INVESTIGATION OF BLAST INDUCED GROUND VIBRATION AND AIR
BLAST AROUND UŞAK KIŞLADAĞ GOLD MINE

A THESIS SUBMITTED TO
THE GRADUATE SCHOOL OF NATURAL AND APPLIED SCIENCES
OF
MIDDLE EAST TECHNICAL UNIVERSITY

BY

ESRA NUR TANRISEVEN

IN PARTIAL FULFILLMENT OF THE REQUIREMENTS
FOR
THE DEGREE OF DOCTOR OF PHILOSOPHY
IN
MINING ENGINEERING

SEPTEMBER 2018

Approval of the thesis:

INVESTIGATION OF BLAST INDUCED GROUND VIBRATION AND AIR BLAST AROUND UŞAK KIŞLADAĞ GOLD MINE

submitted by **ESRA NUR TANRISEVEN** in partial fulfillment of the requirements for the degree of **Doctor of Philosophy in Mining Engineering Department, Middle East Technical University by,**

Prof. Dr. Halil Kalıpçılar
Dean, Graduate School of **Natural and Applied Sciences** ————————

Prof. Dr. Celal Karpuz
Head of Department, **Mining Engineering** ————————

Assoc. Prof. Dr. Hasan Aydın Bilgin
Supervisor, **Mining Engineering Department, METU** ————————

Examining Committee Members:

Assoc. Prof. Dr. Mehmet Ali Hindistan
Mining Engineering Dept., Hacettepe University ————————

Assoc. Prof. Dr. Hasan Aydın Bilgin
Mining Engineering Dept., METU ————————

Assoc. Prof. Dr. Hasan Öztürk
Mining Engineering Dept., METU ————————

Asst. Prof. Dr. İbrahim Ferid Öge
Mining Engineering Dept., Muğla Sıtkı Koçman University ————————

Asst. Prof. Dr. Mustafa Erkayaoğlu
Mining Engineering Dept., METU ————————

Date: 04/09/2018

I hereby declare that all information in this document has been obtained and presented in accordance with academic rules and ethical conduct. I also declare that, as required by these rules and conduct, I have fully cited and referenced all material and results that are not original to this wok.

Name, Last name: Esra Nur Tanrıseven

Signature   :

ABSTRACT

INVESTIGATION OF BLAST INDUCED GROUND VIBRATION AND AIR BLAST AROUND UŞAK KIŞLADAĞ GOLD MINE

Tanrıseven, Esra Nur

Ph.D, Department of Mining Engineering

Supervisor: Assoc. Prof. Dr. Hasan Aydın Bilgin

September 2018, 210 pages

The objective of this study is to evaluate the effects of blasting operations conducted in Kışladağ Open Pit Gold Mine on surrounding villages in terms of ground vibration and air shock in the light of commonly used regulations. Moreover, it is aimed to give site specific propagation laws for future blasts and to determine safe explosive amounts that can be blasted at the same time not to exceed safe ground vibration limits in the villages. Kışladağ Gold Mine is located in the middle of three settlements; Gümüşkol, Karapınar and Katrancılar villages. Data are obtained from the monitoring stations located on the paths towards villages. Blasting operations are evaluated under two classes due their different loading and stemming characteristics; production blasts and presplit blasts. For ground vibration and air shock prediction linear regression analysis and multiple linear regression (MLR) analysis are used and their performances are compared by means of statistical parameters. The performances of analyses from both unclassified and classified data according location of blast round in the pit are tested and compared. Different input combinations for multiple linear regression analysis are tested by using scaled distance, charge weight, distance, and elevation difference between blast round and monitoring station. The results indicate that linear regression analysis has better performance for ground vibration prediction and blast round location affects the ground vibration levels. Whereas, for air blast

prediction MLR is a better tool and elevation difference has an important effect on air blast levels.

Keywords: Ground vibration, air blast, production blast, presplit blast, Multiple Linear Regression Analysis

ÖZ

UŞAK KIŞLADAĞ ALTIN MADENİ ÇEVRESİNDE PATLATMA KAYNAKLI YER TİTREŞİMİ VE HAVA ŞOKUNUN DEĞERLENDİRİLMESİ

Tanrıseven, Esra Nur

Doktora, Maden Mühendisliği Bölümü

Tez Yöneticisi: Doç. Dr. Hasan Aydın Bilgin

Eylül 2018, 210 sayfa

Bu tez çalışmasının amacı, Kışladağ Altın Madeni Yerüstü Ocak İşletmesi'nde yapılmakta olan patlatmaların yarattığı etkilerin yer titreşimi ve hava şoku bakımından ölçülmesi ve çevredeki köyler üzerindeki etkilerinin sıklıkla kullanılan yönetmeliklere göre değerlendirilmesini kapsamaktadır. Ayrıca araziye özgü sönümlenme eşitliklerinin ve köylerde güvenli titreşim limitlerini geçmeyecek şekilde gecikme başına patlatılabilecek maksimum patlayıcı miktarının belirlenmesi amaçlanmıştır. Kışladağ Altın Madeni, Gümüşkol, Karapınar ve Katrancılar Köylerinin ortasında yer almaktadır. Veri köylere giden yollar üzerinde konumlandırılmış ölçüm istasyonlarından elde edilmiştir. Patlatmalar değerlendirilirken sıkılama ve patlayıcı miktarlarına göre üretim patlatmaları ve ön kesme patlatmaları olarak iki ayrı sınıf altında incelenmiştir. Bu çalışmada yer titreşimi ve hava şoku tahmini için doğrusal regresyon ve çoklu doğrusal regresyon analizi kullanılmış olup performansları istatiksel parametreler kullanılarak kıyaslanmıştır. Ayrıca patlatma grubunun ocak içerisindeki konumuna göre sınıflandırılmış ve sınıflandırılmamış veri üzerinde analizler yapılarak sonuçlar karşılaştırılmıştır. Çoklu doğrusal regresyon analizi için ölçekli mesafe, patlayıcı miktarı, mesafe, patlatma ve ölçüm istasyonu arasındaki kot farkı kullanılarak farklı girdi parametreleri kombinasyonları denenmiştir. Sonuçlar yer

titreşimi tahmini için doğrusal regresyon yönteminin daha iyi sonuç verdiğini ve patlatma grubu konumunun yer titreşimi üzerinde etkili bir faktör olduğunu göstermektedir. Hava şoku tahmini için çoklu doğrusal regresyon analizi daha iyi sonuçlar vermiştir ve kot farkının hava şoku üzerinde önemli bir etkisi olduğu görülmüştür.

Anahtar Sözcükler: Yer titreşimi, hava şoku, üretim patlatması, ön kesme patlatması, Çoklu doğrusal regresyon

To My Family

ACKNOWLEDGMENTS

TABLE OF CONTENTS

LIST OF TABLES

xv

LIST OF FIGURES

FIGURES

xviii

LIST OF ABBREVIATIONS

PPV	Peak Particle Velocity
MLR	Multiple Linear Regression
SD	Scaled Distance
RMSE	Root Mean Square Error
R	Correlation coefficient
R^2	Square of correlation coefficient
r^2	Coefficient of determination
MIC	Maximum Instantaneous Charge
USBM	United States Bureau of Mines
OSMRE	Office of Surface Mining Reclamation and Enforcement
OSM	Office of Surface Mining
RI	Report of Investigation
CFR	Code of Federal Regulations
N-NE	North Northeast
N-NW	North Northwest
S-SE	South Southeast
S-SW	South Southwest
E-NE	East Northeast
W-NW	West Northwest
E-SE	East Southeast
W-SW	West Southwest

CHAPTER 1

INTRODUCTION

Ground vibration, air blast, and dust are common results of blasting operations and can even result in damage in nearby buildings and disturbance of people settling around the mine. Charge amount, distance to blast site, face height and orientation, diameter and length of blasthole, type of rock mass, explosive type, and stemming amount are mostly known factors that are affecting the damage levels of a blast. Complaints of local people about vibrations, noise, and damage in the houses led to this study. In this study, ground vibrations and air overpressure induced by production blasting and presplit blasting are predicted by using linear regression analysis and Multiple Linear Regression (MLR) analysis to estimate their damage potential and to minimize disturbance in Gümüşkol, Karapınar, and Katrancılar villages.

1.1 Objectives and Scope of the Study

This research aims to evaluate the environmental impacts of the blasting operations conducted in Kışladağ Gold Mine and to give safe explosive amounts which do not create any structural damage. The scope of this study includes ground vibration and air blast overpressure monitoring on the determined paths towards the villages around the mine and their evaluation. In this context designated steps are followed;

1) Locations of monitoring stations are determined around the mine toward the surrounding villages.

2) Ground vibration and air blast records are collected by means of seismographs.

3) Monitoring stations are selected according to wind direction and location of the blast group, daily.

4) Maximum instantaneous charge (MIC) of blasts and distance of blastholes (giving MIC) to measurement stations are obtained.

5) Daily meteorological data at the time of blasting are obtained.

6) Production blasts and presplit blasts are investigated separately with linear regression analysis and MLR method. The best method is determined by using statistical parameters.

7) The site-specific propagation laws are obtained for each village with linear regression analysis.

8) Obtained site-specific propagation laws are used to determine safe explosive amounts to minimize the damage risk and public complaints from the surrounding villages.

9) Measured ground vibration and air blast levels are evaluated according to regulations.

1.2 Research Methodology

This research study is comprised of two parts; these are data acquisition and classification and their analysis. A four-month period was allocated for data acquisition stage. Presplit blasts and production blasts are investigated separately due to their different characteristics. Then, data are categorized according to the blast location within the pit (both for ground vibration and air shock analysis) and wind direction at the moment of blast (for air shock analysis). Then site-specific propagation laws are determined for each village using least squares regression analysis that will be used for the determination of maximum allowable charge according to blast location for later blasting operations. For this purpose, cube root scaled distance versus air blast level and square root scaled distance versus peak particle velocity are graphed in logarithmic-logarithmic scale. Ground vibration and air blast levels are evaluated according to regulations and legislations. Research methodology and number of records related to each blasting type is given in Figure 1.1.
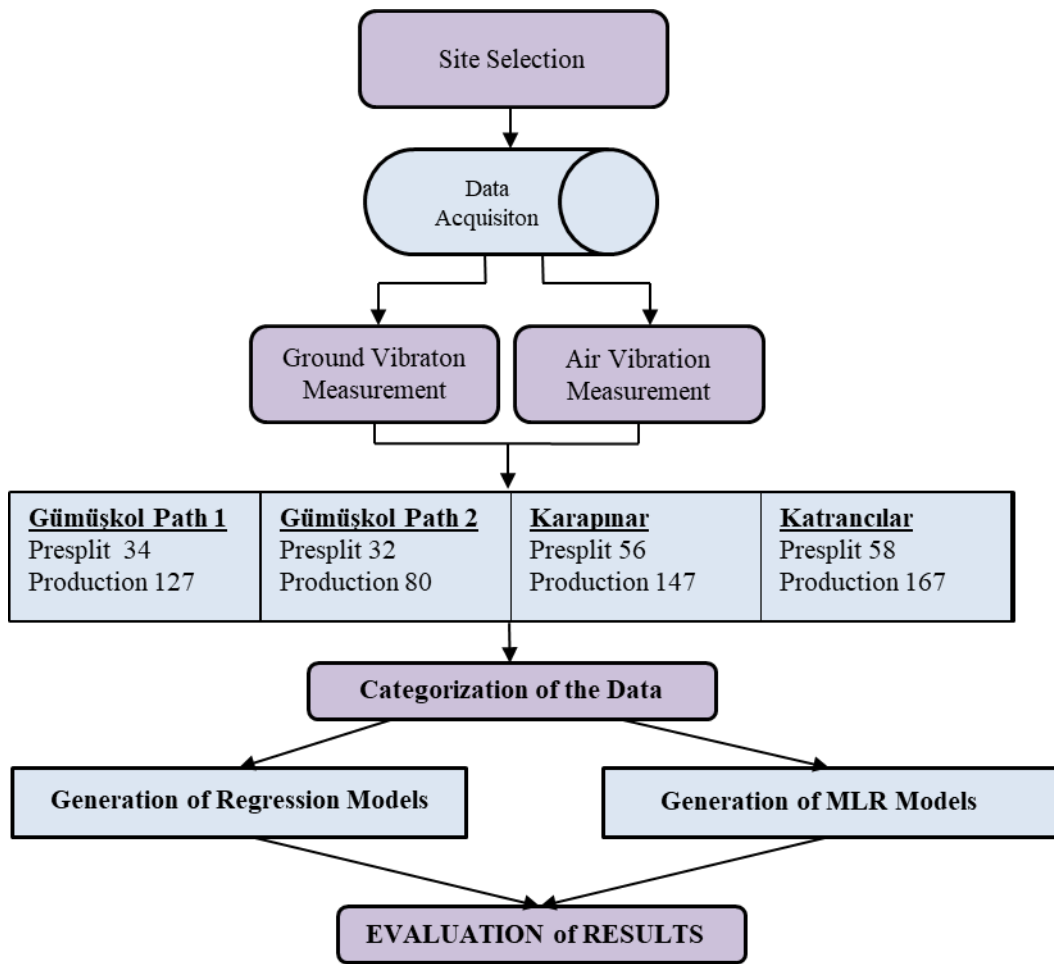
Figure 1.1 Research methodology of the study

CHAPTER 2

LITERATURE REVIEW

2.1   Ground Vibration

When an explosive charge in a blasthole is detonated, a certain amount of energy is released and the rock surrounding the charged blasthole is subjected to stress and fractures. At some distance from the blasthole, the explosion energy decreases to a level, which does not induce more shattering or displacement, and proceeds to travel through the rock as an elastic vibration (Richards & Moore, 2009a). The ground vibration radiates from the blasthole and its intensity decreases with distance to below perception levels. Ground vibration at sufficiently high levels will damage buildings; however, people can feel levels below structural damage levels. Figure 2.1 shows the behavior of the waves radiating from the blasthole.
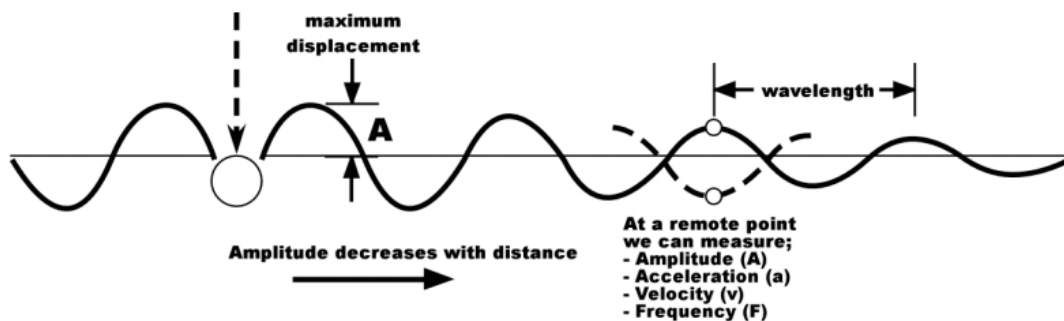
Figure 2.1 Wave terminology (Richards & Moore, 2009a).

2.1.1   Wave Types

Ground vibrations are the common outcome of blasting operations, and vibrations are composed of two types of waves; body waves and surface waves.

2.1.1.1 Body Waves

Body waves are produced by the initial pressure pulse. Compressional (P or primary wave) and shear waves (S or secondary wave) are generally referred to as body waves,

since they travel through rock body (Richards & Moore, 2009a). Figure 2.2 illustrates deformation characteristics of P and S waves. Compressional wave is the fastest wave travelling through the ground. Compressional waves move radially from the blasthole in all directions. The particles in the wave move in the same direction as the propagation of the wave (Richards & Moore, 2009a).
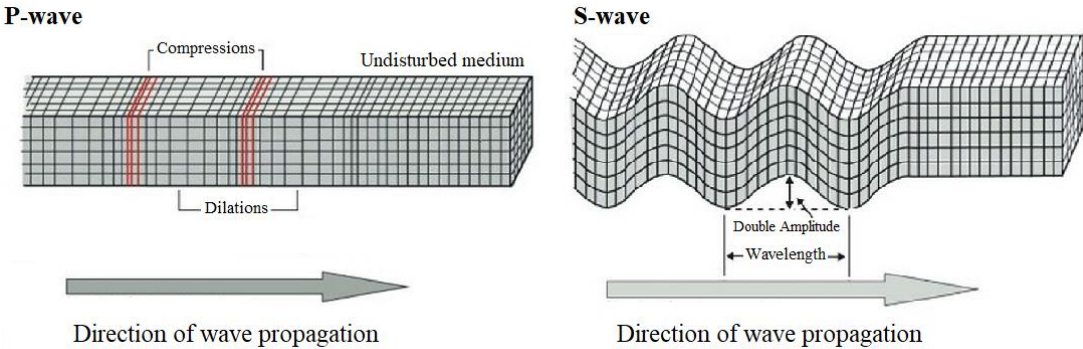
Figure 2.2 Deformation characteristics of Primary and Secondary waves (SOS-LIFE Earthquake early warning system, 2015)

Shear wave has a propagation velocity of 50-60% of the P waves. The particles within the wave move at right angles to the wave propagation direction. This type of wave is formed when the medium particles oscillate perpendicular to the direction of propagation (Prdhan & Das, 2007).

2.1.1.2 Surface Waves

Surface waves are the slowest in propagation velocity and far more the most destructive type of waves due to lowest decay with distance. Surface waves attenuate more rapidly with depth than body waves. These waves travel along the surface as two types of waves; Rayleigh wave (R-wave) and Love wave (Q-wave). These waves cause the most of complaints and vibration problems (Prdhan & Das, 2007). Figure 2.3 shows deformation characteristics of Q and R waves. Love wave is faster than Rayleigh wave. Love waves are characterized by particle vibration of shear in horizontal transverse direction (Prdhan & Das, 2007).
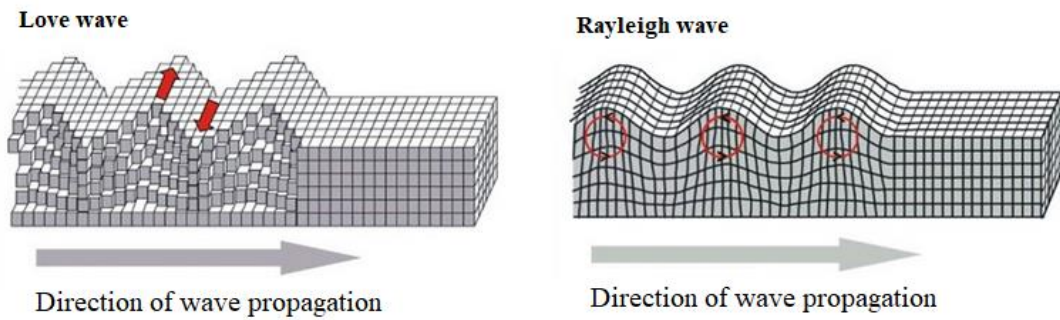
Figure 2.3 Deformation characteristics Love and Rayleigh waves (SOS-LIFE Earthquake early warning system, 2015)

Whereas, the particles within the Rayleigh wave move in an elliptical path in a vertical plane in the direction of propagation and have no transverse component (Richards & Moore, 2009a). The wave motions of all three types of waves are illustrated in Figure 2.4.
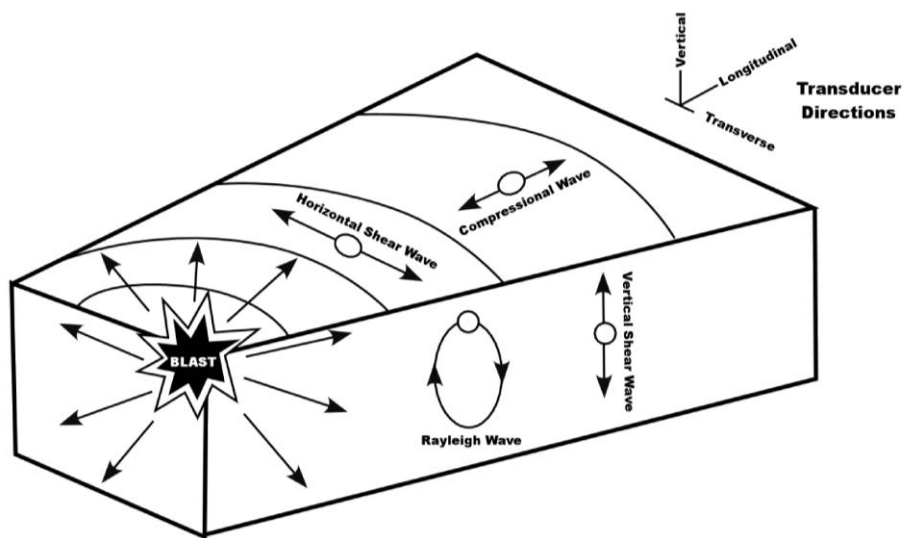
Figure 2.4 Particle motion associated with the different wave types (Richards & Moore, 2009a)

2.1.2   Ground Vibration Level

Ground vibration prediction is a prominent issue and various researchers proposed different formulas to represent ground vibration. Five basic relations are given for particle velocity prediction due to blasting.

2.1.2.1 USBM Formula

Assuming that explosives have cylindrical geometry, Duvall & Petkof (1959); Duvall & Fogelson (1962); Daemen et al.(1983); Duvall et al. (1963) concluded that the actual distance should be divided by the square of the charge mass (Pal Roy, 2005).

V = peak particle velocity (mm/s)

B = slope of the best fit straight line of the velocity vs $(D/\sqrt{Q})$ plot on log-log scale

K = intercept on velocity axis when $(D/\sqrt{Q}) = 1$ (rock transmission factor)

Q = charge mass (kg)

D = distance (m)

$$V = K\left(\frac{D}{\sqrt{Q}}\right)^{-B}$$

2.1.2.2 Langefors-Kihlstrom Formula

Langefors et al. (1958) suggested the following relationship for various charging levels to estimate peak particle velocity (Pal Roy, 2005). This formula was based on blasting in hard rock. The rock transmission factor allows for prediction of PPV for varying rock types and confinement conditions (Richards & Moore, 2009a).

$$V = K\left(\sqrt{\frac{Q}{D^{2/3}}}\right)^{B}$$

2.1.2.3 Ambraseys-Hendron Formula

For spherical symmetry Ambraseys and Hendron (1968) suggested an inverse power law to relate amplitude of seismic waves and scaled distance (Pal Roy, 2005). They also suggested cube root scaled distance.

$$V = K\left(\frac{D}{\sqrt[3]{Q}}\right)^{-B}$$

2.1.2.4 Indian Standard Formula

Indian Standard (1973) used a concept in which blast is scaled to the equivalent distance (Pal Roy, 2005), the relation is expressed as:

$$V = K\left(\frac{Q^{2/3}}{D}\right)^{B}$$

2.1.2.5 CMRI (Central Mining Research Intitute) Formula

The formula takes into consideration only the geometrical spreading as the reason for attenuation of ground vibrations (Mohamed, 2010). This equation is valid only in the zone of disturbance, namely when Q>0 and V>0 (Pal Roy, 2005).

$$V = n + K\left(\frac{\sqrt{Q}}{D}\right)$$

where n is related to the category of parameters, which are influenced by rock properties and geological discontinuities (Prdhan & Das, 2007). K is related to design parameters such as; charge weight, distance to blasting, charge diameter, delay, spacing, burden, stemming, and sub drilling (Prdhan & Das, 2007). Predictor equations are summarized in Table 2.1.

Table 2.1 Predictor equations

Name of Predictor Equation	Equations
USBM (Duvall and Fogelson, 1962)	$V = K\left(\frac{D}{\sqrt{Q}}\right)^{-B}$
Langefors-Kihlstrom (1978)	$V = K\left(\sqrt{\frac{Q}{D^{2/3}}}\right)^{B}$
Ambraseys-Hendron (1968)	$V = K\left(\frac{D}{\sqrt[3]{Q}}\right)^{-B}$
Indian Standard Predictor (1973)	$V = K\left(\frac{Q^{2/3}}{D}\right)^{B}$
CMRI (or CMRS)	$V = n + K\left(\frac{\sqrt{Q}}{D}\right)$

2.2   Air Vibration

Air blast (or air vibration) arises from the stemming release and gas release pulses along with rock and air pressure pulses and radiates in air from an exploding charge (Jimeno et al., 1995). When a pressure wave passes through a place, the pressure of the air increases very rapidly then decreases more slowly to a level below the

atmospheric pressure before maintaining the atmospheric value (Richards & Moore, 2009a). A characteristic air vibration wave trace for a single hole blast is given in Figure 2.5. A multi hole blasting results in a more complex wave trace, since the waves of the individual holes interact with each other.
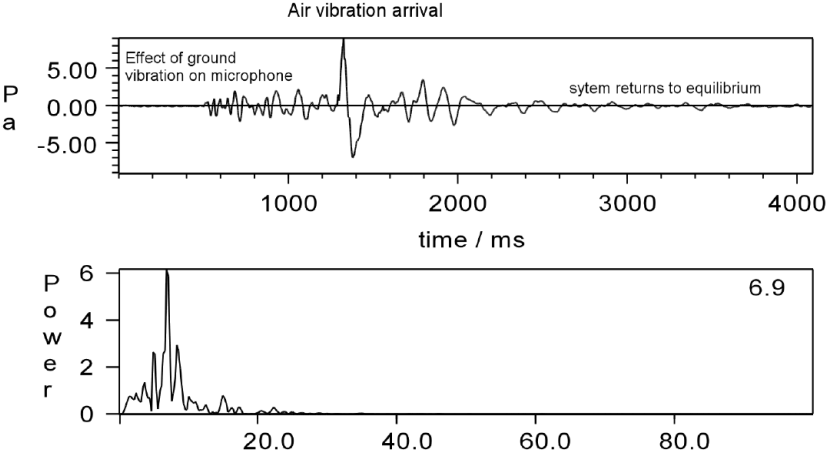
Figure 2.5 Air vibration (Pascal) wave trace for a single hole firing (Richards & Moore, 2009b)

The air blast curve from a single hole has an 'N' shape, formed from an initial positive phase followed by a negative phase and then several minor fluctuations (Richards & Moore, 2006). The 'N' wave shape varies depending on whether air vibration is recorded in front of a free vertical face or behind a free face (Richards & Moore, 2006). Typically, the positive phase has higher pressure than the negative phase but has a shorter duration as shown in Figure 2.6.
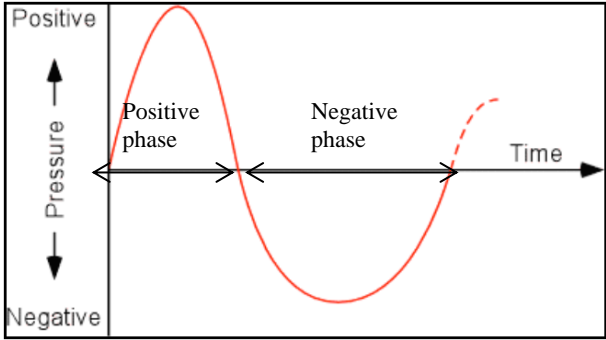
Figure 2.6 Synthesized air blast 'N' wave from single hole blasting (Richards & Moore, 2006)

10

Mohamed (2010) stated that generally four mechanisms are responsible for the formation of air vibrations: the venting of gases to the atmosphere from unconfined explosive charges (i.e. presplit blasts), release of gases to the atmosphere from exposed detonating fuse (initiation system), ground motions resulting from the blast, and the motion of rock at the bench face.

Audible air blast is called noise while air blast at frequencies below 20 Hz and inaudible to the human ear is called infrasound (Mohamed, 2010). Human ear can hear the sound at frequencies between 20 Hz and 20000 Hz (Siskind, 2000). The noise can be continuous (duration>1 second) or impulsive (such as shock) (Mohamed, 2010). Air blast is generally expressed in terms of Pascal (Pa), decibels (dB), or pounds per square inch (psi). The audible portion of air blast ranges between different amplitudes and frequencies, thus the decibel scale is generally used to describe sound level based on human hearing (Persson et al., 1994). The below relationship gives air blast in decibels (dB) where P is the measured peak sound pressure and P_o is the reference pressure of 2.9×10^{-9} psi (20×10^{-6} Pa) (Mohamed, 2010). The logarithmic decibel scale is appropriate for acoustic measurements where human disturbance is the case (Persson et al., 1994).

$$dB = 20 \log_{10}\left(P\big/P_0\right)$$

Maximum instantaneous charge blasted per delay and distance from the blasthole are the main factors affecting air blast level. Moreover, it is extremely affected by atmospheric conditions (such as strength and direction of wind, humidity, temperature, and cloudy weather) and topographical shielding. These factors absorb some part of the overpressure waves and deflect some part of it and the remaining part travels long distances without loss (Dowding, 1985). Air blast can be identified with only one transducer, different from ground vibrations, since air pressure is equal in all directions (Mohamed, 2010). Various sources of air blast are shown in Figure 2.7
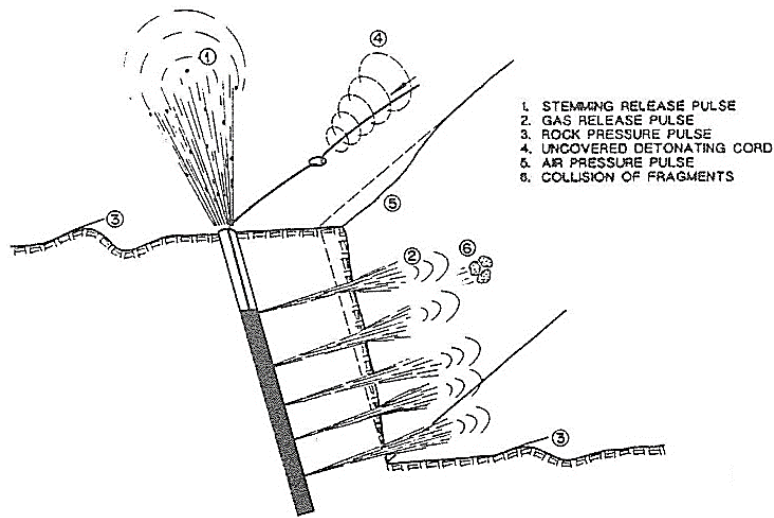
Figure 2.7 Sources of air blast (Jimeno et al., 1995)

Richards (2013) pointed out important factors influencing air blast levels are:

1) Charge mass and distance from blast

2) Face height and orientation

3) Topographic shielding

4) Stemming height and type

5) Blasthole diameter to burden ratio

6) Burden, spacing, and sequential initiation timing

7) Meteorological conditions.

2.2.1   Charge mass and weight

Air blast level increases with increasing charge mass and decreasing distance from the blast site. Air vibration level is assessed using the following cube root scaling formula.

$$P = K \left(\frac{D}{\sqrt[3]{Q}} \right)^a$$

P is Pressure (Pa), Q is the charge mass (kg), D is the distance from charge (m), K is the site constant and a is the site exponent. Siskind et al. (1980a) emphasized that air vibration is proportional to the cube root of the charge mass. Thus, reduction in charge mass could not decrease air vibration levels effectively (Siskind et al., 1980a).

12

2.2.2 Face height and orientation

When a blasthole is fired towards a free face, the resulting air vibration is greater in front of the face (the blast is located behind the pit with respect to village) than behind the face (the blast is located in front of the pit with respect to village) due to the shielding effect of the face (Richards, 2013). Figure 2.8 shows the effect of face orientation.
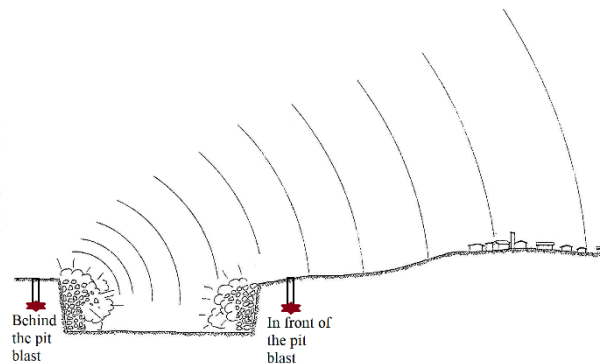
Figure 2.8 Effect of face orientation (Jimeno et al., 1995)

An elliptical contour model was developed to assess air blast levels in the area surrounding the blast site using the data measured at one or more positions (Richards, 2013). Richards (2013) pointed out the elliptical contours are stretched in front of the face and mostly flattened behind the face. These contour maps may be used to analyze air vibration measurements and to assess air vibration levels at unmonitored locations (Richards, 2013). Richards (2013) indicated that, if there is no free face or the air vibration is primarily controlled by the stemming height, air blast contours become circular. The size of the contours can be determined from the inputs: charge mass, stemming height, and hole diameter. Figure 2.9 shows decibel contours placed over a plan of the area.
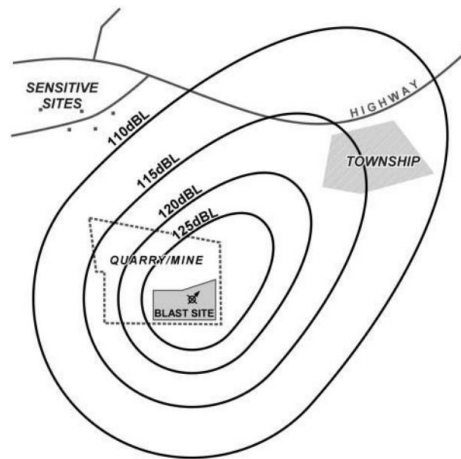
Figure 2.9 Decibel contours placed over area plan (Richards, 2013)

2.2.3 Topographical shielding

In hilly regions, or deep excavations, air vibration levels are decreased by topographic shielding in the surrounding area (Richards & Moore, 2009b). Shielding is affected by effective barrier height and incident angle. Figure 2.10 illustrates the terminology.
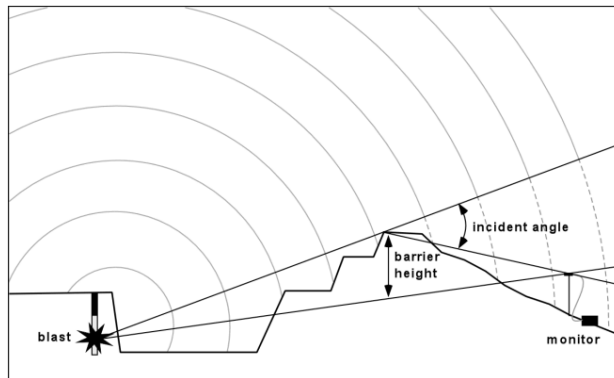
Figure 2.10 Shielding terminology (Richards & Moore, 2009b)

The association between barrier height, incident angle and shielding measured in decibels linear (dBL) is depicted in Figure 2.11. This relationship allows making adjustments to sound pressure levels (dBL) determined by the air blast contour model, to increase the model precision. The following formula may also be used to determine

the effect of shielding, which is based on the graphical analysis illustrated in Figure 2.12. Where H is the barrier height (m) and θ is the incident angle.

$$Shielding\,(dBL) = 15log_{10}(H)sin(\theta)^{1.17} - 10.8sin(\theta)^{1.17} - 0.6$$
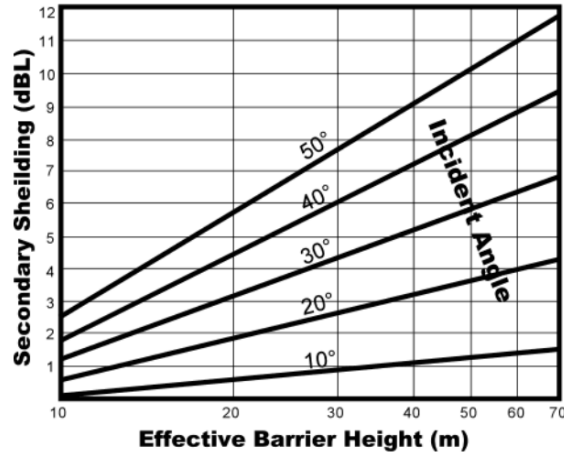
Figure 2.11 Estimation graph for secondary shielding (Richards & Moore, 2009b)
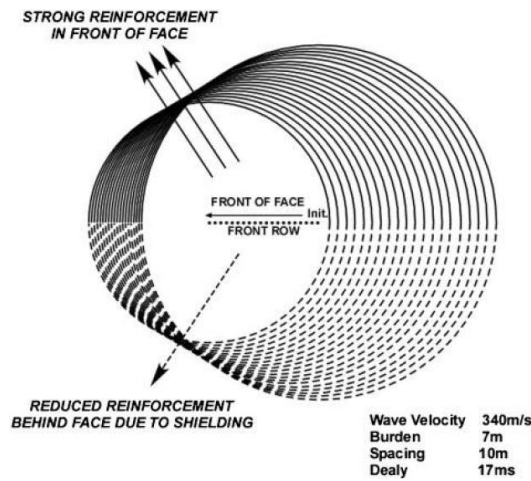
Figure 2.12 Wavefront diagram showing reinforcement (Richards, 2013)

Figure 2.12 shows strong reinforcement taking place in front of the face because of strong emission from front row blastholes (Richards, 2013).

2.2.4 Meteorological conditions

When a blasthole is fired, air vibration wavefront travels outwards from the blasthole in all directions at the speed of sound. Atmospheric temperature, wind speed and direction affect the speed of the wavefront (Richards, 2013). Reinforcement takes place when the sound rays are deflected by variation in temperature or wind and are concentrated at the surface as shown in Figure 2.13 (Richards, 2013).
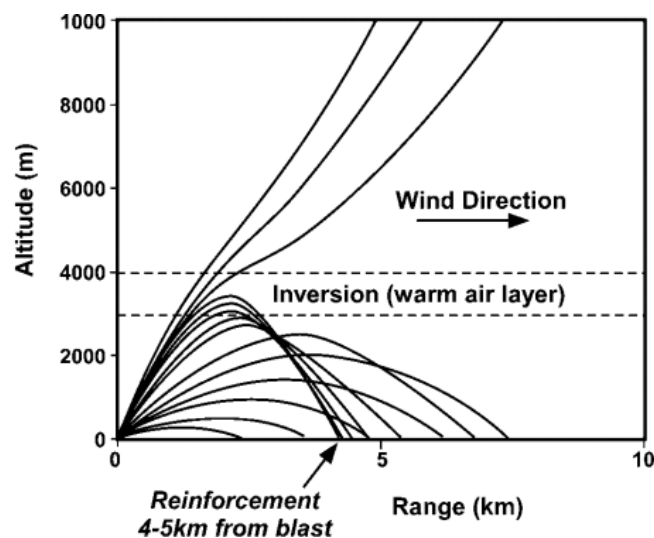
Figure 2.13 Meteorological reinforcement caused by warm air inversion layer (Richards, 2013)

Richards (2013) stated this situation leads to higher air vibration level than that usually arises from the normal attenuation rate. In fact, the significance of the reinforcement may sometimes lead to complaints at distances of several kilometers from the blast site. The reinforcement may result in 10-20 dBL increase at distances greater than 1 km from the blast site (Richards, 2013). In order to identify the effects of the meteorological conditions on air overpressure, meteorological data are required above the ground (Richards, 2013).

2.2.5 Combined effect of burden, spacing and sequential initiation timing

A vibration wavefront is formed when a blasthole is fired, which radiates at the propogation speed uniformly in all directions (Richards, 2013). Richards (2013) stated

16

that if the distance between blastholes coincides with the wavefront travel distance, then reinforcement takes place. Figure 2.14 shows the wavefront reinforcement diagram for blasting of a row of blastholes 3 m apart with a 9 ms delay, a substantial increase occurs in air vibration in the direction of initiation (Richards, 2013).
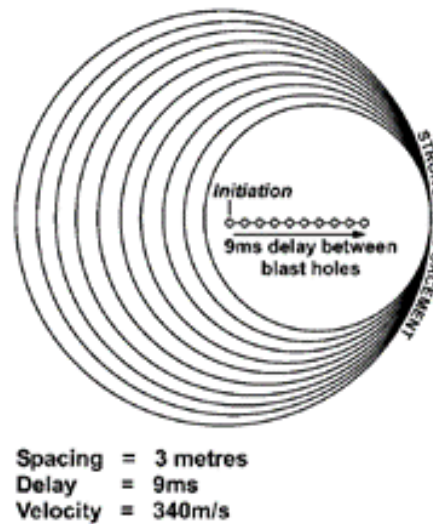
Figure 2.14 Wavefront reinforcement (Richards, 2013)

Wavefront reinforcement model can be used to evaluate the combined effect of sequential initiation sequence and drilling pattern (Richards, 2008). Burden, spacing, delay sequence of each blasthole are the inputs for the model.

Richards (2013) pointed out the model was used to obtain a graphical output for the determination of the direction and extent of increases in air blast overpressure. Figure 2.15 indicates the influence of this strong reinforcement in air blast contour map placed over scaled air photo of the site (Richards, 2013). The contour assessment compares the basic emission case (without wavefront reinforcement) with the total emission case (due to effect of reinforcement) (Richards, 2013).

17
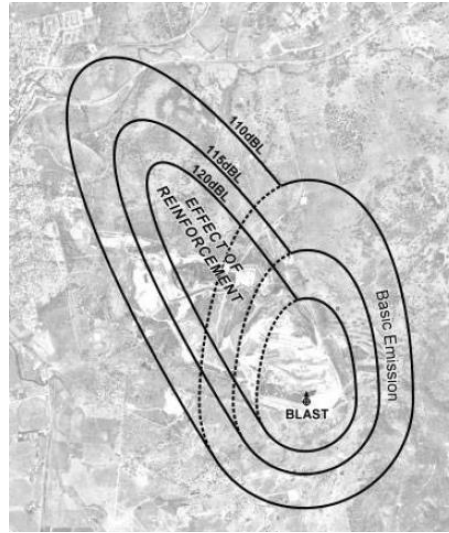
Figure 2.15 Basic air blast emission with wavefront reinforcement (Richards, 2013)

2.3   Scaled Distance

Scaled distance formulas are developed mainly from coal overburden blasting. The square root scaled distance formula is more commonly used and depends on the idea that the charge is distributed in the blast hole; therefore, the diameter of the hole is proportional to the square root of the charge weight (Richards & Moore, 2009a). However, as the hole length shortens compared to the diameter, the charge mass approaches a spherical shape, in which case the diameter is proportional to the cube root of the charge weight (Richards & Moore, 2009a).

$$\text{Square root scaled distance} = \frac{D}{\sqrt{Q}}$$

$$\text{Cube root scaled distance} = \frac{D}{\sqrt[3]{Q}}$$

Blasting energy decay may depend on waveform of the energy and the distance. Namely, at short distances to blast site body waves may be dominant, however at far distances energy may dissipate mainly through surface waves. Sometimes charge mass may be a more complicated function than cube or square root where V is PPV, however the general equation is:

18

$$V = K \left(\frac{D}{Q^n} \right)^{-B}$$

Square root scaled distance is used to collect data from many blasts, perform a statistical analysis to determine the site exponent 'B' and site constant 'K' (Richards & Moore, 2009a). High site exponent results in rapid drops in ground vibration and lower vibration levels at long distances (Richards & Moore, 2009a). Cube root scaled distance is more useful for air blast analysis, since air blast intensity decreases more rapidly with distance than ground vibrations (Ratcliff et al., 2011).

2.4   Amplification Factor and Resonance

Resonant frequency of a system is the value at which the maximum amplitude of natural oscillation occurs. A system oscillates with greater amplitude at some frequencies than the others. Ground has a resonant frequency; hard bedrocks have higher frequencies than soft sediments. When the resonant frequency of the building and the ground matches, it goes under the highest oscillations and suffer the greatest damage. Short buildings on hard bedrock and tall buildings on soft sediments suffer more from ground motions. Short buildings on soft sediment and tall buildings on hard rock are safer. If resonant frequency of the ground beneath the building is known, building design can be modified and the damage from resonance can be prevented.

When explosion frequencies do not match the natural frequency of the buildings, ground vibrations may result in damage (Svinkin, 2008). Such consequences may occur within a distance equal to excavation depth (close-range explosion), however the distance may be much higher for susceptible structures (Svinkin, 2008). The closeness of the dominant frequency of ground vibrations to the natural frequency of the structure may magnify structural vibrations and even result in resonance (Svinkin, 2008). Figure 2.16 shows vibration records on the ground and in the building with close frequencies, structural vibrations amplified 2.7 times compared to ground vibrations. Structural vibrations started to magnify after the first cycle of vibrations.

Resonance does not take place, if only a couple of cycles of ground vibrations with dominant frequency arises (Svinkin, 2008). The resonance may be provoked even at more than one km from the explosion. Resonance of horizontal component of structural vibrations within 2-12 Hz frequency range is the major concern (Svinkin, 2008).
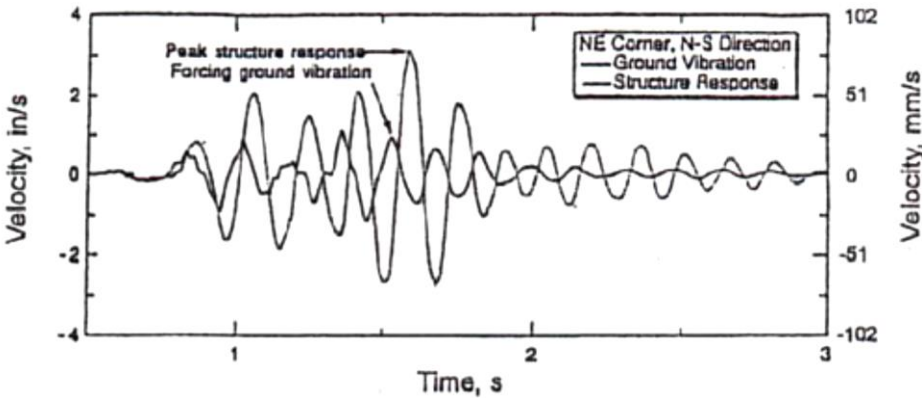
Figure 2.16 Ground and structure vibrations with frequency of 5.8 Hz near structure resonance from Siskind (2000) (Svinkin, 2008)

The probability of building damage also depends on the natural frequency of the ground and the building. The most critical situation takes place when explosion frequency is 8 Hz - 10 Hz in single story buildings, 5 Hz in two story buildings and 2 Hz in 5 story buildings when it is close or equal to natural resonant frequency of the building. In this case, the building resonates even when the wave passes by (Bilgin et al., 2015).

When the building resonates, if the vibration velocity is below the limit values given in the regulations and standards, it does not damage the building, but may result in disturbance of people. However, if the vibration velocity has high amplitude while the building resonates, the building is damaged. In another case, even if the amplitude of the seismic wave is not high enough, the resonance of the building can amplify this amplitude several times and may result in damage of the building (Bilgin et al., 2015).

20

According to Dowding (1992), natural frequency of 1 to 2 story buildings is between 5-10 Hz. Thus, it is expected that the amplification of PPV occurs when the frequency of the seismic wave is equal to 5-10 Hz. As the number of story in a building increases, natural frequency decreases. The ceilings and walls have natural frequencies between 12-20 Hz and resonates independently from the superstructure (Siskind et al., 1980).

When a structure oscillates at resonant frequency it absorbs most of the energy and oscillates for a long time with a higher amplitude. Amplification (magnification) factor is the ratio of vibration amplitude measured at the upper story of a structure to the amplitude at the base (Adhikari et al., 2005). Siskind (2000) pointed out higher amplification factors correspond to frequencies between 4-12 Hz. Svinkin (2015) stated that direct structural damage of 1-2 story buildings without resonance effect were seen within 33-191 mm/s velocity range for 2-5 Hz frequencies and within 102-254 mm/s velocity range for 60–450 Hz frequencies.

2.5 Allowable Ground Vibration Levels

US Office of Surface Mining Reclamation and Enforcement (OSMRE) suggested maximum allowable peak particle velocity limits for the distances from the blasting site (Table 2.2). These criteria are included in US Code of Federal Regulations (CFR).

Table 2.2 Allowable peak particle velocity with respect to distances from the blasting site (Office of Surface Mining Reclamation and Enforcement (OSM), 1983)

Distance from the blast site, m (ft)	Maximum allowable PPV, mm/s (in/sec)	Scaled distance to be applied without seismic monitoring
0-92 (0-300)	31.75 (1.25)	50
92-1524 (301-5000)	25.40 (1.00)	55
>1524 (≥5001)	19.05 (0.75)	65

However, given maximum allowable ground vibration limits do not take frequency and type of structure into account and the tabulated limits are for engineered structures built according to standards.

It is necessary to consider the dominant ground vibration frequency and structure vibrations in order to evaluate the effects of ground vibration on structures. Svinkin (2015) stated that the primary objective of the subsequent USBM study was to prevent the resonant horizontal house vibrations.

Table 2.3 shows the safe ground vibration levels for residential structures, a sudden rise exists above 40 Hz frequency. Nevertheless, the limiting value 12.7 mm/s suggested by Siskind et al. (1980b) is more appropriate to be cautious, since it is lower than PPV values in Table 2.2 (19.05 mm/s or 25.40 mm/s) for the distances from the blasting site.

Table 2.3 Safe ground vibration levels for residential structures (Siskind et al., 1980b)

Structure Type	Ground Vibration - PPV (mm/s)	
	At low frequency (<40 Hz)	At high frequency (>40 Hz)
Modern homes, Drywall interiors	19.05	50.80
Older Homes, Plaster on wood lath construction for interior walls	12.70	50.80

USBM and US Office of Surface Mining Reclamation and Enforcement (OSM) suggested an alternative criterion, which takes into account the frequency of ground vibrations. Figure 2.17 is the graphical representation of these criteria. USBM values were generated from surface coal mine blasting. Within the frequency range of 2.5-10 Hz, 12.7 mm/s and in the range of 40-100 Hz, 50.8 mm/s peak particle velocity is allowable according to USBM. Despite this, US OSM proposed different ground vibration levels, for 4-10 Hz frequency range 19.0 mm/s and for 30-100 Hz frequency range 50.8 mm/s ground vibration is allowed. Moreover, Turkish Regulations (tabulated in Table 2.4) proposed similar levels to US OSM regulations, allowable ground vibration levels are 19.0 mm/s (for 4-10 Hz frequency range) and 50.0 mm/s (for 30-100 Hz frequency range). These values assume that cosmetic cracking (hairline cracks in plaster and shallow cracks) probability can be at most % 5. In other words, these limits guarantee non-occurrence of even superficial cracks with % 95 probability (Siskind et al., 1980b).
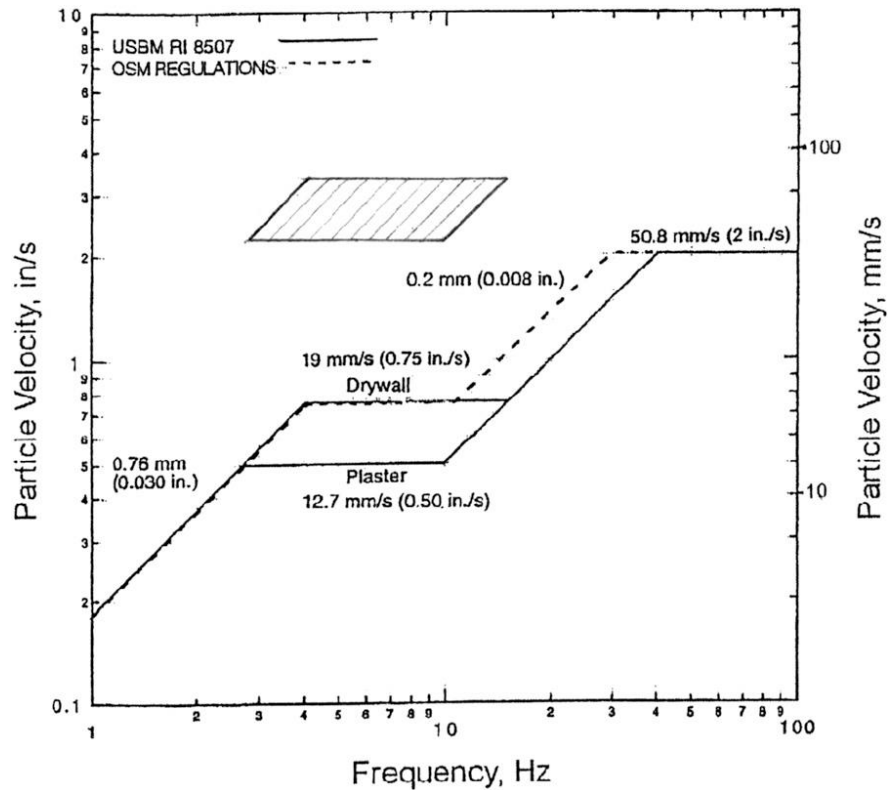
Figure 2.17 Safe ground vibration level criteria from USBM RI 8507 and OSM surface coal mine regulations; shaded area shows structural vibration velocity with amplification of 4.5 at resonance (Siskind, 2000 and Svinkin, 2008)

Table 2.4 Turkish Regulations for safe ground vibration levels (Bilgin et al., 2014)

Vibration Frequency (Hz)	Maximum Allowable Peak Particle Velocity (mm/s)
1	5
4-10	19
30-100	50

German DIN 4150 standard labels a structure as 'damaged' even when either formation of superficial cracks in mortar and cement render or expansion of already existing cracks or detachment of intermediate walls from support walls takes place. If one of the aforementioned damage takes place without exceedance of allowable limits, the reason maybe other causes (DIN 4150–3:1999–02, 1999). This standard is given in Table 2.5 and combined version of USBM RI 8507 and DIN 4150-3 standards are shown in Figure 2.18. Before EU Legislation 2002/49/EC became valid, DIN 4150-1

23

German vibration standard, which is known as the most conservative standard, was under action. This standard is intended not only to avoid structural damage but also to reduce the human annoyance to a minimum and to eliminate the complaints, which are known to occur at levels much lower than the damage levels (Siskind, 2000).

Table 2.5 DIN 4150–3 Vibration standards for structure types

Group	Type of Structure	Peak vibration velocity, mm/s			At upper floors
		At foundation at a frequency of			
		<10 Hz	10-50 Hz	50-100 Hz	All frequencies
1	Buildings used for commercial purposes, industrial buildings and buildings of similar design	20	20-40	40-50	40
2	Dwellings and buildings of similar design and/or use	5	5-15	15-20	15
3	Structures that because of their particular sensitivity to vibration, do not correspond to those listed in groups 1 or 2 and have intrinsic value (e.g. buildings that are under a preservation order)	3	2-8	8-10	8
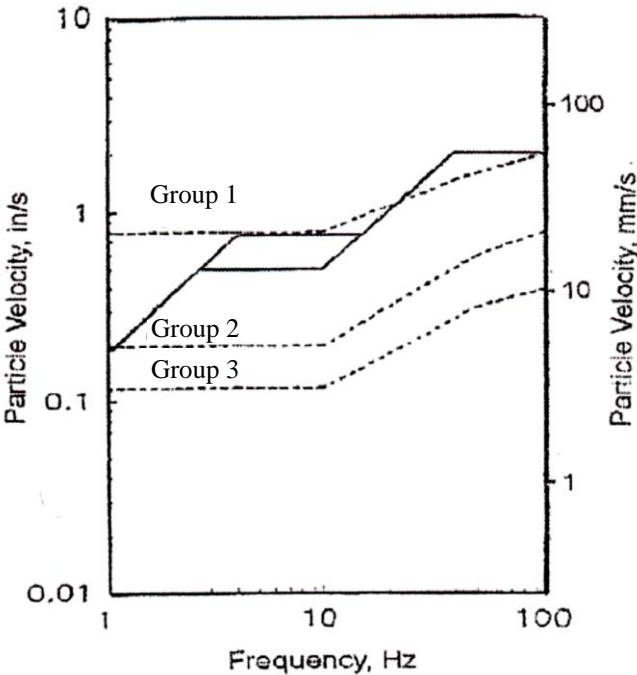
Figure 2.18 Vibration guidelines - USBM RI 8507 (solid line) compared to DIN 4150 (dashed line). Group 1, Group 2, Group 3. From AASHTO Designation: R 8-96 (Svinkin, 2008)

2.6   Human Response to Ground Vibrations

The reaction of human to blast-induced ground vibrations can sometimes be the most decisive factor in ground vibration control. People are very sensitive to ground vibration levels, far lower than the safe limits that will not cause any structural damage. The ground vibration that can be perceived by people is around 1.5 mm/s. Human response depends not only on the amplitude of the seismic wave but also on the frequency and duration (Bilgin et al., 2015). Figure 2.19 shows human perception of ground vibrations depending on the duration of the vibration (Siskind et al., 1980b). Figure 2.20 shows the perception levels with respect to vibration duration (0.1-5.0 seconds) and the frequency range (4-25 Hz).
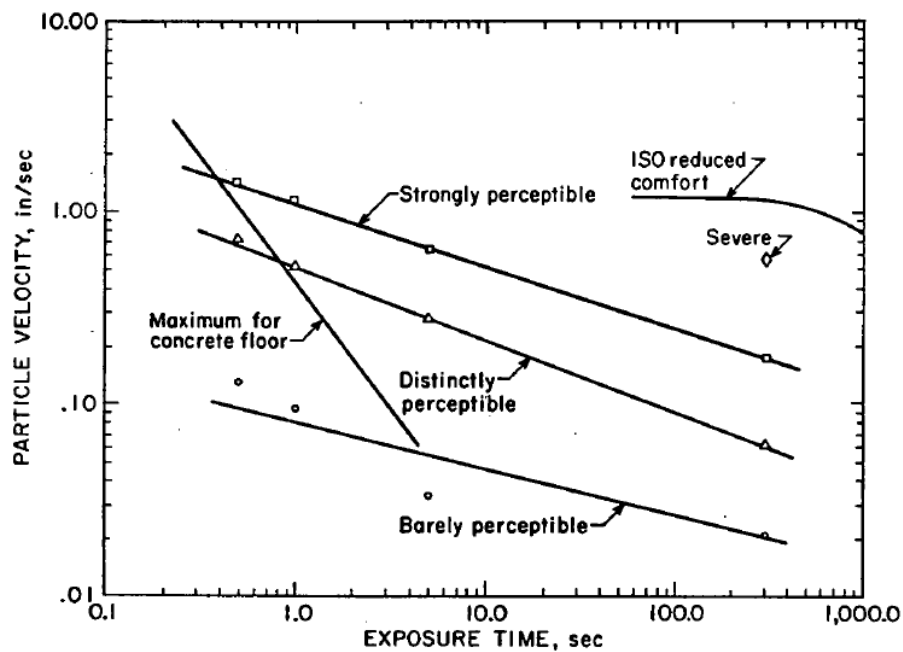
Figure 2.19 Human response to vibrations of various durations, summary. ISO values are from Standard 2631 (Siskind et al., 1980b)

This standard does not apply to people who are not directly exposed to vibration but are exposed to the secondary effects of ground vibrations, such as window rattling, noise from the skeleton of the building (creaking, crackling, etc.), movement of items on the shelves. This standard is given in Table 2.6 and it shows the maximum

25

permissible vibration limits for 1-second duration, transient (such as blasting) vibrations. It is recommended to use lower limits for exposures more than one second.
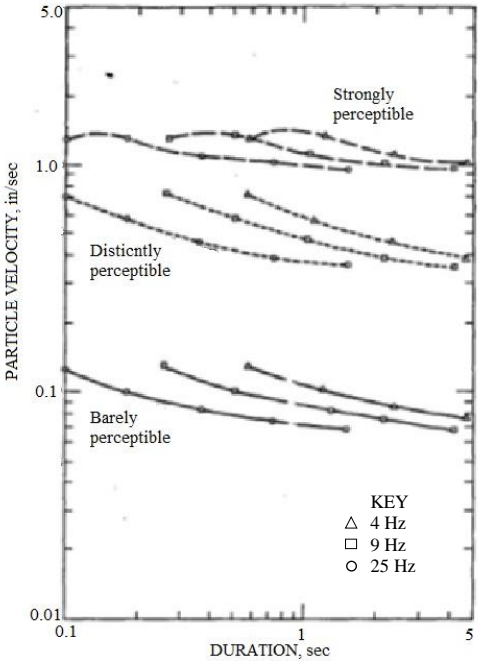
Figure 2.20 Human response to transient vibration velocities of various durations (Siskind et al., 1980b)

Table 2.6 The maximum vibration velocity tolerable by humans in buildings (American National Standards Institute (ANSI S3.29), 1983)

Daily blast count	1	12	26
Dwelling (night)	0.20 mm/s	0.09 mm/s	0.07 mm/s
Dwelling (day)	12.70 mm/s	6.35 mm/s	4.30 mm/s
Office, workshop	18.00 mm/s	8.90 mm/s	6.10 mm/s

In order to prevent human disturbance American National Standards Institute recommends 6.35 mm/s vibration limit for daytime blasts if the daily explosion count is between 2-12. Allowable vibration velocity for explosions with frequency lower than 10 Hz given by DIN 4150 standard provides a safer limit (5 mm/s).

2.7 Allowable Air Blast Levels

As is known, airborne sound (air pressure) waves are one of the side effects that detonation generates. In order to reduce the intensity of air shock in open pit mines, the holes are filled with stemming material such as crushed rock after the explosive is placed in the blasting holes and this is called stemming. It works like a plug, preventing air shock and fly rock. However, presplitting practice generates high levels of air shock due to lack of stemming in the holes as a result of the particular blasting technique (Bilgin et al., 2015).

Frequently, ground vibrations are held responsible for structural vibrations which are commonly the result of long distance air blast waves under favorable weather conditions (Bilgin et al., 2015). Air shock is important for three reasons. First, the audible part produces direct noise. Secondly, the inaudible part causes structural motion by itself or with the ground vibration, which creates noise. Thirdly, it can break window panes, but the air shock must be extraordinarily high for such situation (Bilgin et al., 2015). There are four weighting systems for noise measurement. These are A-, B-, C- and L-weighting. A, B and C weightings are designed to replicate the hearing capability of the human ear at various intensities, they are for low, medium and high sound pressure levels, respectively (Bender, 2006). Figure 2.21 shows attenuation curves for these weighting systems and 0 dB line represents the linear (L-scale) sound level.

It is not possible for humans to hear low-frequency sound waves; however, buildings are mostly sensitive to low-frequency waves and the highest air pressures occur at these inaudible frequencies (Bender, 2006). For this reason, in this research study, noise measurements were made with L scale and unit is expressed as decibel (dB).
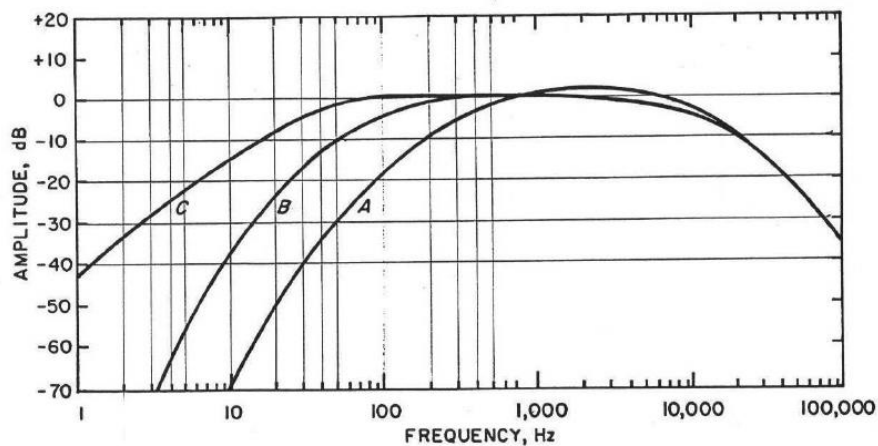
Figure 2.21 Standard sound measurement weighting scales (Bender, 2006).

Air blast has low frequency and medium-high frequency components, mostly it is below 2 Hz that is hard to be audible by humans (Siskind, 2000). However, in cases of inadequate stemming and no stemming (presplit blasting), sudden and high frequency (audible) air blast overpressure levels are generated (Bilgin et al., 2014). Sub-audible air blast (infrasound) may give rise to audible response of the structures (Richards, 2010). Turkish Regulations about allowable noise levels are proposed for sources of sound other than blasting (Bilgin et al., 2014). OSM suggested maximum allowable air blast levels for the given frequency limits as given in Table 2.7. Figure 2.22 shows air blast overpressure levels and their possible outcomes in terms of structural damage and human response. Complaints are likely to occur at 117 dB level, windows and dishes start to rattle. Annoyance and pain threshold level is 120 dB. No structural damage level is 140 dB, where US OSM suggested lower air blast levels 129 dB or 133 dB. At 150 dB poorly mounted windows can break. At 180 dB level hairline cracks at the plaster are observed.

Table 2.7 Allowable air blast levels for given frequency levels (Office of Surface Mining Reclamation and Enforcement, 1983)

Lower frequency limit of measuring system, Hz	Maximum air blast level, dB
0.1 Hz or lower -- flat response	134 peak
2 Hz or lower -- flat response	133 peak
6 Hz or lower -- flat response	129 peak

28

Decibels lb/in²

```
180 — 3          — Structures damaged
    — 1          — Most windows break                    Airblast
160 — 0.3                                                  from
    — 0.1        — Some windows break                   explosions
140 — 0.03       — "No damage" level
    — 0.01
120 — 0.003      — Threshold of pain
    — 0.001      — Threshold of complaints
                    (dishes and windows rattle)
100 — 0.0003     — Riveter
    — 0.0001
 80 — 3 ×10⁻⁵
 60 — 3 ×10⁻⁶    — Ordinary conversation
 40 — 3 × 10⁻⁷   — Hospital room
 20 — 3 × 10⁻⁸   — Whisper
  0 — 3 × 10⁻⁹   — Level of hearing
```
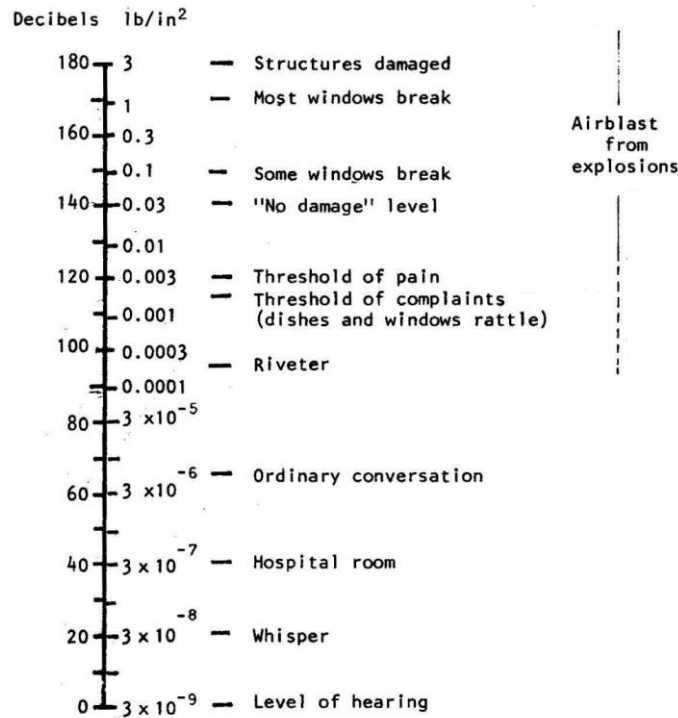
Figure 2.22 Human and structural response to sound pressure levels (Ladegaard-Pedersen & Dally, 1975)

2.8 Previous Studies

In this chapter previous studies are reviewed which are mainly about ground vibration and air shock prediction by using different statistical methods.

Hudaverdi (2012) conducted a multivariate analysis for the prediction of blast induced ground vibrations. In this respect an extensive blast database was created from the blasts that was performed in a sandstone quarry. Blast design parameters and ground vibration related parameters were considered to carry out multivariate analysis. Blast data were classified into different groups according to similarities, for that purpose cluster analysis was performed. Discriminant analysis was used to analyze group memberships. Then, regression analysis was performed to generate prediction equation for peak particle velocity for each group. Eventually, test blasts were performed in order to validate the suggested equations.

Dehghanin and Ataee-pour (2011) analyzed blast induced ground vibration by including rock strength and blast design making use of ANN (artificial neural network) and dimensional analysis. At first a 3 layer, feed forward back propogation neural network with 9 input parameters and 25 hidden neurons was modeled. 116 datasets were used to train the model and 17 datasets were used to check the performance of the ANN model to predict ground vibration. And then, a sensitivity analysis was conducted on the ANN model. Afterwards, dimensional analysis was performed on the results of the sensitivity analysis of the ANN model in order to develop a new formula. Results from the new formula were compared with the previous PPV predictor equations on the basis of correlation coefficient and root mean square error (RMSE).

Ak et al. (2009) in their studies presented the analyses of ground vibrations resulted from bench blasting in an open pit mine. The objective of the study was to estimate peak particle velocity and to determine the slope of the attenuation curve of the site. To this end, blast design parameters and ground vibration components of 43 blast datasets were used. The site constants were determined with regression analysis. After statistical analysis, a relationship between PPV and scaled distance was established with the USBM predictor equation. Maximum charge weight and scaled distance graphs for different structures were proposed to perform controlled blasts.

Alipour and Ashtiani (2011) predicted maximum charge per delay by means of conventional method (predictor equations) and ANFIS (Adaptive Neuro Fuzzy Inference System) method using admissable PPV and distance between blast site and monitoring point. ANFIS is a soft computing technique, which integrates the fuzzy logic into neural network. It analyzes the relation between input and output in order to determine optimum distribution of membership function. Input parameters were distance and PPV, and the output parameter was charge quantity per delay. The comparison between methods showed that, ANFIS model output gives better correlation with the measurements compared to other methods.

Mohamed (2011) analyzed the ground vibration and air shock using fuzzy logic, artificial neural network (ANN) and regression analysis by incorporating maximum charge per delay and the distance between blast and monitoring point as input parameters. Square root scaling distance was used to derive PPV prediction model and cube root scaling distance was used to derive dB prediction model. 136 datasets were used to train the model, and 26 datasets were used to validate the model. Performance of the models were assessed by using variance account for (VAF), root mean square error (RMSE) and coefficient of determination indices. These indices showed that fuzzy model has better prediction performance than ANN and regression analysis.

Singh and Singh (2005) in their studies predicted ground vibrations using ANN and multi variate regression analysis. Then, the results were compared to the measured field data. If high non-linearity is the case, statistical methods have some limitations. Finally, ANN was found more accurate.

Khandelwal and Singh (2006) concentrated on the prediction of frequency and amplitude of ground vibration with ANN and MVRA (multi variate regression analysis). In order to verify the ANN model, the results were compared with MVRA results. ANN model gave higher correlation coefficient than MVRA for predicted and measured values of PPV and frequency. The performance of the models were evaluated with the mean absolute percentage error (MAPE) and coefficient of correlation between the predicted and observed values. MAPE, correlation coefficient and number of predicted parameters showed that ANN is accurate for the prediction of PPV and its frequency. Consequently, ANN has the superiority over MVRA especially when variable number is too many.

Khandelwal and Singh (2007) concentrated on the estimation of blast induced ground vibrations at a magnesite mine. Blasting records were used to calculate amount of explosive to minimize ground vibrations. Charge mass and PPV parameters were recorded for 150 blast datasets. At first these datasets were used to predict site constants for widely used ground vibration predictor equations (USBM, Ambraseys–

Hendron, Langefors–Kihlstrom, Indian Standard Predictor equations). And then, another 20 blast datasets were utilized and analyzed with ground vibration predictors to estimate PPV. Calculated vibration levels from these predictors were compared with actual field data. The same datasets were also used for the prediction by ANN. All of the vibration predictors gave a very poor correlation between calculated and measured ground vibrations. However, ANN provided a high degree of correlation.

Khandelwal and Singh (2009) evaluated ground vibrations and frequency of ground vibrations using ANN by incorporating rock properties, blast design and explosive parameters and distance to monitoring point from the blast face as input parameters. Rock samples were used in order to determine poisson's ratio, blastability index, P-wave velocity and Young's modulus. Same datasets were used to predict PPV from commonly used vibration predictors and MVRA. Results were compared on the basis of coefficient of determination and mean absolute error (MAE) between monitored and predicted values of PPV and frequency. Prediction of ANN model was closer to measured data, whereas prediction from MVRA and predictor equations had wide variation.

Fişne et al. (2011) compared the performance of Fuzzy logic and classical regression analysis for the prediction of PPV. For that purpose VAF and RMSE performance indexes were used to assess the performance of the models.

Konya & Konya (2015) focused on the air overpressure in the near field. Major construction projects were analyzed in order to designate new air overpressure propagation equations for construction blasting. Then these new prediction equations were used to compare calculated results analyzed from field data with other existing air overpressure prediction equations. Production blasting and presplit blasting were studied separately in order to compare air overpressure levels.

Konya et al. (2000) pointed out proper stemming is crucial to make sure that gas confinement is conserved and intensity of the blasting is reduced. In this study, the

design criteria for stemming amounts were determined by trial and error. There are several approaches to define stemming depths; some operators use stemming depths equal to the burden distance, while others use 50%, 70%, 85% of the burden distance (Konya et al., 2000). Proper burden distance changes with rock type, harder rocks need smaller burdens and short stemming (Konya et al., 2000).

Burgher (2000) conducted small-scale test shots to determine when the meteorological conditions favour the air blast overpressure levels. For this purpose, 205 test shots were performed and the overpressure levels, meteorological and topographical data were collected. A site-specific empirical equation was developed with SPSS regression.

Kopp (2000) focused on two objectives. First objective of the study was to analyze the effect of orientation of the blasting on vibration levels. For this reason, four directions were taken into consideration and regression analysis was done for each direction. Then, one-way analysis of variance test conducted to designate the significance of blast parameter in the study. Second objective was to determine the effects of varying blasthole delay intervals on air blast and ground vibrations. Because, both the amplitude and the frequency of vibrations are important for preventing the damage. For this purpose, 52 production blasts were monitored at a surface coal mine.

Richards and Moore (2009b) established a real-time system in order to predict the effects of meteorology on air blast overpressure levels. Real time meteorological data and a predictive meteorological model were the inputs to an atmospheric refraction model that allows the interpretation of the effect of meteorological conditions on air blast overpressure levels. The model enables to decide the suitable times for blasting not to exceed the allowable air blast level.

Richards (2010) focused on elliptical air blast overpressure model in order to assess air blast levels surrounding the blast site. For this purpose, air blast levels were measured and predicted at one or more positions. This model yields decibel contour plans that can be superimposed on plans or air photos of the site. It was found that the

elliptical air blast overpressure model allows to determine air blast levels more accurately than cube root scaling methods. However, when delay sequence, topographic shielding or meteorological conditions have significant effect, their effect must be evaluated and added to the value from the elliptical air blast model.

Kima and Lee (2000) analyzed various ground vibrations caused by train loading, blasting, friction pile driving, and hydraulic hammer compaction by making use of 3D geophones inside the borehole and on the ground surface. Propagation and attenuation characteristics of these vibrations were investigated by examining source characteristics and geotechnical properties. With the purpose of geometric modeling of different types of vibrations, source types, and their induced waves were identified, and the geometric damping coefficients were determined.

Wu and Hao (2005) analyzed the simultaneous effect of ground shock and air blast overpressure on structural response and damage. Parametric numerical simulations of surface explosions were performed, moreover, time lag between ground shock and air blast overpressure was determined. Finally, empirical expressions of air blast-time history were derived as a function of charge weight, distance to structure, structure height, ground shock-time history spectral density function, envelope function and duration; which can be used in structural response analysis to surface explosions.

Alcudia and Stewart (2008) combined air blast and seismic data to reduce the air shock related noise from seismic records. The basic concept behind this method is the design of non-stationary filter in the time-frequency domain. A type of localized Fourier transform was developed by using Gabor transform in the time-frequency domain. A mask function was generated from Gabor spectrum by applying a threshold to Gabor coefficients. Then multiplying the geophone Gabor spectrum with the mask function cancels the air blast component in the seismic signal. As, the highest noise levels were from air blast, the method enabled the removal of air blast induced seismic signals.

Hongmian and Jing (2010) analyzed five different blast waves obtained from weapon air blast tests. In this study, digital filtering and wavelet denoising methods were used to remove vibration signals overlapping with shock wave signals. And, in order to search for the best fitting curve for time and pressure relationship, least square method was used.

Colombero et al. (2015) analyzed the attenuation of peak particle velocity with distance generated from drop load tests using finite element analysis. Velocity-time recordings attained at various distances from the drop load were compared to computed velocity-time histories. These computations were carried out by modelling the layered soil profile and simulating the drop load.

Casarotti et al. (2007) focused on seismic wave propagation with spectral element method in complex geological models by using CUBIT to form an advanced 3D unstructured hexahedral mesh. They provided tools to understand the effect of surface topography and subsurface structures on seismic phenomena.

CHAPTER 3

GEOLOGICAL SETTING OF THE STUDY AREA

3.1 Regional Geology

The Kışladağ deposit is situated in a mid- to late-tertiary volcanic complex in western Turkey, related to subduction along the Hellenic Trench (Juras et al., 2010). In the area, these volcanics erupted onto schist-gneiss basement at the northeast border of an uplifted terrain known as the Menderes Massif. The lithologies of the project area can be seen in Figure 3.1.
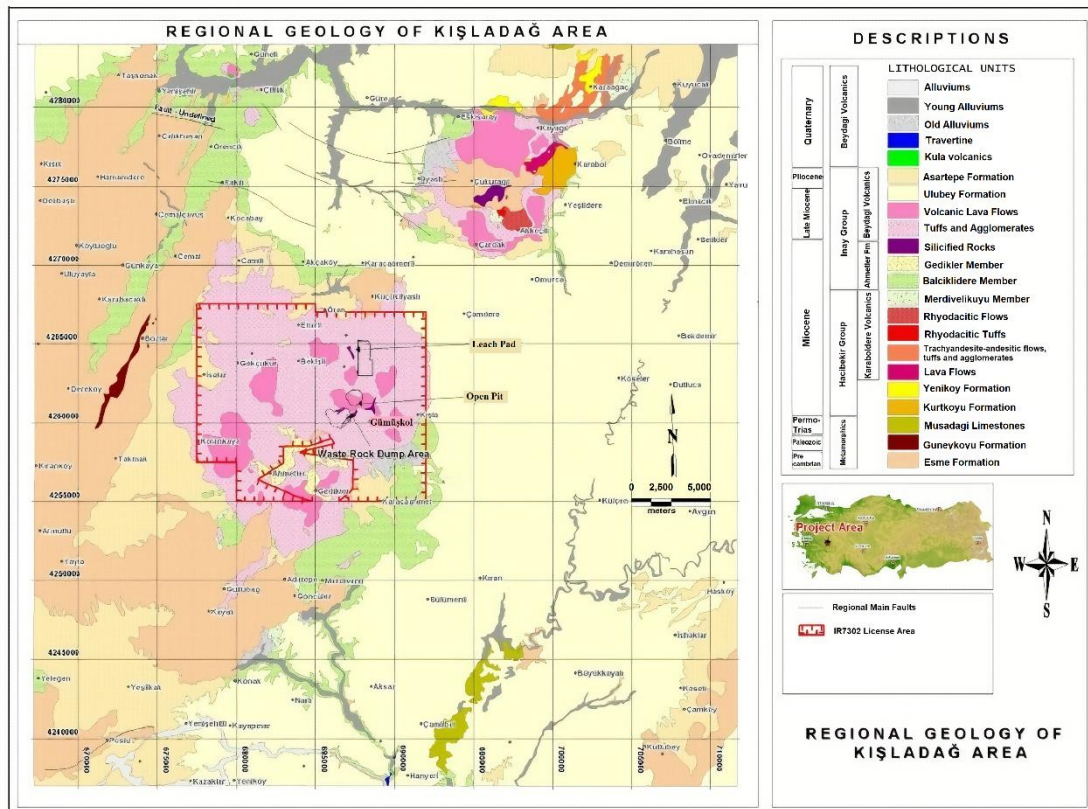
Figure 3.1 Kışladağ regional geology (Yazicigil et al., 2000)

The topography of the project area is composed of valleys with 900 m elevation and hills with 1100 m elevation above sea level. This topography is the result of erosion of

the plateau which is generated from metamorphic rocks at the bottom; the lacustrine limestones and volcanic rocks with lateral transitions at the top. Topographically higher sections are generally represented by volcanic rock formations.

The region includes, peneplain plains developed on metamorphic foundation in the west, plateaus of Neogene sedimentary rocks in horizontal position in the east and large volcanic cones in the middle among them. The volcanic plateaus are located in Eskisaray, Çardak and Karabol villages in the north east and in the vicinity of Akçaköy, Gümüşkol, Kışlaköy, Gedikler, Ahmetler and Kolankaya in the central part (Yazicigil et al., 2000).

The most significant feature of the local morphology, which is well preserved and easily detectable in satellite images, is the Kışladağ Volcanic Complex. This structure consists of two volcanic cones approximately in the direction of the Northeast-Southwest. Beydağı volcanic cone is located in the Southwest and Kışla volcanic cone is located in the Northeast. Dimensions of the volcanic complex are about 10 km to 9 km. When going out of the volcanic cone, the volcanic outcrops on the sides of the volcano are crossed with Neogene lacustrine limestones and shales.

3.1.1 Pre-Tertiary Rocks

The basic rock that forms the foundation of the project region is the northeast extension of Menderes Crystalline Massif which composes the main rock of Aegen region. Within the Menderes metamorphic complex there are three main formations (Ercan et al., 1978). These units are Güneyköyü Formation, Eşme Formation, and Musadağı Marbles.

3.1.1.1 Güneyköyü Formation

The unit consists of granitic gneisses and aplitic, quartz dykes crossing them (Ercan et al., 1978). It is accepted that granitic gneisses with lateral and vertical transitions with ocular gneiss constitute the core of Menderes Massif. The age of the Güneyköyü

formation is Paleozoic and/or Precambrian, and it has been outcropped around the Bozlar Village in the west of the project area.

3.1.1.2 Eşme Formation

Eşme formation outcrops at the West and Southeast parts of the project area (Ercan et al., 1978). The formation starts with ocular gneiss at the bottom and continues upwards with small crystalline gneisses, sericitic schists and finally calcschists and marbles. It is accepted that the schists overlie the granitic gneiss core. The age of the formation is mapped as Precambrian. Eşme formation is mainly seen in Eşme village and its West along with East of İlyaslı town and outcrops at far Southeast of Ulubey village.

3.1.1.3 Musadağı Marbles

Local outcrops of marble are seen along the Banaz Creek Valley in the South of Ulubey. They are formed of white light gray metamorphic dolomitic limestones. The marbles are with coarse crystals and contain black bands and diasporite lenses in places have more than 150 m thickness. Karstic structures and voids increase the storage properties of marbles and give them an aquifer property. The age of the marbles is considered Permian-Triassic (Ercan et al., 1978).

3.1.2   Tertiary Rocks

Tertiary Rocks include Hacıbekir and İnay Groups (Ercan et al., 1978).

3.1.2.1 Hacıbekir Group

Hacıbekir group includes Kürtköyü Formation, Yeniköy Formation and Karaboldere Volcanics.

3.1.2.1.1   KÜRTKÖYÜ FORMATION

Kürtköyü formation locally outcrops at the East of İlyaslı town and the North Yeşildere village. The formation consists of conglomerates and sandstones. The components of the conglomerates are poorly sized, semi-angular, and semi-round. The formation contains deposits of cone sediments formed in Early Miocene (Ercan et al., 1978).

3.1.2.1.2 YENIKÖY FORMATION

Local outcrops of Yeniköy Formation can be seen between Karaağaç - Eskisaray - Kayağıl villages in the north of the project area. It consists of multi-component conglomerate, sandstone, clayey and sandy limestone, and tuffite alternation. The unit is formed in the stream environment. Groundwater is not a problem due to both the formation of the clay component and the limited occurrence of the cliffs. The age of the formation is considered to be Miocene (Ercan et al., 1978).

3.1.2.1.3 KARABOLDERE VOLCANICS

It is composed of Rhyodacite, tephritic lavas, tuff, and agglomerates with trachyandesite character. The presence of volcanic rocks is partly acidic and partly basic is an indication of multi-stage formation (Ercan et al., 1978). It outcrops at Northwest of Karabol village, north and southeast of İlyaslı town, north of Akkeçili village and near Kayağıl village.

3.1.2.2 İnay Group

The main rocks forming the group are Ahmetler Formation, Beydağı Volcanics, and Ulubey Formation from oldest to youngest.

3.1.2.2.1 AHMETLER FORMATION

It is composed of three groups; Merdivenlikuyu member, Balçıklıdere member, and Gedikler members (Ercan et al., 1978).

3.1.2.2.1.1 Merdivenlikuyu member

The unit is composed of obscure bedded old slope debris, usually formed from angular blocks, derived from metamorphic basement rocks. The survey area has very small outcrops approximately with 60 m thickness. The age of the unit is assumed to be Upper Miocene. Outcrops have been exposed in between Merdivenli, Adatepe, Göncüler villages, and Southeast of Göncüler villages (Ercan et al., 1978).

3.1.2.2.1.2 Balçıklıdere member

It commonly outcrops at West and South of Güre and Southwest of İnay. It is also observed at Kumsüren and Deredamı river valleys. The member consists of alternating conglomerates, sandstones, marls, and limestones, which are usually deposited in the stream environment. The thickness of this member is less than 200 meters. The rock units are white, light gray, yellowish, bluish and greenish. It is usually layered horizontally or close to the horizontal. The coarse-grained units are at the bottom and the grain size diminishes upward. The tuff levels within the unit are products of Beydağı volcanics (Ercan et al., 1978).

3.1.2.2.1.3 Gedikler member

It outcops in the vicinity of Ahmetler and Gedikler. The unit, which is composed of alternating light yellow, light green, gray siltstone, claystone and tuffite, approximately 60 meters thick, conformably covers Balçıklıdere member. In places, 5-10 cm thick bituminous units and 2-3 cm thick gypsum bands alternates with fine grained clastic units. Lapilli and ash size Beydağı volcanics in the stack form tuffite levels. The volcano bombs and blocks inside the member are proof that the age of the unit is the same as Beydağı volcanics (Ercan et al., 1978).

3.1.2.2.2 Beydağı Volcanics

It is known that Miocene aged latite, latitic-andesite, and traki-andesitic composition contributes to lower levels of Ahmetler Formation and Ulubey Formation. Volcanic structure comes into prominence with two volcanic centers; Ahmetler village in the South and Kışladağ Hill in the North. Beydağı volcanics are composed of purple to pinkish lava flows and agglomerates and whitish-yellowish tuffs with altered silicified and calcified rocks of these units. It is very common in Uşak and in the central part of the study area (Ercan et al., 1978).

3.1.2.2.3 Ulubey Formation

It is the most common rock unit in the project area. It is exposed in large areas in Uşak, Ulubey, Inay, Sülümenli, Narlı and Güre and covers the Ahmetler Formation. It is

usually composed of lacustrine limestones. The formation starts with alternation of siltstone, claystone, marl and clayey limestone and continues with pinkish and grayish lacustrine limestones. There are thin sandstone and conglomerate levels in the limestones. The most beautiful faces of the Ulubey formation are seen in the canyon formed by the Yavu stream. Here, about 150 m thick limestone and clayey limestone and/or marl alternation can be observed continuously (Ercan et al., 1978).

The limestones are medium-thick bedded, very porous, irregular, cracked, karstic, and locally silicic. Lithological features and fossil content indicate that the formation precipitated in the lacustrine environment. Concretions in some places indicate a turbulent environment (Ercan et al., 1978).

3.1.3 Quaternary aged rocks

The Quaternary units include Asartepe Formation, Kula Volcanics, travertines, and sediment cone sediments.

3.1.3.1 Asartepe Formation

There are different crop outs belonging to Asartepe formation in the project area. The widest outcrops are located in the vicinity of Eşme. The formation covers the older rocks unconformably. It is horizontal or slightly inclined. It is composed of weak cemented red, brown, dirty yellow, dirty white, medium - thick bedded conglomerate, sandstone, siltstone alternation. It contains marl and claystone in places.

Grains of conglomerate are generally derived from metamorphic rocks. The grains are well rounded and semi-angular. The matrix of conglomerate is composed of sand, silt and clay sized granules.

Tile - colored sandstones and siltstones are usually thin - medium bedded and loosely cemented. Between the sandstone and siltstone layers there are white marls and carbonate-rich lenses in places. It is considered it was formed in the stream

environment of Asartepe Formation during Upper Pliocene - Lower Quaternary (Ercan et al., 1978).

3.1.3.2 Kula Volcanics

They represent the youngest volcanic activity of the region. It is made up of dark colored basalt lavas and tuffs. Basalt lavas are the first products of volcanic activity and tuffs are the last products. They are not very common in the field of investigation. They are exposed at a small area at the West-Northwest of Çiftlik Village (Ercan et al., 1978).

3.1.3.3 Travertines

They are associated with fault controlled thermal sources. The main rocks are gneisses and the volcanites are the heat source. It is not observed around the project site in a regional sense, only a small area was exposed near Hamam Village in the far South of the project area (Ercan et al., 1978).

3.1.3.4 Terrace Deposits (Old Alluvium)

They are formed by Gediz River and Banaz Stream. They are shown as old alluvials on the map (Figure 3.1) and comprised of loose cemented gravel, sand and silt. Their thickness is less than 40 meters. Despite the boundaries of the presented map, they are exposed in large areas around the Gediz River and the Banaz Creek, but they are exposed in small areas around the project site and near İlyaslı, İnay and Konak (Ercan et al., 1978).

3.1.3.5 Deposition Cone Deposits, Colloids and Alluviums

Depositional sediments are not very common. Alluviums formed in river beds and mapped as the newest alluvial unit which contains pebbles, sand, silt and clay (Ercan et al., 1978).

3.2 Kışladağ Gold Mine Geology

Kışladağ Gold Mine is formed buried in either the intrusive, extrusive and Pre-Cretaceous aged basement schists and gneisses of the Menderes Metamorphic

Complex or within the overlying volcanoclastic rocks of the eroded Eocene stratovolcano (Orhan, 2004). The volcanic rocks and intrusive rocks of Kışladağ extend to the outside of the mine boundaries and extend to Beydağı Volcanic Unit. As moving away from the volcanic centers, the Beydağı volcanic rocks pass partly to the clastic sedimentary rocks of the Ahmetler formation and Ulubey lacustrine limestones of the same age. Rocks belonging to Beydağı Volcanic Sequence are exposed at Gümüşkol Village, Micanlar Neighborhood, Katrancılar and Karapınar Neighborhood, which are located in the vicinity of the mine. Almost everywhere, except for the places where the rocks are exposed, there is at least 0.2-0.4 m of light brown soil. The depth of the soil reaches to 1.0-1.50 m in places, and it is rarely higher in the agricultural areas.

Most of the volcanic rocks of Beydağı Volcanic Unit are porphyritic and include phenocrystal plagioclase, K-feldspar, biotite, hornblende and occasionally quartz minerals. It is likely that it is in a narrow compositional range in the comagmatic environment, and petrological studies show that they have latite composition (Lewis Geoscience Services Inc., 2002). In previous studies these volcanics were determined to be andesitic and have latitic composition in the study area (Orhan, 2004).

To the north of the mine, massive, flow-banded latite flows with quartz rarely occur. It is found in discontinuous masses of several meters in thickness, successively stratified by clastic rocks. To the south of the mine (towards Gümüşkol Village) massive porphyritic latite flows of quartz show 10-20 m thickness in volcanoclastic rocks (Orhan, 2004).

To summarize, the main rock units are latitic, massive or flow banded, non-quartziferous or quartziferous flows, volcanic breccia, stratified tuffite and epiclastic rocks, volcanic conglomerates, fine-grained tuffs, lapilli tuffs or tuffy siltstone. The neighboring settlements are usually located on the Beydağı Volcanic Units (Orhan, 2004).

The rocks belonging to the Kışladağ Gold Mine area are composed of extrusive and intrusive rocks of Beydağı Volcanic Unit and stratovolcanics resulting from erosion of these rocks together with Menderes metamorphic rocks which are base rocks in the region. Miocene old intrusive rocks are composed of schist and gneiss and buried in the Paleozoic old rocks which are called the Menderes Massif. Although the rocks of the Menderes massif are basement rocks and covered with a very thick volcanic cover, they are exposed at the north of the project area in the form of windows and heads due to erosion (Kışladağ Altın Madeni, 2013).

Volcanic and intrusive rocks of Kışladağ are spreading out of the mine area. As moved away from the stack, the Beydağı volcanics show a transition to the lacustrine limestones and the clastic sedimentary rocks belonging to the Ulubey and Ahmetler Formations (Kışladağ Altın Madeni, 2013).

Several different volcanic activities in the area, as well as the overlap of volcanoclastics in different stacks, resulted in a very complicated volcanostratigraphic structure. Figure 3.2 shows mine site geology. Figure 3.3 and Figure 3.4 show the profiles of A-A' and B-B' cross sections through the deposit which are indicated in Figure 3.2. The volcanic stratigraphy of the region is a mixture of fine-grained crystalline tuffs, eruption and flow breccia and sub-volcanic intrusives. Six rock units are defined in the mine area. These units are stacked in the following order, from top to bottom (Lewis Geoscience Services Inc., 2002).

1) Breccia - Porphyritic, latitic clastics (PBb),

2) Porphyritic, Latitic lava flows (PBF),

3) Breccia, tuff, sandstone, claystone volcanoclastics (PBvc),

4) Porphyritic, Quartz-Latitic lava flows (PBq),

5) Porphyritic, Latitic intrusions (PBi),

6) Monolithologic volcanic conglomerates (PBcg).

Porphyritic, latitic intrusions (PBi) are divided into four sub-units (Juras et al., 2010) (see Figure 3.2).

1- Coarse size porphyritic primary intrusive rocks (PBi1) formed before the mineralization; this rock has undergone a hydrothermal alteration on a scale that occupies very dense and wide areas and at the same time has been exposed to a gold mineralization which is roughly uniformly distributed throughout the rock. The alteration from the initial potassic phase later influenced the initial potassic alteration of secondary and tertiary phases as quartz - tourmaline and very advanced argillic (clay) alteration.

2- Secondary intrusive rock (PBi2) with a medium-size but almost identical composition formed simultaneously with ore yield; this rock has undergone potassic alteration like the primary intrusive and quartz - tourmaline and argillic alteration in weakly graded and confined areas. The secondary intrusive rock itself was formed in two phases as PBi2 and PBi2A, and PBi2A is exposed to a stronger kaolinitic clay alteration and the gold grade is slightly lower than PBi2.

3-Tertiary intrusive rock (PBi3) with fine-medium grain size and same mineralogical composition after mineralization; unlike the first two intrusive rocks, this rock has undergone a weak alteration that is somewhat propylated and somewhat fresh. The rock has a distinctive alteration which can be distinguished macroscopically-naked eye.

4- Tourmaline matrix intrusive breccia (PBib); It is a structural element in the typical breccia character formed by angular, semi-rounded block and/or fine millimetric granular particles of after mineralization and pre-existing intrusive rocks.
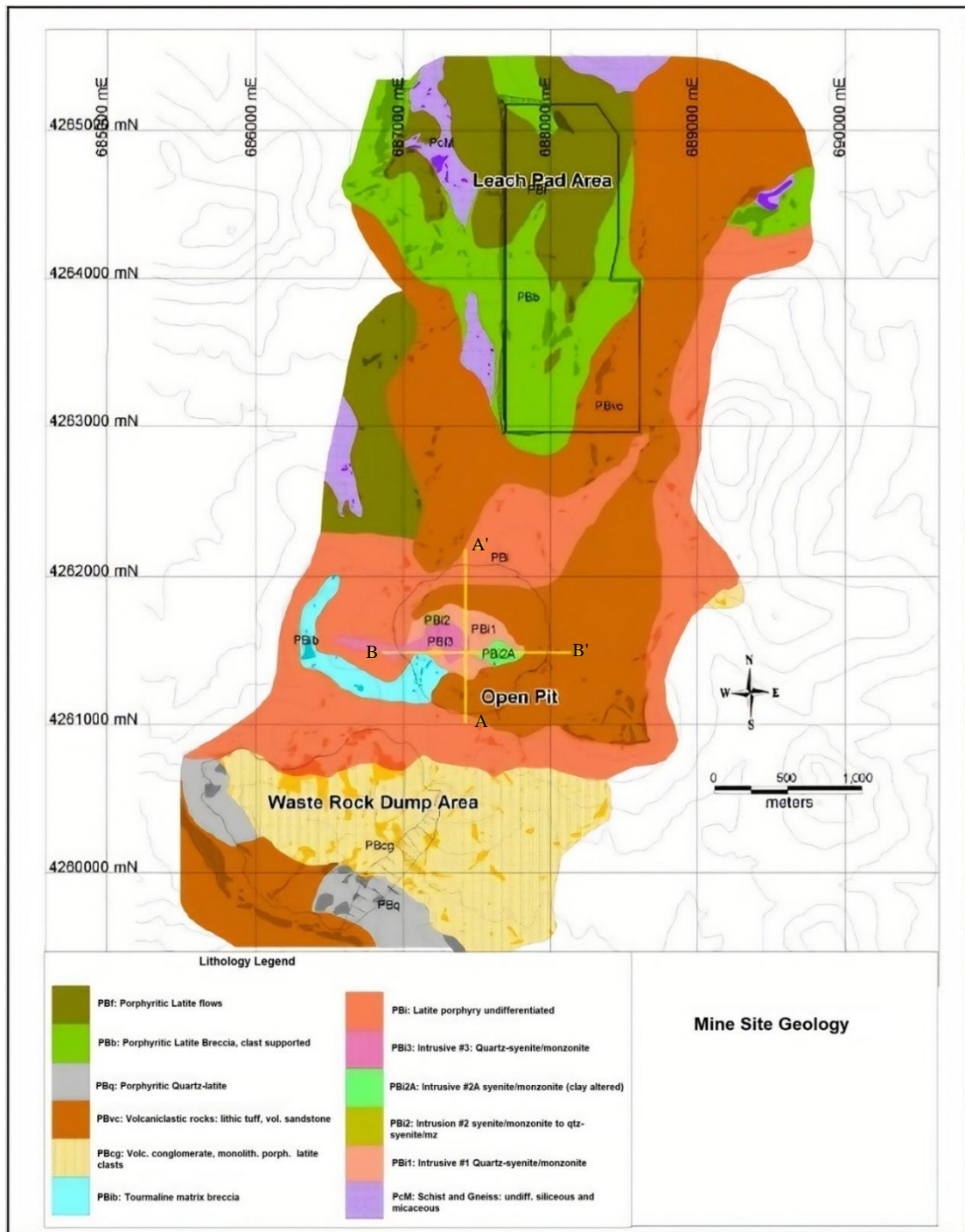
Figure 3.2 Mine site geology (Juras et al., 2010)
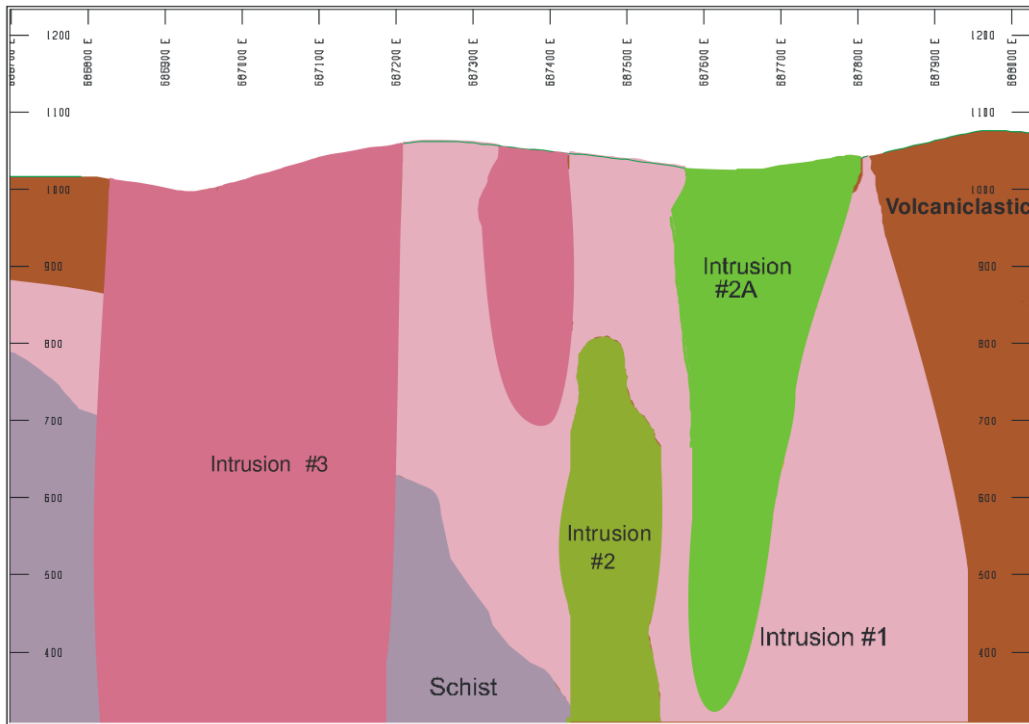
Figure 3.3 B-B' Cross-Section at 4261500N with Lithologies (looking north) (Juras et al., 2010)
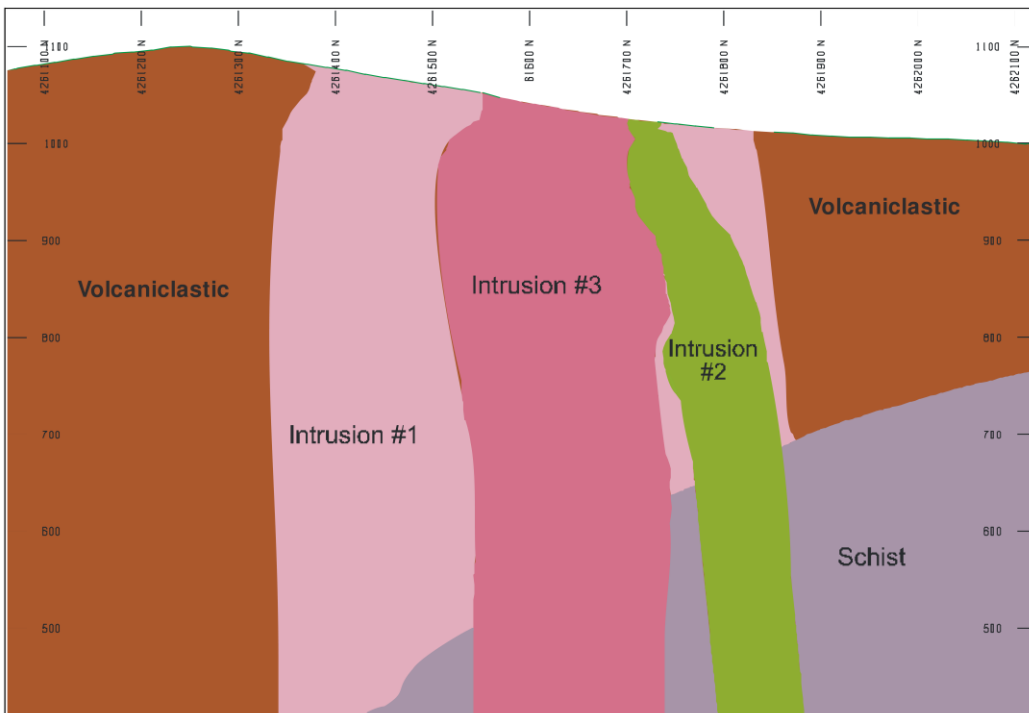
Figure 3.4 A-A' Cross-Section at 687300E, Looking West (Juras et al., 2010)

3.3   Structural Geology

The deposit lies within the core of a Miocene stratovolcano complex which has gone under slight structural alteration. Lithologic contacts in the region are basically intrusive or depositional and do not include any mappable fault offsets. The most prominent feature at the site is a northeast-striking sub-vertical fault at the east part of the deposit and concluded from the existence of silicified ridges on surfaces and distinct difference in gold grade and intrusive phases at that part of the deposit (Juras et al., 2010).

Variation related to this property can be detected from south of the deposit into the waste dump area. Bedding slopes are low to moderate. Mostly the strata replicate the probable shape of the actual stratovolcano which dips away from the deposit. Slopes do not show induced inclination on the contrary they display mainly the depositional dips (Juras et al., 2010).

The deposit and neighboring rocks involve many low-displacement brittle discontinuities, however, there are no major faults. Most of the detectable discontinuities are classified as joints (stationary sub-parallel fractures) and low-displacement faults (centimeters to decimeters range displacement magnitudes) and have continuity limited to a maximum of few tens of meters (Juras et al., 2010).

The most continuous faults apparent in the pit are steeply dipping sub-vertical East-West striking faults which are passing through a passage along the pit center. Intrusion 1 is parallel to these faults and dyke-shaped part of Intrusion 3 is situated across the western part of this fault corridor. All these characteristics jointly indicate that the deposit and intrusions are confined along the East-West fault zone, proof for which is widely destroyed by intrusions and related hydrothermal activity (Juras et al., 2010).

Various joint sets are pervasive in pit exposures and are distinguished by orientation data obtained from oriented drill core. Joints widely take place in orientation specific

clusters or structural passages, though they do not show radial or concentric orientation dispersions in the region. NNE striking joints steeply dipping towards West constitute the most ubiquitous set in the pit, which dominates the structural attribute of the Eastern third part of the pit (Juras et al., 2010). Figure 3.5 shows stereographic projection of mentioned discontinuities (faults and joint) within the pit cone.
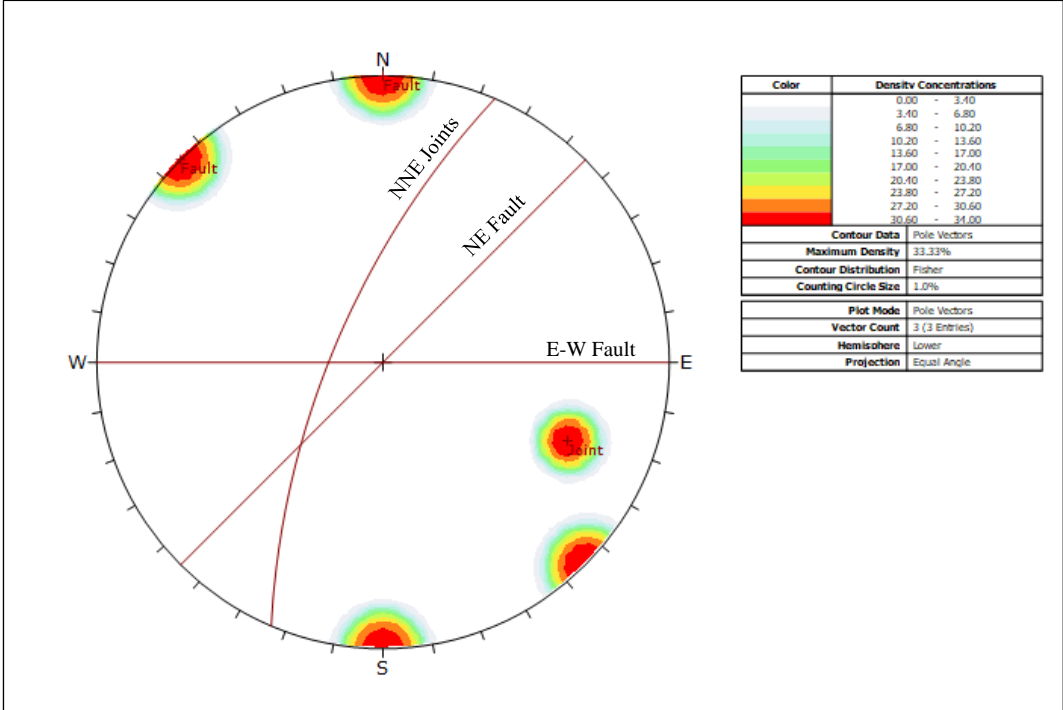
Figure 3.5 Discontinuity mapping of the pit cone (Rocscience Dips version 7)

3.4 Deposit Type

Juras et al. (2010) stated that; "The Kışladağ deposit consists of porphyry-style gold mineralization centered on a series of overlapping sub-volcanic intrusives of quartz-syenite to quartz-monzonite composition."

In the feasibility report prepared by HATCH (2003) it is indicated that; "A lesser amount of mineralization is hosted by subaerial volcanics, which surround and partially overlap the mineralized intrusives along their southern and eastern margins."

Geological consultant Richard Sillitoe concluded in his report that after his visit in 2000; "Kışladağ is confirmed to be a true porphyry gold deposit, albeit possessing several distinctive geological features. These include the paucity of quartz veinlets, the dominance of molybdenum over copper and the exceptionally high gold values. The deposit is centred on a steep, multiphase latite porphyry intrusion of alkaline affiliation. Younger intrusive phases were emplaced progressively nearer the centre of the stock and are characterized by increasingly weaker alteration of lower gold contents. The centrally positioned late-mineral phase is essentially barren."

CHAPTER 4

FIELD STUDIES AND DATA COLLECTION

On the basis of the inquiry made by Tüprag Metal Mining Company to assess the vibration and airblast levels in the surrounding settlements of the mine, investigations were carried out in Gümüşkol, Karapınar, and Katrancılar villages. The measurement stations are placed on four main cross sections towards the villages surrounding the mine (Figure 4.1). These monitoring paths are named as KP (Karapınar), KT (Katrancılar), and GK (Gümüşkol path 1 and path 2). Toward Gümüşkol, two paths were chosen in order to investigate the effect of topographical shielding along Gümüşkol Path 2. The coordinates of the monitoring stations are given in Appendix A and cross sections of monitoring paths are given in Appendix C.

All blasting operations in mine are conducted during daytime and usually more than one blasting, daily. A total number of 521 ground vibration records (from production blasts) and 180 air blast records (from presplit blasts) were obtained at the data collection stage. Table 4.1 shows the distribution of the collected data for each village. During monitoring stage of the investigation, the number of presplit blasts recorded in Karapınar, Katrancılar, Gümüşkol path 1 and Gümüşkol path 2 monitoring paths are 56, 58, 34, 32, respectively. In addition, the number of production blasts recorded are 147, 167, 127, 80 in the same order.

Table 4.1 Distribution of collected data

Cross-section Name	Presplit blast	Production blast
Gümüşkol Path 1	34	127
Gümüşkol Path 2	32	80
Karapınar	56	147
Katrancılar	58	167

The measurements were classified and analyzed in detail to provide a guidance for future blasts and to evaluate environmental impacts. Safe explosive amounts that can be blasted per delay were calculated from the propagation laws on four paths obtained with regression analyses.
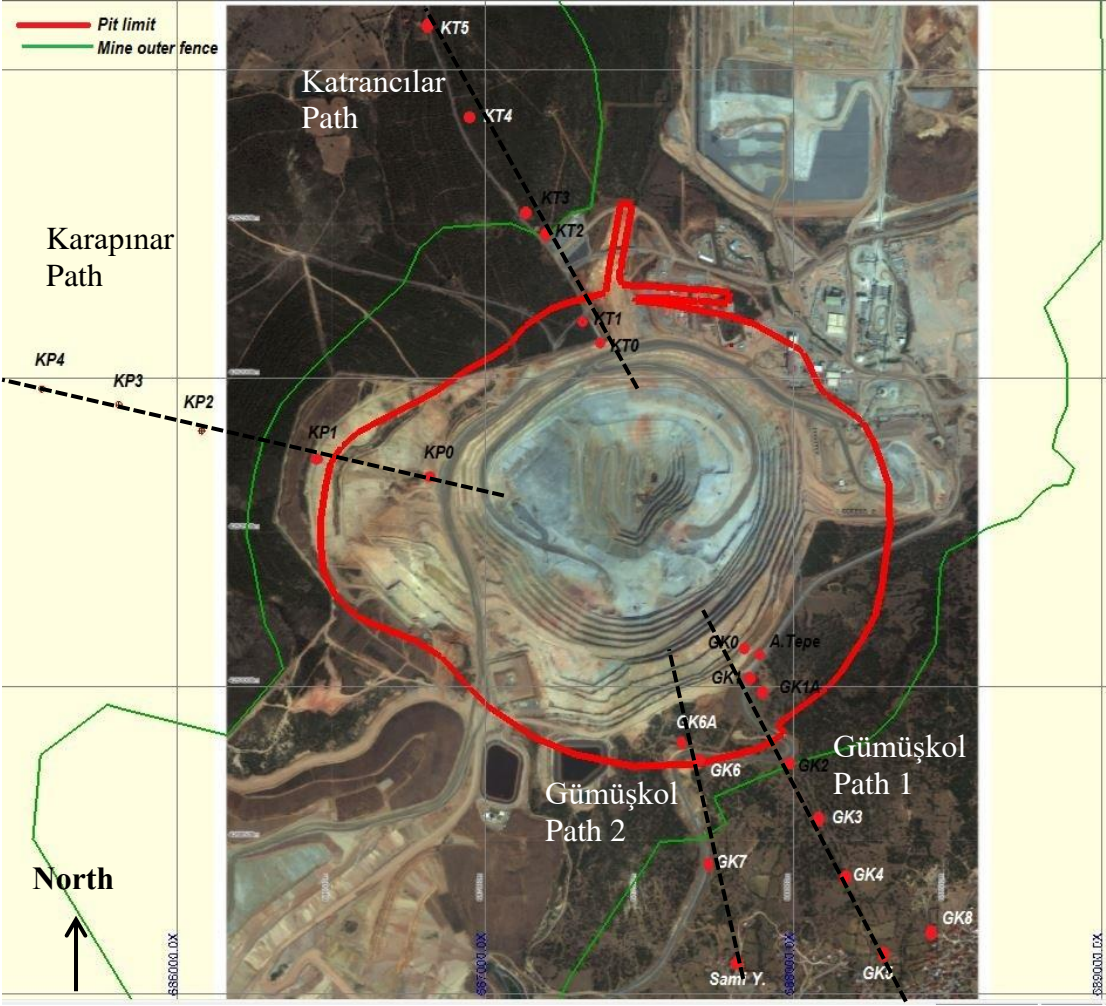
Figure 4.1 Monitoring paths and stations

The data collected from field studies are;

1) Air overpressure level

2) Ground vibration level

3) Maximum instantaneous charge

4) Distance between monitoring station and blasting location

5) Average air temperature

6) Wind speed and direction

Blast pattern and the coordinates of the blast holes for each operation were provided daily by the blasting team of the company.

4.1 Blasting Practices

In this study, production blasts and presplit blasts were investigated separately in terms of ground vibration and air shock because of their different loading and stemming characteristics. For presplit blasting, less amount of charge is loaded compared to production blasting and no stemming is carried out to get a clean break at the boundary of the blast holes. These specifications lead to low ground vibration and comparatively higher air blast levels. Whereas, in production blasting the case is the opposite, and thus lower air blast and higher ground vibration levels are measured.

Ground vibration analyses were conducted only on the data collected from production blasts. Whereas, air shock analyses were performed both for presplit and production blasts. When calculating maximum instantaneous charge for presplit and production blasts, great care has to be given. For presplit blasts the total amount of explosives should be used for scaled distance calculation because all the blast holes are detonated at the same time. Whereas, for production blasts the amount of explosive from blast holes detonated at the same time was calculated with JKSimBlast software. The distance between monitoring station and blasting is calculated from the nearest blast hole exploding at the same time.

4.1.1 Presplit Blasting

Presplit blasting is a method that is introducing a separating face between the rock to be blasted and stationary rock. That face optimizes the breakage effect of blasts and

prevents the propagation of stresses through the back wall and hinder over break (Berta, 1990).

All shots are fired simultaneously if possible. If this is not the case, micro delays are used. The general energy balance formula could not be applied to presplitting, since the energy transmission to the rock is different from that in production blasting (Berta, 1990). The reason is that no energy is consumed for rock breakage and displacement (Berta, 1990). Presplitting technique uses;
1) A row of very closely spaced holes, through the excavation perimeter
2) Decoupled charges (that means the explosive does not fill the borehole).

In order to increase slope stability and to create stable benches after blasting, presplit blasting is carried out before production blasting. Therefore, one can think presplit blasts create a faulty structure in the rock which results in lower ground vibrations from production blasts than the ground vibrations from production blasts without presplitting practice.

In Kışladağ Gold Mine, angled holes are drilled in a single row for presplitting operations. Generally, 30 holes are blasted at the same time and between each 30-hole group, 25 ms or 67 ms delay is used (Figure 4.2).
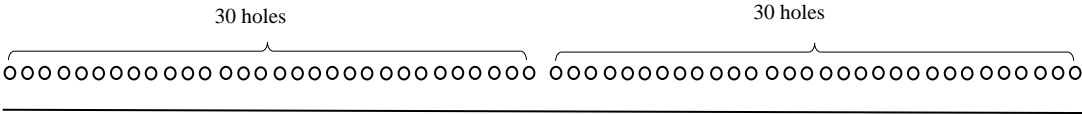
Figure 4.2 Presplitting hole pattern

Presplit blast holes are drilled with 95 mm diameter, 10 m depth and 1 m spacing. For presplit blast holes decoupled charging is satisfied by partially loading the blast holes. Decoupled charging with no stemming used for presplit blasts results in higher air blast levels compared to production blasts. These holes are loaded with detonating cord

(with 10 gr/m explosive) and dynamite cartridges (approximately 8 kg dynamite per hole).

4.1.2 Production Blasting

The pit is formed of regular benches with 10 m bench height. Usually 165 mm and rarely 152 mm diameter holes are drilled in a certain order for stripping blasts to remove the overburden covering the ore and for production blasts to obtain the ore. Burden x hole spacing are; 4.8 m x 6.2 m for stripping of overburden, 4.5 m x 5.2 m for production blasts of ore which is crushed before spreaded over leach pad and 3.6 m x 4.1 m for production blasts of ore which is directly spreaded over leach pad without crushing. Number of blast holes depends on panel dimensions, they are at least 40-50 and at most 300-320. For initiation of blast holes; non-electric millisecond (ms) delayed in-hole and surface capsules are used for stripping and production blasts. Whole in-hole capsules have 500 ms delay time. An example for delay firing pattern is given in Figure 4.3, delay periods between holes in the same row are 25 ms and 67 ms between the rows. The first hole in the second row explodes at 634th ms and the fourth hole in the first row detonates at 642nd ms.

With that technique a minimum of 8 ms delay is provided between blast holes and each hole is ensured to detonate at a different time. The main purpose of that practice is to control vibration by restricting the explosive amount blasted at the same time. There is no specific hole pattern for production blasting. Delay intervals within rows are 25 ms and between rows are 67 ms, generally. Lately, 109 ms delay intervals within rows and 67 ms between rows are started to be used to provide more efficient vibration control.

The main charge, ANFO with a density of 0.8 kg/dm^3, is used in dry holes, and emulsion type water resistant blasting agent with a density of 1.20 kg/dm^3 is used in wet holes. Hole depths are changing between 10.8 and 11.0 m. Charge height is 6.5-7.5 m for dry holes and 6.0-7.0 m for wet holes. Stemming length is 3.5-4.0 m. Linear

charge density (concentration) for blast holes are around 17.10 kg/m for ANFO and 25.65 kg/m for emulsion. Based on this information it can be said that 110-125 kg ANFO is used in dry holes and 154-180 kg emulsion is used in wet holes. For blast groups with large number of blast holes when the delay time between two holes less than or equal to 8 ms, 2 or 3 blast holes may detonate practically at the same time and the maximum instantaneous charge increases.
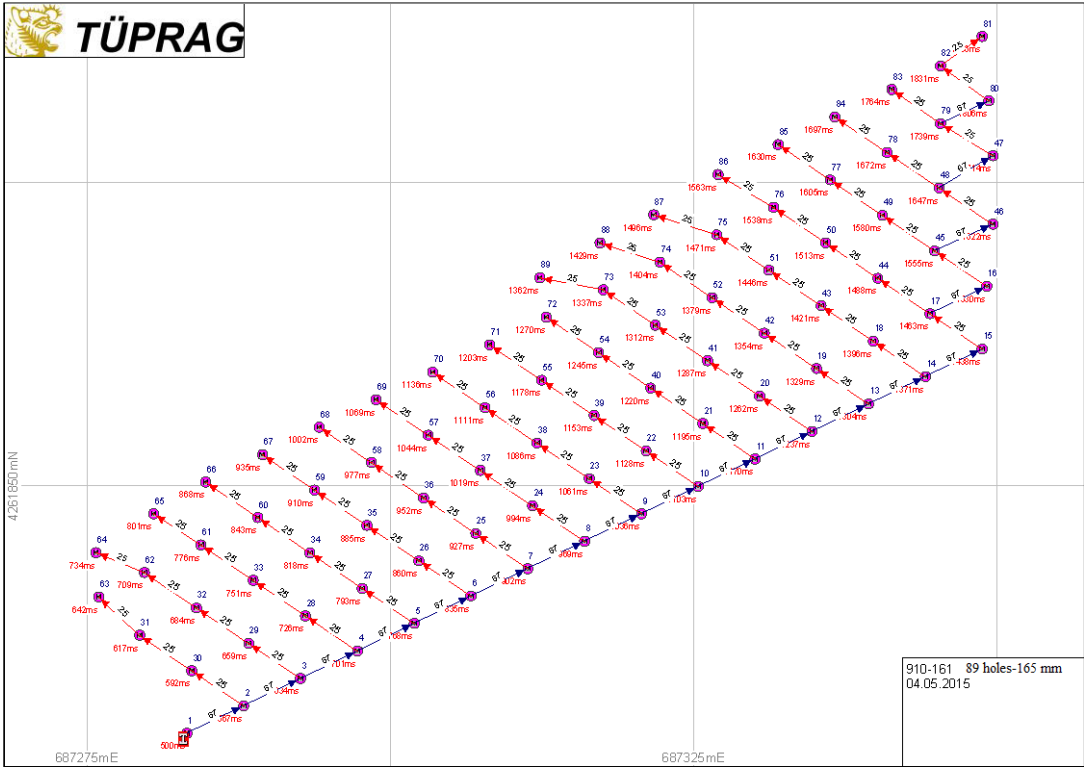
Figure 4.3 Initiation pattern using 25 ms in row and 67 ms inter row delay periods

4.2   Technical Features of Buildings

The damage possibility of the buildings resulting from ground vibrations and air shock depends on blasting characteristics as well as on the technical features of the buildings. In other words, depending on the technical specifications, the level of vibration and air shock that each building can tolerate without damage is different. For this reason, at the beginning of the research, the nearest settlements were visited, and the existing structures were investigated from the technical point of view. The settlement units

58

examined are Gümüşkol Village, Micanlar Quarter of this village and Karapınar and Katrancılar Villages.

Structures in the settlements are usually one or two-story buildings. The foundations and walls of the buildings are mostly made of rubble stone using mud mortar (Figure 4.4, Figure 4.5a). Dimension stones were used at the corners of some buildings (Figure 4.4, Figure 4.5a). Some of the structures are mixed and masonry structures since stone and brick were used simultaneously for construction. A close view of the rubble stone and mud mortar wall is given in Figure 4.5b. As is known, mud mortar has no tensile strength. In order to eliminate this drawback and to prevent damage due to foundation settlement or to strengthen the building against earthquake usually wooden beams are used at different levels of the wall. However wooden beams are rarely used at the wall of the buildings in investigated residential areas.

Figure 4.4 Mud mortared rubble stone building in Gümüşkol Village (Bilgin et al., 2015)

In single-story buildings, the wooden beam is used only above the walls for ceiling construction (Figure 4.4, Figure 4.5a). Since the majority of structures have walls with no tensile strength, this has to be taken into account in ground vibration analysis. As a result of the lack of beams on the walls, there were pre-existing damages (not

originating from explosions) in some buildings due to weak foundation, foundation settlement or water seepage into foundation.

In the residential areas, lime mortared brick walled, and/or reinforced concrete structures are seen in small numbers in comparison to mud-mortared rubble stone buildings (Figure 4.6). However, none of these buildings are engineered structures, they were constructed by local craftsmen. In Figure 4.7, there is a two story (ground + first floor) structure built with mud mortar rubble stone from Gümüşkol Village, Micanlar District. Probable reasons of damages of first floor walls might be inadequate strength in the foundation of the building, in the ground floor walls or water seepage into the foundation, deformation caused by stretching or bending of the first-floor wooden flooring.

Figure 4.5 a) Mud mortared building in Katrancılar village constructed in 1945, b) A close view of the rubble stone and mud mortar wall (Bilgin et al., 2015).

Figure 4.6 Various structure types: mud mortared rubble stone building on the right, lime mortared brick walls and reinforced concrete structures in the middle and on the left (Bilgin et al., 2015).

Figure 4.7 Two-story, mud mortared rubble stone building belonging to Sami Yıldırım (Bilgin et al., 2015)

In Figure 4.8, the house of Sami Yıldırım built with mud mortar-rubble stones and the first-floor wooden beams and wooden floors are shown. The wooden beam in the middle sits on the inner wall of the ground floor, which is made of mud mortar and rubble stone, and does not bend too much. However, the other two wooden beams, shown on sides, are above the doors and stretches too much, which causes vertical tension cracks above the door corners at the upper floor (given in Figure 4.9).

A similar situation is the vertical crack created on the ground floor outer wall window given in Figure 4.10. This crack is wider at the top, and it is narrowing and disappearing downwards. This proves that this crack occurs as a result of a tensile force acting along the wall plane and within the wall plane. A technical drawing describing the crack formation mechanism is given in Figure 4.11 on the right with MODEL NVTC-1 code (Audell, 1996). In Figure 4.11, thick black arrows indicate the vertical movement of the foundation, and the resulting tension created in the wall plane is shown by the two-way white arrow.

Figure 4.8 Mud-mortared walls and wooden beams in the basement of Sami Yıldırım's house (Bilgin et al., 2015)

Figure 4.9 Normal vertical tension cracks above the door corners in the first floor of Sami Yıldırım's house (Bilgin et al., 2015)

Figure 4.10 Normal vertical tension crack above the window in the basement of Sami Yıldırım's house (Bilgin et al., 2015)
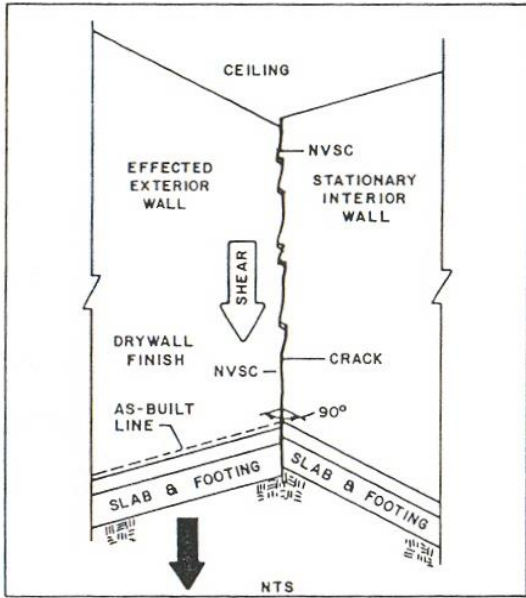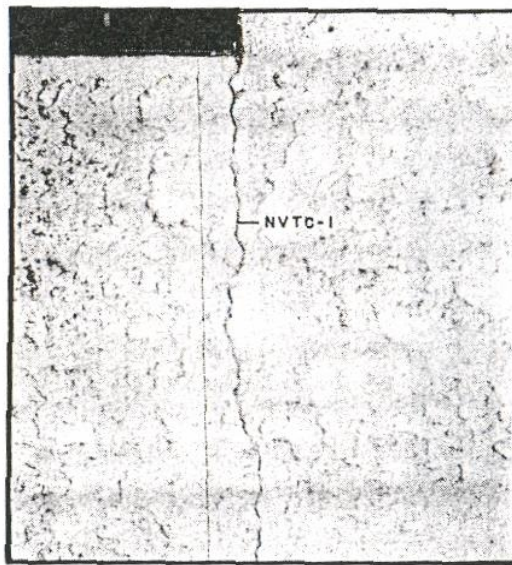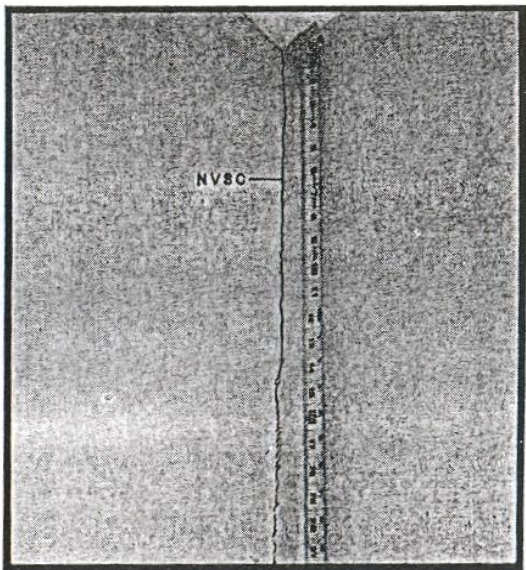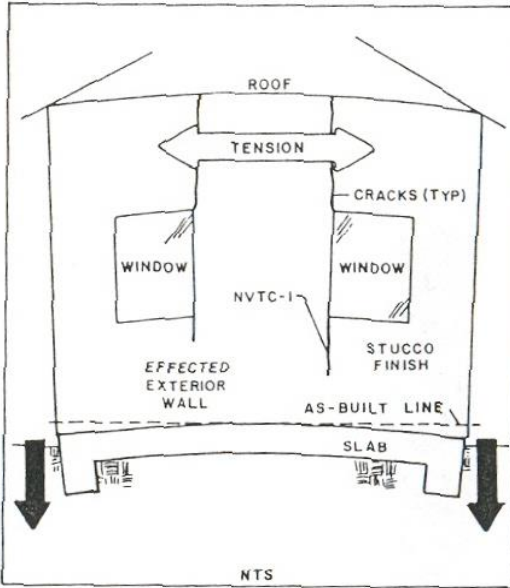
Figure 4.11 Crack forming mechanisms (normal vertical shear crack on the left and normal vertical tension crack on the right) (Audell, 1996)

Figure 4.12 and Figure 4.13 show vertical cracks at the joint of two walls resulting from the vertical differential movement of the walls. In Figure 4.12, wall on the right is inner partition wall and the wall on the left is the outer wall. At first glance, a non-

64

specialist may think that this vertical crack at the junction of the walls is the result of vibration. However, this is not the case, as evidenced by the vibration measurements provided and evaluated in Chapter 5.

Vibration levels measured at the ground of Sami Yıldırım's house proved that the highest PPV was 1.49 mm/s for 'in front of the pit' blasts and 1.206 mm/s for 'behind the pit' blasts, which are lower than the damage levels, and compatible with the Turkish Regulations. The crack at the wall corner stems from the fact that vertical shear movement of the inner partition wall, located on the right, sitting on the wooden floor (Figure 4.12) due to downward stretching of the wooden floor. A technical drawing describing this mechanism is given on the left-hand side of Figure 4.11 with MODEL NVSC code (Audell, 1996). Figure 4.12 shows the vertical shear force with thick arrow. As explained in detail above, it is well proven that the cracks in this house were not formed due to seismic effect. This is also confirmed by dirt and dust within the cracks (see Figure 4.13).
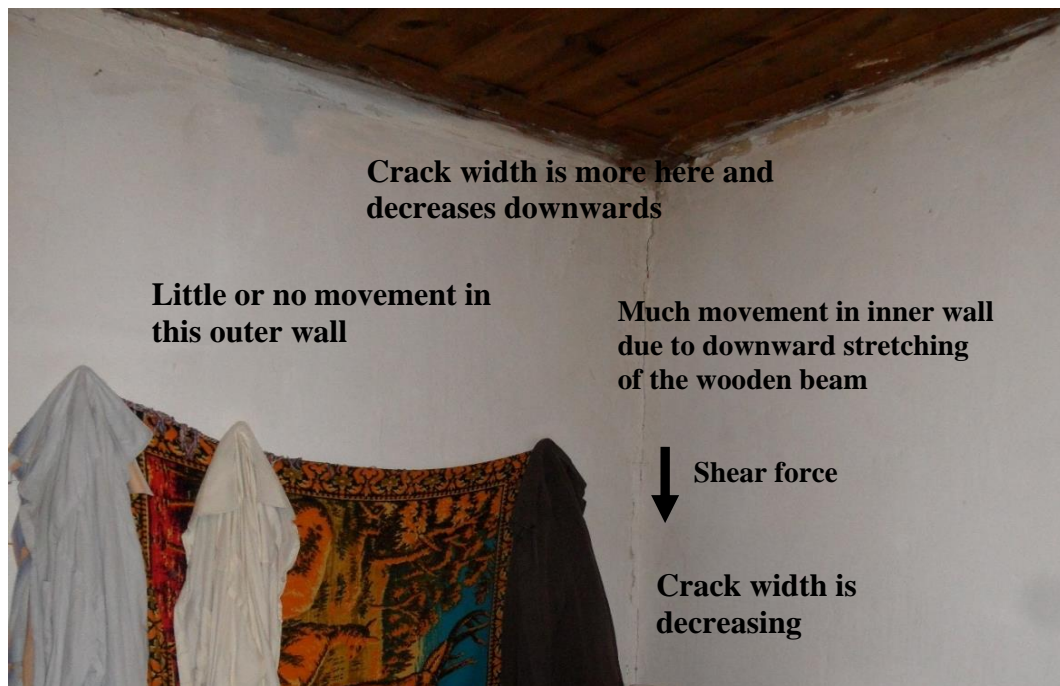
Figure 4.12 Normal vertical shear crack at the joint of inner wall and outer wall of first floor of Sami Yıldırım's house (Bilgin et al., 2015)
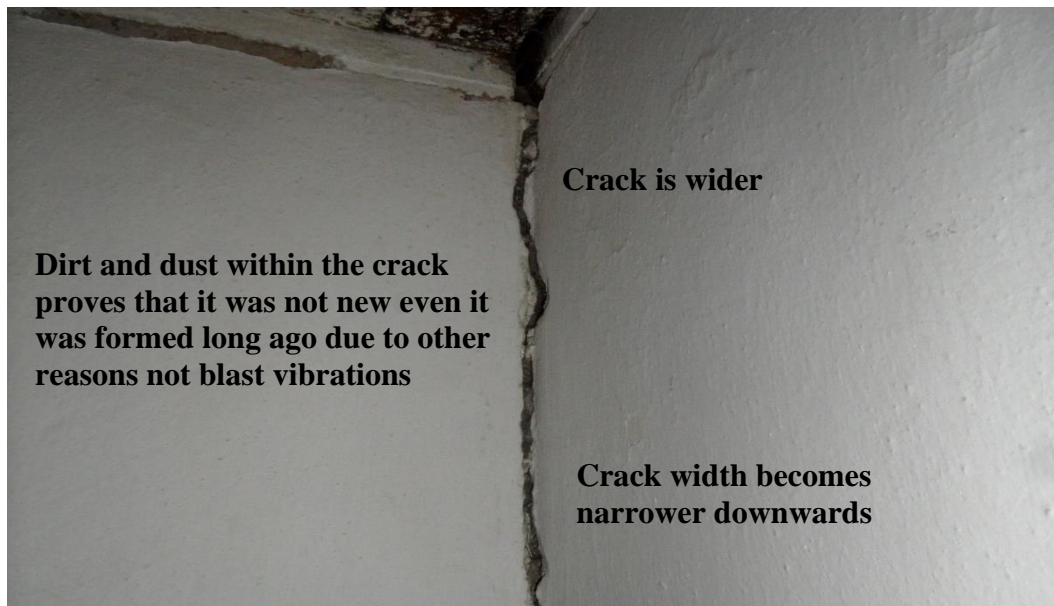
Figure 4.13 Normal vertical shear crack at the joint of inner and outer walls at the first floor of Sami Yıldırım's house (Bilgin et al., 2015)

4.3 Statistical Analysis of Collected Data

This chapter presents statistical analysis of data obtained during the field studies. In accordance with this purpose, analysis of wind speed and wind directions at the moment of blasting is presented for each path. Moreover, statistical analysis of air blast levels resulted from presplit blasting and peak particle velocity and air blast levels resulted from production blasting is given for each path, separately. But firstly, pie charts of the data are formed to gain an insight into the distribution of the collected data according to location and elevation of blast groups. Figure 4.14 shows the distribution of blast records with respect to location of blast group within the pit and elevation of blast groups for presplit blasts. Blast groups are located mostly at the southwest and south-southwest part of the pit and 66% of the presplit blasts are located at 910 m elevation. Figure 4.15 shows distribution of records with respect to location of blast group within the pit and elevation of blast groups for production blasts, respectively. Blast groups are located mostly at the southwest and south-southwest part of the pit and 41% of the production blasts are located at 920 m elevation.
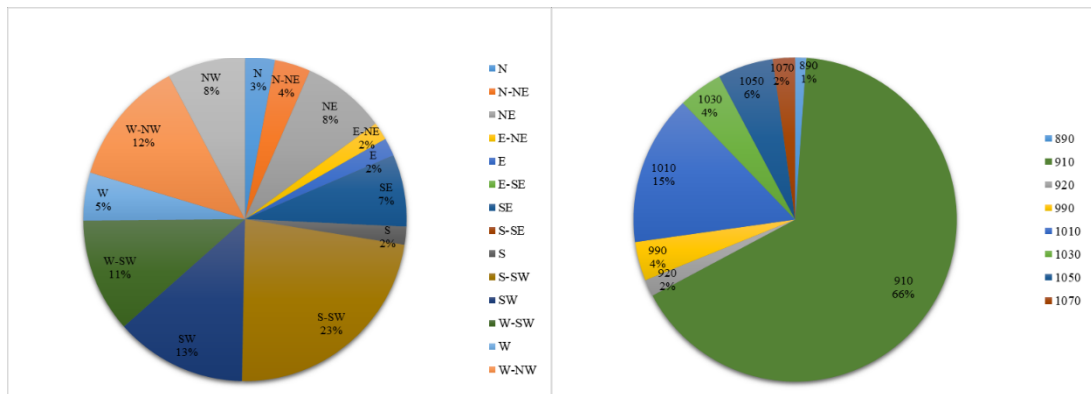
Figure 4.14 Distribution of presplit blasts with respect to location of blast group within the pit and elevation of blast group
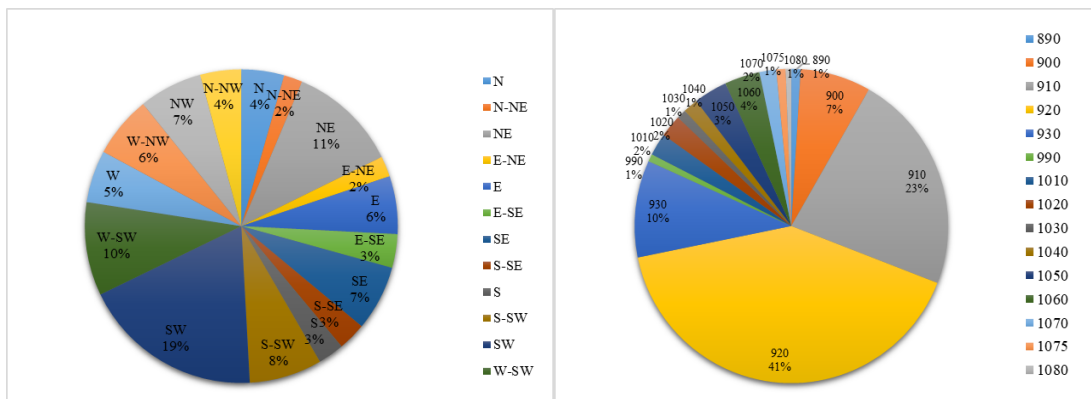
Figure 4.15 Distribution of production blasts with respect to location of blast group within the pit and elevation of blast group

Figure 4.16 and Figure 4.17 show boxplots of air blast levels from presplit blasts and production blasts respectively for each monitoring path. Figure 4.18 shows boxplots of PPV from production blasts for each cross section. Boxplots can be used to detect the outliers in air blast level and PPV data. Boxplots show the distribution of air blast levels from presplit blasts are skewed to left and distribution of PPV from production blasts are skewed to right. Star symbols may indicate possible outliers whereas sometimes it can represent heavily tailed distribution of data. General behavior of the data must be taken into consideration for outlier detection. The data from on-site meteorological station during the project span were used to obtain the wind rose of Kışladağ (Figure 4.19).
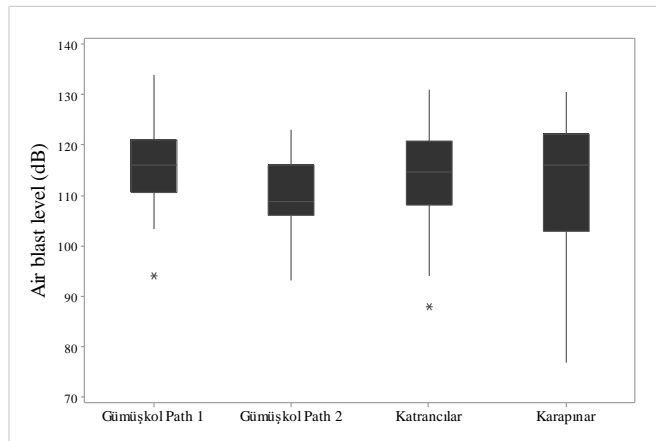
Figure 4.16 Boxplots of air blast levels from presplit blasts with respect to villages
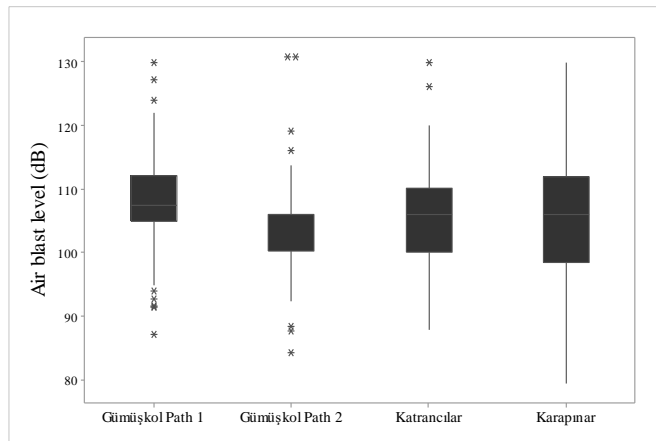
Figure 4.17 Boxplots of air blast levels from production blasts with respect to villages
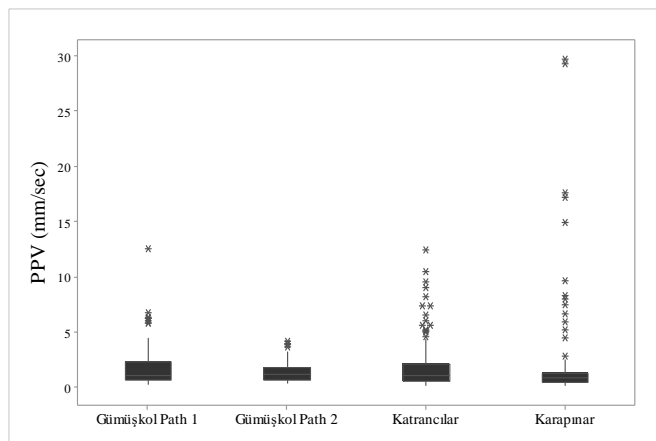
Figure 4.18 Boxplots of PPV from production blasts with respect to villages
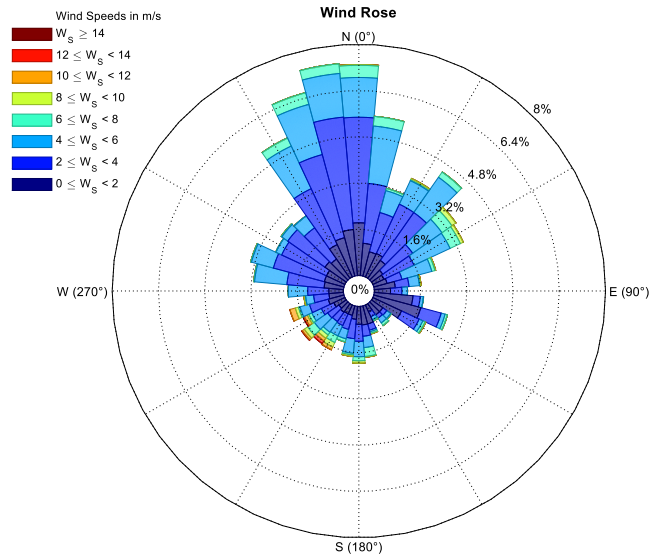
Figure 4.19 Wind rose for Kışladağ between April-July

4.3.1 Katrancılar Data Analysis

Figure 4.20 and Figure 4.21 show the distribution of wind direction and wind speed at the time of blast, while monitoring is along Katrancılar. Northern winds were the most frequently observed wind direction in the field, 54% of all wind directions. Wind speeds were generally in the range of 1.5-5.5 m/s, which constitutes 77% of all winds. Lowest and highest wind speeds were 1.02 m/s and 7.35 m/s, respectively.
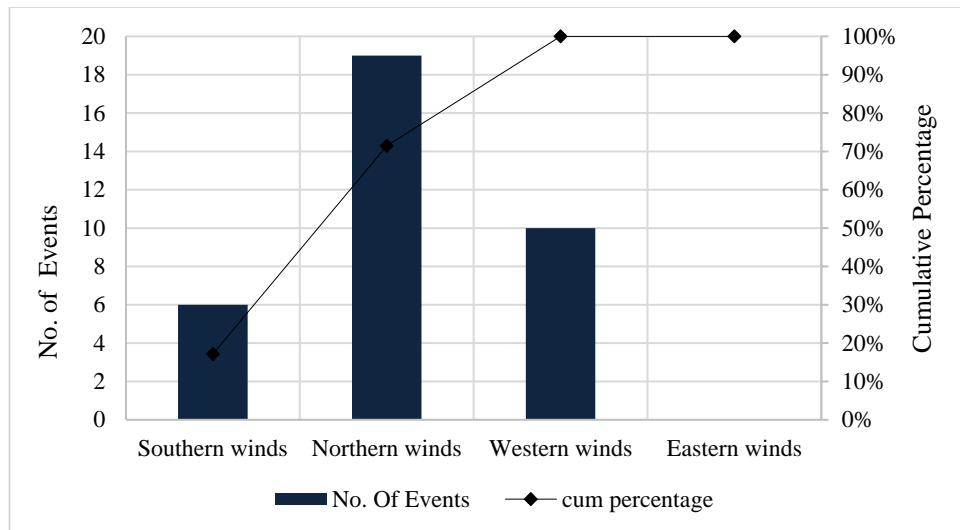
Figure 4.20 Frequency distribution of wind directions at the moment of blasting for Katrancılar

58 presplit blasting air blast data were collected along Katrancılar path, mean of the air blast levels is 114.20 dB. Figure 4.22 shows frequency distribution of air blast levels from presplit blasting. The air blast level between 109.00 dB and 115.00 dB has the highest frequency. Noise level between 88.00 dB and 99.00 dB was observed only three times. Noise level between 104.00-126.00 dB are the most common. This is attributed to the close distance between the village and the monitoring stations.
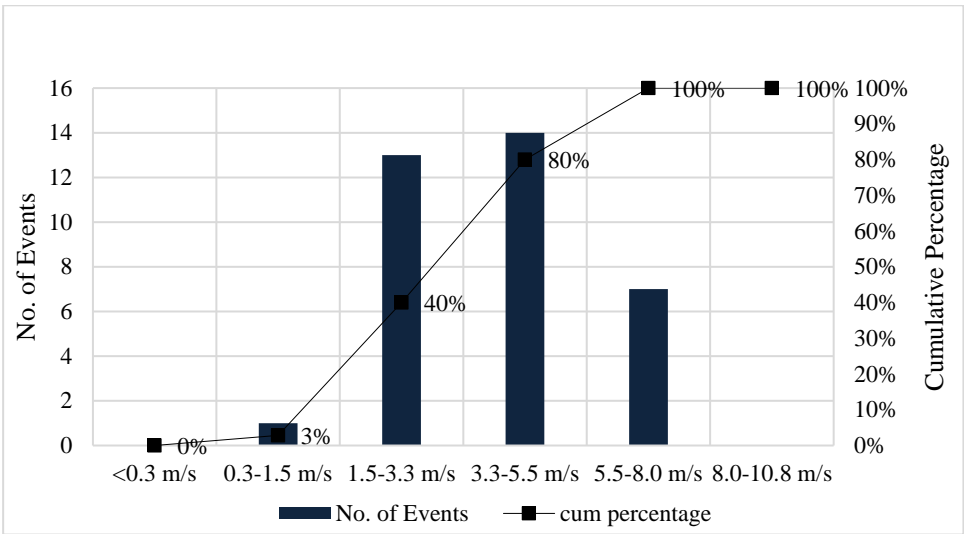
Figure 4.21 Frequency distribution of wind speeds at the moment of monitoring for Katrancılar
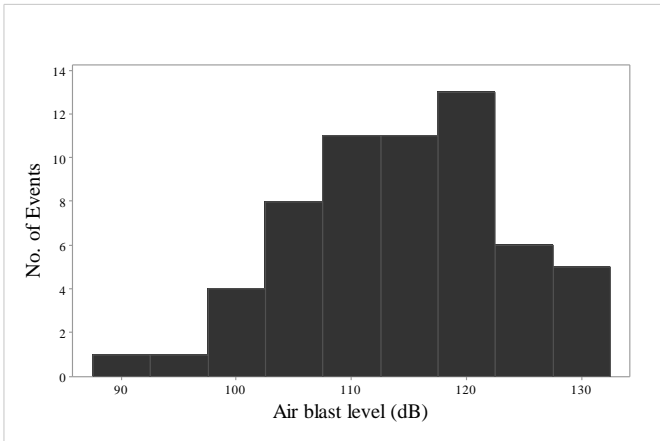
Figure 4.22 Katrancılar presplit blasting air blast histogram

Measured highest air blast level was 130.90 dB (with 5.63 Hz frequency) which was recorded at KT1 station (close to pit). For this blasting maximum instantaneous charge (MIC) is 170.00 kg, distance is 238.20 m and cube root scaled distance 43.00 m/$\sqrt[3]{kg}$. Lowest air blast level was 88.00 dB (with 2.75 Hz frequency) which was recorded at KT4 station (close to village). For this blasting MIC is 180.00 kg, distance is 1900.00 m and cube root scaled distance 336.51 m/$\sqrt[3]{kg}$.

167 ground vibration data from production blasting were collected along Katrancılar path, mean of the peak particle velocity (PPV) is 1.82 mm/s. Figure 4.23 shows frequency distribution of PPV from production blasts. Great majority of PPVs were in the range of 0.10-1.70 mm/s. Ground vibrations stronger than 6.30 mm/s were rare and measured at the closest monitoring stations to the pit.

The lowest and highest PPV levels were 0.14 mm/s (with 4.88 and 13.75 Hz frequency) (KT3 station) and 12.40 mm/s (with 16.75 Hz frequency) (KT0 station, closest to the pit), respectively. Lowest PPV was measured when MIC 357.00 kg, distance 1293.03 m and square root scaled distance 68.43 m/$\sqrt{kg}$. Highest PPV measured when MIC 394.00 kg, distance 189.00 m and square root scaled distance 9.52 m/$\sqrt{kg}$.
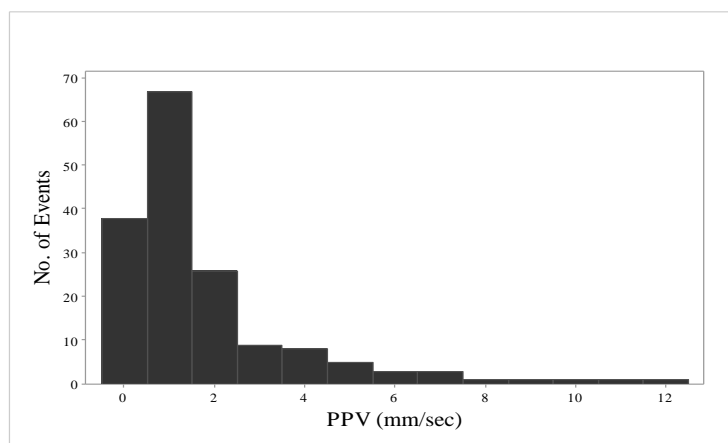
Figure 4.23 Katrancılar production blasting PPV histogram

71

123 air blast records from production blasts were collected along Katrancılar path, mean of the air blast levels is 104.90 dB. Figure 4.24 shows frequency distribution of air blast levels from production blasting. The air blast levels between 104.00 dB and 109.00 dB occupy the great majority.

Measured highest air blast level was 129.90 dB (with 8.31 Hz frequency) which was recorded at KT0 station. For this blasting MIC is 506.00 kg, distance is 635.00 m and cube root scaled distance 79.69 m/$\sqrt[3]{}$kg. Lowest air blast level was 87.90 dB (with 3.69 Hz frequency) which was recorded at KT5 station, the farthest station to the mine. For this blasting MIC is 213.00 kg, distance is 1852.60 m and cube root scaled distance 310.21 m/$\sqrt[3]{}$kg.
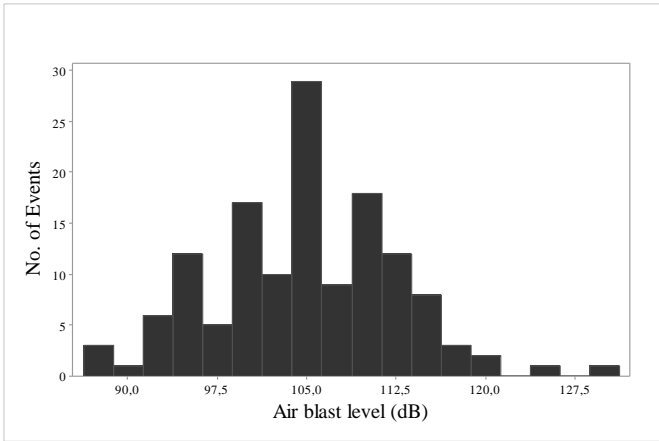
Figure 4.24 Katrancılar production blasting air blast histogram

4.3.2   Karapınar Data Analysis

Figure 4.25 and Figure 4.26 show the distribution of wind direction and wind speed at the time of blast, while monitoring is along Karapınar. Northern winds were the most frequently observed wind direction in the field, 50% of all wind directions. Wind speeds were generally in the range of 1.50-5.50 m/s, which constitutes 62% of all winds. Lowest and highest wind speeds were 0.79 m/s and 10.02 m/s, respectively.

56 production blasting air blast data were collected along Karapınar path, mean of the air blast levels is 112.80 dB. Figure 4.27 shows the frequency distribution of air blast

levels from presplit blasts. The air blast level between 115.00-123.00 dB has the highest frequency, and 100.00-107.00 dB range follows it. 77.00-92.00 dB was observed only two times.

Measured highest air blast level was 130.40 dB (with 9.81 Hz frequency) which was recorded at KP0 station (closest to the pit). For this blasting MIC is 240.00 kg, distance is 193.40 m and cube root scaled distance 31.12 m/$\sqrt[3]{}$kg. Lowest air blast level was 76.90 dB (with 4.25 Hz frequency) which was recorded at KP3 station, the farthest station to the mine. For this blasting MIC is 210.00 kg, distance is 1630.00 m and cube root scaled distance 274.23 m/$\sqrt[3]{}$kg.
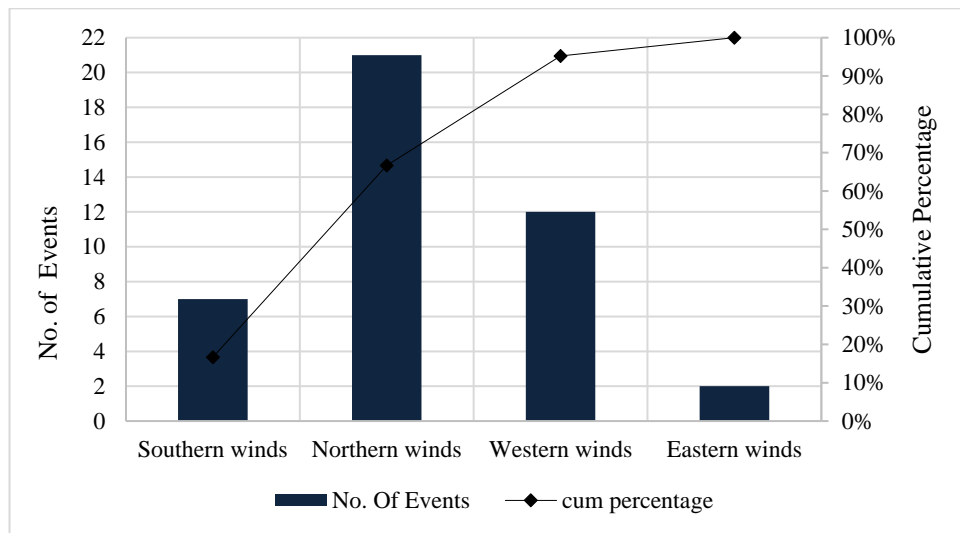
Figure 4.25 Frequency distribution of wind directions at the moment of blasting for Karapınar
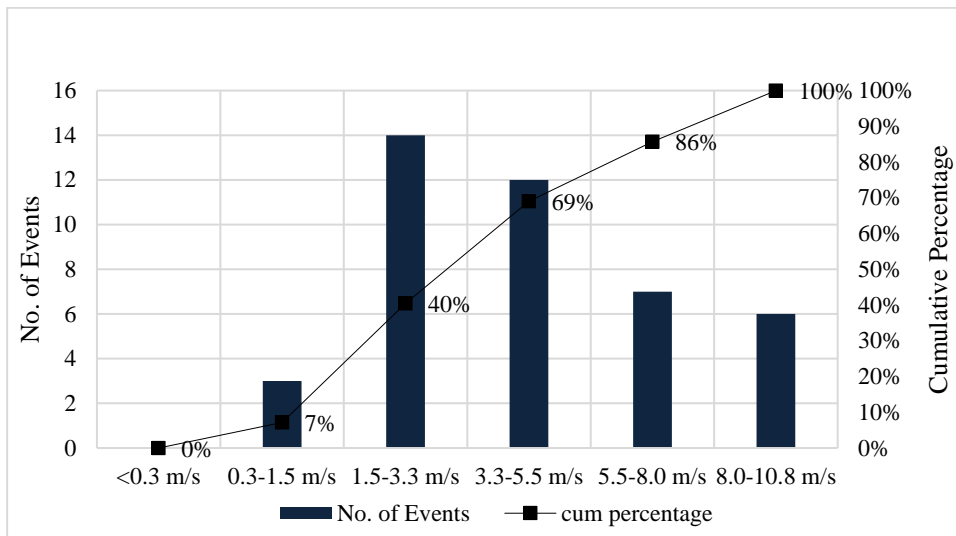
Figure 4.26 Frequency distribution of wind speeds at the moment of monitoring for Karapınar
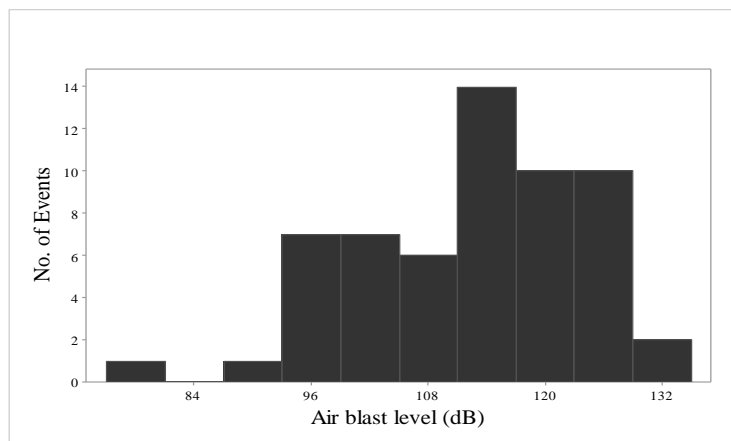
Figure 4.27 Karapınar presplit blasting air blast histogram

147 ground vibration records from production blasting were collected along Karapınar path, mean of the PPV is 1.91 mm/s. Figure 4.28 shows the frequency distribution of PPVs from production blasts. Generally, ground vibrations in the range of 0.10-1.40 mm/s were observed at the field. Ground vibrations stronger than 2.70 mm/s were unusual and recorded at the monitoring stations close to the pit, rather than the settlement.
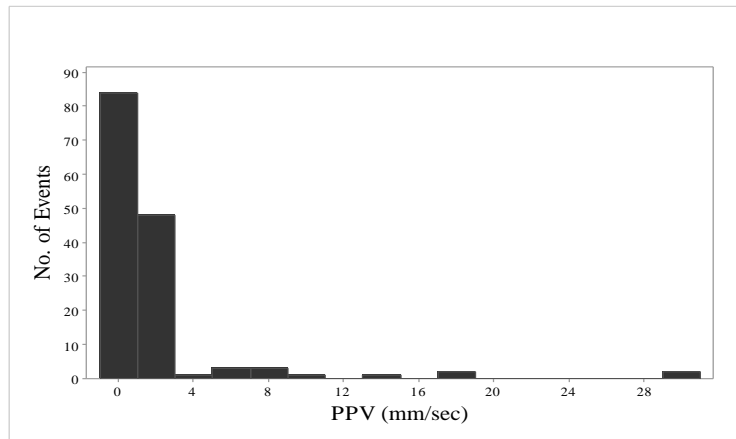
Figure 4.28 Karapınar production blasting PPV histogram

The lowest and highest PPV levels were 0.13 mm/s (with 12.63 Hz frequency) (KP3 station) and 29.70 mm/s (with 25.75 Hz frequency) (KP0 station), respectively. Lowest PPV was measured when MIC 343.00 kg, distance 1843.00 m and square root scaled distance 99.51 m/$\sqrt{}$kg. Highest PPV measured when MIC 506.00 kg, distance 225.00 m and square root scaled distance 10.00 m/$\sqrt{}$kg.

124 air blast records from production blasts were collected along Karapınar path, mean of the air blast levels is 105.80 dB. Figure 4.29 shows the frequency distribution of air blast levels from production blasting. The air blast level between 93.00 dB and 107.00 dB has the highest frequency. Air blast levels ranging between 107.00-114.00 dB has the second highest frequency.

Measured highest air blast level was 130.00 dB (with 11.50 Hz frequency) which was recorded at KP0 station. For this blasting MIC is 506.00 kg, distance is 225.00 m and cube root scaled distance 28.24 m/$\sqrt[3]{}$kg. Lowest air blast level was 79.40 dB (with 8.38 Hz frequency) which was recorded at KP4 station, the farthest station to the mine. For this blasting MIC is 363.00 kg, distance is 1900.00 m and cube root scaled distance 266.35 m/$\sqrt[3]{}$kg.

75
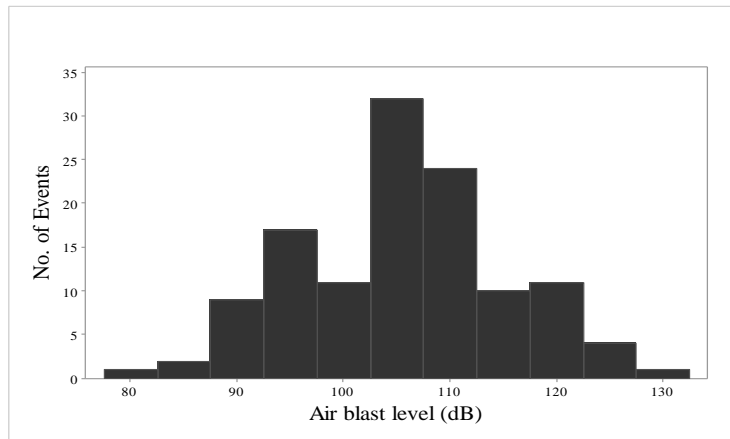
Figure 4.29 Karapınar production blasting air blast histogram

4.3.3 Gümüşkol Village Path 1 Data Analysis

Figure 4.30 and Figure 4.31 show the distribution of wind direction and wind speed at the time of blast, while monitoring is along Gümüşkol path 1. Northern winds were the most frequently observed wind direction in the field, 50% of all wind directions. Wind speeds were generally in the range of 1.50-5.50 m/s, which constitutes 68% of winds. Lowest and highest wind speeds were 0.79 m/s and 10.02 m/s, respectively.
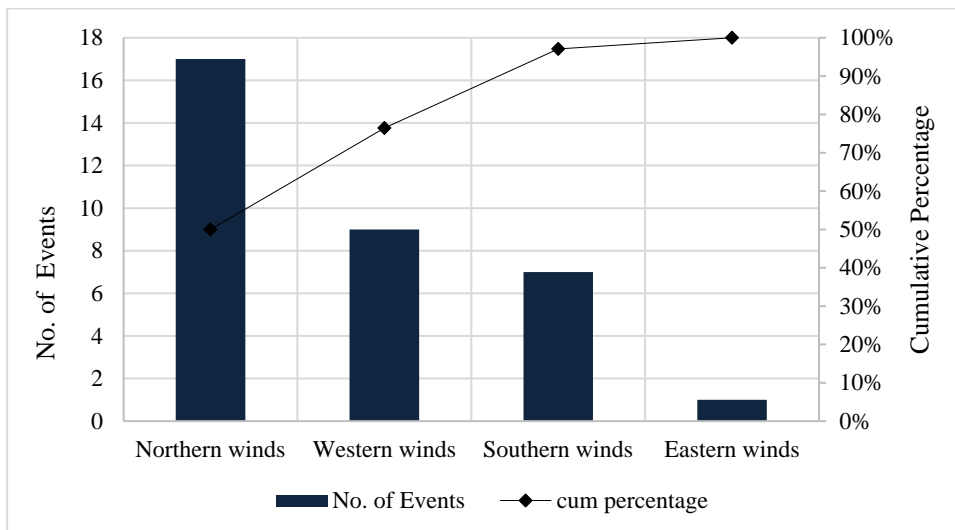
Figure 4.30 Frequency distribution of wind directions at the moment of blasting for Gümüşkol path 1
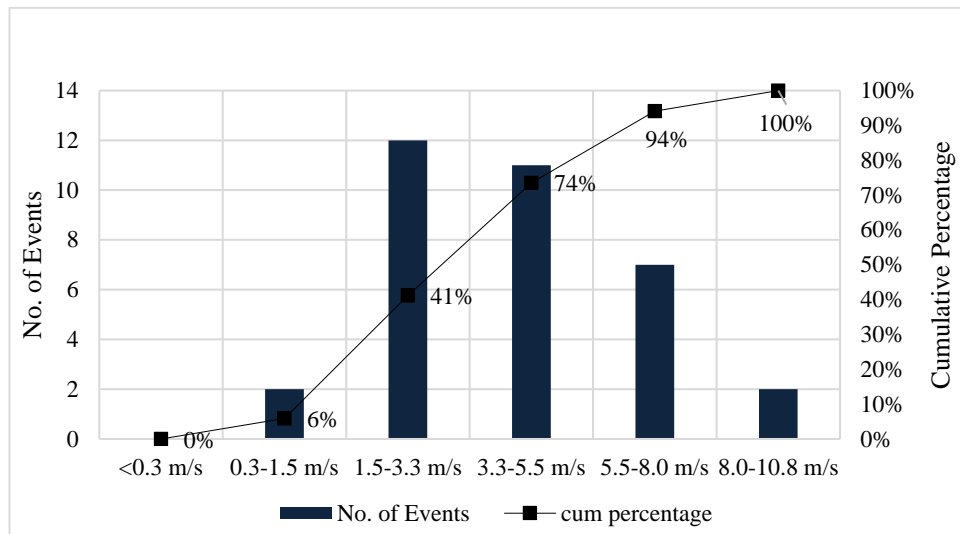
Figure 4.31 Frequency distribution of wind speeds at the moment of monitoring for Gümüşkol path 1

34 air blast records from presplit blasts were collected through Gümüşkol Path 1, mean of the air blast levels is 115.70 dB. Figure 4.32 shows the frequency distribution of air blast levels from presplit blasting. The air blast level between 109.00 dB and 124.00 dB has the highest frequency, constitutes 65% of all measurements. Measured highest air blast level was 134.00 dB. For this blasting MIC is 160.00 kg, distance is 1019.00 m and cube root scaled distance 187.70 m/$\sqrt[3]{}$kg. Noise levels between 124.00 dB and 134.00 dB are 16% of the collected data and noise levels over 129.00 dB are only 7% of the data, which are recorded at the nearest station to the mine. Lowest air blast level was 94.05 dB which was recorded at GK5 station, the farthest station to the mine. For this blasting MIC is 200.00 kg, distance is 1944.10 m and cube root scaled distance 332.44 m/$\sqrt[3]{}$kg.

127 ground vibration records from production blasting were collected through Gümüşkol Path 1, mean of the PPV is 1.72 mm/s. Figure 4.33 shows the frequency distribution of peak particle velocity from production blasts. Generally, ground vibrations in the range of 0.10-1.80 mm/s were observed at the field which is 67% of all events. Ground vibrations stronger than 5.00 mm/s were rare (5%) and recorded at the monitoring stations close to the pit which are away from residential area.
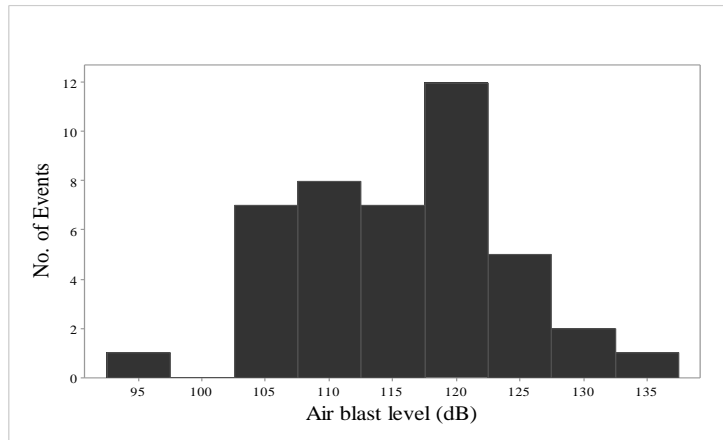
Figure 4.32 Gümüşkol Path 1 presplit blasting air blast histogram

The lowest and highest PPV levels were 0.21 mm/s (GK2 station) and 12.57 mm/s (Araptepe station), respectively. Lowest PPV was measured when MIC 310.19 kg, distance 1308.81 m and square root scaled distance 74.31 m/√kg. Highest PPV measured when MIC 363.00 kg, distance 297.00 m and square root scaled distance 15.59 m/√kg.
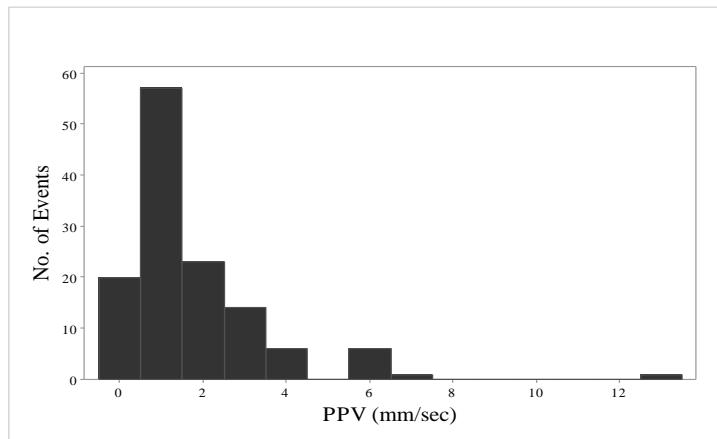
Figure 4.33 Gümüşkol Path 1 production blasting PPV histogram
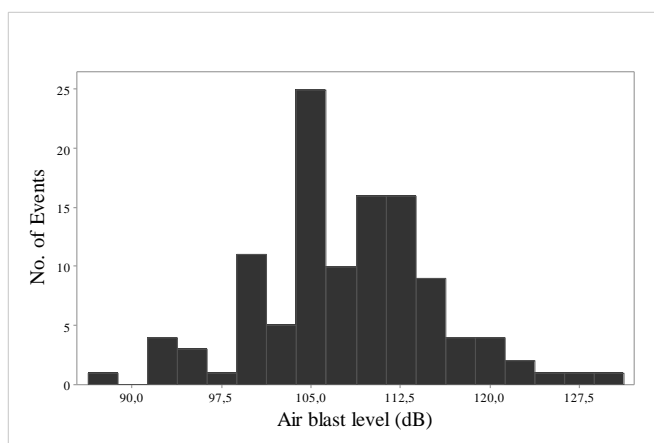
Figure 4.34 Gümüşkol Path 1 production blasting air blast histogram

102 air blast records from production blasts were collected along Gümüşkol Path 1, mean of the air blast levels is 108.20 dB. Figure 4.34 shows the frequency distribution of air blast levels from production blasting. The air blast level between 102.00 dB and 112.00 dB has the highest frequency, 49% of all data. The lowest and highest air blast levels were 87.00 dB and 130.00 dB, respectively. Air blast levels equal to and higher than 120.00 dB constitutes 8% whereas air blast levels over 129.00 dB constitutes 1% of the data. Lowest air blast level was recorded at GK5 station, the farthest station to the mine. For this blasting MIC is 514.70 kg, distance is 1645.50 m and cube root scaled distance 205.33 m/$\sqrt[3]{}$kg. For the highest air blast level MIC is 506.00 kg, distance is 930.00 m and cube root scaled distance 116.71 m/$\sqrt[3]{}$kg.

4.3.4 Gümüşkol Village Path 2 Data Analysis

Figure 4.35 and Figure 4.36 show the distribution of wind direction and wind speed at the time of blast, while monitoring is along Gümüşkol path 2. Northern winds were the most frequently observed wind direction in the field, 58% of all wind directions. Wind speeds were generally in the range of 3.30-5.50 m/s, which constitutes 46% of all winds. Lowest and highest wind speeds were 0.79 m/s and 10.02 m/s, respectively.

32 air blast data from presplit blasts were collected through Gümüşkol Path 2, mean of the air blast levels is 110.10 dB. Figure 4.37 shows frequency distribution for air

blast levels from presplit blasting. The air blast level between 106.00 dB and 110.00 dB has the highest frequency with 29%.
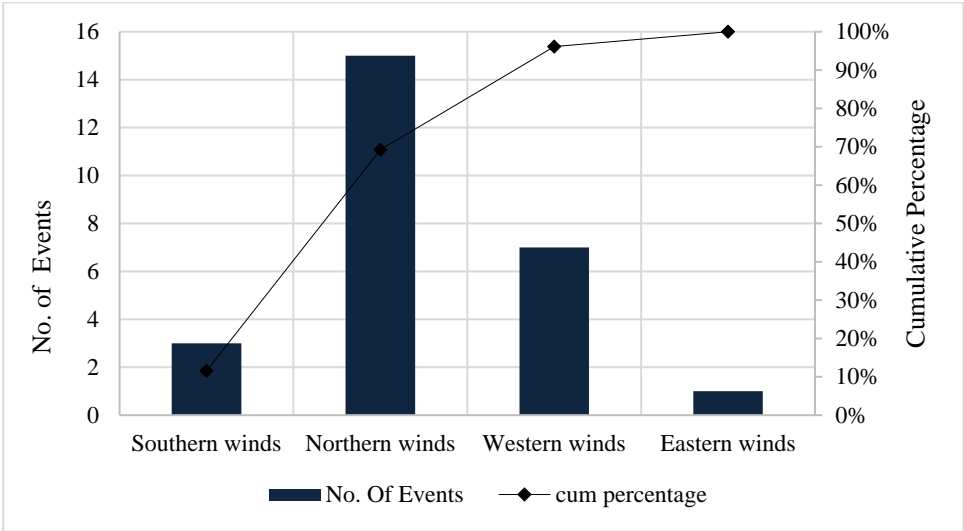
Figure 4.35 Frequency distribution of wind directions at the moment of blasting for Gümüşkol path 2
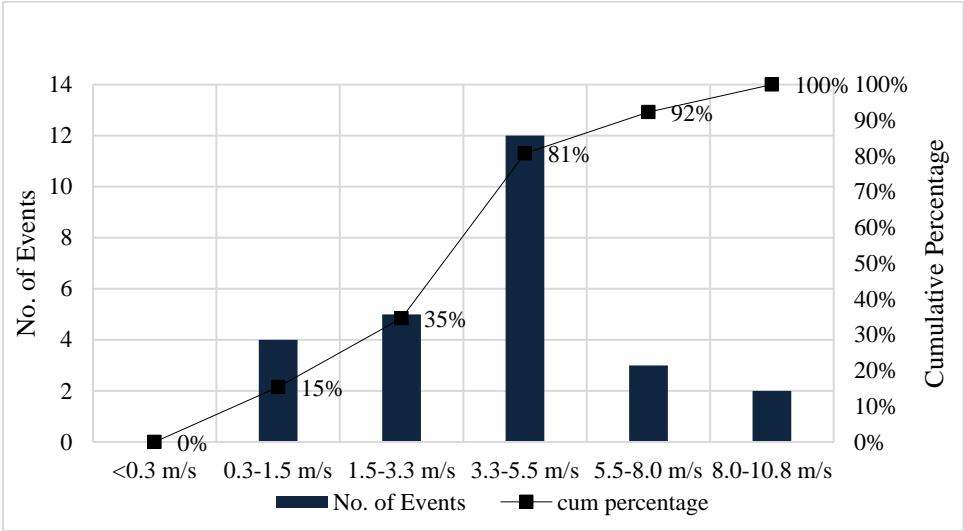
Figure 4.36 Frequency distribution of wind directions at the moment of blasting for Gümüşkol path 2

Measured highest air blast level was 123.00 dB (with 9.38 Hz frequency) at GK6 station. For this blasting MIC is 260.00 kg, distance is 1242.00 m and cube root scaled distance 194.59 m/$\sqrt[3]{}$kg. Lowest air blast level was 93.10 dB (with 4.63 Hz frequency)

which was recorded at the nearest house to the mine in that path, also the farthest station to the mine. For this blasting MIC is 120.00 kg, distance is 1631.00 m and cube root scaled distance 330.67 m/$\sqrt[3]{}$kg.
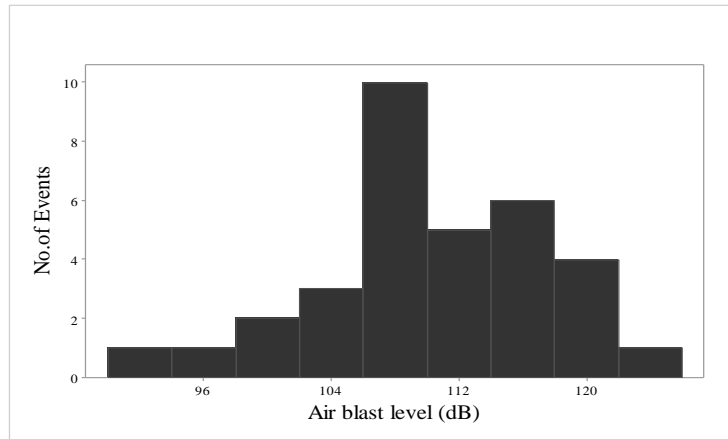
Figure 4.37 Gümüşkol Path 2 presplit blasting air blast histogram

80 ground vibration records from production blasts were collected through Gümüşkol Path 2, mean of the PPV is 1.37 mm/s. Figure 4.38 shows frequency distribution of peak particle velocity from production blasts. Ground vibrations in the range of 0.30-0.80 mm/s constitute 31% of all data. However, ground vibrations in the range of 0.80-1.80 mm/s occupy a greater share (43% of all data).
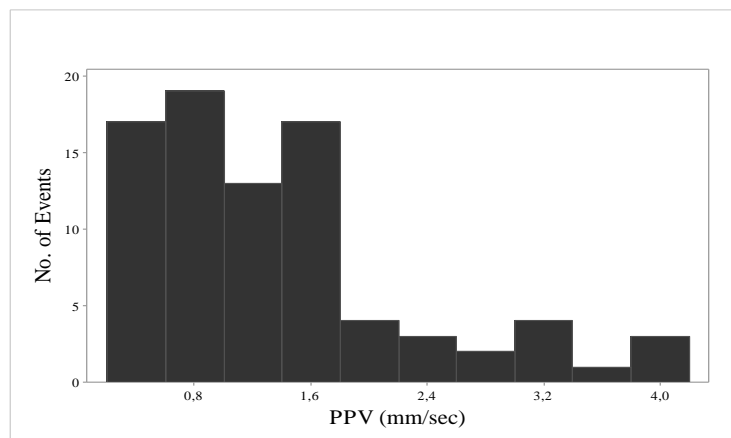
Figure 4.38 Gümüşkol Path 2 production blasting PPV histogram

The lowest and highest PPV levels were 0.29 mm/s (with 14.88 and 8.50 Hz frequency) (GK7 station) and 4.19 mm/s (with 19.31 Hz frequency) (GK6 station), respectively. Lowest PPV was measured when MIC 266.00 kg, distance 1548.00 m and square root scaled distance 94.91 m/√kg. Highest PPV measured when MIC 458.00 kg, distance 1109.00 m and square root scaled distance 51.82 m/√kg.

72 air blast records from production blasts were collected through Gümüşkol Path 2, mean of the air blast levels is 104.40 dB. Figure 4.39 shows frequency distribution of air blast levels from production blasts. The air blast level between 104.00 dB and 110.00 dB has the highest frequency (43% of all events), while that between 97.00 dB and 104.00 dB has the second highest frequency (29% of all events).

Measured highest air blast level was 130.80 dB (with 81 Hz frequency) which was recorded at GK7 station. For this blasting MIC is 177.00 kg, distance is 1485.00 m and cube root scaled distance 264.49 m/$\sqrt[3]{kg}$. Lowest air blast level was 84.24 dB (with 8.88 Hz frequency) which was recorded at the nearest house to the mine, also the farthest station to the mine. For this blasting MIC is 305.00 kg, distance is 1807.00 m and cube root scaled distance 268.45 m/$\sqrt[3]{kg}$.
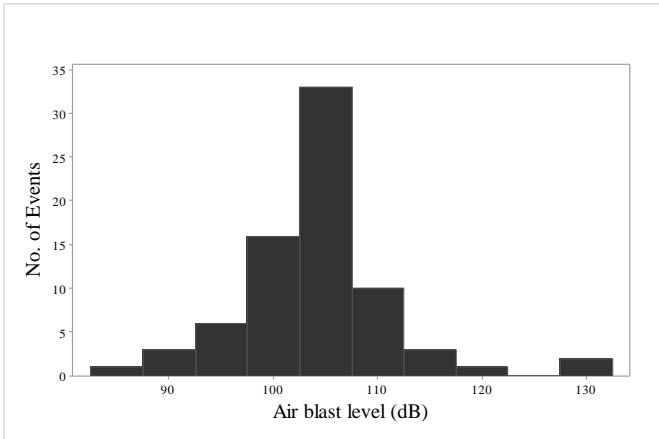
Figure 4.39 Gümüşkol Path 2 production blasting air blast histogram

CHAPTER 5

CONVENTIONAL ANALYSES OF GROUND VIBRATION AND AIR SHOCK

Linear least squares regression analyses were carried out on the collected datasets to obtain site-specific propagation equations for each direction. Analyses were performed using square root scaled distance versus peak particle velocity for ground vibration and cube root scaled distance versus air blast level for air shock. Ground vibration and air shock analyses were carried out on production blast records. However, only air shock analyses were conducted on presplit blast records since most of the energy produced is used on air shock formation due to no-stemming practice.

The collected data were divided into two parts; to form the regression models and to test the models. 10 % of the data were allocated to test the model response. In order to judge the performance of the regression models root-mean square error (RMSE), correlation coefficient (R), coefficient of determination (r^2) were calculated by using measured and predicted values both for modelling set and for testing set. RMSE is calculated with the following relation, where n is the sample size, y_i is predicted value and f_i is measured value.

$$RMSE = \sqrt{\frac{1}{n}\sum_{i=1}^{n}\left(y_i - f_i\right)^2}$$

Correlation coefficient defines the relationship between two variables, here this parameter is used to see the relation between predicted and measured values. R=1 shows perfect correlation and R=-1 shows inverse perfect correlation. Correlation coefficient (Pearson correlation coefficient) is calculated with the following relation, where μ_m and σ_m are the mean and standard deviation of measured values, whereas, μ_p and σ_p are the mean and standard deviation of predicted values. y_i and f_i are measured and predicted values, respectively.

$$R = \frac{1}{n-1}\sum_{i=1}^{n}\left(\frac{\overline{y_i - \mu_m}}{\sigma_m}\right)\left(\frac{f_i - \mu_p}{\sigma_p}\right)$$

The other statistical parameter used for model evaluation is the coefficient of determination (r^2) which should not be confused with the square of correlation coefficient (R^2) given for line equations. $\bar{y}$ is the mean of the measured data, y_i and f_i are the measured data and predicted values, respectively. If negative r^2 values are obtained, it means that the mean of the measured data provides a better consistency than the predicted values.

$$r^2 = 1 - \frac{\sum_i (y_i - f_i)^2}{\sum_i (y_i - \bar{y})^2} \qquad \bar{y} = \frac{1}{n}\sum_{i=1}^{n} y_i$$

5.1 Ground Vibration Analyses

For ground vibration analyses logarithmic plots of square root scaled distance versus PPV are obtained. Two propagation equations with related R^2 (square of correlation coefficient between SD and PPV) are obtained for each dataset these are mean value equation (belonging to the below line) and 95% confidence interval line equation (belonging the upper line) (can be seen in Figure 5.1). These equations are in the form of $PPV = Kx(SD)^{-\beta}$. Where K is rock transmission factor and β is attenuation constant. In this study, 95% confidence interval line equation (the upper line) is used to calculate safe explosive amounts per delay and to predict PPV for future blasts. It implies that the future PPV measurements can be higher than the predicted value only with 5% possibility.

As a preliminary step to detailed ground vibration analyses, all the collected data were analyzed in the same graph regardless of the location of monitoring stations (Figure 5.1). The performance indicators calculated for modelling and testing set are given in Table 5.1. These values are later compared to regression analyses of the classified data.
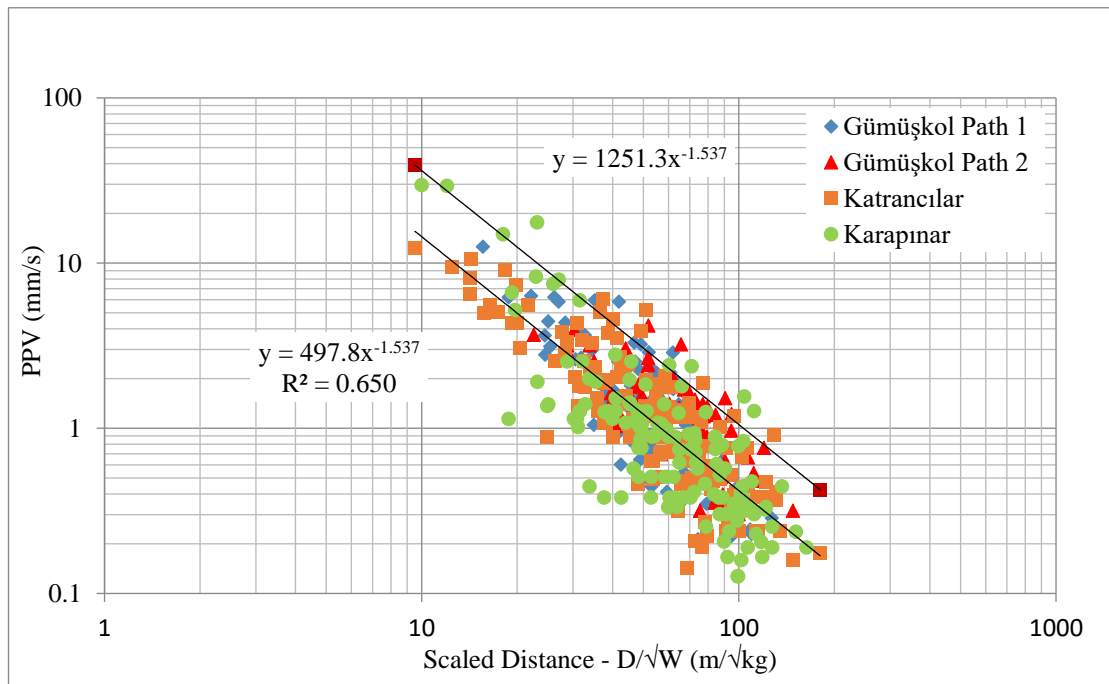
Figure 5.1 PPV prediction from whole production blast data

Table 5.1 Performance indicators for the whole-data model

		R	r^2	RMSE
Whole data	Modelling Set	0.813	0.612	1.673
	Testing set	0.924	0.803	1.174

Figure 5.2 shows the division of the pit according to blast group location within the pit which will be later used for ground vibration analyses for each village. Blast groups were classified in 16 groups before analyzing. The ground vibrations from blast groups behind the pit follow a longer path than the blast groups in front of the pit to reach to the monitoring station. In other words, they travel through the pit cone therefore their blast vibrations are expected to be lower.
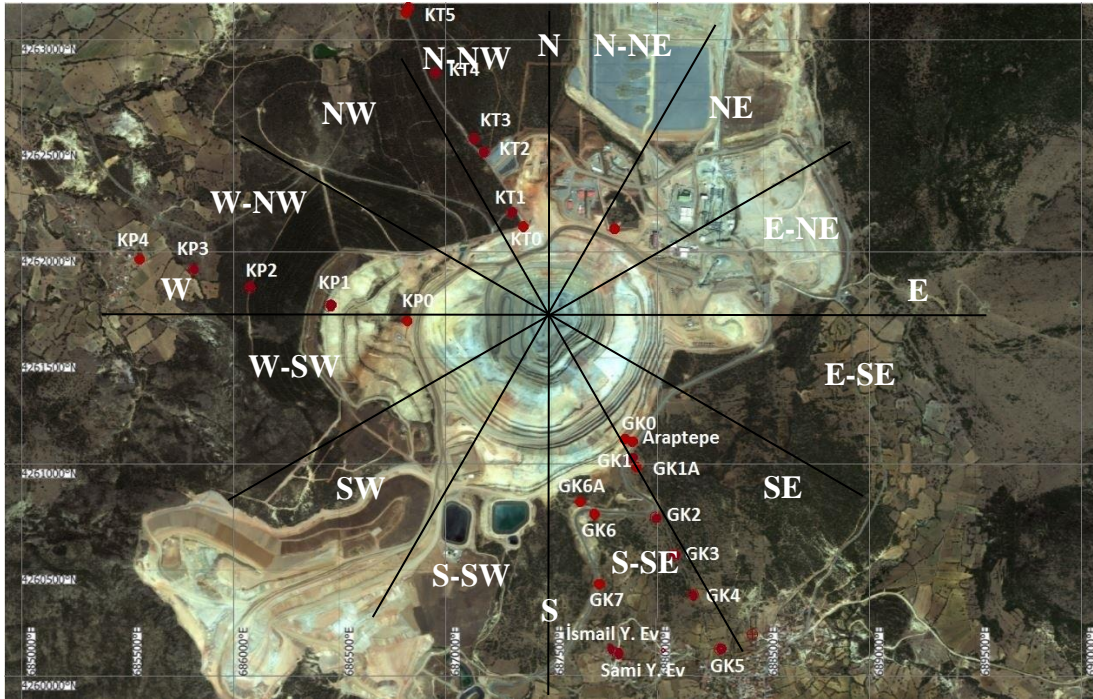
Figure 5.2 Division of the pit according to directions

5.1.1 Katrancılar village

167 ground vibration records were obtained from production blasts. Production blasts were conducted at minimum 1293.8 m and maximum 1902.2 m horizontal distances to this village. In production blasting both ground vibration and air blast are felt from Katrancılar village. 10% of the collected data were separated as testing set in order to test the developed regression model. The highest PPV level from production blasting is 1.876 mm/s (transverse component) with 5.63 Hz predominant frequency (at 1447.3 m). According to US OSM Regulations (Figure 2.17) for 5.63 Hz frequency value, maximum allowable ground vibration level is 19 mm/s.

Ground vibration data from production blasting were divided into two parts according to location of blast holes within the pit with respect to Katrancılar; i.e. in front of the pit and behind the pit. Figure 5.3 shows behind the pit and in front of the pit concepts for Katrancılar stations (KT0 to KT6).
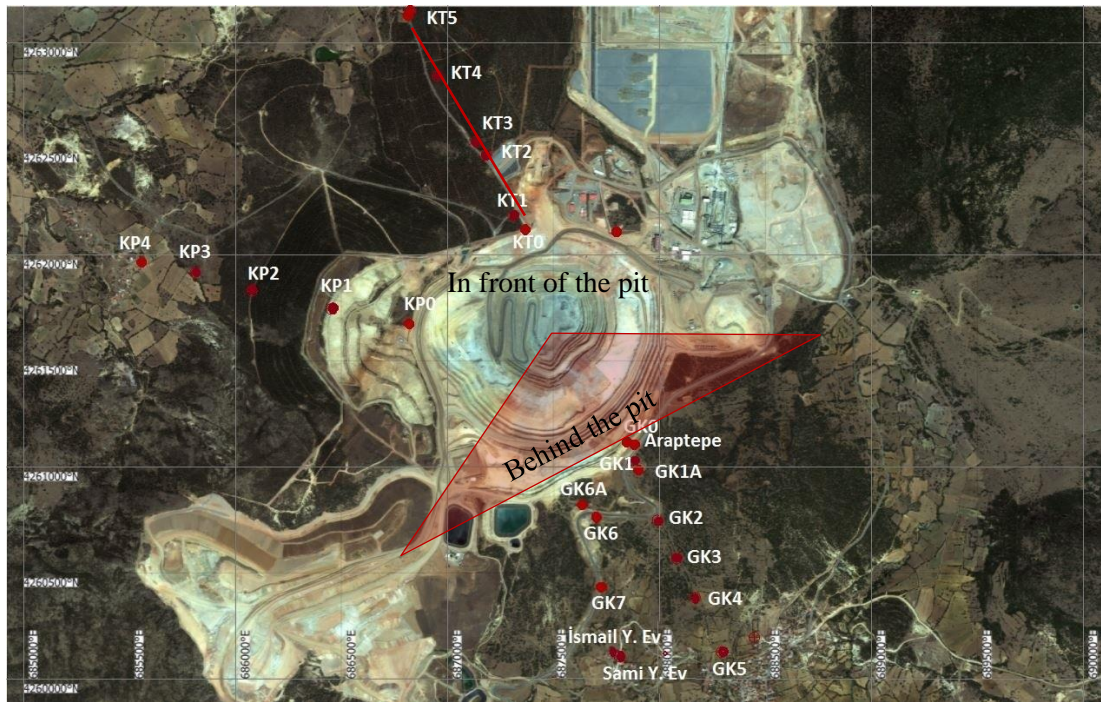
Figure 5.3 'behind the pit' and 'in front of the pit' concepts for Katrancılar

8 different pit classification scenarios were tested and evaluated by using model records and test records and compared to the regression analysis from unclassified data. Table 5.2 shows the directions included in the analysis, line equation and R^2 (square of correlation coefficient), which shows the correlation between square root scaled distance and PPV. To evaluate the performance of the models; correlation coefficient, coefficient of determination and Root-Mean Square Error (RMSE) were calculated and compared in Table 5.3. All the models gave more or less the same results, but the best result is obtained for model 1 combination. Figure 5.4 shows ground vibration attenuation relation for unclassified production blast data.

Table 5.2 Katrancılar properties of the formed models

	Pit location	Directions included	Line equation	
Unclassified	-	-	$y = 453.7 * x^{-1.51}$	$R^2= 0.722$ R=-0.850
Model 1	In front of the pit	N, NE, SW, W, NW, NNW	$y = 250.1 * x^{-1.33}$	$R^2=0.732$ R=-0.856
	Behind the pit	ENE, E, SE, S, SSW	$y = 376.7 * x^{-1.55}$	$R^2=0.566$ R=-0.752
Model 2	In front of the pit	N, NE, W, NW, NNW	$y = 222.0 * x^{-1.28}$	$R^2=0.748$ R=-0.865
	Behind the pit	ENE, E, SE, S, SSW, SW, WSW	$y = 386.9 * x^{-1.51}$	$R^2=0.540$ R=-0.735
Model 3	In front of the pit	N, NE, WSW, W, NW, NNW	$y = 228.2 * x^{-1.29}$	$R^2=0.739$ R=-0.860
	Behind the pit	ENE, E, SE, S, SW	$y = 320.8 * x^{-1.47}$	$R^2=0.476$ R=-0.690
Model 4	In front of the pit	N, NE, E, ESE, NW, NNW	$y = 316.4 * x^{-1.39}$	$R^2=0.748$ R=-0.865
	Behind the pit	SE, S, SW, WSW, W	$y = 432.5 * x^{-1.53}$	$R^2=0.579$ R=-0.761
Model 5	In front of the pit	N, NE, ENE, W, NW, NNW	$y = 217.0 * x^{-1.27}$	$R^2=0.743$ R=-0.862
	Behind the pit	E, SE, S, SW, WSW	$y = 364.1 * x^{-1.50}$	$R^2=0.545$ R=-0.738
Model 6	In front of the pit	N, NE, E, WNW, NW, NNW	$y = 305.5 * x^{-1.38}$	$R^2=0.749$ R=-0.865
	Behind the pit	ESE, SE, S, SW, W	$y = 389.5 * x^{-1.51}$	$R^2=0.577$ R=-0.760
Model 7	In front of the pit	N, NE, WNW, NW, NNW	$y = 223.2 * x^{-1.28}$	$R^2=0.763$ R=-0.873
	Behind the pit	ENE, E, SE, S, SW, W	$y = 547.1 * x^{-1.59}$	$R^2=0.580$ R=-0.762
Model 8	In front of the pit	N, NE, ENE, WNW, NW, NNW	$y = 218.1 * x^{-1.28}$	$R^2=0.758$ R=-0.871
	Behind the pit	E, SE, S, SSW, SW, W	$y = 526.0 * x^{-1.58}$	$R^2=0.586$ R=-0.766

Table 5.3 Katrancılar performance indicators for the models

	Modelling Set			Testing Set		
	R	**r^2**	**RMSE**	**R**	**r^2**	**RMSE**
Unclassified	0.887	0.777	0.995	0.948	0.889	0.588
Model 1	**0.893**	**0.791**	**0.965**	**0.965**	**0.906**	**0.540**
Model 2	0.895	0.794	0.957	0.954	0.894	0.574
Model 3	0.894	0.792	0.963	0.957	0.895	0.572
Model 4	0.892	0.789	0.970	0.953	0.889	0.587
Model 5	0.896	0.795	0.955	0.954	0.895	0.571
Model 6	0.895	0.794	0.957	0.964	0.902	0.553
Model 7	0.894	0.791	0.964	0.952	0.889	0.588
Model 8	0.895	0.792	0.962	0.954	0.892	0.581
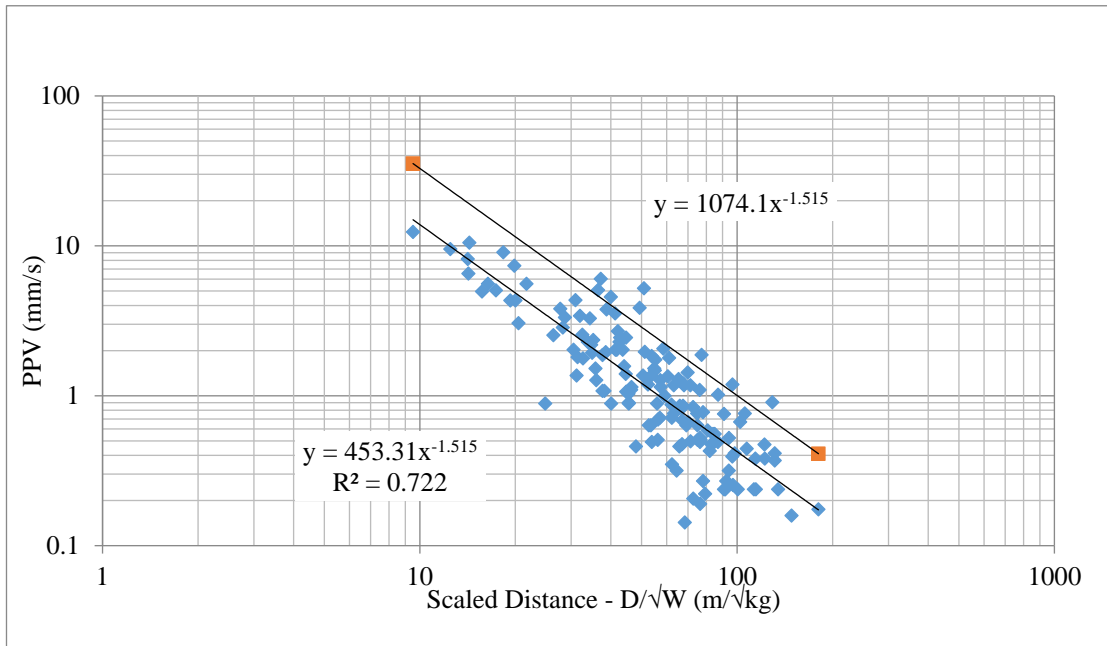
Figure 5.4 Katrancılar unclassified production blasting PPV values

5.1.1.1 Katrancılar Village – in front of the pit analysis

The highest PPV level from in front of the pit production blasts is 1.876 mm/s (transverse component) with 5.63 Hz predominant frequency (at 1447.3 m). According to US OSM Regulations (Figure 2.17) for 5.63 Hz frequency value, maximum allowable ground vibration level is 19 mm/s.

SD vs PPV graph was used to determine propagation-attenuation equation for stripping-production blasts on this path (Figure 5.5). The attenuation relation for in front of the pit blasts is $PPV = 529.48*SD^{-1.326}$. Distance-explosive amount graph obtained from this equation for various PPV levels is shown in Figure 5.6. This graph is used to determine the safe explosive amount per delay when the distance between the blast site and the relevant structure is known. The distance between KT5 station (the closest building in the village to the mine) and north border of the mine is 1150 m and the distance between KT5 and the center of the open pit is 1610 m. The lowest measured frequency value is 3.813 Hz on this path and the allowable PPV is 16.40 mm/s for this frequency value.

89
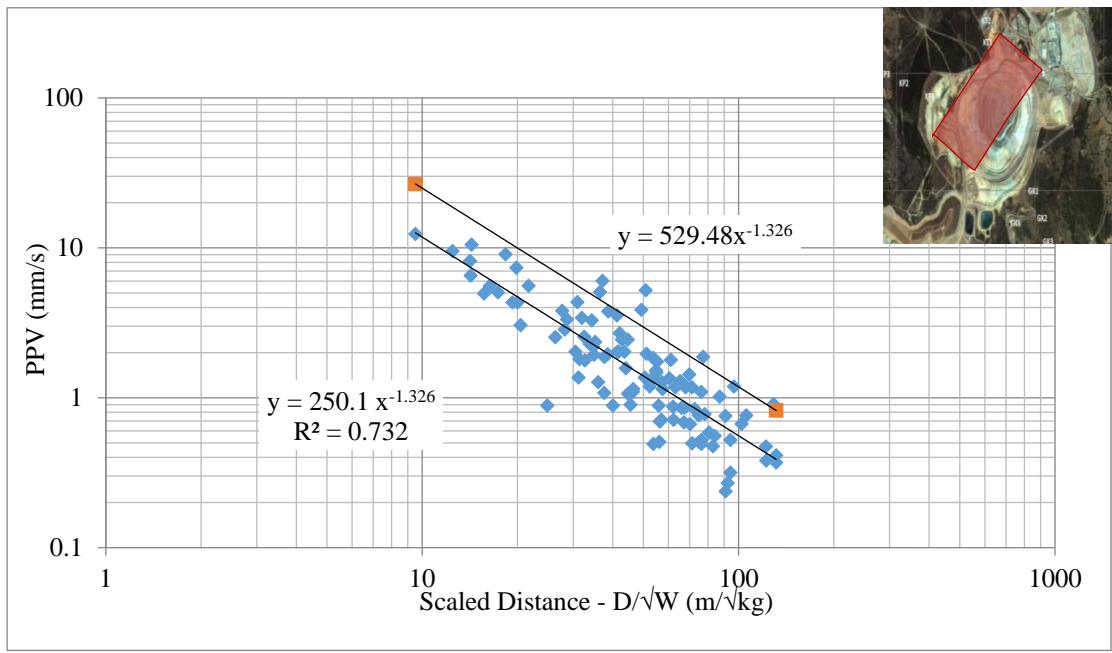
Figure 5.5 Katrancılar production blasting PPV values (Pit location- NE, N, W, SW- in front of the pit)
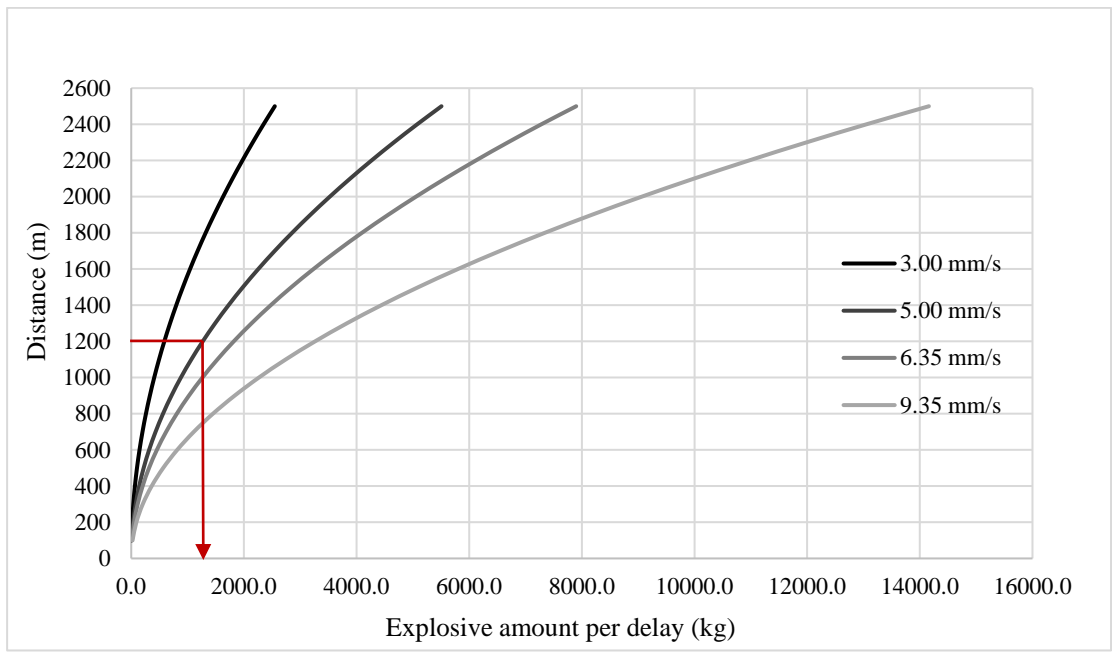
Figure 5.6 Safe explosive amounts for Katrancılar village for 'in front of the pit' blasts

However, it was aimed not to exceed at worst 5.00 mm/s or normally 3.00 mm/s since some of the buildings in the village were constructed by using mud mortar and rubble stone. For example, if the distance between KT5 station and the blast site is 1200 m and 5.00 mm/s was decided as the PPV limit, the safe amount of explosive that can be blasted at the same time is 1269.0 kg.

5.1.1.2 Katrancılar Village – behind the pit analysis

The highest PPV level from production blasting is 1.429 mm/s (transverse component) with 13.88 Hz predominant frequency (at 1328.0 m). According to US OSM Regulations (Figure 2.17) for 13.88 Hz frequency value, maximum allowable ground vibration level is 25.8 mm/s. SD vs PPV graph was used to determine propagation-attenuation equation for stripping-production blasts on this path (Figure 5.7). The attenuation relation for behind the pit blasts is $PPV = 881.28 * SD^{-1.55}$. Distance-explosive amount graph obtained from this equation for various PPVs is shown in Figure 5.8. This graph is used to determine the safe explosive amount per delay when the distance between the blast site and the relevant structure is known.
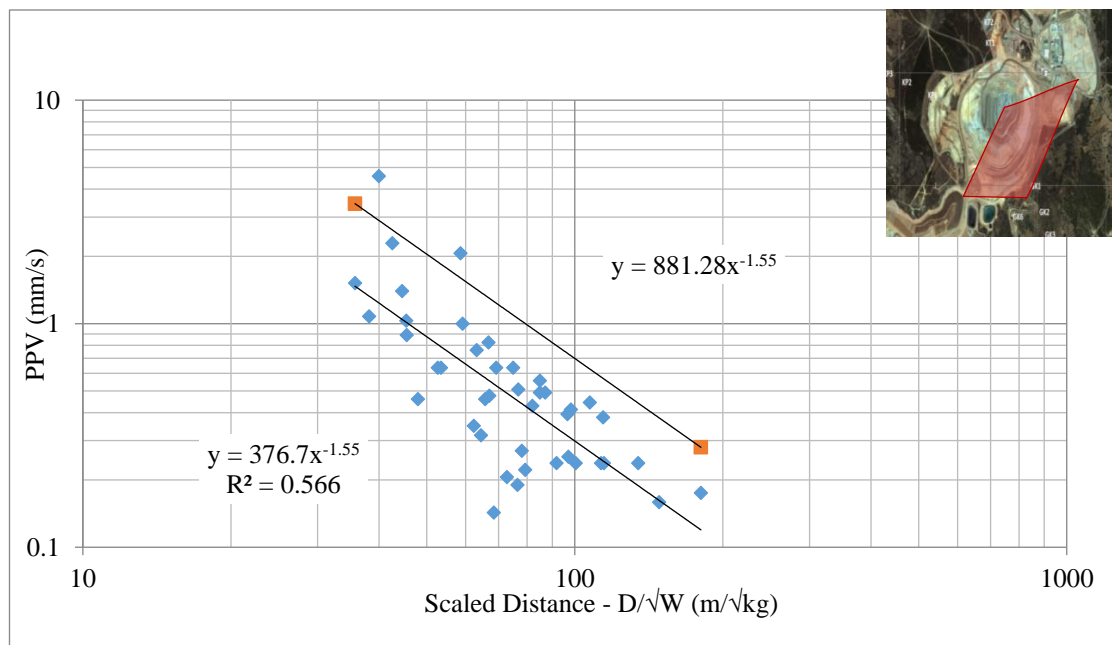
Figure 5.7 Katrancılar production blasting PPV values (Pit location- SSW, S, E, ENE- behind the pit)
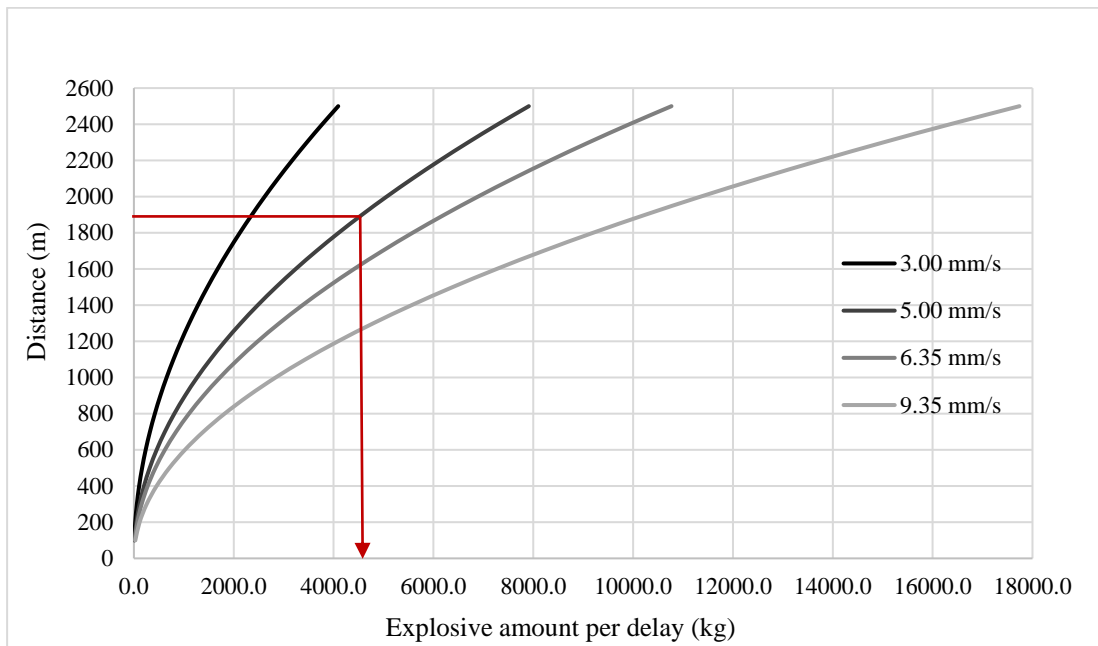
Figure 5.8 Safe explosive amounts for Katrancılar village for 'behind the pit' blasts

The distance between KT5 station (the closest building to the mine) and south border of the mine is 2310 m and the distance between KT5 and the center of the open pit is 1610 m. The lowest measured frequency value is 4.125 Hz on this path and the allowable PPV is 19 mm/s for this frequency value. However, it was aimed not to exceed at worst 5.00 mm/s or normally 3.00 mm/s since some of the buildings in the village was constructed by using mud mortar and rubble stone. For example, if the distance between KT5 station and the blast site is 1900 m and 5.00 mm/s was decided as the PPV limit, the safe amount of explosive that can be blasted at the same time is 4569.5 kg.

5.1.2 Karapınar Village

147 ground vibration records were obtained from production blasts. Production blasts were conducted at minimum 1249.50 m and maximum 2248.65 m horizontal distances to this village. In production blasting both ground vibration and air blast are felt from this village. The highest PPV level from production blasting is 2.372 mm/s (transverse component) with 7.94 Hz predominant frequency (at 1381.0 m). According to US

OSM Regulations (Figure 2.17) for 7.94 Hz frequency value, maximum allowable ground vibration level is 19 mm/s.

Ground vibration data from production blasting were divided into two parts according to location of blast holes within the pit with respect to the settlement location; i.e. in front of the pit and behind the pit. Figure 5.9 shows behind the pit and in front of the pit concepts for Karapınar stations.

Figure 5.9 'behind the pit' and 'in front of the pit' concepts for Karapınar

9 different pit classification scenarios were tested and evaluated by using model records and test records and compared to the regression analysis from unclassified data. Table 5.4 shows the directions included in the analysis, line equation and R^2 (square of correlation coefficient, which shows the relation between SD and PPV). To evaluate the performance of the models; correlation coefficient, coefficient of determination and Root-Mean Square Error (RMSE) were calculated and compared in Table 5.5.

Table 5.4 Karapınar properties of the formed models

	Pit location	Directions included	Line equation		
Unclassified	-	-	$y = 469.7 * x^{-1.56}$	$R^2=0.654$	$R=-0.809$
Model 1	In front of the pit	NNE, N, W, S, SSE	$y = 313.6 * x^{-1.44}$	$R^2=0.642$	$R=-0.801$
	Behind the pit	NE, E, SE	$y = 1542.7 * x^{-1.91}$	$R^2=0.573$	$R=-0.757$
Model 2	In front of the pit	N, W, S, SSE	$y = 311.9 * x^{-1.44}$	$R^2=0.647$	$R=-0.804$
	Behind the pit	NNE, NE, E, SE	$y = 803.3 * x^{-1.77}$	$R^2=0.538$	$R=-0.733$
Model 3	In front of the pit	NE, N, W, S, SSE	$y = 336.7 * x^{-1.46}$	$R^2=0.627$	$R=-0.792$
	Behind the pit	ENE, E, SE	$y = 927.1 * x^{-1.81}$	$R^2=0.685$	$R=-0.828$
Model 4	In front of the pit	NNE, N, W, SSW	$y = 281.7 * x^{-1.41}$	$R^2=0.624$	$R=-0.790$
	Behind the pit	NE, E, SE, S	$y = 1314.9 * x^{-1.87}$	$R^2=0.612$	$R=-0.782$
Model 5	In front of the pit	NNW, W, S, SSE	$y = 325.5 * x^{-1.45}$	$R^2=0.652$	$R=-0.807$
	Behind the pit	N, NE, E, SE	$y = 649.0 * x^{-1.71}$	$R^2=0.529$	$R=-0.727$
Model 6	In front of the pit	NNE, N, W, S	$y = 286.5 * x^{-1.42}$	$R^2=0.629$	$R=-0.793$
	Behind the pit	NE, E, SE, SSE	$y = 1493.6 * x^{-1.90}$	$R^2=0.619$	$R=-0.787$
Model 7	In front of the pit	NNW, W, SSW	$y = 289.2 * x^{-1.41}$	$R^2=0.632$	$R=-0.795$
	Behind the pit	N, E, S	$y = 658.1 * x^{-1.70}$	$R^2=0.569$	$R=-0.754$
Model 8	In front of the pit	N, W, SSW	$y = 277.9 * x^{-1.40}$	$R^2=0.628$	$R=-0.792$
	Behind the pit	NNE, E, S	$y = 770.3 * x^{-1.75}$	$R^2=0.581$	$R=-0.762$
Model 9	In front of the pit	SW, W, NNW	$y = 298.7 * x^{-1.42}$	$R^2=0.618$	$R=-0.786$
	Behind the pit	N, E, SSW	$y = 212.0 * x^{-1.43}$	$R^2=0.498$	$R=-0.706$

Regression model from unclassified data gives the best performance indicators among all and the second-best result is obtained for model 5 combination. Figure 5.10 shows ground vibration attenuation relation for unclassified production blast data.

Table 5.5 Karapınar performance indicators for the models

	Modelling Set			Testing Set		
	R	**r^2**	**RMSE**	**R**	**r^2**	**RMSE**
Unclassified	0.881	0.512	2.924	0.933	0.751	2.071
Model 1	0.867	0.469	3.050	0.917	0.685	2.326
Model 2	0.866	0.473	3.037	0.915	0.688	2.316
Model 3	0.868	0.480	3.017	0.917	0.698	2.279
Model 4	0.864	0.456	3.087	0.916	0.668	2.387
Model 5	**0.871**	**0.475**	**3.034**	**0.927**	**0.702**	**2.264**
Model 6	0.864	0.458	3.081	0.915	0.670	2.380
Model 7	0.864	0.466	3.058	0.916	0.680	2.346
Model 8	0.862	0.460	3.077	0.914	0.670	2.381
Model 9	0.865	0.475	3.032	0.915	0.690	2.309
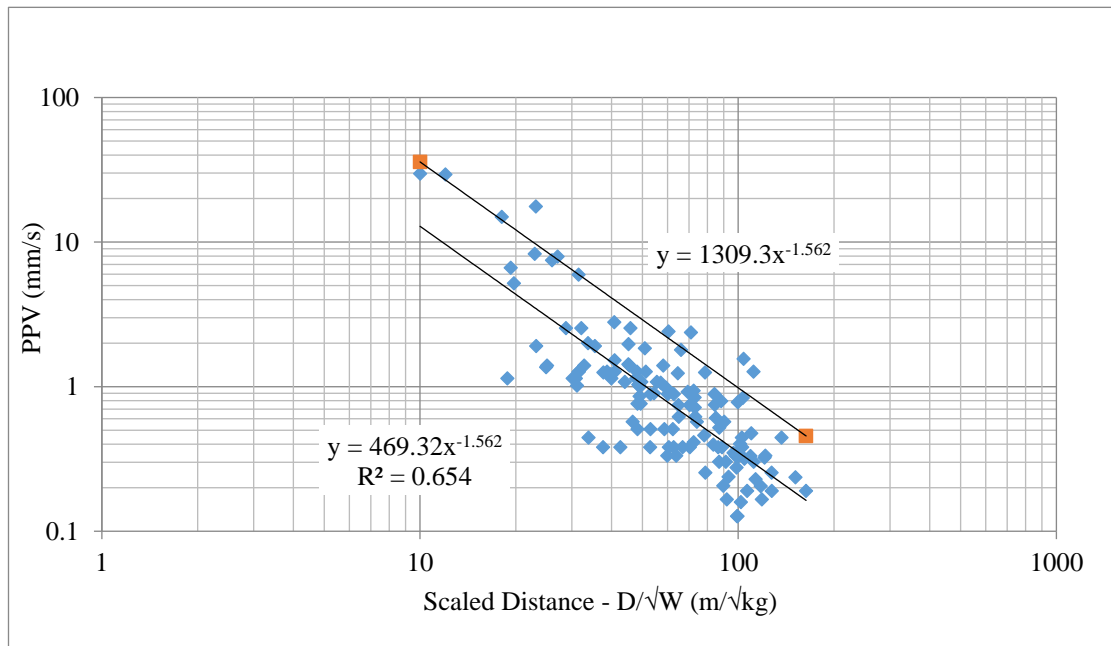
Figure 5.10 Karapınar unclassified production blasting PPV

5.1.2.1 Karapınar village – in front of the pit analysis

From production blasting both ground vibration and air blast are felt from this village. The highest PPV level from production blasting is 2.372 mm/s (transverse component) with 7.94 Hz predominant frequency (at 1381.0 m). According to US OSM Regulations (Figure 2.17) for 7.94 Hz frequency value, maximum allowable ground vibration level is 19 mm/s.

SD vs PPV graph was used to determine propagation-attenuation equation for stripping-production blasts on this path (Figure 5.11). The attenuation relation for in front of the pit blasts is PPV = 891.1*SD$^{-1.445}$. Distance-explosive amount graph obtained from this equation for various PPV values is shown in Figure 5.12. This graph is used to determine the safe explosive amount per delay when the distance between the blast site and the relevant structure is known. The distance between KP4 station (the closest building in the village to the mine) and west border of the mine is 930 m and the distance between KP4 and the center of the open pit is 1968 m.
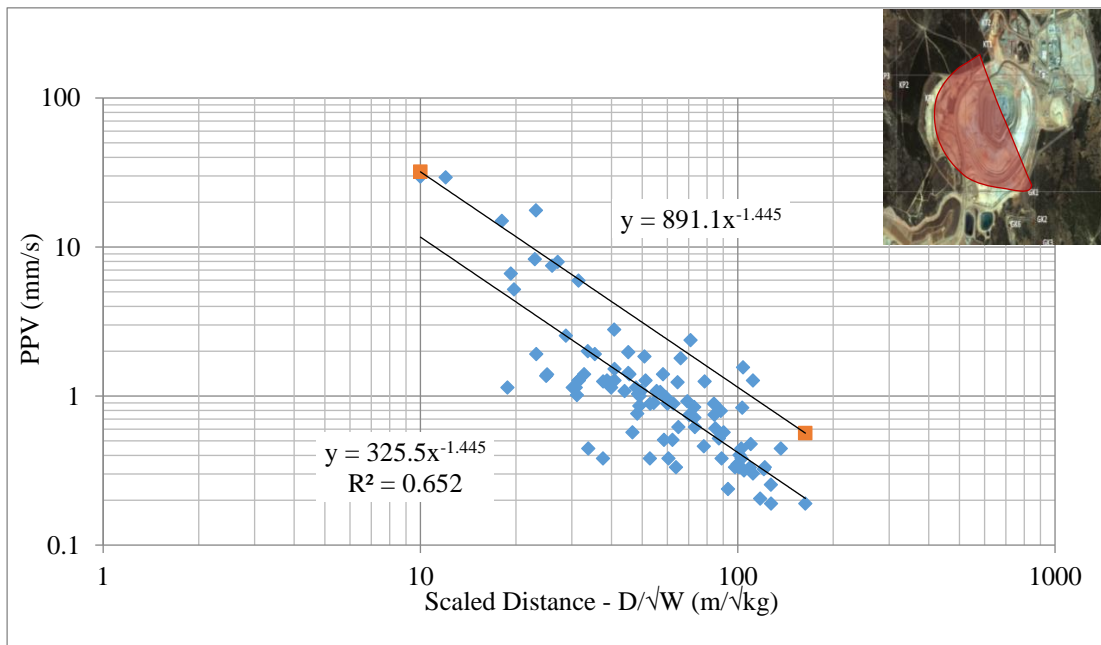
Figure 5.11 Karapınar production blasting PPV values (Pit location- NNW, W, S, SSE- in front of the pit)
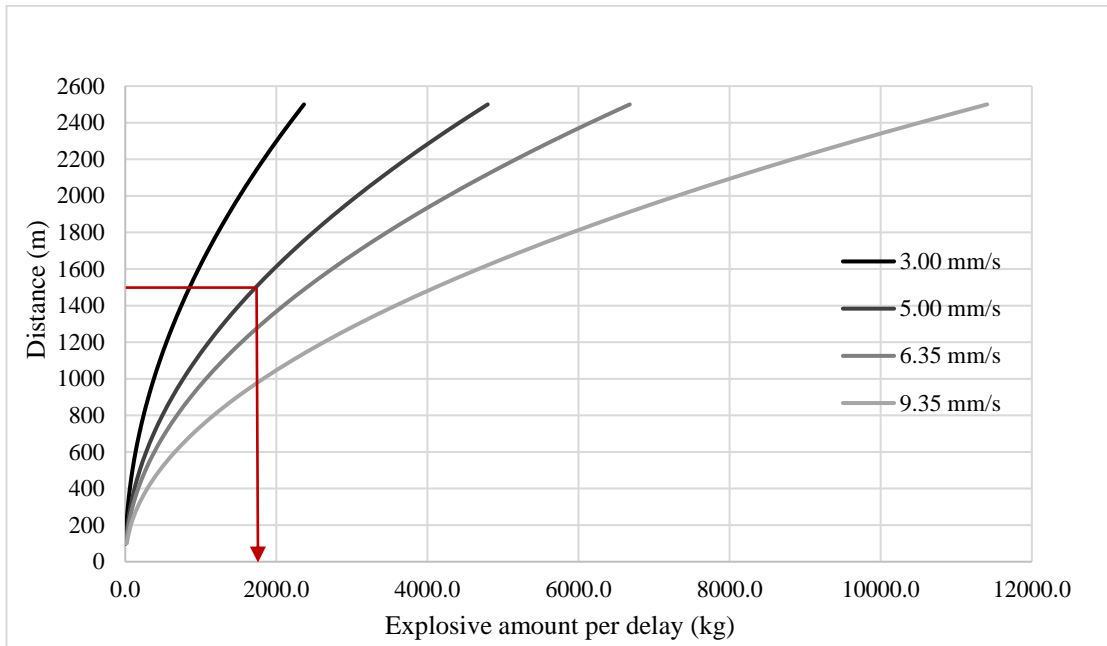
Figure 5.12 Safe explosive amounts for Karapınar village for 'in front of the pit' blasts

The lowest measured frequency value is 6.25 Hz on this path and the allowable PPV is 19 mm/s for this frequency value. However, it was aimed not to exceed at worst 5.00 mm/s or normally 3.00 mm/s since some of the buildings in the village was constructed by using mud mortar and rubble stone. For example, if the distance between KP4 station and the blast site is 1500 m and 5.00 mm/s was decided as the PPV limit, the safe amount of explosive that can be blasted at the same time is 1727.1 kg.

5.1.2.2 Karapınar village – behind the pit analysis

The highest PPV level from production blasting is 0.780 mm/s (radial component) with 8.25 Hz predominant frequency (at 1900.0 m). According to US OSM Regulations (Figure 2.17) for 8.25 Hz frequency value, maximum allowable ground vibration level is 19 mm/s. The measured maximum velocity value is even less than the allowable velocity limit which is 5 mm/s for 1 Hz the frequency. Moreover, it is less than the human perception level that is 1.50 mm/s (given in Chapter 2.6). It can be felt only when the people are in a building due to resonance effect of the structure.

SD vs PPV graph was used to determine propagation-attenuation equation for stripping-production blasts on this path (Figure 5.13). The attenuation relation for behind the pit blasts is PPV = $1635.9 * SD^{-1.705}$. Distance-explosive amount graph obtained from this equation for various PPVs is shown in Figure 5.14. This graph is used to determine the safe explosive amount per delay when the distance between the blast site and the relevant structure is known. The distance between KP4 station (the closest building in the village to the mine) and east border of the mine is 2530 m and the distance between KP4 and the center of the open pit is 1968.0 m.

The lowest measured frequency value is 3.38 Hz on this path and the allowable PPV is 14.80 mm/s for this frequency value. However, it was aimed not to exceed at worst 5.00 mm/s or normally 3.00 mm/s since some of the buildings in the village was constructed by using mud mortar and rubble stone.
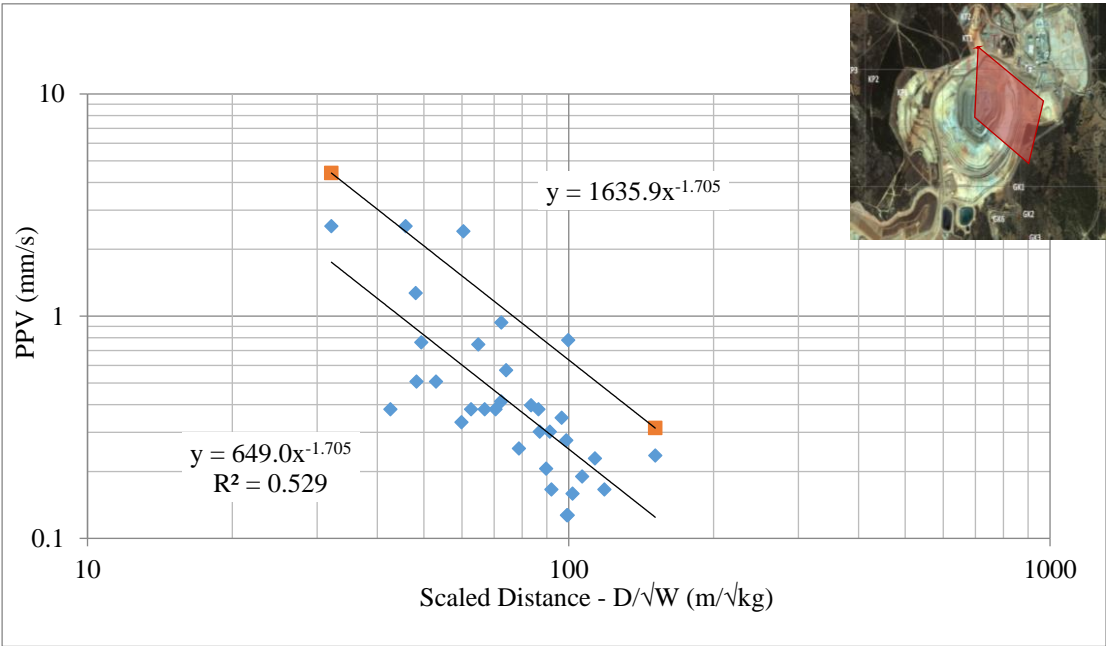
Figure 5.13 Karapınar production blasting PPV values (Pit location- N, NE, E, SE - behind the pit)

98
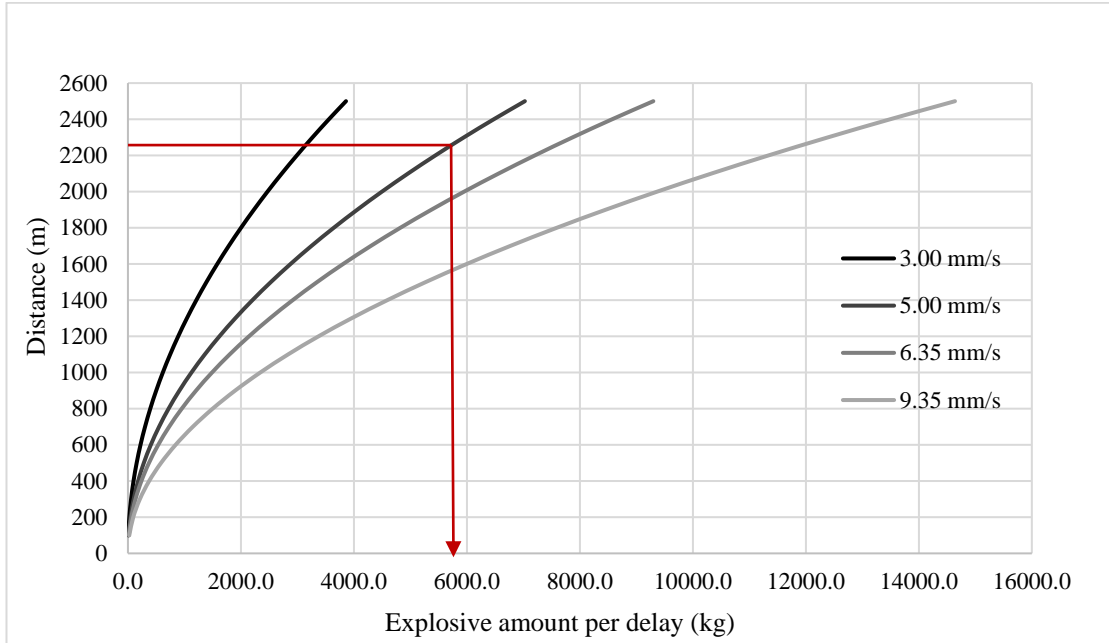
Figure 5.14 Safe explosive amounts for Karapınar village for 'behind the pit' blasts

For example, if the distance between KP4 station and the blast site is 2250 m and 5.00 mm/s was decided as the PPV limit, the safe amount of explosive that can be blasted at the same time is 5691.4 kg.

5.1.3 Gümüşkol Village Path 1

127 ground vibration records were obtained from production blasts. Production blasts were conducted at minimum 1457.3 m and maximum 1869.3 m horizontal distances to this village. In production blasting both ground vibration and air blast are felt from this village. The highest PPV level from production blasting at the village is 0.741 mm/s (transverse component) with 12.81 Hz predominant frequency (at 1707.9 m). According to US OSM Regulations (Figure 2.17) for 12.81 Hz frequency value, maximum allowable ground vibration level is 24.10 mm/s.

Ground vibration data from production blasting were divided into two parts according to location of blast holes within the pit with respect to settlement location; i.e. in front of the pit and behind the pit. Figure 5.15 shows behind the pit and in front of the pit

concepts for Gümüşkol Path 1 monitoring line (GK1 to GK5). Figure 5.16 shows ground vibration attenuation relation for unclassified production blast data.

Figure 5.15 'behind the pit' and 'in front of the pit' concepts for Gümüşkol Path 1

9 different pit classification scenarios were tested and evaluated by using model records and test records and compared to the regression analysis from unclassified data. Table 5.6 shows the directions included in the analysis, line equation and R^2 (square of correlation coefficient, which shows the relation between SD and PPV).

To evaluate the performance of the models; correlation coefficient, coefficient of determination and Root-Mean Square Error (RMSE) were calculated and compared in Table 5.7. All the models gave more or less the same results, but the best result is obtained for model 3 combination. Figure 5.16 shows ground vibration attenuation relation for unclassified production blast data.

Table 5.6 Gümüşkol Path 1 properties of the formed models

	Pit location	Directions included	Line equation		
Unclassified	-	-	$y = 1366.9 * x^{-1.80}$	$R^2= 0.649$	R=-0.806
Model 1	In front of the pit	SW, S, E, NE	$y = 1177.8 * x^{-1.75}$	$R^2= 0.749$	R=-0.865
	Behind the pit	WSW, W, NW, N, NNE	$y = 3111.8 * x^{-2.01}$	$R^2= 0.275$	R=-0.524
Model 2	In front of the pit	WSW, SW, S, E, NE	$y = 1100.9 * x^{-1.73}$	$R^2= 0.731$	R=-0.855
	Behind the pit	W, NW, N, NNE	$y = 9007.5 * x^{-2.28}$	$R^2= 0.318$	R=-0.564
Model 3	In front of the pit	W, WSW, SW, S, E, NE	$y = 1176.9 * x^{-1.76}$	$R^2= 0.685$	R=-0.828
	Behind the pit	WNW, N, NNE	$y = 41931.5 * x^{-2.62}$	$R^2= 0.480$	R=-0.693
Model 4	In front of the pit	W, WSW, S, E, ENE	$y = 1104.6 * x^{-1.75}$	$R^2= 0.713$	R=-0.844
	Behind the pit	WNW, NW, N, NE	$y = 103176.5 * x^{-2.83}$	$R^2= 0.536$	R=-0.732
Model 5	In front of the pit	ESE, SE, SSE, S	$y = 1283.5 * x^{-1.80}$	$R^2= 0.839$	R=-0.916
	Behind the pit	N, NE, E, SSW, W, NNW	$y = 1775.7 * x^{-1.86}$	$R^2= 0.552$	R=-0.743
Model 6	In front of the pit	SE, SSE, S	$y = 1293.1 * x^{-1.79}$	$R^2= 0.838$	R=-0.915
	Behind the pit	N, NE, E, ESE, SSW, W, NNW	$y = 1539.7 * x^{-1.82}$	$R^2= 0.571$	R=-0.756
Model 7	In front of the pit	SE, SSE	$y = 1341.2 * x^{-1.81}$	$R^2= 0.846$	R=-0.920
	Behind the pit	N, NE, E, ESE, S, SSW, W, NNW	$y = 1606.4 * x^{-1.83}$	$R^2= 0.578$	R=-0.760
Model 8	In front of the pit	SE, SSE, S, SSW	$y = 1225.0 * x^{-1.76}$	$R^2=0.719$	R=-0.848
	Behind the pit	N, NE, E, ESE, SW, W, NNW	$y = 1274.9 * x^{-1.78}$	$R^2=0.529$	R=-0.727
Model 9	In front of the pit	ESE, SE, SSE, S, SSW	$y = 1262.1 * x^{-1.77}$	$R^2=0.736$	R=-0.858
	Behind the pit	N, NE, E, SW, W, NNW	$y = 1492.7 * x^{-1.82}$	$R^2=0.494$	R=-0.703

Table 5.7 Gümüşkol Path 1 performance indicators for the models

	Modelling Set			Testing Set		
	R	**r²**	**RMSE**	**R**	**r²**	**RMSE**
Unclassified	0.855	0.714	0.933	0.933	0.860	0.684
Model 1	0.865	0.721	0.923	0.933	0.849	0.710
Model 2	0.856	0.711	0.939	0.934	0.857	0.691
Model 3	**0.855**	**0.711**	**0.938**	**0.934**	**0.860**	**0.684**
Model 4	0.874	0.725	0.915	0.831	0.573	1.193
Model 5	0.861	0.714	0.933	0.933	0.851	0.706
Model 6	0.856	0.711	0.939	0.937	0.859	0.685
Model 7	0.857	0.709	0.941	0.939	0.857	0.690
Model 8	0.855	0.713	0.935	0.930	0.855	0.695
Model 9	0.856	0.712	0.936	0.934	0.860	0.684
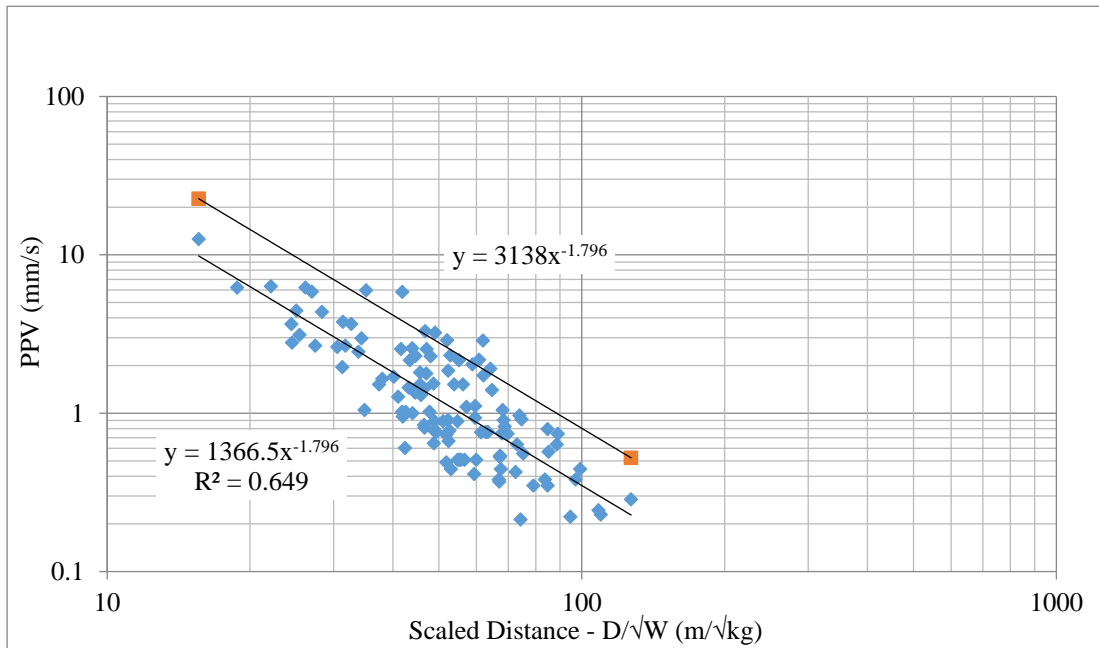
Figure 5.16 Gümüşkol Path 1 unclassified production blasting PPV values

5.1.3.1 Gümüşkol Village Path 1– in front of the pit analysis

The highest PPV level from production blasting is 0.741 mm/s (transverse component) with 12.81 Hz predominant frequency (at 1707.9 m). According to US OSM Regulations (Figure 2.17) for 12.81 Hz frequency value, maximum allowable ground vibration level is 24.10 mm/s. The maximum measured velocity value is less than the allowable velocity limit (5 mm/s) given for 1 Hz frequency. Moreover, it is less than the human perception level that is 1.50 mm/s.

SD vs PPV graph was used to determine propagation-attenuation equation for stripping-production blasts on this path (Figure 5.17). The attenuation relation for in front of the pit blasts is PPV $= 2607.3*SD^{-1.761}$. Distance-explosive amount graph obtained from this equation for various PPV values is shown in Figure 5.18. This graph is used to determine the safe explosive amount per delay when the distance between the blast site and the relevant structure is known.
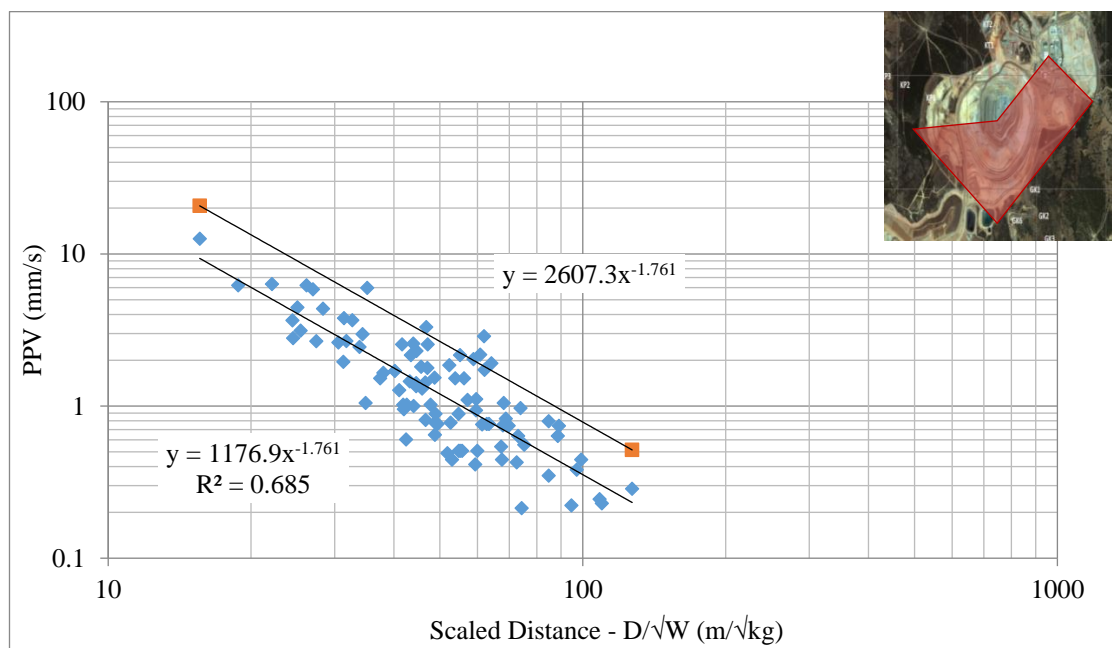
Figure 5.17 Gümüşkol Path 1 production blasting PPV values (Pit location-W, WSW, SW, S, E, NE-in front of the pit)
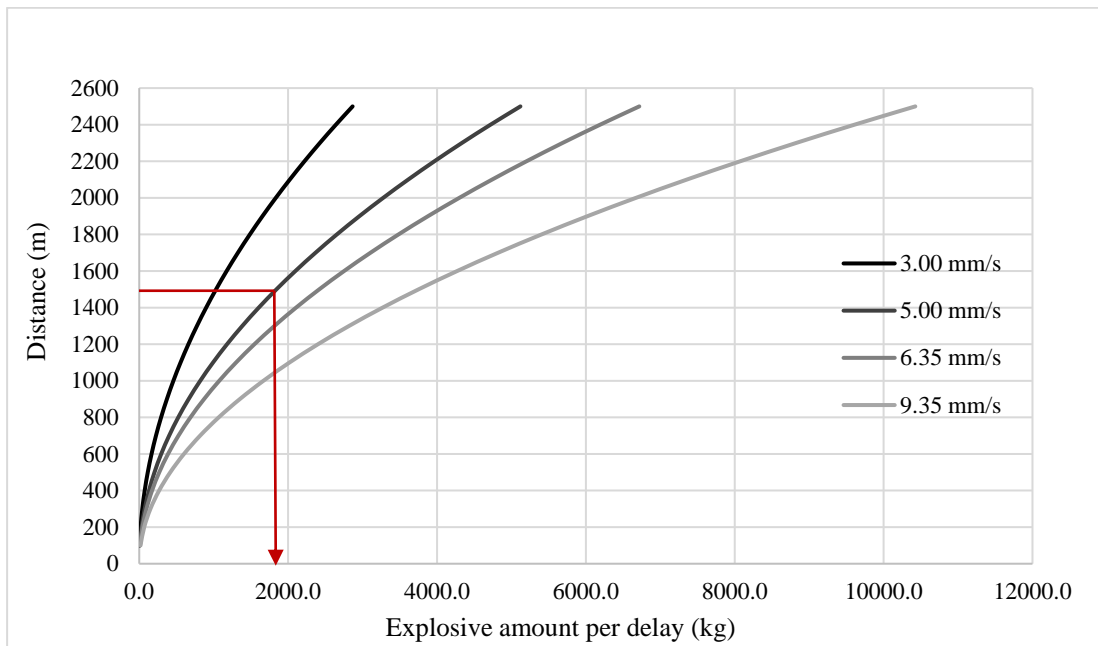
Figure 5.18 Safe explosive amounts for Gümüşkol village Path 1 for 'in front of the pit' blasts

The distance between GK5 station (the closest building in the village to the mine) and south border of the mine is 1069 m and the distance between GK5 and the center of the open pit is 1735 m. The lowest measured frequency value is 4.625 Hz on this path and the allowable PPV is 19 mm/s for this frequency value. However, it was aimed not to exceed at worst 5.00 mm/s or normally 3.00 mm/s since some of the buildings in the village was constructed by using mud mortar and rubble stone. For example, if the distance between GK5 station and the blast site is 1500 m and 5.00 mm/s was decided as the PPV limit, the safe amount of explosive that can be blasted at the same time is 1843.45 kg.

5.1.3.2 Gümüşkol Village Path 1– behind the pit analysis

The highest PPV level measured at GK4 station from production blasting is 0.968 mm/s (radial component) with 34.63 Hz predominant frequency (at 1653.78 m). According to US OSM Regulations (Figure 2.17) for 34.63 Hz frequency value, maximum allowable ground vibration level is 50.0 mm/s.

SD vs PPV graph was used to determine propagation-attenuation equation for stripping-production blasts on this path (Figure 5.19). The attenuation relation for behind the pit blasts is PPV = $110800 \cdot SD^{-2.623}$. Distance-explosive amount graph obtained from this equation for various PPV values is shown in Figure 5.20. This graph is used to determine the safe explosive amount per delay when the distance between the blast site and the relevant structure is known. The distance between GK5 station (the closest building in the village to the mine) and north border of the mine is 2050 m and the distance between GK5 and the center of the open pit is 1735 m.

The lowest measured frequency value is 19 Hz on this path and the allowable PPV is 33.7 mm/s for this frequency value. However, it was aimed not to exceed at worst 5.00 mm/s or normally 3.00 mm/s since some of the buildings in the village was constructed by using mud mortar and rubble stone. For example, if the distance between GK5 station and the blast site is 1900 m and 5.00 mm/s was decided as the PPV limit, the safe amount of explosive that can be blasted at the same time is 1756.38 kg.
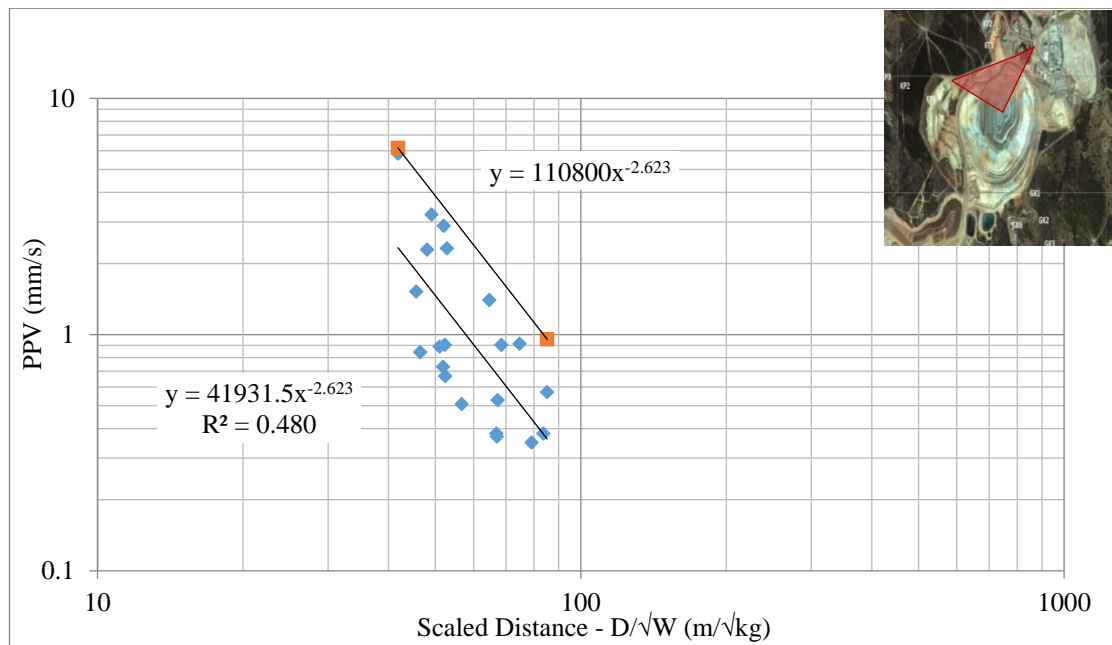
Figure 5.19 Gümüşkol Path 1 production blasting PPV values (Pit location- WNW, N, NNE- behind the pit)
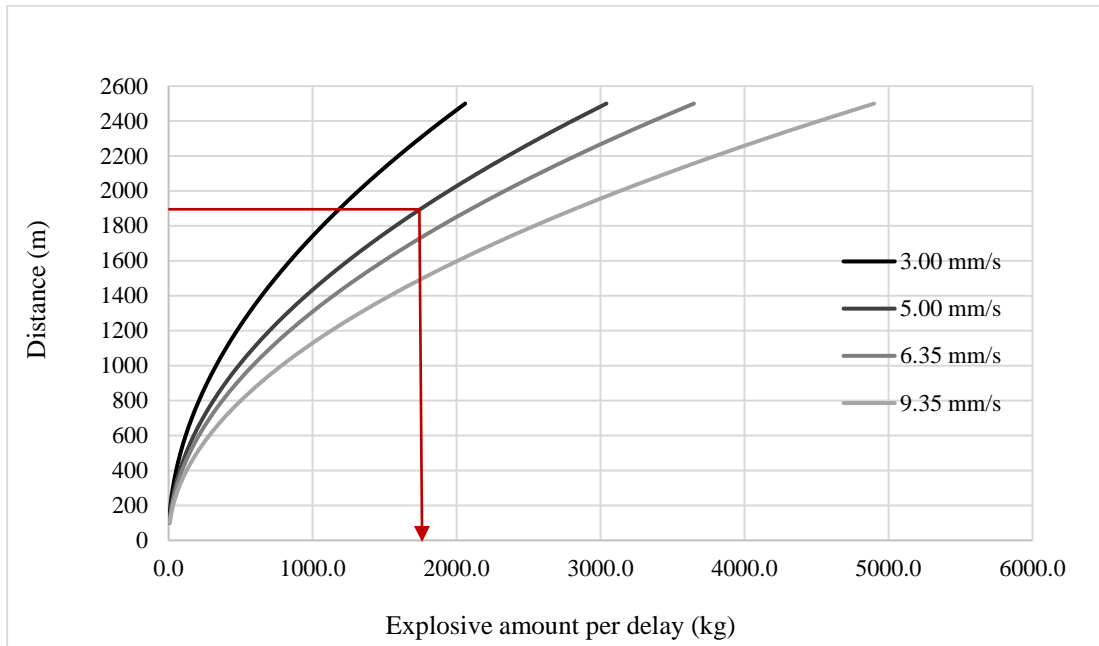
Figure 5.20 Safe explosive amounts for Gümüşkol village Path 1 for 'behind the pit' blasts

5.1.4 Gümüşkol Village Path 2

80 ground vibration records have been obtained from production blasts. Production blasts were conducted at minimum 1242.0 m and maximum 1807.0 m horizontal distances to this village. In production blasting both ground vibration and air blast are felt from this village. The maximum PPV level from production blasting is 1.490 mm/s (transverse component) with 13.13 Hz predominant frequency (at 1641.16 m). According to US OSM Regulations (Figure 2.17) for 13.13 Hz frequency value, maximum allowable ground vibration level is 25.17 mm/s.

Ground vibration data from production blasts were divided into two parts according to location of blast holes within the pit with respect to the settlement location; i.e. in front of the pit and behind the pit. Figure 5.21 shows behind the pit and in front of the pit concepts for Gümüşkol Path 2 monitoring line.

106

Figure 5.21 'behind the pit' and 'in front of the pit' concepts for Gümüşkol Path 2

8 different pit classification scenarios were tested and evaluated by using model records and test records and compared to the regression analysis from unclassified data. Table 5.8 shows the directions included in the analysis, line equation and R^2 (square of correlation coefficient, which shows the relation between SD and PPV).

To evaluate the performance of the models; correlation coefficient, coefficient of determination and Root-Mean Square Error (RMSE) were calculated and compared in Table 5.9. All the models gave more or less the same results, but the best result is obtained for model 7 combination. Figure 5.22 shows ground vibration attenuation relation for unclassified production blast data.

Table 5.8 Gümüşkol Path 2 properties of the formed models

	Pit location	Directions included	Line equation	
Unclassified	-	-	$y = 328.8 * x^{-1.36}$	$R^2= 0.559$ $R=-0.748$
Model 1	In front of the pit	WNW, W, S, E, ENE	$y = 142.6 * x^{-1.17}$	$R^2= 0.565$ $R=-0.752$
	Behind the pit	N, NE, NW	$y = 13664.0 * x^{-2.21}$	$R^2= 0.639$ $R=-0.800$
Model 2	In front of the pit	SSW, S, E, ENE	$y = 365.7 * x^{-1.42}$	$R^2= 0.689$ $R=-0.830$
	Behind the pit	SW, W, NW, N, NE	$y = 781.9 * x^{-1.55}$	$R^2= 0.475$ $R=-0.689$
Model 3	In front of the pit	WSW, S, E, ENE	$y = 202.8 * x^{-1.26}$	$R^2= 0.623$ $R=-0.789$
	Behind the pit	W, NW, N, NE	$y = 4197.5 * x^{-1.94}$	$R^2= 0.517$ $R=-0.719$
Model 4	In front of the pit	SW, S, E, ENE	$y = 185.6 * x^{-1.23}$	$R^2= 0.632$ $R=-0.795$
	Behind the pit	WSW, W, NW, N, NE	$y = 1538.1 * x^{-1.72}$	$R^2= 0.468$ $R=-0.684$
Model 5	In front of the pit	SE, SSE, S, SSW	$y = 472.8 * x^{-1.48}$	$R^2= 0.692$ $R=-0.832$
	Behind the pit	N, NE, ESE, SW, W, NNW	$y = 423.6 * x^{-1.42}$	$R^2= 0.448$ $R=-0.669$
Model 6	In front of the pit	ESE, S, SSW	$y = 472.8 * x^{-1.48}$	$R^2= 0.692$ $R=-0.832$
	Behind the pit	N, NE, E, SW, W, NNW	$y = 423.6 * x^{-1.42}$	$R^2= 0.448$ $R=-0.669$
Model 7	In front of the pit	SE, SSE, S	$y = 649.1 * x^{-1.55}$	$R^2= 0.623$ $R=-0.789$
	Behind the pit	N, NE, ESE, SSW, W, NNW	$y = 309.5 * x^{-1.35}$	$R^2= 0.511$ $R=-0.715$
Model 8	In front of the pit	SE, SSE	$y = 784.9 * x^{-1.59}$	$R^2= 0.530$ $R=-0.728$
	Behind the pit	N, NE, E, S, SW, W, NNW	$y = 307.1 * x^{-1.35}$	$R^2= 0.555$ $R=-0.745$

Table 5.9 Gümüşkol Path 2 performance indicators for the models

	Modelling Set			Testing Set		
	R	**r^2**	**RMSE**	**R**	**r^2**	**RMSE**
Unclassified	0.739	0.522	0.639	0.956	0.649	0.632
Model 1	0.808	0.637	0.557	0.946	0.523	0.737
Model 2	0.748	0.542	0.626	0.966	0.552	0.714
Model 3	0.792	0.613	0.575	0.949	0.545	0.720
Model 4	0.755	0.555	0.617	0.949	0.561	0.707
Model 5	0.737	0.518	0.642	0.961	0.600	0.675
Model 6	0.737	0.518	0.642	0.961	0.600	0.675
Model 7	**0.738**	**0.518**	**0.642**	**0.958**	**0.694**	**0.590**
Model 8	0.742	0.523	0.638	0.959	0.660	0.622
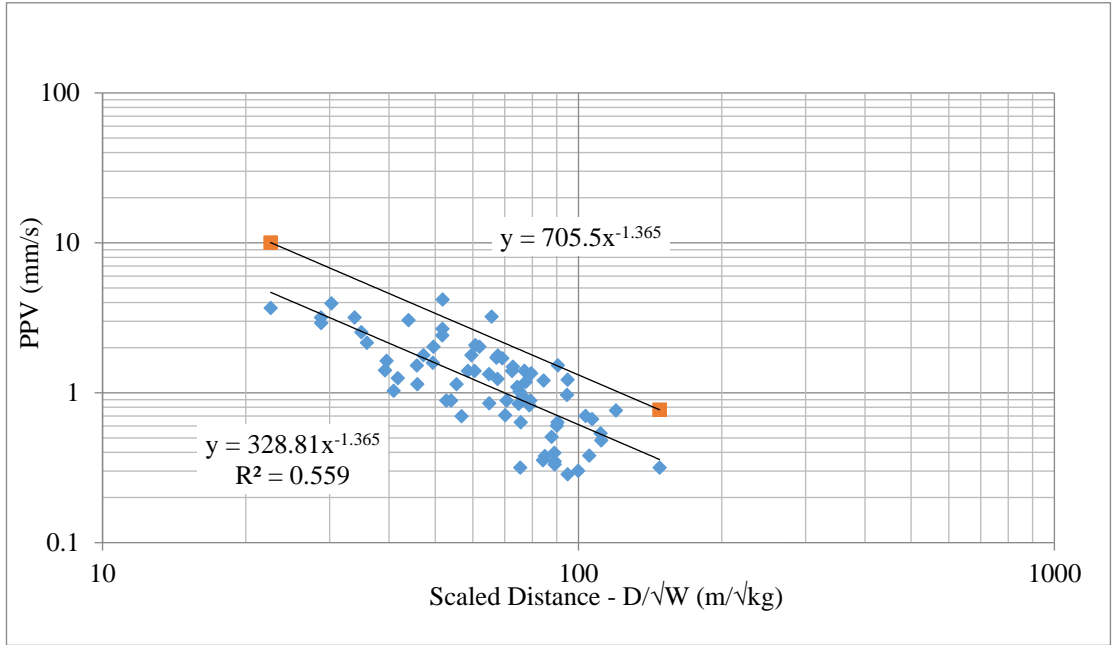
Figure 5.22 Gümüşkol Path 2 unclassified production blasting PPV values

5.1.4.1 Gümüşkol Village Path 2– in front of the pit analysis

The highest PPV level measured at Sami Y.'s house from production blasts is 1.413 mm/s (transverse component) with 18.13 Hz predominant frequency (at 1262.03 m). According to US OSM Regulations (Figure 2.17) for 18.13 Hz frequency value, maximum allowable ground vibration level is 33.87 mm/s.

SD vs PPV graph was used to determine propagation-attenuation equation for stripping-production blasts on this path (Figure 5.23). The attenuation relation for in front of the pit blasts is PPV = $1367.6 \ast SD^{-1.549}$. Distance-explosive amount graph obtained from this equation for various PPV values is shown in Figure 5.24. This graph is used to determine the safe explosive amount per delay when the distance between the blast site and the relevant structure is known. The distance between Ismail Y.'s house station (the closest building in the village to the mine) and south border of the mine is 880 m and the distance between Ismail Y.'s house and the center of the open pit is 1597 m.
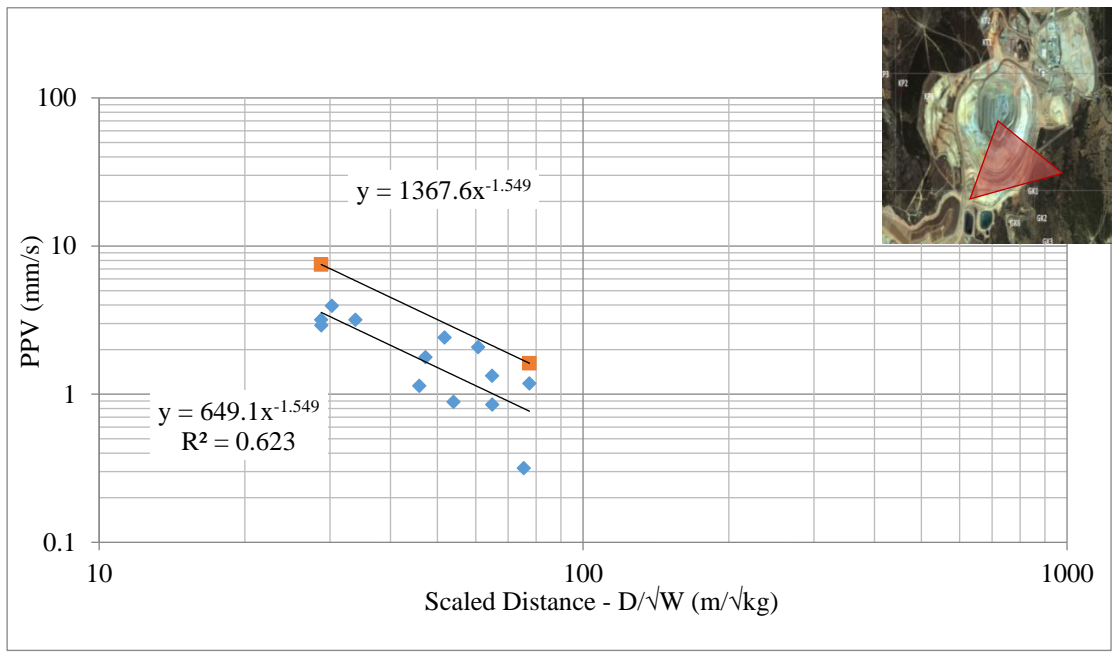
Figure 5.23 Gümüşkol Path 2 production blasting PPV values (Pit location- S, SSE, SE - in front of the pit)
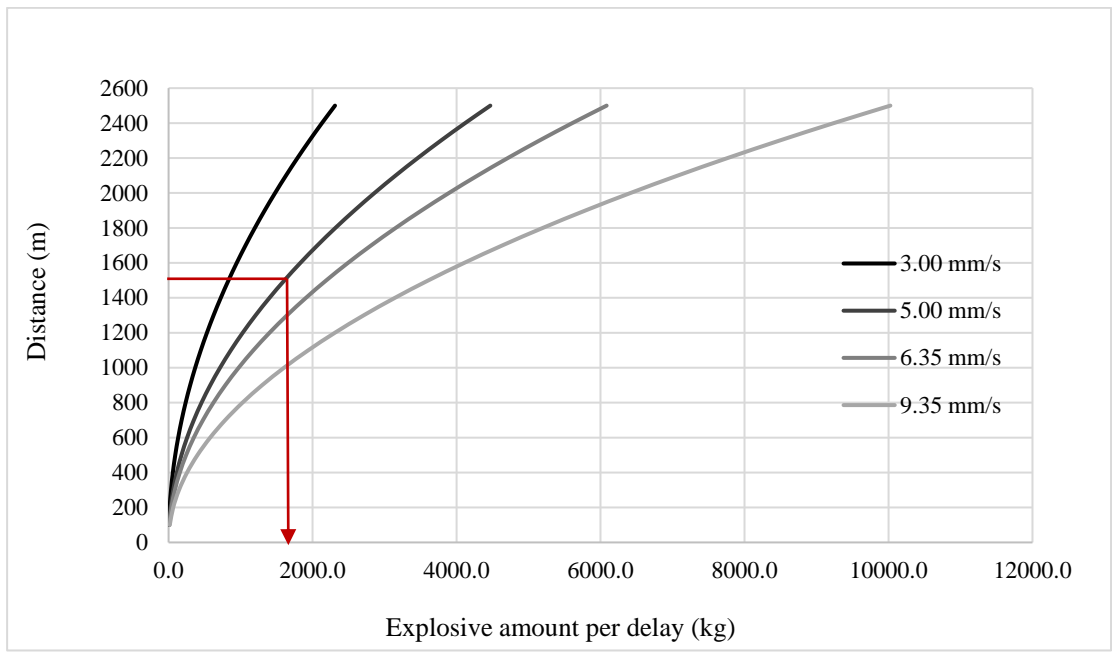
Figure 5.24 Safe explosive amounts for Gümüşkol village Path 2 for 'in front of the pit' blasts

The lowest measured frequency value is 10 Hz on this path and the allowable PPV is 19 mm/s for this frequency value. However, it was aimed not to exceed at worst 5.00 mm/s or normally 3.00 mm/s since some of the buildings in the village was constructed by using mud mortar and rubble stone.

For example, if the distance between Ismail Y.'s house and the explosion is 1500 m and 5.00 mm/s was decided as the PPV limit, the safe amount of explosive that can be blasted at the same time is 1608.98 kg.

5.1.4.2 Gümüşkol Village Path 2– behind the pit analysis

The highest PPV level measured at Sami Y.'s house from production blasts is 1.490 mm/s (transverse component) with 13.13 Hz predominant frequency (at 1641.16 m). According to US OSM Regulations (Figure 2.17) for 13.13 Hz frequency value, maximum allowable ground vibration level is 25.17 mm/s.

$y = 673.75x^{-1.349}$

$y = 309.51x^{-1.349}$
$R^2 = 0.511$
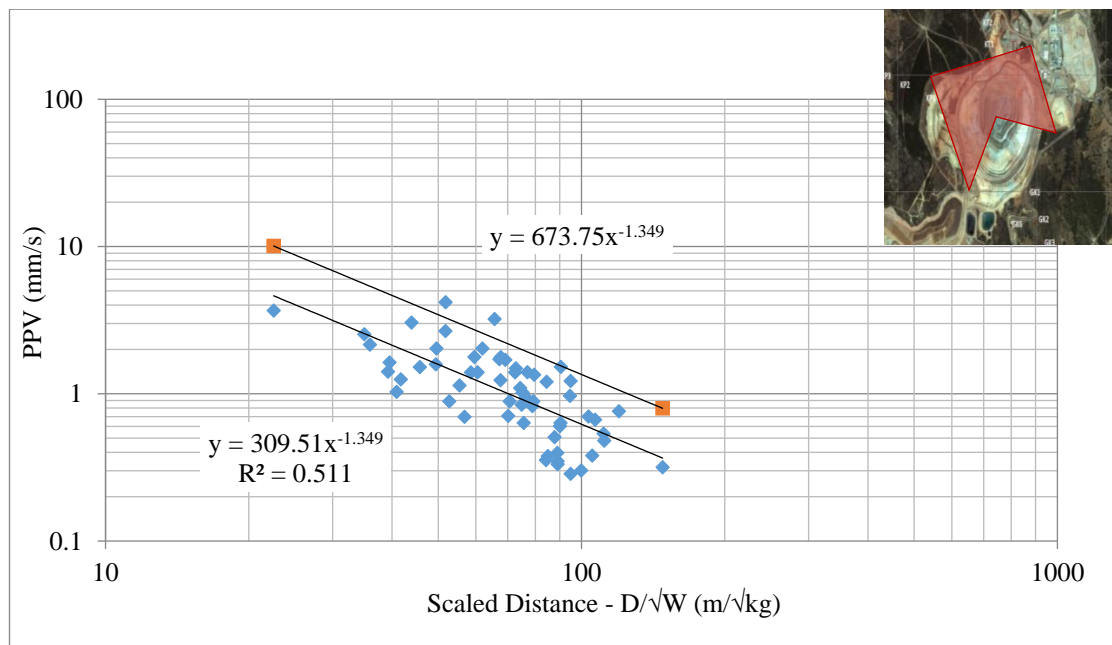
Figure 5.25 Gümüşkol Path 2 production blasting PPV values (Pit location- N, E, ESE, SSW, W, NNW- behind the pit)

SD vs PPV graph was used to determine propagation-attenuation equation for stripping-production blasts on this path (Figure 5.25). The attenuation relation for behind the pit blasts is PPV = $673.75*SD^{-1.349}$. Distance-explosive amount graph obtained from this equation for various PPV levels is shown in Figure 5.26. This graph is used to determine the safe explosive amount per delay when the distance between the blast site and the relevant structure is known. The distance between Ismail Y.'s house (the closest building in the village to the mine) and north border of the mine is 1912 m and the distance between Ismail Y.'s house and the center of the open pit is 1597 m.

The lowest measured frequency value is 6.25 Hz on this path and the allowable PPV is 19 mm/s for this frequency value. However, it was aimed not to exceed at worst 5.00 mm/s or normally 3.00 mm/s since some of the buildings in the village was constructed by using mud mortar and rubble stone. For example, if the distance between Ismail Y.'s house and the blast site is 1700 m and 5.00 mm/s was decided as the PPV limit, the safe amount of explosive that can be blasted at the same time is 2008.24 kg.
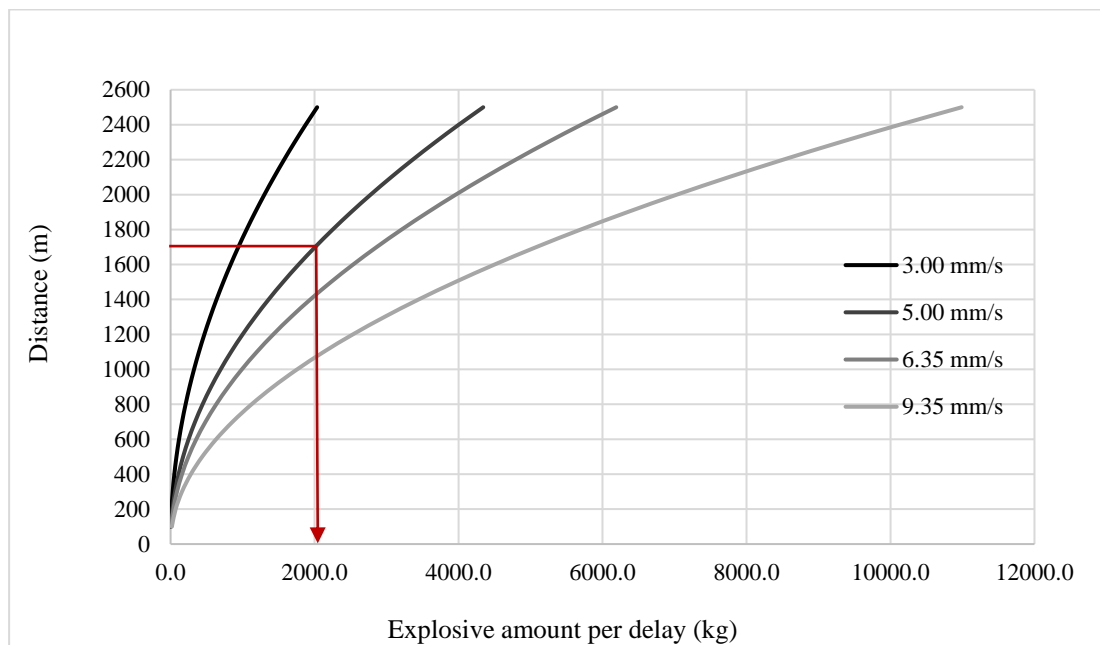
Figure 5.26 Safe explosive amounts for Gümüşkol village Path 2 for 'behind the pit' blasts

5.2 Air Shock Analyses

For air shock analyses logarithmic plots of cube root scaled distance versus air blast level are obtained. Two propagation equations are obtained for each dataset these are mean value equation (belonging to the below line) and 95% confidence interval line equation (belonging the upper line) (can be seen in Figure 5.27). These equations are in the form of Air blast level (dB) $= Kx(SD)^{-a}$, where K is the site constant and a is the site exponent. 95% confidence interval line equation is used to predict air blast level for future blasts. Air shock analyses were performed on presplit and production blasting data. The results will be presented for presplit and production blasts separately in the following sections.

5.2.1 Presplit Blasting

Before detailed air shock analyses, all the collected data were analyzed in the same graph regardless of the location of the monitoring station (Figure 5.27). The performance indicators calculated for modelling and testing set are given in Table 5.10.
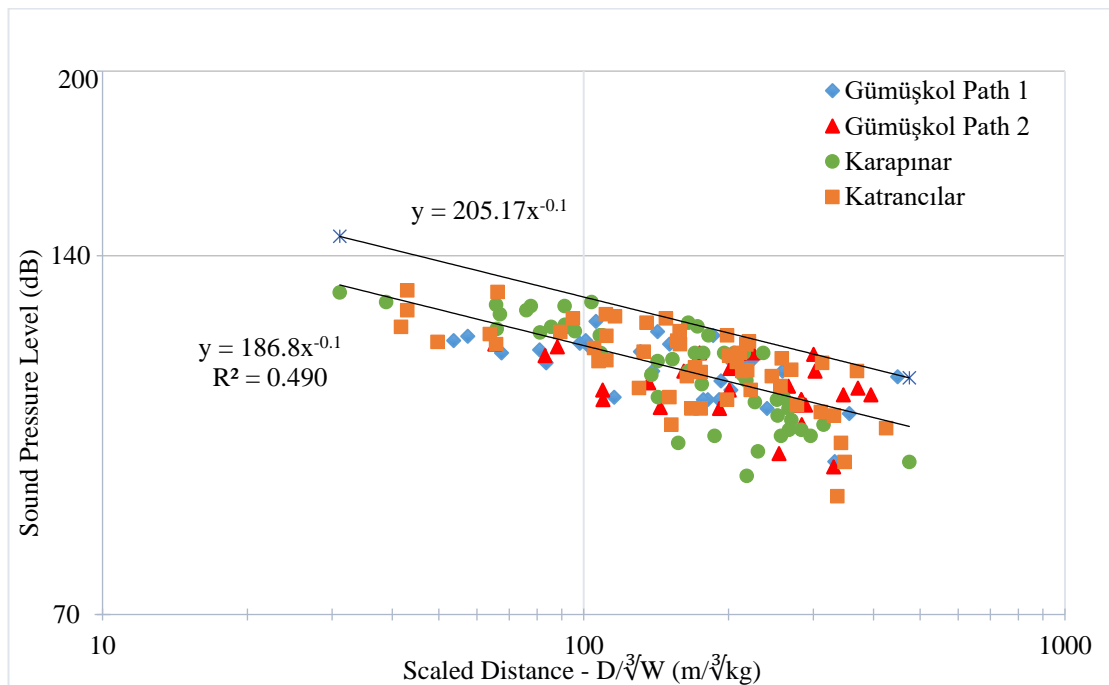
Figure 5.27 Air shock prediction from whole presplit blast data

113

These values are later compared to classified regression analyses for which the blast group location classification given in Figure 5.2 is used.

Table 5.10 Performance indicators for the whole-data model

		R	r^2	RMSE
Whole data	Modelling Set	0.708	0.501	6.191
	Testing set	0.718	0.496	6.553

5.2.1.1 Katrancılar Village

58 air blast records were obtained from presplit blasts. Presplit blasts were performed at minimum 1453.4 m and at maximum 2002.5 m horizontal distances to this village. In Katrancılar, the maximum air blast overpressure level from presplit blasts at the house nearest to the pit border from presplit blasting is 112 dB with 6.5 Hz predominant frequency (at 1824.0 m). Air blast levels from presplit blasts are lower than the permitted values given in US OSM Regulations (133 dB) (in Table 2.7). Moreover, they are even less than the threshold level of complaints (117 dB) (in Figure 2.22).

For air shock analyses both the effects of location of blast group within the pit and wind direction classification were tested. 8 different pit classification scenarios were compared to the regression analysis from unclassified data by using model set and test set. Table 5.11 shows the directions included in the analysis, line equation and R^2 (square of correlation coefficient).

To evaluate the performance of the models; correlation coefficient, coefficient of determination and Root-Mean Square Error (RMSE) were calculated and compared in Table 5.12. The best result is obtained for model 1 combination. Moreover, it can be said that blast group location serves better classification than wind direction classification.

Table 5.11 Katrancılar properties of the formed models

	Pit location	Directions included	Line equation		
Unclassified	-	-	$y = 184.1 * x^{-0.10}$	$R^2= 0.478$	R=-0.691
Model 1	In front of the pit	N, NE, SW, W, NW, NNW	$y = 389.1 * x^{-0.23}$	$R^2= 0.618$	R=-0.786
	Behind the pit	ENE, E, SE, S, SSW	$y = 178.8 * x^{-0.09}$	$R^2= 0.522$	R=-0.722
Model 2	In front of the pit	N, NE, W, NW, NNW	$y = 193.4 * x^{-0.11}$	$R^2= 0.644$	R=-0.802
	Behind the pit	ENE, E, SE, S, SSW, SW, WSW	$y = 315.4 * x^{-0.19}$	$R^2= 0.555$	R=-0.745
Model 3	In front of the pit	N, NE, WSW, W, NW, NNW	$y = 182.1 * x^{-0.10}$	$R^2= 0.574$	R=-0.758
	Behind the pit	ENE, E, SE, S, SW	$y = 356.5 * x^{-0.21}$	$R^2= 0.624$	R=-0.790
Model 4	In front of the pit	N, NE, E, ESE, NW, NNW	$y = 197.1 * x^{-0.12}$	$R^2= 0.665$	R=-0.815
	Behind the pit	SE, S, SW, WSW, W	$y = 288.8 * x^{-0.18}$	$R^2= 0.607$	R=-0.779
Model 5	In front of the pit	N, NE, ENE, W, NW, NNW	$y = 193.4 * x^{-0.11}$	$R^2= 0.644$	R=-0.802
	Behind the pit	E, SE, S, SW, WSW	$y = 315.4 * x^{-0.19}$	$R^2= 0.555$	R=-0.745
Model 6	In front of the pit	N, NE, E, WNW, NW, NNW	$y = 197.1 * x^{-0.12}$	$R^2= 0.665$	R=-0.815
	Behind the pit	ESE, SE, S, SW, W	$y = 288.8 * x^{-0.18}$	$R^2= 0.607$	R=-0.779
Model 7	In front of the pit	N, NE, WNW, NW, NNW	$y = 197.1 * x^{-0.12}$	$R^2= 0.665$	R=-0.815
	Behind the pit	ENE, E, SE, S, SW, W	$y = 288.8 * x^{-0.18}$	$R^2= 0.607$	R=-0.779
Model 8	In front of the pit	N, NE, ENE, WNW, NW, NNW	$y = 197.1 * x^{-0.12}$	$R^2= 0.665$	R=-0.815
	Behind the pit	E, SE, S, SSW, SW, W	$y = 288.8 * x^{-0.18}$	$R^2= 0.607$	R=-0.779
Model 9	Northern winds	N, NE, NW	$y = 184.57 *x^{-0.1}$	$R^2 = 0.417$	R=-0.646
(Wind direction Classification)	Southern winds	WSW, W, SSE, S	$y = 170.63*x^{-0.08}$	$R^2 = 0.563$	R=-0.750

Figure 5.28 shows air blast attenuation relation before classification of the data. The graph for presplit blasts when winds blown from north is given in Figure 5.29. The minimum and the maximum northern wind speed were 2.668 m/s and 6.808 m/s, respectively. The graph for presplit blasts for southern winds is given in Figure 5.30. The minimum and the maximum southern wind speed were 2.825 m/s and 7.244 m/s, respectively. Figure 5.31 and Figure 5.32 show regression analyses for 'in front of the pit' and 'behind the pit' blast groups for model 1, respectively. Analysis for 'in front of the pit' case gives higher correlation.

Table 5.12 Katrancılar performance indicators for the models

	Modelling Set			Testing Set		
	R	**r²**	**RMSE**	**R**	**r²**	**RMSE**
Unclassified	0.697	0.485	6.356	0.707	0.455	6.802
Model 1	**0.765**	**0.585**	**5.706**	**0.705**	**0.442**	**6.880**
Model 2	0.788	0.620	5.461	0.687	0.365	7.343
Model 3	0.783	0.613	5.512	0.736	0.420	7.017
Model 4	0.806	0.649	5.247	0.652	0.315	7.627
Model 5	0.788	0.620	5.461	0.687	0.365	7.343
Model 6	0.806	0.649	5.247	0.652	0.315	7.627
Model 7	0.806	0.649	5.247	0.652	0.315	7.627
Model 8	0.806	0.649	5.247	0.652	0.315	7.627
Model 9	0.707	0.500	6.268	0.707	0.439	6.904
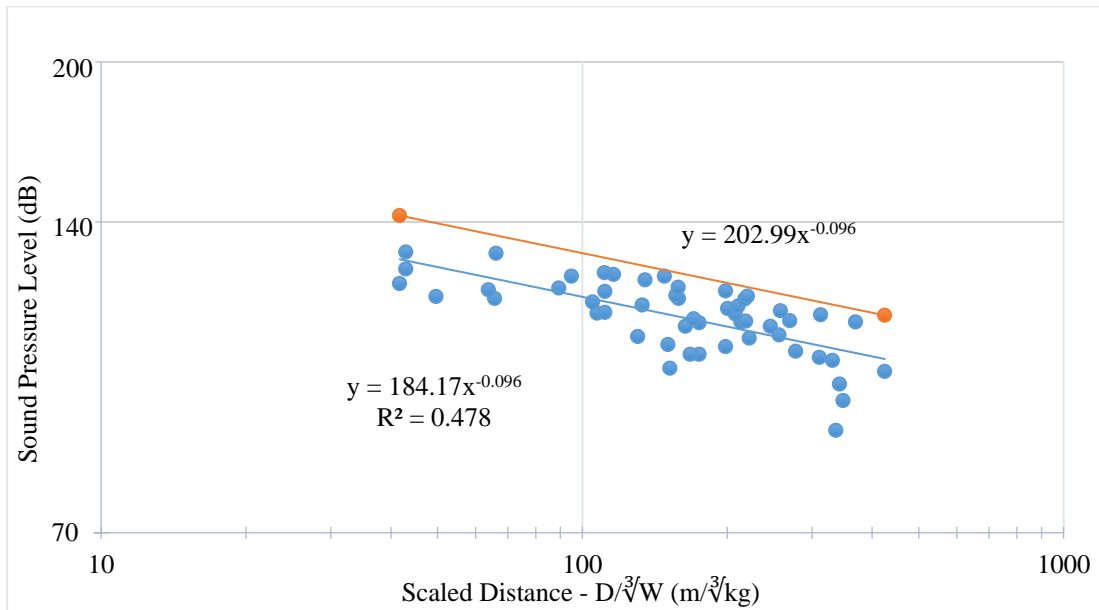
Figure 5.28 Katrancılar unclassified presplit blasting air blast overpressure levels in dB

116

$$y = 205.08x^{-0.097}$$

$$y = 184.57x^{-0.097}$$
$$R^2 = 0.417$$

Figure 5.29 Katrancılar presplit blasting air blast overpressure levels in dB (Northern winds-N, NE, NW)

$$y = 183.04x^{-0.077}$$

$$y = 170.63x^{-0.077}$$
$$R^2 = 0.563$$
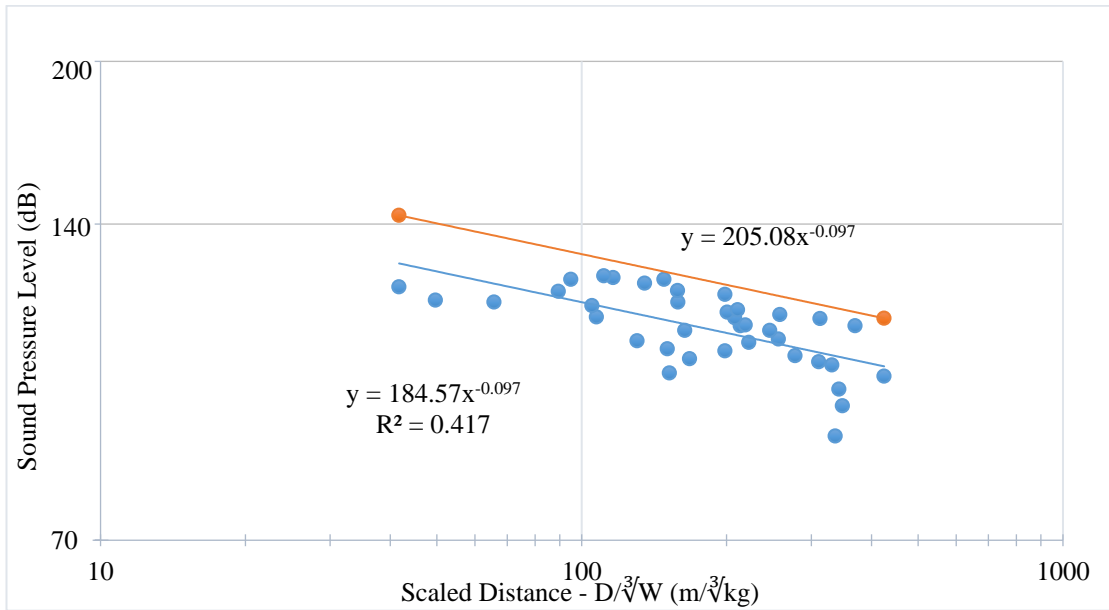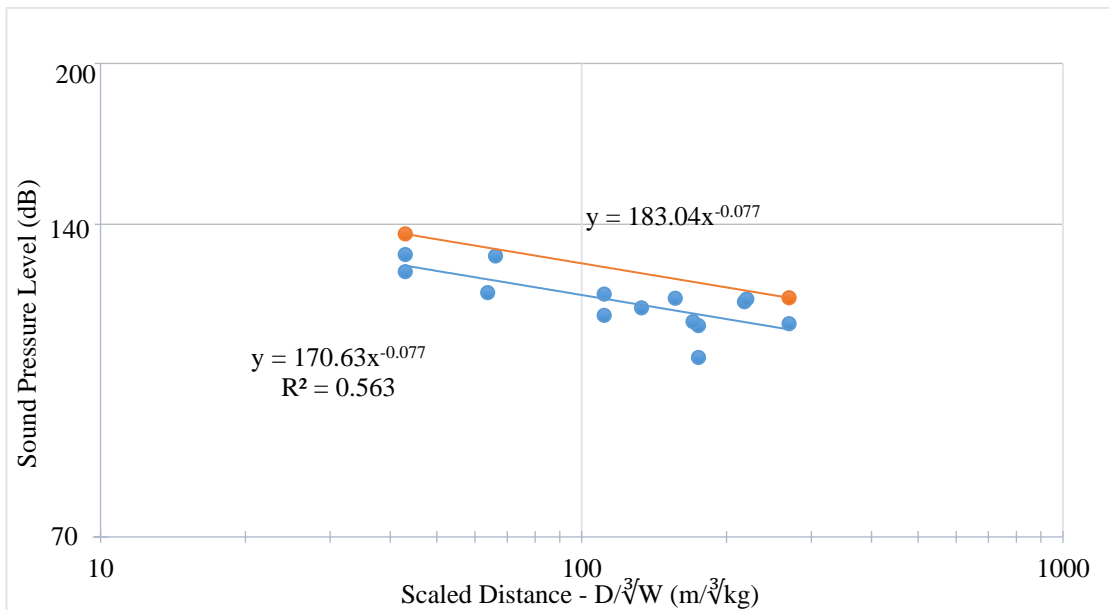
Figure 5.30 Katrancılar presplit blasting air blast overpressure levels in dB (Southern winds-WSW, W, SSE, S)
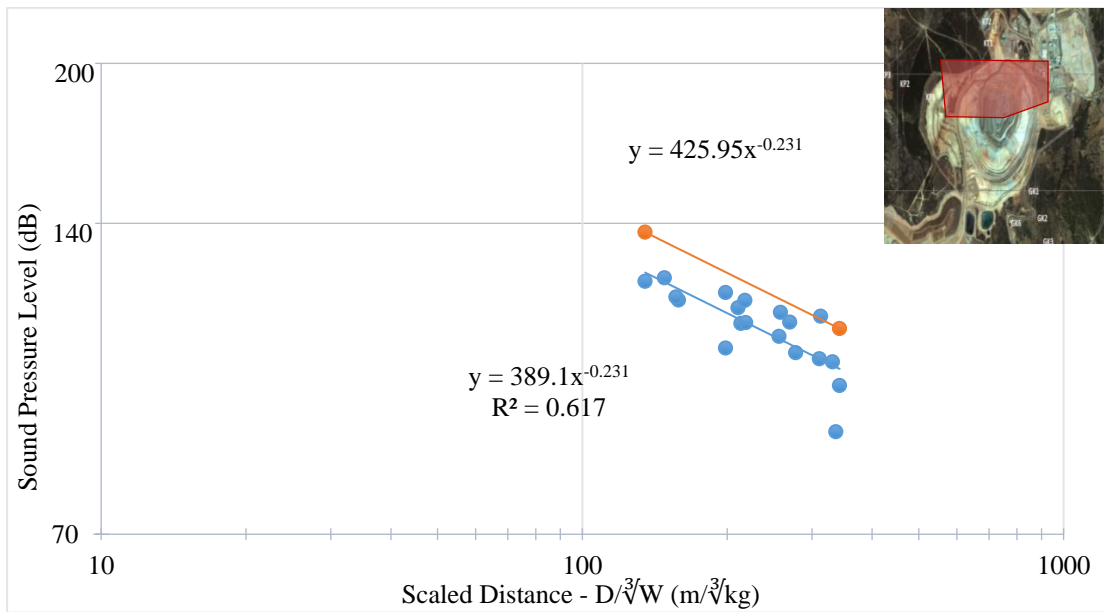
Figure 5.31 Katrancılar presplit blasting air blast overpressure levels in dB (Pit location- NE, N, NW, W- in front of the pit)

In the first figure the fitted equations are:

$$y = 425.95x^{-0.231}$$

$$y = 389.1x^{-0.231}$$
$$R^2 = 0.617$$
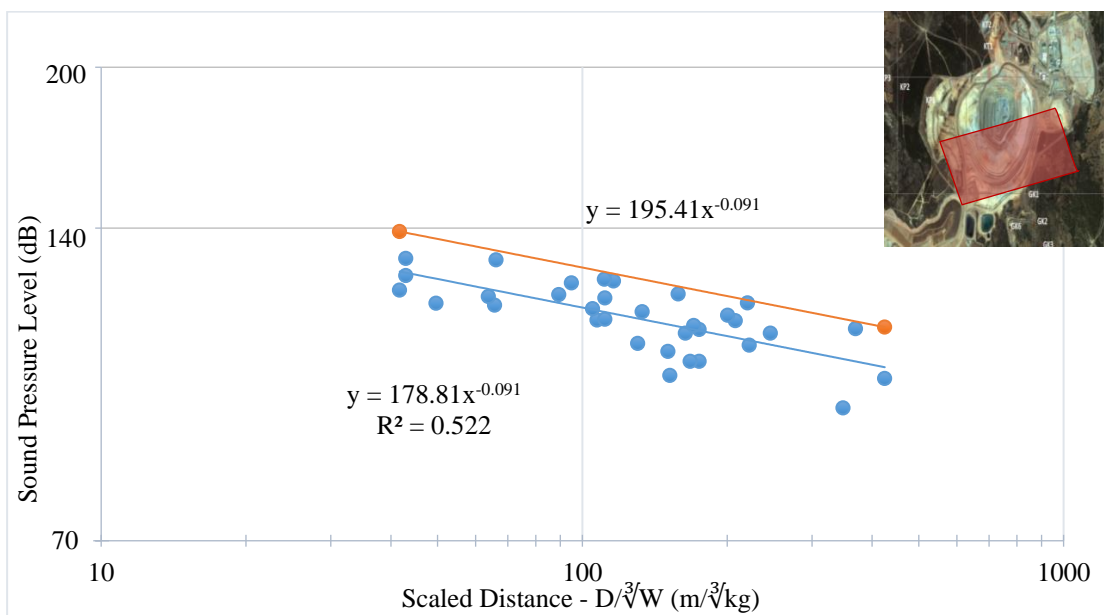
Figure 5.32 Katrancılar presplit blasting air blast overpressure levels in dB (Pit location- S, E, ENE, SSW - behind the pit)

In the second figure the fitted equations are:

$$y = 195.41x^{-0.091}$$

$$y = 178.81x^{-0.091}$$
$$R^2 = 0.522$$

5.2.1.2 Karapınar Village

56 air blast records were obtained from presplit blasts which are conducted at minimum 1078.9 m and maximum 2289.0 m horizontal distances to this village. In Karapınar, the maximum air blast overpressure level at the nearest house to the pit border is 112 dB with 12.38 Hz predominant frequency (at 1078.9 m). Air blast levels from presplit blasts are below the values given in US OSM Regulations (129 dB) (in Table 2.7). Moreover, they are even less than the threshold level of complaints (117 dB) (in Figure 2.22).

For air shock analyses both the effects of blast group location within the pit and wind direction classification were tested. 9 different pit classification scenarios were evaluated by using model set and test set and compared to the regression analysis from unclassified data. Table 5.13 shows the directions included in the analysis, line equation and R^2 (square of correlation coefficient). To evaluate the performance of the models; correlation coefficient, coefficient of determination and Root-Mean Square Error (RMSE) were calculated and compared in Table 5.14. The best result is obtained for model 9 combination.

Figure 5.33 shows air blast attenuation relation from the unclassified data. The graph for air blast analysis of presplit blasts when winds blown from west is given in Figure 5.34. The minimum and the maximum western wind speed were 2.471 m/s and 7.918 m/s, respectively.

The graph for presplit blast air blast analysis for eastern winds is given in Figure 5.35. The minimum and the maximum eastern wind speed were 0.792 m/s and 6.808 m/s, respectively. Figure 5.36 and Figure 5.37 show regression analyses for blast groups in front of the pit and behind the pit for model 9, respectively. Analysis for 'in front of the pit' case provides higher correlation.

Table 5.13 Karapınar properties of the formed models

	Pit location	Directions included	Line equation	
Unclassified	-	-	$y = 222.0 * x^{-0.14}$	$R^2= 0.643$ R=-0.802
Model 1	In front of the pit	NNE, N, W, S, SSE	$y = 225.7 * x^{-0.14}$	$R^2= 0.670$ R=-0.819
	Behind the pit	NE, E, SE	$y = 355.8 * x^{-0.21}$	$R^2= 0.758$ R=-0.871
Model 2	In front of the pit	N, W, S, SSE	$y = 224.3 * x^{-0.14}$	$R^2= 0.659$ R=-0.812
	Behind the pit	NNE, NE, E, SE	$y = 380.2 * x^{-0.23}$	$R^2= 0.734$ R=-0.857
Model 3	In front of the pit	NE, N, W, S, SSE	$y = 225.1 * x^{-0.14}$	$R^2= 0.679$ R=-0.824
	Behind the pit	ENE, E, SE	$y = 117.9 * x^{-0.004}$	$R^2= 0.0001$ R=-0.01
Model 4	In front of the pit	NNE, N, W, SSW	$y = 225.7 * x^{-0.14}$	$R^2= 0.670$ R=-0.819
	Behind the pit	NE, E, SE, S	$y = 355.8 * x^{-0.21}$	$R^2= 0.758$ R=-0.871
Model 5	In front of the pit	NNW, W, S, SSE	$y = 221.3 * x^{-0.14}$	$R^2= 0.666$ R=-0.816
	Behind the pit	N, NE, E, SE	$y = 356.6 * x^{-0.22}$	$R^2= 0.564$ R=-0.751
Model 6	In front of the pit	NNE, N, W, S	$y = 225.7 * x^{-0.14}$	$R^2= 0.670$ R=-0.819
	Behind the pit	NE, E, SE, SSE	$y = 355.8 * x^{-0.21}$	$R^2= 0.758$ R=-0.871
Model 7	In front of the pit	NNW, W, SSW	$y = 221.3 * x^{-0.14}$	$R^2= 0.666$ R=-0.816
	Behind the pit	N, E, S	$y = 356.6 * x^{-0.22}$	$R^2= 0.564$ R=-0.751
Model 8	In front of the pit	N, W, SSW	$y = 224.3 * x^{-0.14}$	$R^2= 0.659$ R=-0.812
	Behind the pit	NNE, E, S	$y = 380.2 * x^{-0.23}$	$R^2= 0.734$ R=-0.857
Model 9	In front of the pit	SW, W, NNW	$y = 224.2 * x^{-0.14}$	$R^2= 0.695$ R=-0.834
	Behind the pit	N, E, SSW	$y = 433.7 * x^{-0.25}$	$R^2= 0.636$ R=-0.797
Model 10	Western winds	W, SSW, NW, SW, NNW	$y = 240.8 * x^{-0.152}$	$R^2 = 0.686$ R=-0.828
(Wind direction Classification)	Eastern winds	N, NE, E, SSE, SE	$y = 201.9 * x^{-0.116}$	$R^2 = 0.600$ R=-0.775

Table 5.14 Karapınar performance indicators for the models

	Modelling Set			Testing Set		
	R	**r²**	**RMSE**	**R**	**r²**	**RMSE**
Unclassified	0.806	0.649	6.204	0.886	0.701	6.194
Model 1	0.840	0.706	5.679	0.900	0.711	6.088
Model 2	0.823	0.677	5.948	0.885	0.677	6.437
Model 3	0.822	0.675	5.969	0.891	0.716	6.039
Model 4	0.826	0.682	5.902	0.921	0.739	5.791
Model 5	0.818	0.669	6.023	0.906	0.717	6.025
Model 6	0.826	0.682	5.902	0.921	0.739	5.791
Model 7	0.818	0.669	6.023	0.906	0.717	6.025
Model 8	0.823	0.677	5.948	0.885	0.677	6.437
Model 9	**0.826**	**0.682**	**5.902**	**0.921**	**0.739**	**5.791**
Model 10	0.816	0.666	6.050	0.885	0.719	6.004
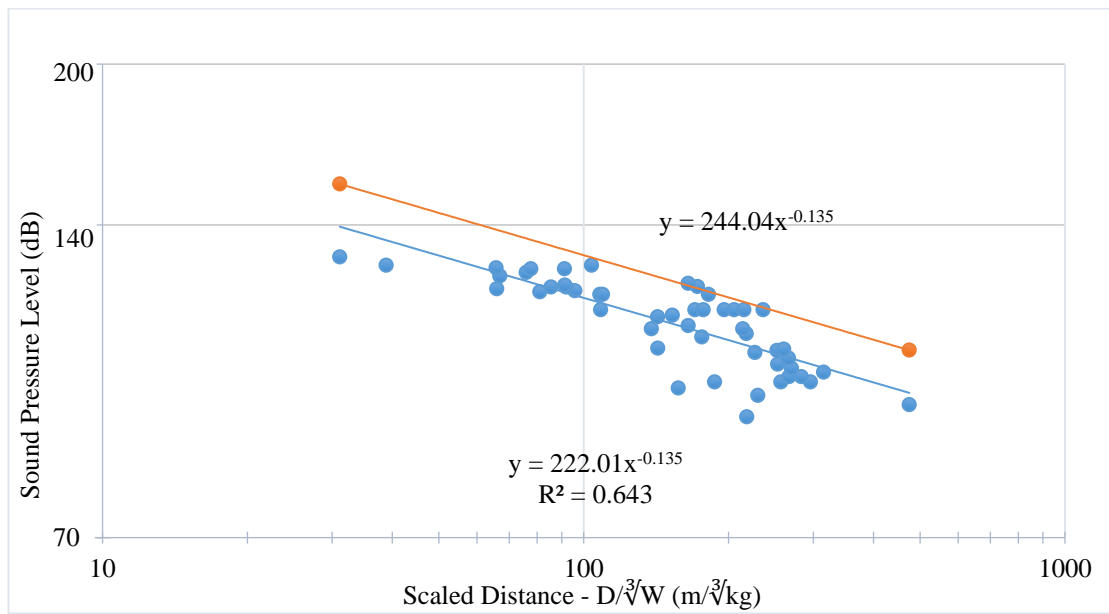
Figure 5.33 Karapınar unclassified presplit blasting air blast overpressure levels in dB

$$y = 244.04x^{-0.135}$$

$$y = 222.01x^{-0.135}$$
$$R^2 = 0.643$$
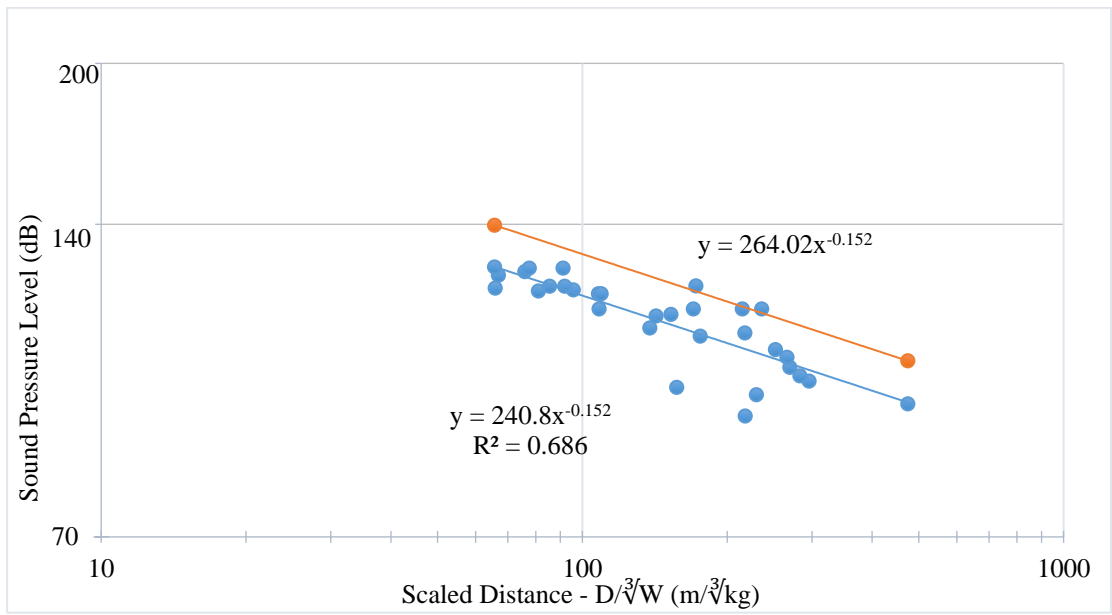
Figure 5.34 Karapınar presplit blasting air blast overpressure levels in dB (Western winds-W, SSW, NW, SW, NNW)
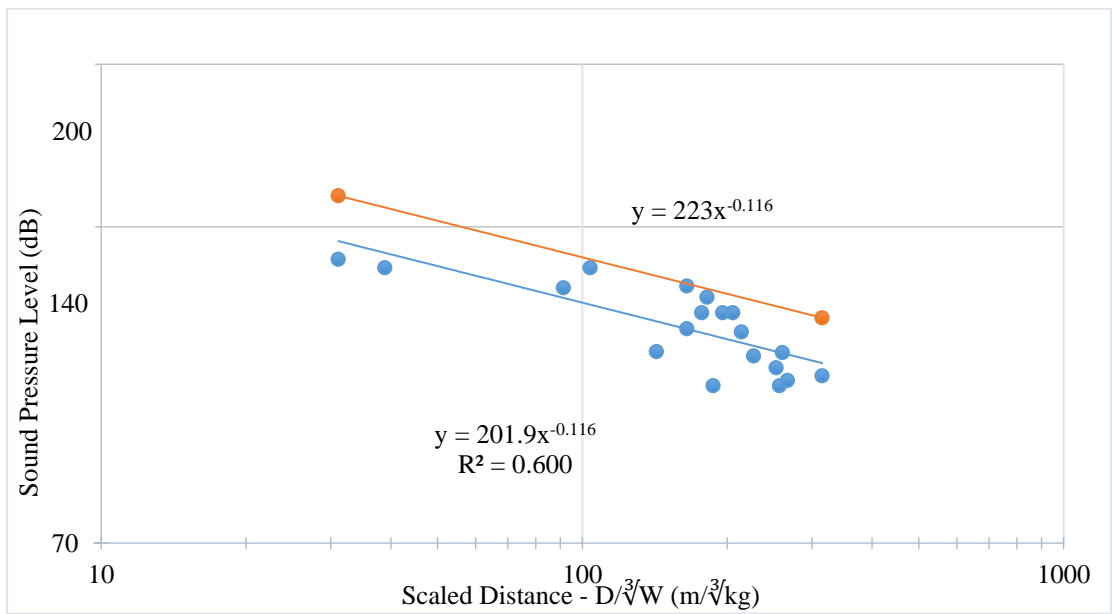
Figure 5.35 Karapınar presplit blasting air blast overpressure levels in dB (Eastern winds-N, NE, E, SSE, SE)
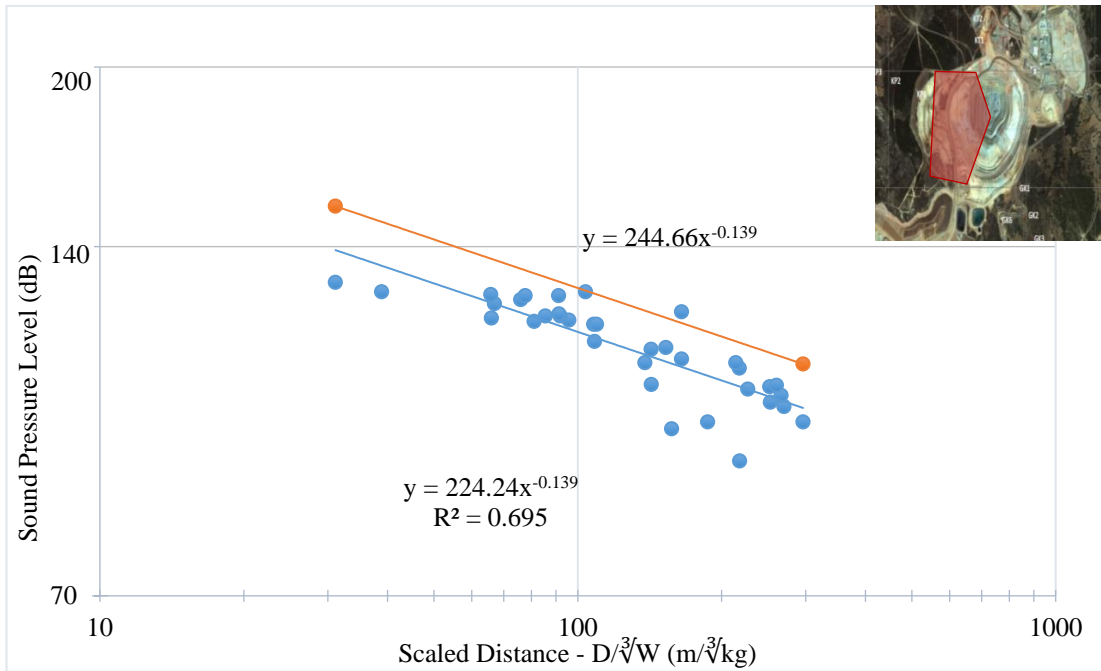
Figure 5.36 Karapınar presplit blasting air blast overpressure levels in dB (Pit location- SW, W, NNW - in front of the pit)
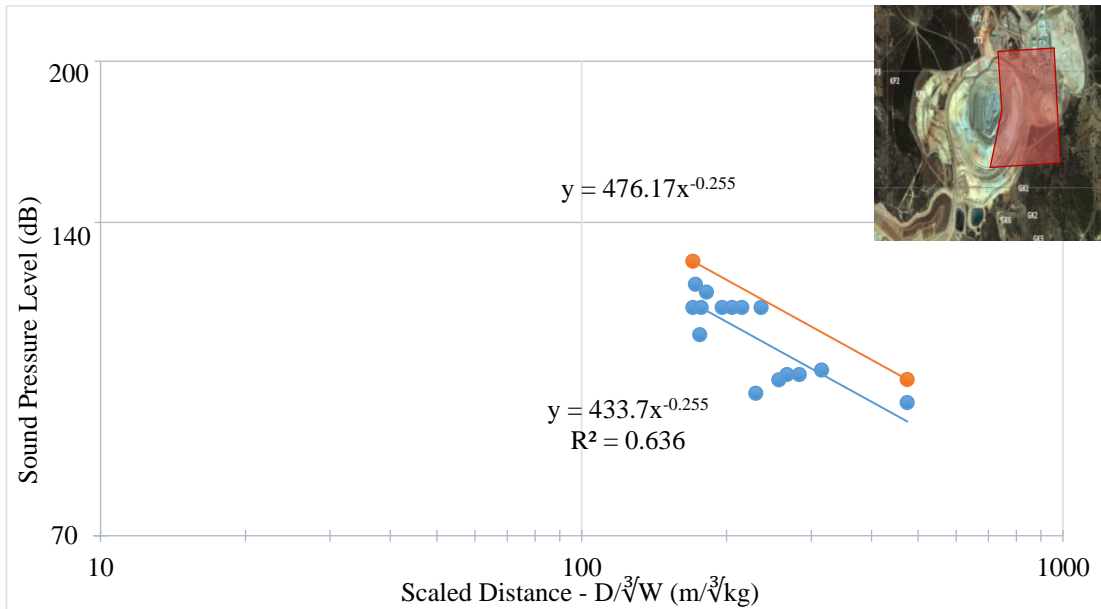
Figure 5.37 Karapınar presplit blasting air blast overpressure levels in dB (Pit location- N, E, SSW - behind the pit)

5.2.1.3 Gümüşkol Village Path 1

For Gümüşkol Path 1, 34 air blast records were obtained from presplit blasts which are conducted at minimum 1944.1 m and maximum 2331 m horizontal distances to this village. The maximum air blast overpressure level at the nearest house to the pit border from presplit blasts is 110.8 dB with 9.81 Hz predominant frequency (at 2331 m). Air blast levels from presplit blasts are below the permitted values given in US OSM Regulations (129 dB) (in Table 2.7). Moreover, they are even less than the threshold level of complaints (117 dB) (in Figure 2.22).

For air shock analyses both blast group location within the pit and wind direction classification were tested. 8 different pit classification scenarios were evaluated by using model set and test set and compared to the regression analysis from unclassified data. Table 5.15 shows the directions included in the analysis, line equation and R^2 (square of correlation coefficient). To evaluate the performance of the models; correlation coefficient, coefficient of determination and Root-Mean Square Error (RMSE) were calculated and compared in Table 5.16 and the best result is obtained for model 7. Moreover, it can be said blast group location serves better classification than wind direction classification.

Figure 5.38 shows air blast attenuation relation for unclassified data. Air blast attenuation graph for northern winds, which is also the dominant wind direction, is given in Figure 5.39. For northern winds the minimum and the maximum wind speed were 2.471 m/s and 7.154 m/s, respectively. Figure 5.40 shows regression analysis of presplit blasts for southern winds. Figure 5.41 and Figure 5.42 show regression analyses for blast groups in front of the pit and behind the pit, respectively. Analysis for 'in front of the pit' case provides higher correlation.

Table 5.15 Gümüşkol Path 1 properties of the formed models

	Pit location	Directions included	Line equation	
Unclassified	-	-	$y = 160.0 * x^{-0.07}$	$R^2 = 0.389$ R=-0.624
Model 1	In front of the pit	SW, S, E, NE	$y = 152.4 * x^{-0.06}$	$R^2 = 0.311$ R=-0.558
	Behind the pit	WSW, W, NW, N, NNE	$y = 201.3 * x^{-0.11}$	$R^2 = 0.275$ R=-0.524
Model 2	In front of the pit	WSW, SW, S, E, NE	$y = 169.5 * x^{-0.08}$	$R^2 = 0.422$ R=-0.650
	Behind the pit	W, NW, N, NNE	$y = 155.5 * x^{-0.06}$	$R^2 = 0.193$ R=-0.439
Model 3	In front of the pit	W, WSW, SW, S, E, NE	$y = 169.1 * x^{-0.08}$	$R^2 = 0.422$ R=-0.650
	Behind the pit	WNW, N, NNE	$y = 160.4 * x^{-0.07}$	$R^2 = 0.185$ R=-0.430
Model 4	In front of the pit	SW, S, E, ENE	$y = 160.7 * x^{-0.07}$	$R^2 = 0.413$ R=-0.643
	Behind the pit	WSW, W, NW, N, NE	$y = 215.1 * x^{-0.12}$	$R^2 = 0.342$ R=-0.585
Model 5	In front of the pit	WSW, S, E, ENE	$y = 178.7 * x^{-0.09}$	$R^2 = 0.531$ R=-0.729
	Behind the pit	W, NW, N, NE	$y = 172.4 * x^{-0.08}$	$R^2 = 0.262$ R=-0.512
Model 6	In front of the pit	W, WSW, S, E, ENE	$y = 177.5 * x^{-0.09}$	$R^2 = 0.526$ R=-0.725
	Behind the pit	WNW, NW, N, NE	$y = 177.5 * x^{-0.09}$	$R^2 = 0.276$ R=-0.525
Model 7	In front of the pit	ESE, SE, SSE, S	$y = 212.6 * x^{-0.15}$	$R^2 = 0.993$ R=-0.996
	Behind the pit	N, NE, E, SSW, W, NNW	$y = 171.3 * x^{-0.08}$	$R^2 = 0.432$ R=-0.657
Model 8	In front of the pit	SE, SSE, S, SSW	$y = 159.2 * x^{-0.07}$	$R^2 = 0.364$ R=-0.603
	Behind the pit	N, NE, E, ESE, SW, W, NNW	$y = 164.0 * x^{-0.07}$	$R^2 = 0.334$ R=-0.578
Model 9	Northern winds	N, NE, NW	$y = 157.66 * x^{-0.067}$	$R^2 = 0.397$ R=-0.630
(Wind direction Classification)	Southern winds	WSW, W, SSE, S	$y = 199.52 * x^{-0.111}$	$R^2 = 0.385$ R=-0.620

Table 5.16 Gümüşkol Path 1 performance indicators for the models

	Modelling Set			Testing Set		
	R	**r²**	**RMSE**	**R**	**r²**	**RMSE**
Unclassified	0.625	0.390	4.960	0.716	0.504	4.259
Model 1	0.641	0.411	4.875	0.692	0.477	4.376
Model 2	0.638	0.407	4.894	0.714	0.461	4.439
Model 3	0.639	0.407	4.890	0.715	0.465	4.426
Model 4	0.665	0.442	4.744	0.689	0.472	4.396
Model 5	0.678	0.459	4.671	0.516	0.096	5.750
Model 6	0.680	0.461	4.664	0.517	0.111	5.704
Model 7	**0.690**	**0.475**	**4.602**	**0.862**	**0.702**	**3.303**
Model 8	0.627	0.392	4.953	0.709	0.500	4.278
Model 9	0.641	0.410	4.878	0.740	0.546	4.077
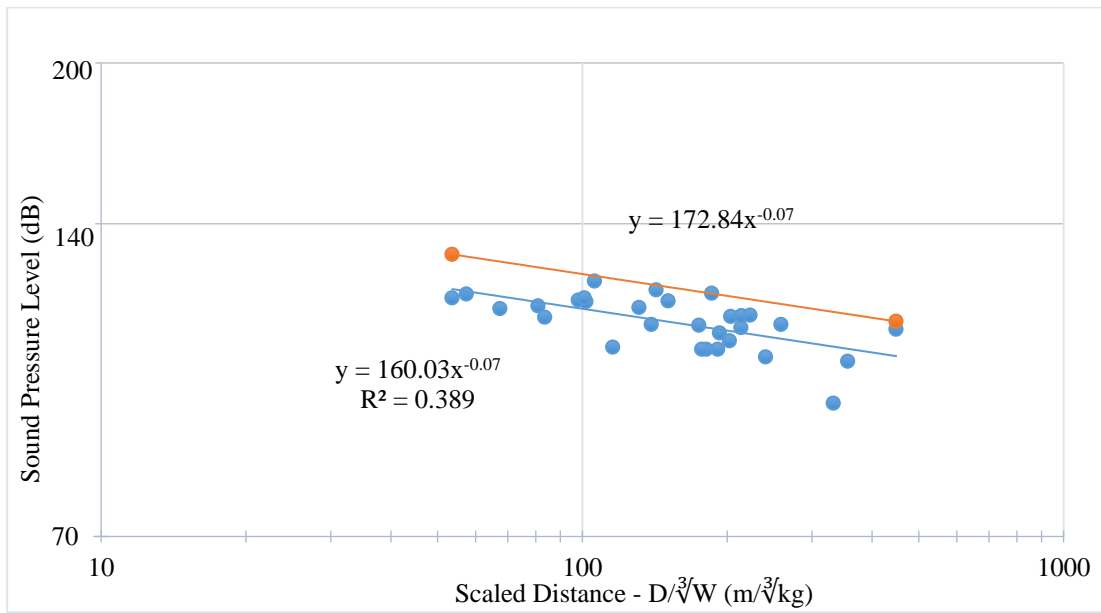
Figure 5.38 Gümüşkol Path 1 unclassified presplit blasting air blast overpressure levels
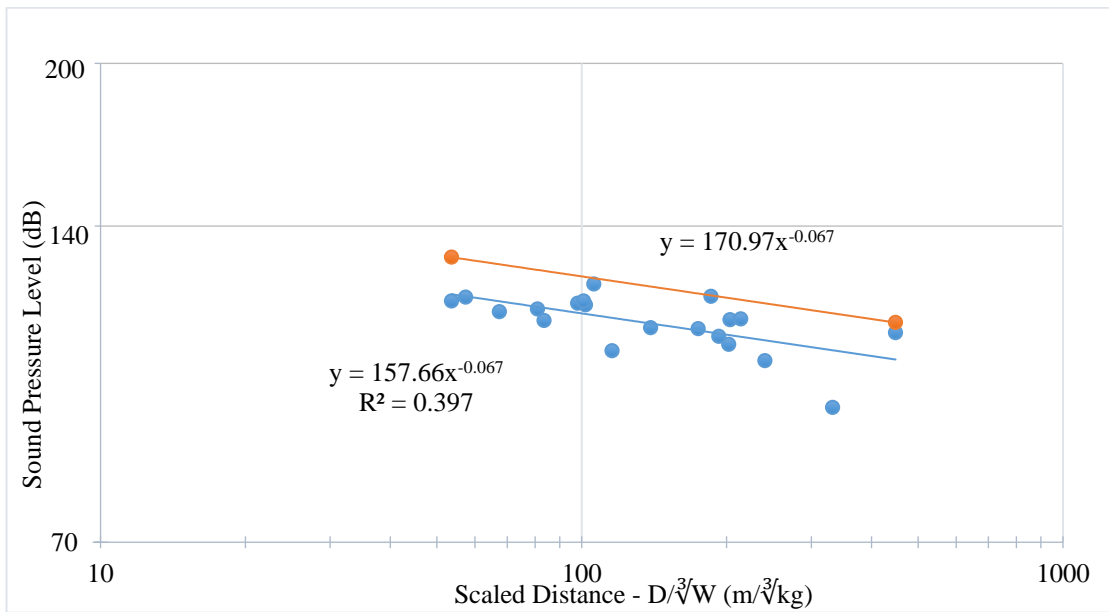
Figure 5.39 Gümüşkol Path 1 presplit blasting air blast overpressure levels (Northern winds-N, NE, NW)
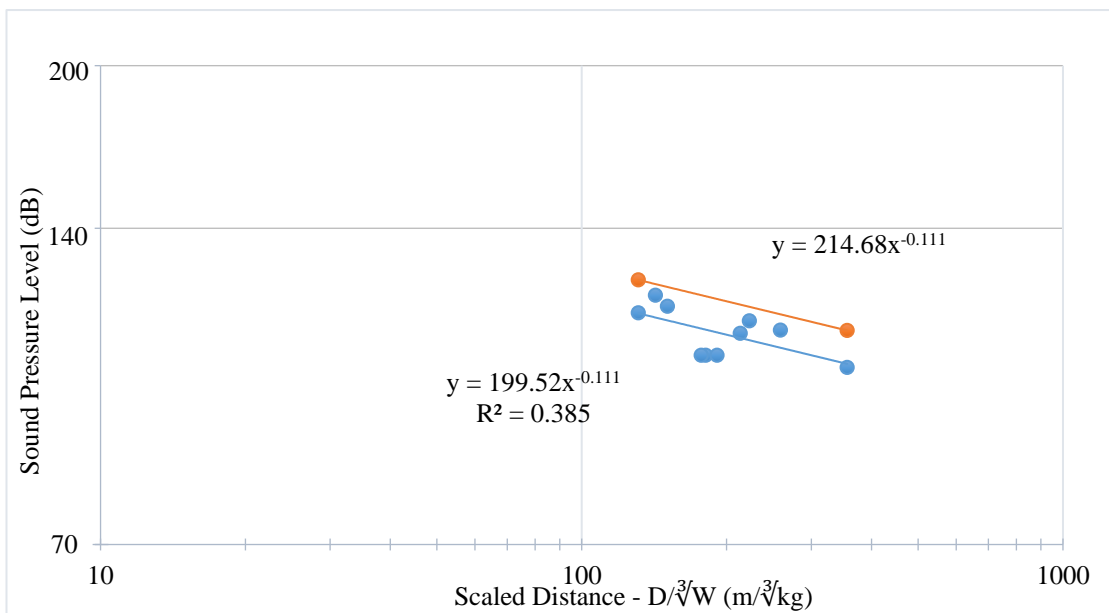
Figure 5.40 Gümüşkol Path 1 presplit blasting air blast overpressure levels (Southern winds-SE, S)

127
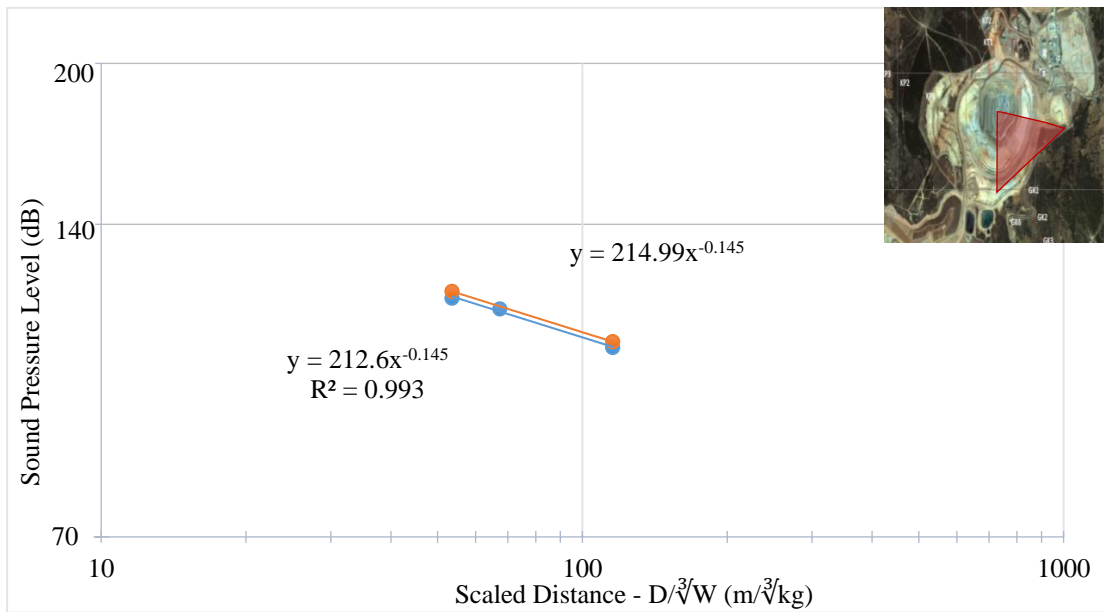
Figure 5.41 Gümüşkol Path 1 presplit blasting air blast overpressure levels (Pit location- ESE, SE, SSE, S - in front of the pit)
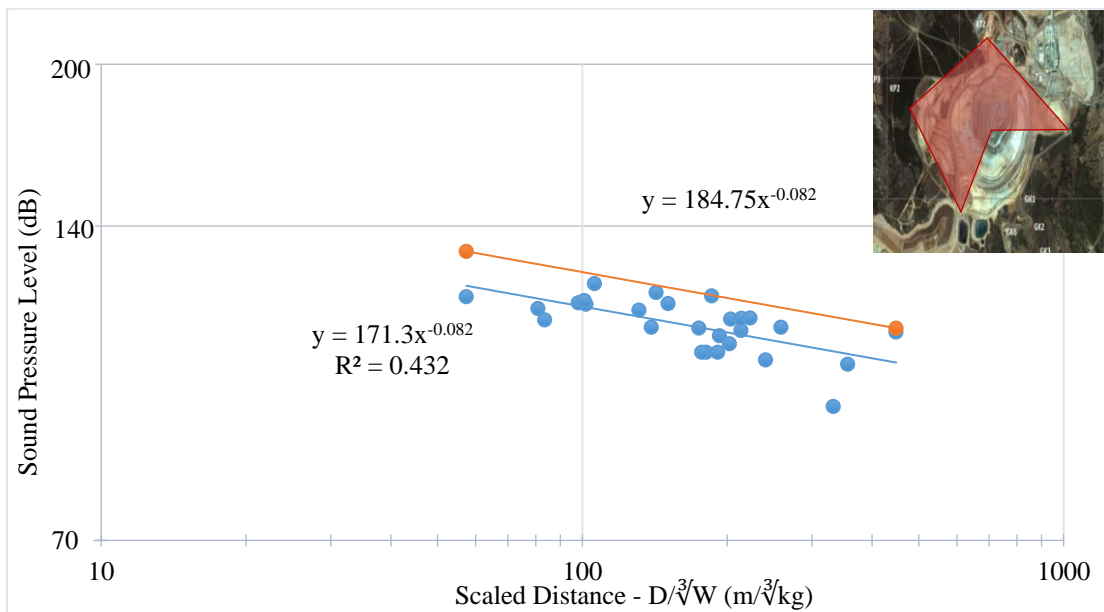
Figure 5.42 Gümüşkol Path 1 presplit blasting air blast overpressure levels (Pit location- N, NE, E, SSW, W - behind the pit)

5.2.1.4 Gümüşkol Village Path 2

32 air blast records were obtained from presplit blasts which are conducted at minimum 1190 m and maximum 2051.4 m horizontal distances to the village. For Gümüşkol Path 2, maximum air blast level at the nearest house to the pit border from presplit blasts is 115.7 dB with 9.25 Hz predominant frequency (at 1917.7 m). Air blast levels from presplit blasts are below the permitted values given in US OSM Regulations (129 dB) (in Table 2.7). Moreover, they are even less than the threshold level of complaints (117 dB) (in Figure 2.22).

For air shock analyses both blast group location within the pit and wind direction classification were tested. 7 different pit classification scenarios were evaluated by using model records and test records and compared to the regression analysis from unclassified data. Table 5.17 shows the directions included in the analysis, line equation and R^2 (square of correlation coefficient). To evaluate the performance of the models; correlation coefficient, coefficient of determination and Root-Mean Square Error (RMSE) were calculated and compared in Table 5.18. The results are not so satisfying, but the best result is obtained for model 3 combination. Moreover, it can be said blast group location serves better classification than wind direction classification. Figure 5.43 shows air blast attenuation relation for unclassified data.

The graph for presplit blasts for northern winds is given in Figure 5.44. The minimum and the maximum northern wind speed were 2.471 m/s and 7.154 m/s, respectively. Figure 5.45 shows regression analysis of presplit blasts for southern wind direction. Figure 5.46 and Figure 5.47 show regression analyses for blast groups in front of the pit and behind the pit, respectively. Analysis for 'in front of the pit' case provides higher correlation.

Table 5.17 Gümüşkol Path 2 properties of the formed models

	Pit location	Directions included	Line equation	
Unclassified	-	-	$y = 145.5 * x^{-0.06}$	$R^2= 0.208$ R=-0.456
Model 1	In front of the pit	WNW, W, S, E, ENE	$y = 152.7 * x^{-0.07}$	$R^2= 0.288$ R=-0.537
	Behind the pit	N, NE, NW	$y = 261.4 * x^{-0.15}$	$R^2= 0.255$ R=-0.474
Model 2	In front of the pit	SSW, S, E, ENE	$y = 177.6 * x^{-0.10}$	$R^2= 0.559$ R=-0.748
	Behind the pit	SW, W, NW, N, NE	$y = 164.2 * x^{-0.07}$	$R^2= 0.140$ R=-0.374
Model 3	In front of the pit	WSW, S, E, ENE	$y = 181.6 * x^{-0.10}$	$R^2= 0.560$ R=-0.748
	Behind the pit	W, NW, N, NE	$y = 179.4 * x^{-0.09}$	$R^2= 0.296$ R=-0.544
Model 4	In front of the pit	SW, S, E, ENE	$y = 188.5 * x^{-0.11}$	$R^2= 0.606$ R=-0.778
	Behind the pit	WSW, W, NW, N, NE	$y = 166.7 * x^{-0.08}$	$R^2= 0.236$ R=-0.486
Model 5	In front of the pit	SE, SSE, S, SSW	$y = 198.7 * x^{-0.12}$	$R^2= 0.748$ R=-0.865
	Behind the pit	N, NE, ESE, SW, W, NNW	$y = 160.1 * x^{-0.07}$	$R^2= 0.116$ R=-0.341
Model 6	In front of the pit	ESE, S, SSW	$y = 198.7 * x^{-0.12}$	$R^2= 0.748$ R=-0.865
	Behind the pit	N, NE, E, SW, W, NNW	$y = 160.1 * x^{-0.07}$	$R^2= 0.116$ R=-0.341
Model 7	In front of the pit	SE, SSE, S	$y = 260.5 * x^{-0.19}$	$R^2= 0.974$ R=-0.987
	Behind the pit	N, NE, ESE, SSW, W, NNW	$y = 154.8 * x^{-0.07}$	$R^2= 0.208$ R=-0.456
Model 8 (Wind direction Classification)	Northern winds	NNE, NNW, WNW	$y = 131.8 * x^{-0.035}$	$R^2 = 0.144$ R=-0.379
	Southern winds	WSW, ESE, S	$y = 166.32 * x^{-0.081}$	$R^2 = 0.289$ R=-0.538

Table 5.18 Gümüşkol Path 2 performance indicators for the models

	Modelling Set			Testing Set		
	R	**r^2**	**RMSE**	**R**	**r^2**	**RMSE**
Unclassified	0.464	0.215	5.390	0.979	0.138	6.748
Model 1	**0.726**	**0.526**	**4.186**	**0.979**	**0.336**	**5.923**
Model 2	0.596	0.354	4.888	0.979	0.296	6.100
Model 3	0.550	0.302	5.083	0.980	0.511	5.084
Model 4	0.705	0.497	4.313	0.979	0.319	6.001
Model 5	0.532	0.282	5.154	0.979	0.230	6.377
Model 6	0.532	0.282	5.154	0.979	0.230	6.377
Model 7	0.535	0.285	5.142	0.979	0.190	6.541
Model 8	0.502	0.251	5.264	0.891	0.212	6.451
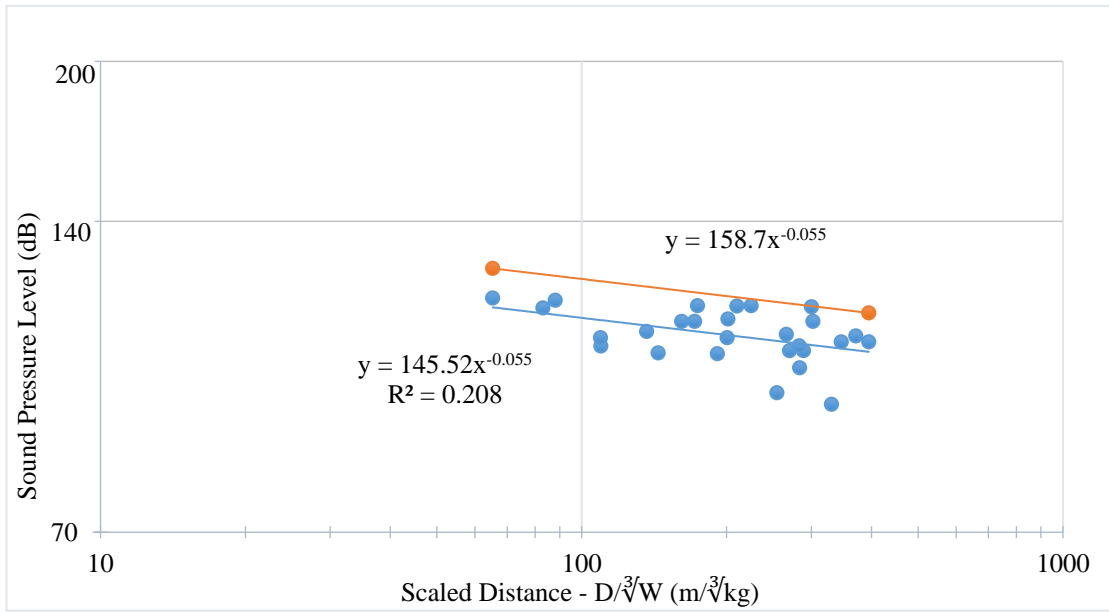
Figure 5.43 Gümüşkol Path 2 unclassified presplit blasting air blast overpressure levels in dB
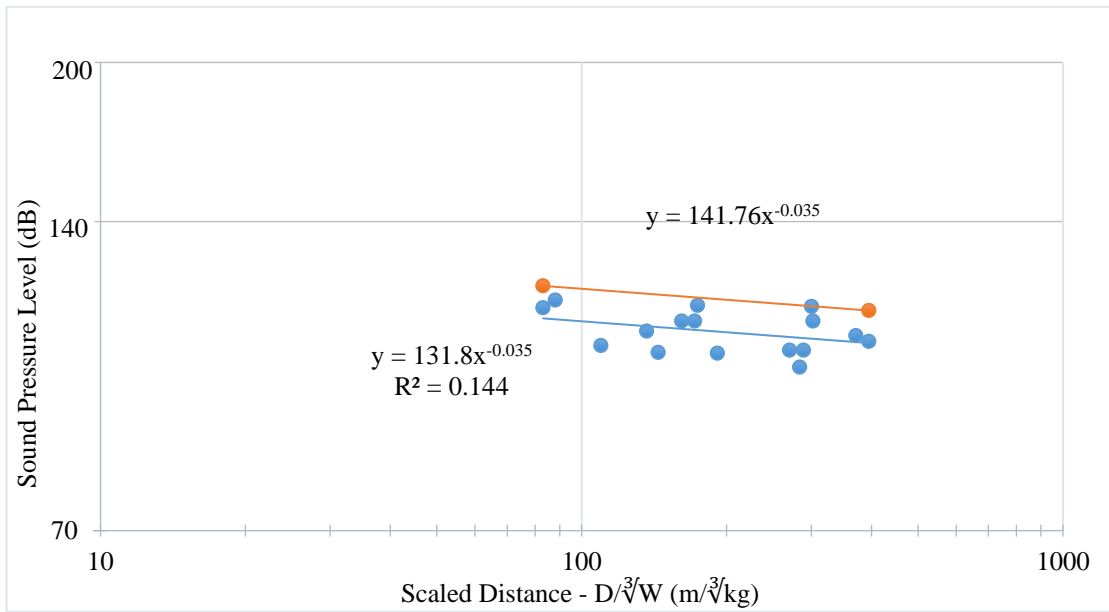
Figure 5.44 Gümüşkol Path 2 presplit blasting air blast overpressure levels in dB (Northern winds-NNE, NNW, WNW)

Figure 5.45 Gümüşkol Path 2 presplit blasting air blast overpressure levels in dB (Southern winds-WSW, S, ESE)
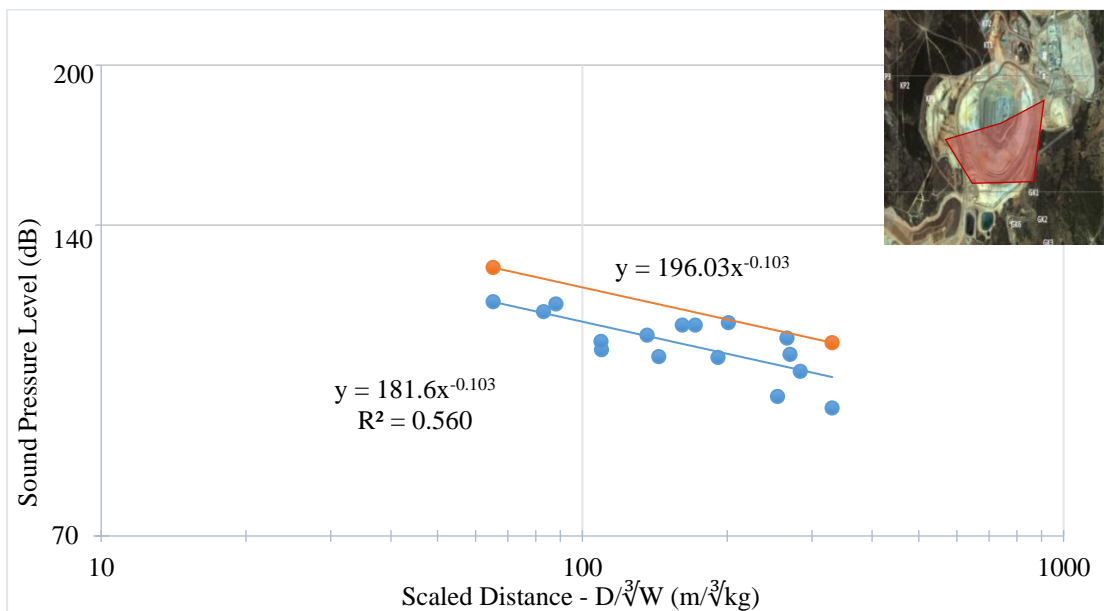
The equations shown on the figure:

$$y = 184.77x^{-0.081}$$

$$y = 166.32x^{-0.081}$$
$$R^2 = 0.289$$

Axis labels: Sound Pressure Level (dB); Scaled Distance - $D/\sqrt[3]{W}$ (m/$\sqrt[3]{kg}$)

Figure 5.46 Gümüşkol Path 2 presplit blasting air blast overpressure levels in dB (Pit location- WSW, S, E, ENE - in front of the pit)

The equations shown on the figure:

$$y = 196.03x^{-0.103}$$

$$y = 181.6x^{-0.103}$$
$$R^2 = 0.560$$

Axis labels: Sound Pressure Level (dB); Scaled Distance - $D/\sqrt[3]{W}$ (m/$\sqrt[3]{kg}$)

132

The chart shows equations:

$$y = 190.34x^{-0.087}$$

$$y = 179.42x^{-0.087}$$
$$R^2 = 0.296$$

With axes: Sound Pressure Level (dB) on the y-axis and Scaled Distance - $D/\sqrt[3]{W}$ (m/$\sqrt[3]{kg}$) on the x-axis.
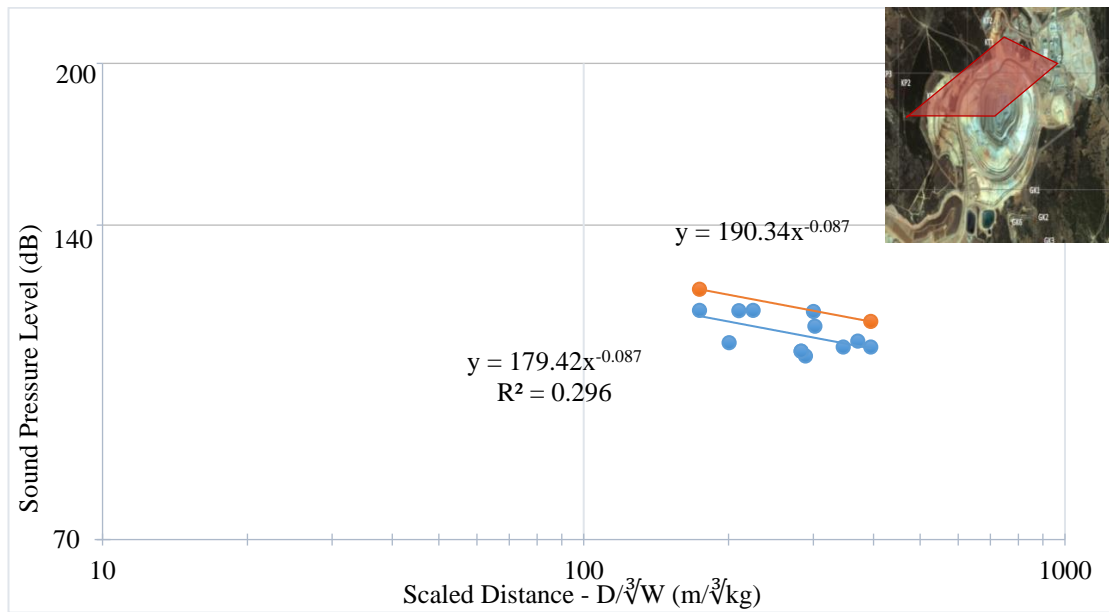
Figure 5.47 Gümüşkol Path 2 presplit blasting air blast overpressure levels in dB (Pit location- W, NW, N, NE- behind the pit)

5.2.2 Production Blasting

Before detailed air blast analyses, all the collected data are analyzed in the same graph regardless of the location of the monitoring station (Figure 5.48). The performance indicators calculated for modelling and testing set are given in Table 5.19. These values are later compared to classified regression analyses for which the blast group location classification given in Figure 5.2 is used.

Table 5.19 Performance indicators for the whole-data model

		R	r^2	RMSE
Whole data	Modelling Set	0.631	0.398	5.977
	Testing set	0.601	0.358	6.701

133
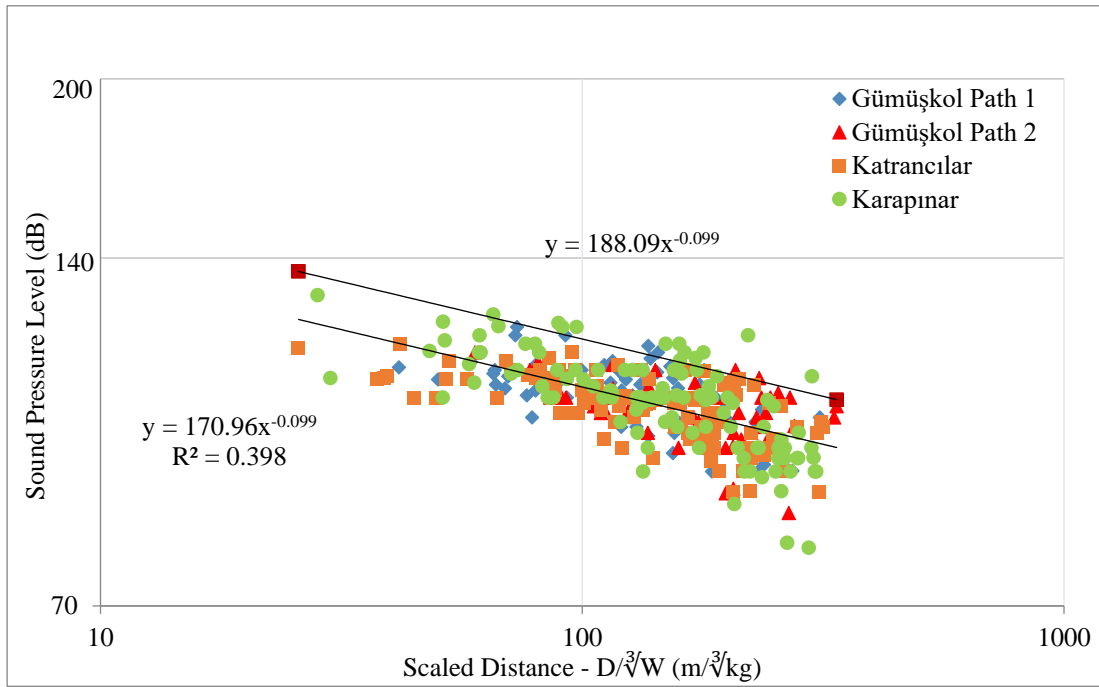
Figure 5.48 Air shock prediction from whole production blast data

5.2.2.1 Katrancılar Village

123 air blast records were gathered from production blasts and the highest air blast level measured at the village from production blasts is 104.9 dB with 3.88 Hz predominant frequency (at 1782.0 m). Air blast levels from production blasts are below the permitted values given in US OSM Regulations (129 dB) (in Table 2.7). Moreover, they are even less than the threshold level of complaints (117 dB) (in Figure 2.22).

For air shock analyses both blast group location and wind direction classification were tested. 8 different pit classification scenarios were tested and evaluated by using model set and test set and compared to the regression analysis from unclassified data. Table 5.20 shows the directions included in the analysis, line equation and R^2 (square of correlation coefficient). To evaluate the performance of the models; correlation coefficient, coefficient of determination and Root-Mean Square Error (RMSE) were calculated and compared in Table 5.21 and the best result is obtained for model 7

combination. Moreover, it can be said blast group location serves better classification than wind direction classification.

Table 5.20 Katrancılar properties of the formed models

	Pit location	Directions included	Line equation		
Unclassified	-	-	$y = 153.7 * x^{-0.08}$	$R^2= 0.400$	$R=-0.632$
Model 1	In front of the pit	N, NE, SW, W, NW, NNW	$y = 157.1 * x^{-0.09}$	$R^2= 0.469$	$R=-0.685$
	Behind the pit	ENE, E, SE, S, SSW	$y = 167.7 * x^{-0.09}$	$R^2= 0.284$	$R=-0.533$
Model 2	In front of the pit	N, NE, W, NW, NNW	$y = 166.4 * x^{-0.10}$	$R^2= 0.647$	$R=-0.804$
	Behind the pit	ENE, E, SE, S, SSW, SW, WSW	$y = 177.7 * x^{-0.11}$	$R^2= 0.338$	$R=-0.581$
Model 3	In front of the pit	N, NE, WSW, W, NW, NNW	$y = 162.0 * x^{-0.09}$	$R^2= 0.563$	$R=-0.750$
	Behind the pit	ENE, E, SE, S, SW	$y = 180.3 * x^{-0.11}$	$R^2= 0.330$	$R=-0.574$
Model 4	In front of the pit	N, NE, E, ESE, NW, NNW	$y = 155.2 * x^{-0.08}$	$R^2= 0.495$	$R=-0.704$
	Behind the pit	SE, S, SW, WSW, W	$y = 184.4 * x^{-0.11}$	$R^2= 0.422$	$R=-0.650$
Model 5	In front of the pit	N, NE, ENE, W, NW, NNW	$y = 165.4 * x^{-0.10}$	$R^2= 0.636$	$R=-0.797$
	Behind the pit	E, SE, S, SW, WSW	$y = 177.7 * x^{-0.11}$	$R^2= 0.338$	$R=-0.581$
Model 6	In front of the pit	N, NE, E, WNW, NW, NNW	$y = 158.1 * x^{-0.09}$	$R^2= 0.554$	$R=-0.744$
	Behind the pit	ESE, SE, S, SW, W	$y = 175.7 * x^{-0.10}$	$R^2= 0.372$	$R=-0.610$
Model 7	In front of the pit	N, NE, WNW, NW, NNW	$y = 163.2 * x^{-0.10}$	$R^2= 0.663$	$R=-0.814$
	Behind the pit	ENE, E, SE, S, SW, W	$y = 180.5 * x^{-0.11}$	$R^2= 0.375$	$R=-0.612$
Model 8	In front of the pit	N, NE, ENE, WNW, NW, NNW	$y = 162.2 * x^{-0.10}$	$R^2= 0.650$	$R=-0.806$
	Behind the pit	E, SE, S, SSW, SW, W	$y = 180.4 * x^{-0.11}$	$R^2= 0.375$	$R=-0.612$
Model 9 **(Wind direction Classification)**	Northern winds	N, NE, NW	$y = 155.93 * x^{-0.083}$	$R^2 = 0.425$	$R=-0.652$
	Southern winds	SSW, SSE, S	$y = 151.04 * x^{-0.076}$	$R^2 = 0.368$	$R=-0.607$

Figure 5.49 shows air blast attenuation relation for unclassified data. The graph for production blasts for northern winds is given in Figure 5.50. The minimum and the maximum northern wind speed were 2.179 m/s and 6.808 m/s, respectively. Air blast analysis of production blasts for southern winds is given in Figure 5.51. The minimum and the maximum southern wind speed were 2.825 m/s and 7.35 m/s, respectively. In addition to wind direction, blast group location was also used for classification of the air blast data. Figure 5.52 and Figure 5.53 show regression analyses for blast groups

in front of the pit and behind the pit for model 7 combination, respectively. Analysis for 'in front of the pit' case provides higher correlation.

Table 5.21 Katrancılar performance indicators for the models

	Modelling Set			Testing Set		
	R	**r²**	**RMSE**	**R**	**r²**	**RMSE**
Unclassified	0.635	0.402	5.177	0.791	0.614	4.332
Model 1	0.652	0.424	5.080	0.796	0.620	4.299
Model 2	0.700	0.489	4.785	0.857	0.727	3.642
Model 3	0.678	0.458	4.928	0.842	0.696	3.842
Model 4	0.684	0.467	4.890	0.841	0.680	3.946
Model 5	0.697	0.485	4.807	0.855	0.723	3.672
Model 6	0.688	0.472	4.864	0.860	0.717	3.710
Model 7	**0.708**	**0.501**	**4.731**	**0.869**	**0.745**	**3.520**
Model 8	0.704	0.496	4.755	0.866	0.740	3.557
Model 9	0.637	0.405	5.167	0.802	0.632	4.230
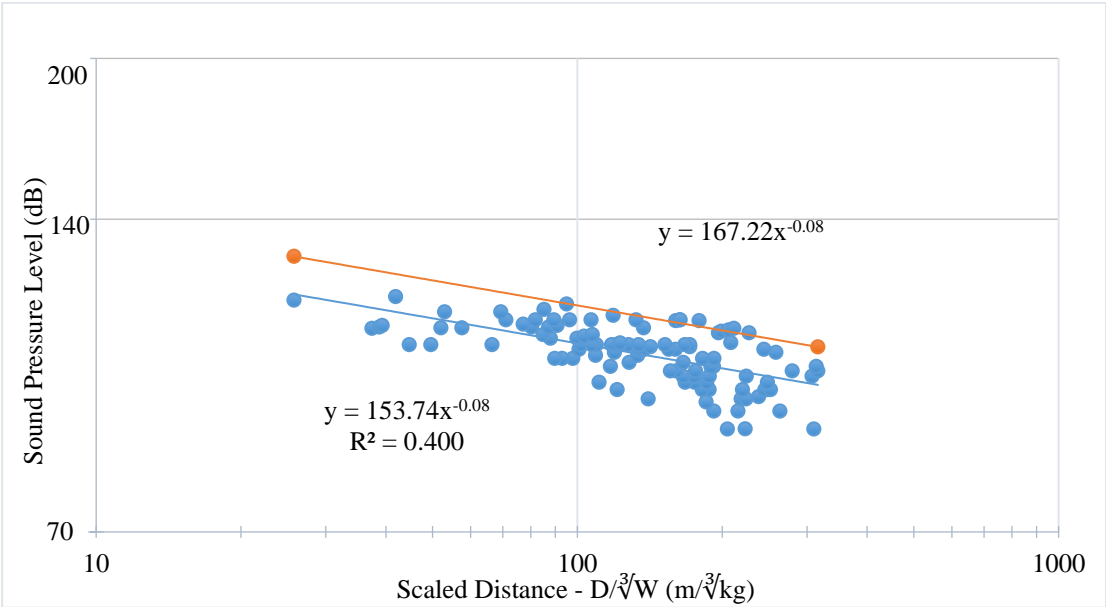
Figure 5.49 Katrancılar unclassified production blasting air blast overpressure levels in dB

136

$y = 169.78x^{-0.083}$

$y = 155.93x^{-0.083}$
$R^2 = 0.425$

Figure 5.50 Katrancılar production blasting air blast overpressure levels in dB (Northern winds-N, NE, NW)

$y = 164.29x^{-0.076}$

$y = 151.04x^{-0.076}$
$R^2 = 0.368$
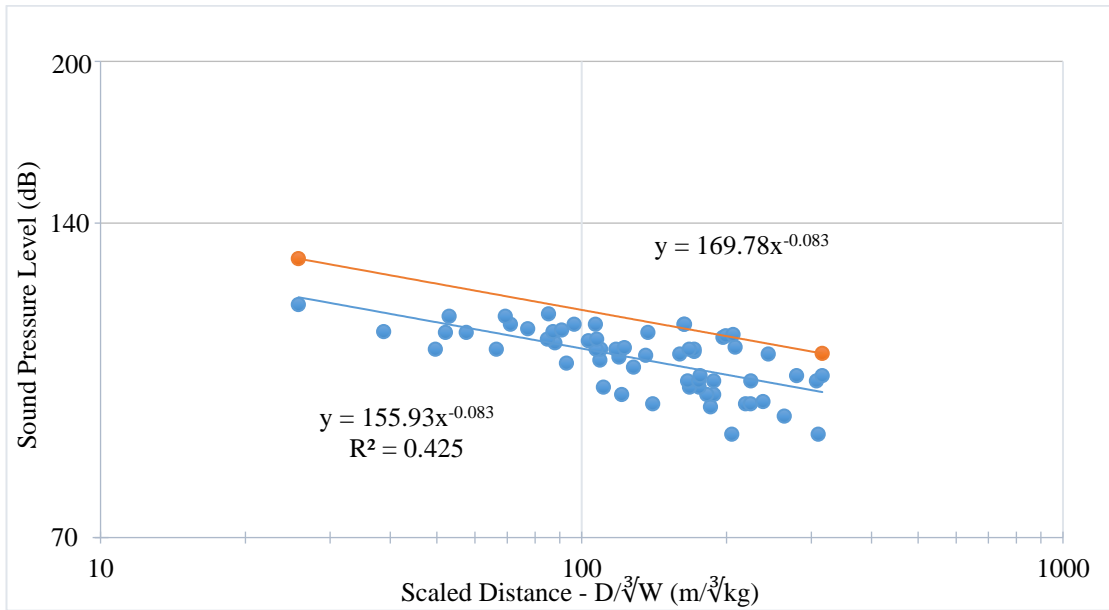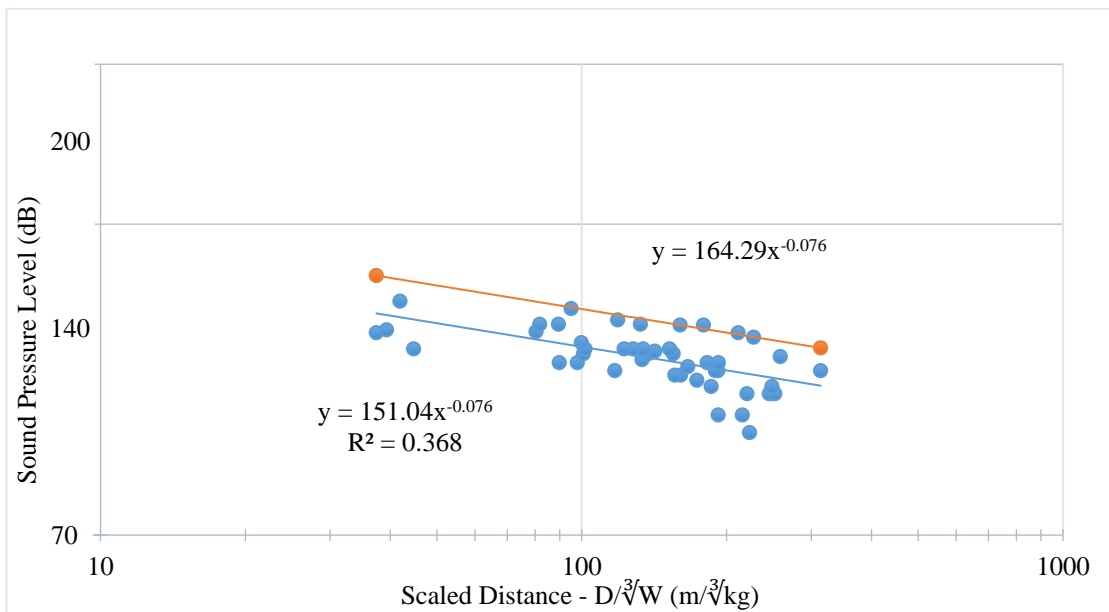
Figure 5.51 Katrancılar production blasting air blast overpressure levels in dB (Southern winds-S, SSE, SSW)

137
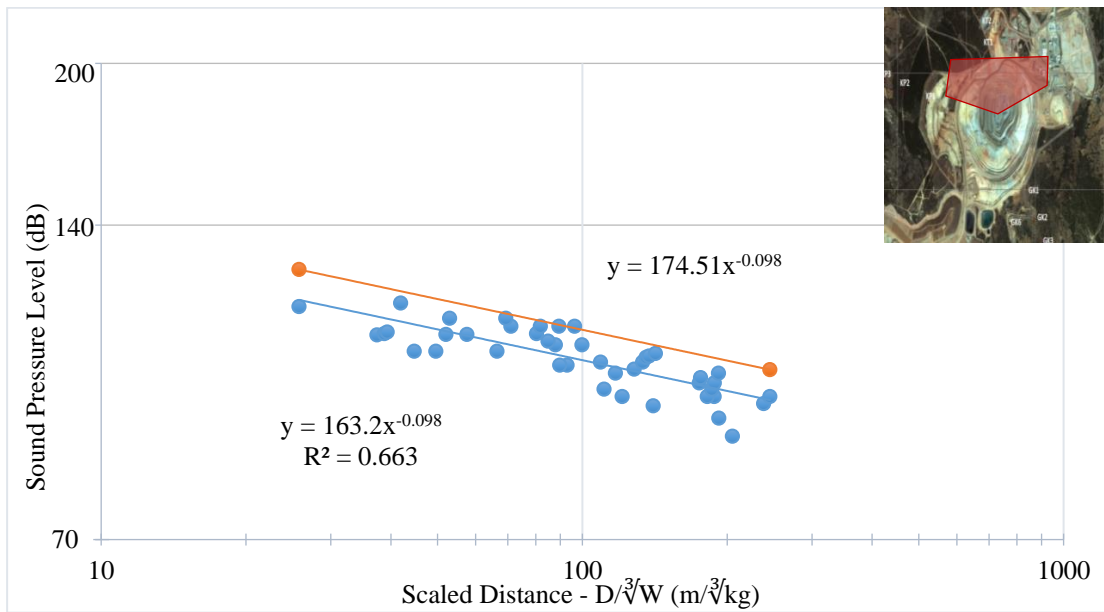
Figure 5.52 Katrancılar production blasting air blast overpressure levels in dB (Pit location- N, NE, WNW, NW, NNW - in front of the pit)
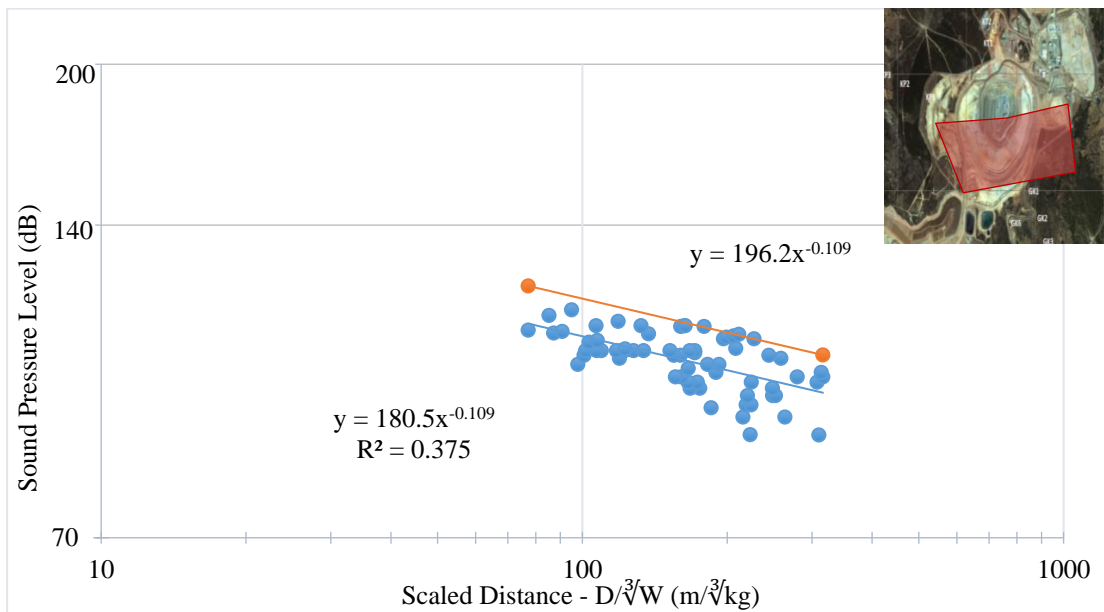
Figure 5.53 Katrancılar production blasting air blast overpressure levels in dB (Pit location- ENE, E, SE, S, SW, W- behind the pit)

5.2.2.2 Karapınar Village

124 air blast records were obtained from production blasts and the highest air blast level measured at the village from production blasts is 110.6 dB with 3.88 Hz predominant frequency (at 2100.0 m). Air blast levels from production blasts are below the permitted values given in US OSM Regulations (129 dB) (in Table 2.7). Moreover, they are even less than the threshold level of complaints (117 dB) (in Figure 2.22).

For air shock analyses both blast group location and wind direction classification were tested. 9 different pit classification scenarios were tested and evaluated by using modelling set and testing set and compared to the regression analysis from unclassified data. Table 5.22 shows the directions included in the analysis, line equation and R^2 (square of correlation coefficient). Performance indicators are given in Table 5.23 and model 3 is selected as the best combination.

Figure 5.54 shows air blast attenuation relation before classification according to wind direction. The graph for production blasting air blast analysis for western winds is given in Figure 5.55. The minimum and the maximum western wind speed were 1.35 m/s and 10.02 m/s, respectively.

The graph of production blasting air blast analysis for eastern winds is given in Figure 5.56. The minimum and the maximum eastern wind speed were 0.792 m/s and 9.06 m/s, respectively. In addition to wind direction classification, blast group location was also used for classification of the air blast data. Figure 5.57 and Figure 5.58 show regression analyses for blast groups in front of the pit and behind the pit, respectively. Analysis for 'in front of the pit' case provides higher correlation.

Table 5.22 Karapınar properties of the formed models

	Pit location	Directions included	Line equation		
Unclassified	-	-	$y = 197.5 * x^{-0.13}$	$R^2 = 0.497$	$R = -0.705$
Model 1	In front of the pit	NNE, N, W, S, SSE	$y = 204.7 * x^{-0.14}$	$R^2 = 0.591$	$R = -0.769$
	Behind the pit	NE, E, SE	$y = 247.5 * x^{-0.16}$	$R^2 = 0.272$	$R = -0.522$
Model 2	In front of the pit	N, W, S, SSE	$y = 205.1 * x^{-0.14}$	$R^2 = 0.589$	$R = -0.767$
	Behind the pit	NNE, NE, E, SE	$y = 246.6 * x^{-0.16}$	$R^2 = 0.292$	$R = -0.540$
Model 3	In front of the pit	NE, N, W, S, SSE	$y = 203.3 * x^{-0.13}$	$R^2 = 0.564$	$R = -0.751$
	Behind the pit	ENE, E, SE	$y = 271.8 * x^{-0.18}$	$R^2 = 0.241$	$R = -0.491$
Model 4	In front of the pit	NNE, N, W, SSW	$y = 199.8 * x^{-0.13}$	$R^2 = 0.589$	$R = -0.767$
	Behind the pit	NE, E, SE, S	$y = 288.7 * x^{-0.20}$	$R^2 = 0.347$	$R = -0.589$
Model 5	In front of the pit	NNW, W, S, SSE	$y = 199.8 * x^{-0.13}$	$R^2 = 0.584$	$R = -0.764$
	Behind the pit	N, NE, E, SE	$y = 258.7 * x^{-0.18}$	$R^2 = 0.325$	$R = -0.570$
Model 6	In front of the pit	NNE, N, W, S	$y = 198.4 * x^{-0.13}$	$R^2 = 0.582$	$R = -0.763$
	Behind the pit	NE, E, SE, SSE	$y = 290.1 * x^{-0.20}$	$R^2 = 0.335$	$R = -0.579$
Model 7	In front of the pit	NNW, W, SSW	$y = 194.1 * x^{-0.13}$	$R^2 = 0.581$	$R = -0.762$
	Behind the pit	N, E, S	$y = 285.0 * x^{-0.20}$	$R^2 = 0.377$	$R = -0.614$
Model 8	In front of the pit	N, W, SSW	$y = 200.1 * x^{-0.13}$	$R^2 = 0.586$	$R = -0.766$
	Behind the pit	NNE, E, S	$y = 284.7 * x^{-0.19}$	$R^2 = 0.359$	$R = -0.599$
Model 9	In front of the pit	SW, W, NNW	$y = 192.6 * x^{-0.12}$	$R^2 = 0.570$	$R = -0.755$
	Behind the pit	N, E, SSW	$y = 287.6 * x^{-0.20}$	$R^2 = 0.393$	$R = -0.627$
Model 10	Western winds	SSW, SW, W, NW, NNW	$y = 199.4 * x^{-0.131}$	$R^2 = 0.495$	$R = -0.704$
(Wind direction Classification)	Eastern winds	SSE, SE, E, NE, NNE	$y = 191.63 * x^{-0.118}$	$R^2 = 0.521$	$R = -0.722$

Table 5.23 Karapınar performance indicators for the models

	Modelling Set			Testing Set		
	R	**r²**	**RMSE**	**R**	**r²**	**RMSE**
Unclassified	0.704	0.494	7.016	0.842	0.547	7.632
Model 1	0.730	0.532	6.750	0.881	0.553	7.577
Model 2	0.730	0.531	6.757	0.880	0.551	7.602
Model 3	**0.711**	**0.504**	**6.952**	**0.882**	**0.635**	**6.852**
Model 4	0.724	0.523	6.816	0.843	0.518	7.872
Model 5	0.719	0.516	6.863	0.822	0.507	7.962
Model 6	0.720	0.517	6.856	0.838	0.520	7.859
Model 7	0.718	0.515	6.871	0.805	0.496	8.052
Model 8	0.724	0.523	6.815	0.844	0.516	7.885
Model 9	0.719	0.515	6.870	0.815	0.523	7.829
Model 10	0.723	0.521	6.830	0.877	0.560	7.524
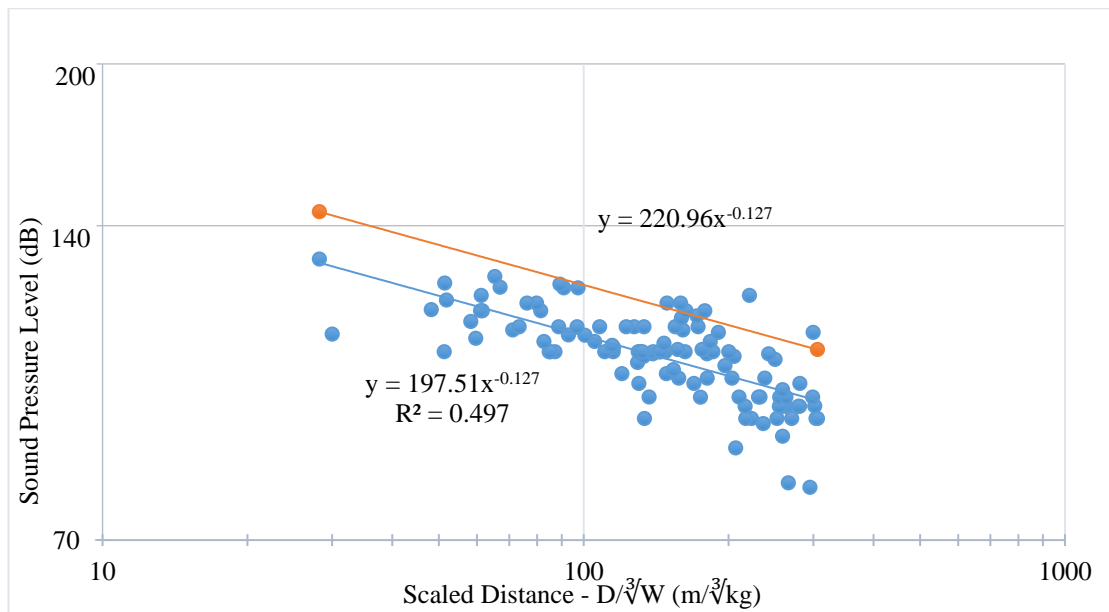
Figure 5.54 Karapınar unclassified production blasting air blast overpressure levels in dB

141
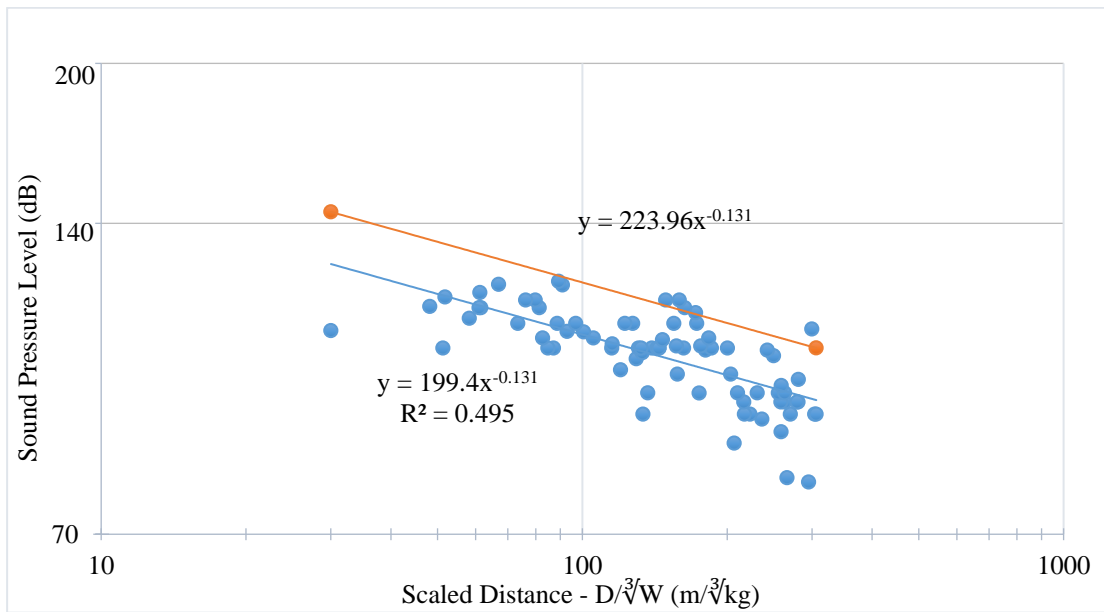
Figure 5.55 Karapınar production blasting air blast overpressure levels in dB (Western winds- SSW, SW, W, NW, NNW)
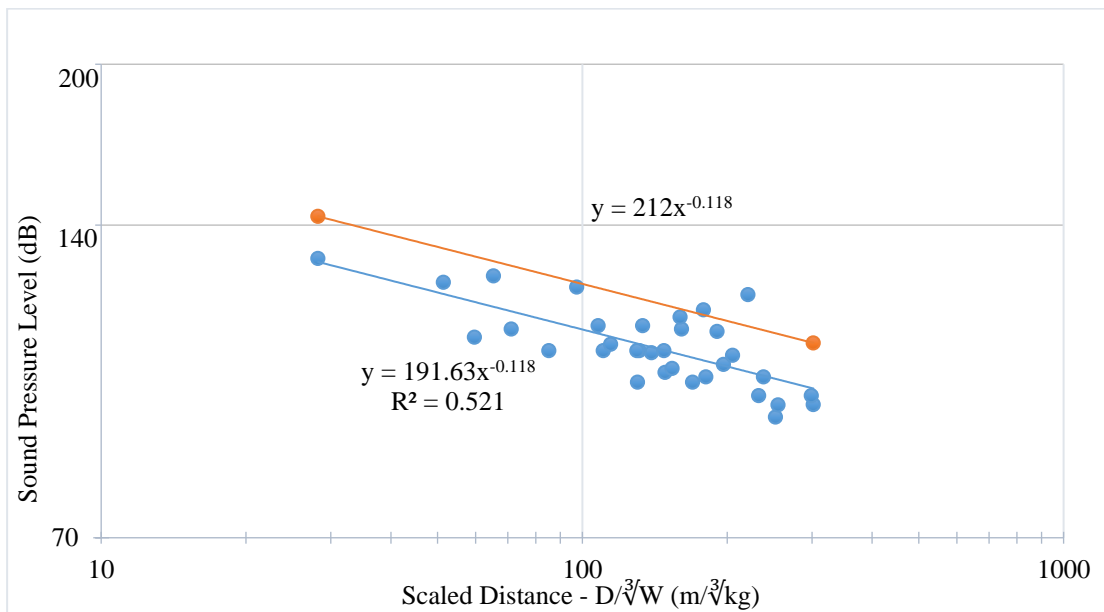
Figure 5.56 Karapınar production blasting air blast overpressure levels in dB (Eastern winds-SSE, SE, E, NE, NNE)
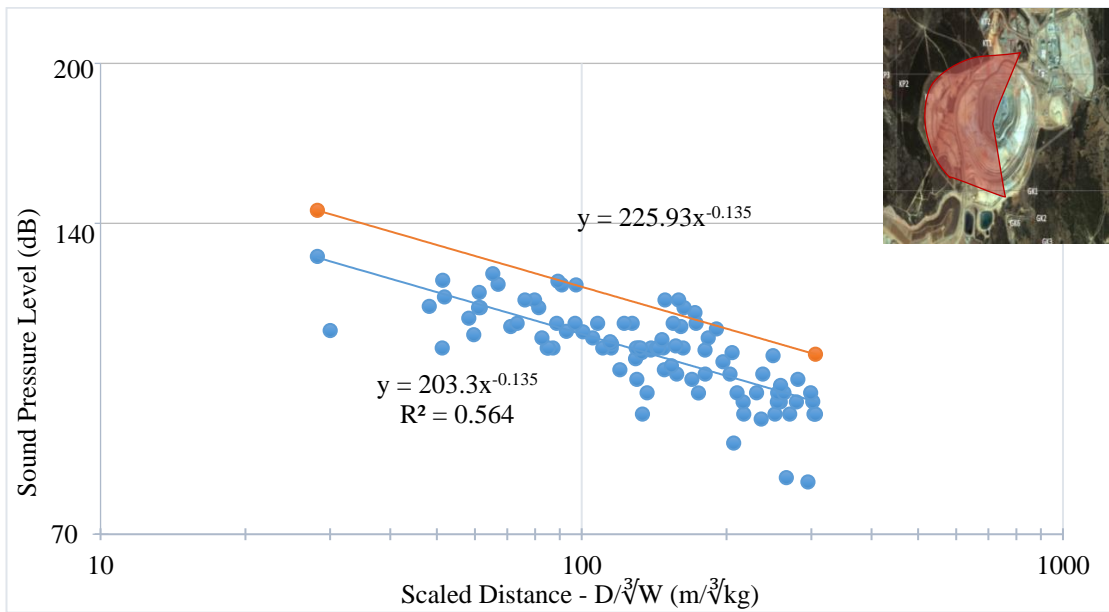
$y = 225.93x^{-0.135}$

$y = 203.3x^{-0.135}$
$R^2 = 0.564$

Figure 5.57 Karapınar production blasting air blast overpressure levels in dB (Pit location- NE, N, W, S, SSE - in front of the pit)
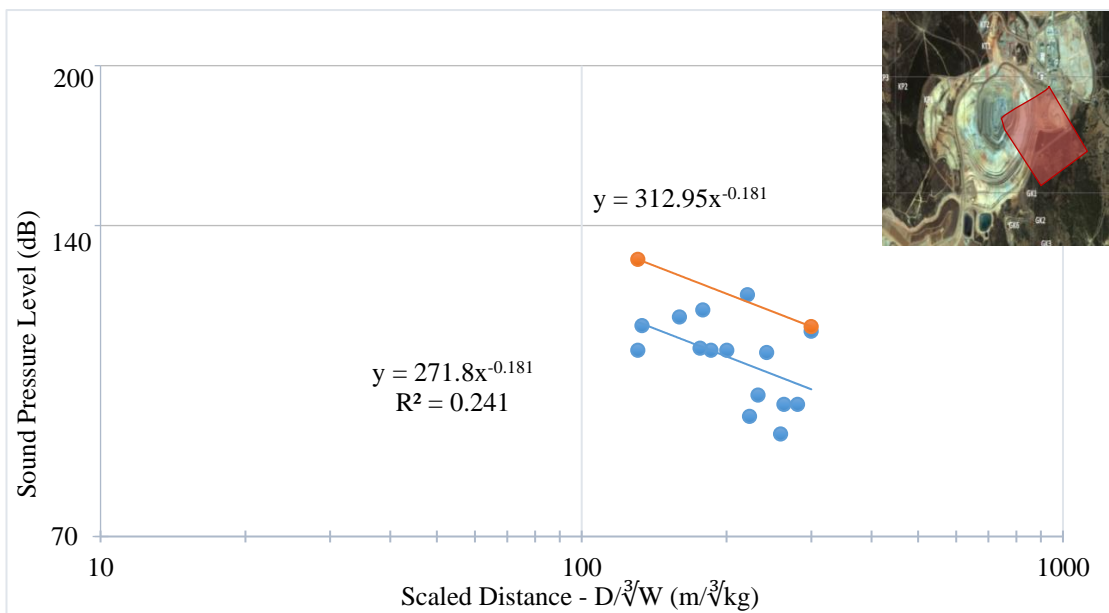
$y = 312.95x^{-0.181}$

$y = 271.8x^{-0.181}$
$R^2 = 0.241$

Figure 5.58 Karapınar production blasting air blast overpressure levels in dB (Pit location- ENE, E, SE - behind the pit)

143

5.2.2.3 Gümüşkol Village Path 1

102 air blast records were obtained from production blasts and the highest air blast level measured at the village from production blasting is 101.9 dB with 3.63 Hz predominant frequency (at 1869.34 m). Air blast levels from production blasts are below the values given in US OSM Regulations (129 dB) (in Table 2.7). Moreover, they are even less than the threshold level of complaints (117 dB) (in Figure 2.22).

For air shock analyses both blast group location and wind direction classification were tested. 8 different pit classification scenarios were evaluated by using model set and test set and compared to the regression analysis from unclassified data. Table 5.24 shows the directions included in the analysis, line equation and R2 (square of correlation coefficient).

To evaluate the performance of the models; correlation coefficient, coefficient of determination and Root-Mean Square Error (RMSE) were calculated and compared in Table 5.25, the best result is obtained for model 8 combination. Moreover, it can be said that blast group location serves better classification than wind direction classification.

Figure 5.59 shows air blast attenuation relation of unclassified data. Air blast analysis of production blasts, for northern winds is given in Figure 5.60. The minimum and the maximum northern wind speed were 2.691 m/s and 10.02 m/s, respectively.

The graph for production blasting air blast analysis for southern winds is given in Figure 5.61. The minimum and the maximum southern wind speed were 0.792 m/s and 7.35 m/s, respectively. In addition to wind direction classification, blast group location was also used for classification of the air blast data. Figure 5.62 and Figure 5.63 show regression analyses for blast groups in front of the pit and behind the pit, respectively. Analysis for 'in front of the pit' case provides higher correlation.

Table 5.24 Gümüşkol Path 1 properties of the formed models

	Pit location	Directions included	Line equation	
Unclassified	-	-	$y = 163.0 * x^{-0.09}$	R^2=0.291 R=-0.539
Model 1	In front of the pit	SW, S, E, NE	$y = 165.3 * x^{-0.09}$	R^2=0.344 R=-0.587
	Behind the pit	WSW, W, NW, N, NNE	$y = 268.2 * x^{-0.18}$	R^2=0.435 R=-0.660
Model 2	In front of the pit	WSW, SW, S, E, NE	$y = 163.0 * x^{-0.09}$	R^2=0.312 R=-0.559
	Behind the pit	W, NW, N, NNE	$y = 280.3 * x^{-0.19}$	R^2=0.501 R=-0.708
Model 3	In front of the pit	SW, S, E, ENE	$y = 164.7 * x^{-0.09}$	R^2=0.349 R=-0.591
	Behind the pit	WSW, W, NW, N, NE	$y = 205.9 * x^{-0.13}$	R^2=0.347 R=-0.589
Model 4	In front of the pit	WSW, S, E, ENE	$y = 162.4 * x^{-0.09}$	R^2=0.314 R=-0.560
	Behind the pit	W, NW, N, NE	$y = 210.4 * x^{-0.14}$	R^2=0.401 R=-0.633
Model 5	In front of the pit	W, WSW, S, E, ENE	$y = 162.1 * x^{-0.09}$	R^2=0.308 R=-0.555
	Behind the pit	WNW, NW, N, NE	$y = 208.8 * x^{-0.13}$	R^2=0.432 R=-0.657
Model 6	In front of the pit	ESE, SE, SSE, S	$y = 153.0 * x^{-0.08}$	R^2=0.602 R=-0.776
	Behind the pit	N, NE, E, SSW, W, NNW	$y = 186.8 * x^{-0.11}$	R^2=0.311 R=-0.558
Model 7	In front of the pit	SE, SSE, S	$y = 162.6 * x^{-0.09}$	R^2=0.775 R=-0.880
	Behind the pit	N, NE, E, ESE, SSW, W, NNW	$y = 179.1 * x^{-0.11}$	R^2=0.293 R=-0.541
Model 8	In front of the pit	SE, SSE	$y = 162.4 * x^{-0.09}$	R^2=0.817 R=-0.904
	Behind the pit	N, NE, E, ESE, S, SSW, W, NNW	$y = 178.9 * x^{-0.11}$	R^2=0.297 R=-0.545
Model 9	Northern winds	N, NW, NE, NNE, ENE	$y = 153 * x^{-0.074}$	R^2 = 0.286 R=-0.535
(Wind direction Classification)	Southern winds	SE, SSW, S	$y = 183.77 * x^{-0.114}$	R^2 = 0.332 R=-0.576

Table 5.25 Gümüşkol Path 1 performance indicators for the models

	Modelling Set			Testing Set		
	R	**r^2**	**RMSE**	**R**	**r^2**	**RMSE**
Unclassified	0.535	0.285	5.379	0.385	0.102	6.550
Model 1	0.599	0.359	5.094	0.441	0.186	6.234
Model 2	0.583	0.340	5.169	0.432	0.181	6.254
Model 3	0.590	0.347	5.140	0.639	0.340	5.614
Model 4	0.573	0.327	5.217	0.614	0.310	5.738
Model 5	0.574	0.329	5.210	0.600	0.278	5.873
Model 6	0.583	0.339	5.171	0.698	0.358	5.536
Model 7	0.579	0.334	5.190	0.736	0.381	5.437
Model 8	**0.583**	**0.339**	**5.172**	**0.751**	**0.392**	**5.388**
Model 9	0.553	0.304	5.305	0.510	0.208	6.148
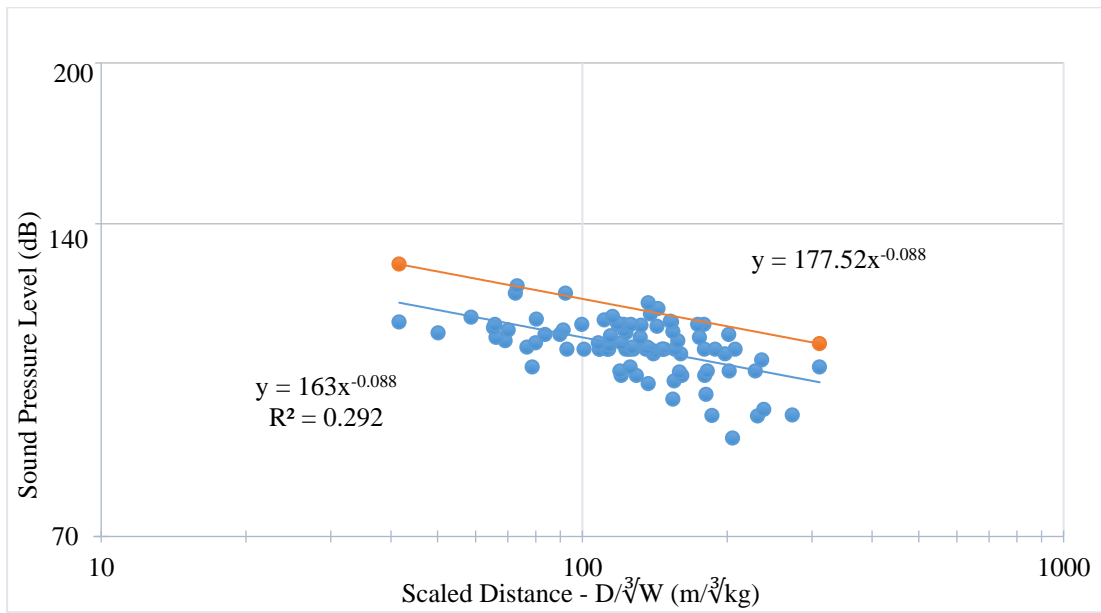
Figure 5.59 Gümüşkol Path 1 unclassified production blasting air blast overpressure levels in dB
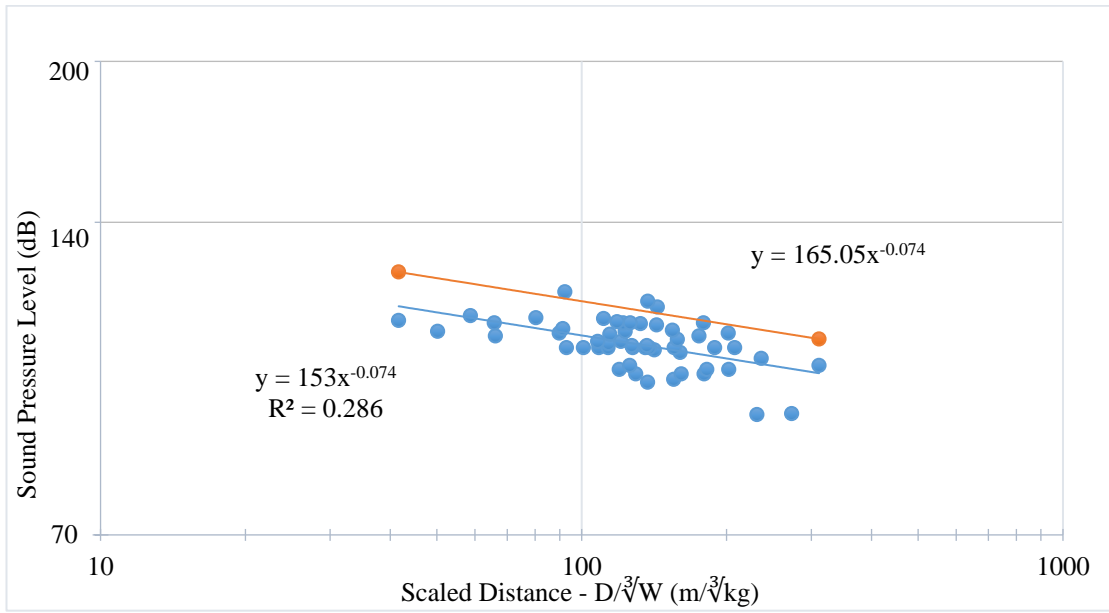
Figure 5.60 Gümüşkol Path 1 production blasting air blast overpressure levels in dB (Northern winds-N, NW, NE, NNE, ENE)

Figure 5.61 Gümüşkol Path 1 production blasting air blast overpressure levels in dB (Southern winds-SE, SSW, S)

147
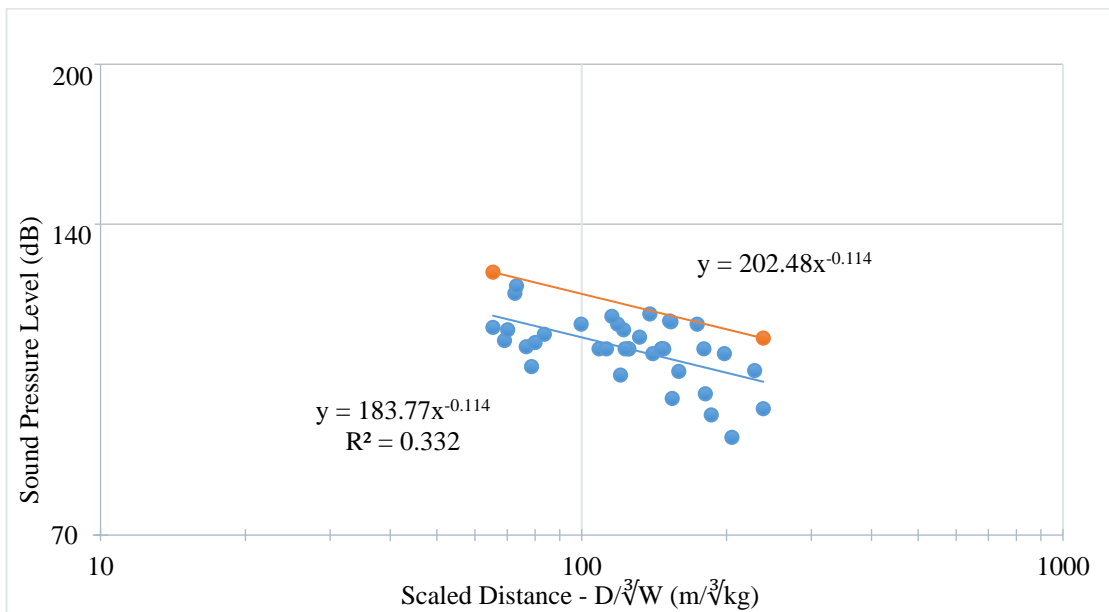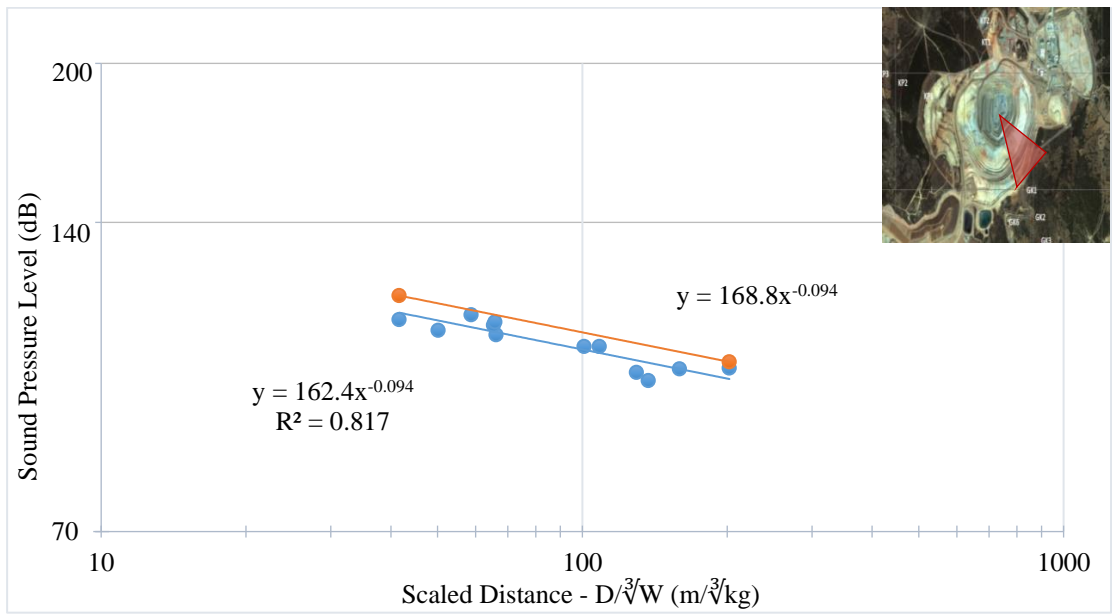
Figure 5.62 Gümüşkol Path 1 production blasting air blast overpressure levels in dB (Pit location- SE, SSE - in front of the pit)
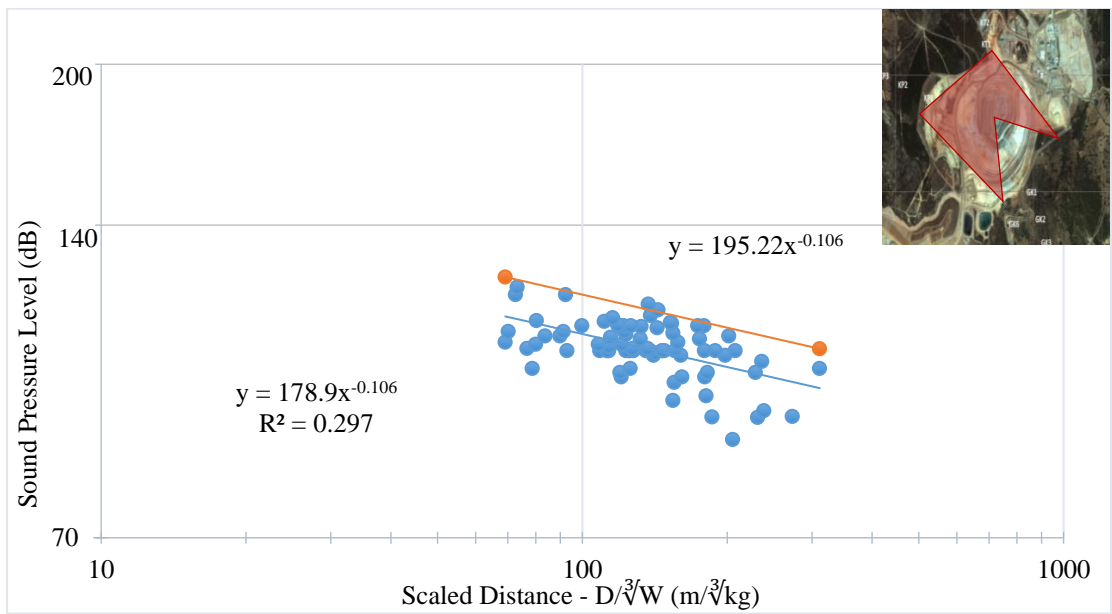
Figure 5.63 Gümüşkol Path 1 production blasting air blast overpressure levels in dB (Pit location- N, NE, E, ESE, S, SSW, W, NNW- behind the pit)

5.2.2.4 Gümüşkol Village Path 2

72 air blast records were obtained from production blasts and the highest air blast level measured at the village from production blasting is 110.2 dB with 3.13 Hz predominant frequency (at 1558 m). Air blast levels from production blasts are below the permitted values given in US OSM Regulations (129 dB) (in Table 2.7). Moreover, they are even less than the threshold level of complaints (117 dB) (in Figure 2.22).

For air shock analyses both blast group location and wind direction classification were tested. 6 different pit classification scenarios were evaluated by using model set and test set and compared to the regression analysis from unclassified data. Table 5.26 shows the directions included in the analysis, line equation and R^2 (square of correlation coefficient). To evaluate the performance of the models; correlation coefficient, coefficient of determination and Root-Mean Square Error (RMSE) were calculated and compared in Table 5.27 and the best result is obtained for model 6 combination.

Figure 5.64 shows air blast attenuation relation from unclassified data. Air blast analysis of production blasts for northern winds is given in Figure 5.65. The minimum and the maximum northern wind speed were 1.02 m/s and 10.02 m/s, respectively. Air blast analysis of production blasts for southern winds is given in Figure 5.66. The minimum and the maximum southern wind speed were 0.957 m/s and 4.109 m/s, respectively. In addition to wind direction classification, blast group location was also used for classification of the air blast data. Figure 5.67 and Figure 5.68 show regression analyses for blast groups in front of the pit and behind the pit, respectively. Analysis for 'in front of the pit' case provides higher correlation.

Table 5.26 Gümüşkol Path 2 properties of the formed models

	Pit location	Directions included	Line equation		
Unclassified	-	-	$Y = 157.1 * x^{-0.08}$	$R^2= 0.268$	R=-0.518
Model 1	In front of the pit	WNW, W, S, E, ENE	$y = 156.1 * x^{-0.08}$	$R^2= 0.273$	R=-0.522
	Behind the pit	N, NE, NW	$y = 168.6 * x^{-0.10}$	$R^2= 0.203$	R=-0.451
Model 2	In front of the pit	SSW, S, E, ENE	$y = 187.5 * x^{-0.12}$	$R^2= 0.518$	R=-0.720
	Behind the pit	SW, W, NW, N, NE	$y = 155.6 * x^{-0.08}$	$R^2= 0.158$	R=-0.397
Model 3	In front of the pit	WSW, S, E, ENE	$y = 153.9 * x^{-0.08}$	$R^2= 0.250$	R=-0.500
	Behind the pit	W, NW, N, NE	$y = 176.1 * x^{-0.10}$	$R^2= 0.226$	R=-0.475
Model 4	In front of the pit	SW, S, E, ENE	$y = 162.7 * x^{-0.09}$	$R^2= 0.293$	R=-0.541
	Behind the pit	WSW, W, NW, N, NE	$y = 176.6 * x^{-0.10}$	$R^2= 0.256$	R=-0.506
Model 5	In front of the pit	SE, SSE, S, SSW	$y = 175.3 * x^{-0.11}$	$R^2= 0.496$	R=-0.704
	Behind the pit	N, NE, ESE, SW, W, NNW	$y = 155.1 * x^{-0.08}$	$R^2= 0.155$	R=-0.394
Model 6	In front of the pit	SE, SSE	$y = 172.6 * x^{-0.11}$	$R^2= 0.458$	R=-0.677
	Behind the pit	N, NE, E, S, SW, W, NNW	$y = 163.2 * x^{-0.09}$	$R^2= 0.275$	R=-0.524
Model 7	Northern winds	N, NE, NW	$y = 149.06 * x^{-0.07}$	$R^2 = 0.334$	R=-0.578
(Wind direction Classification)	Southern winds	SE, ESE	$y = 182.48 * x^{-0.117}$	$R^2 = 0.252$	R=-0.502

Table 5.27 Gümüşkol Path 2 performance indicators for the models

	Modelling Set			Testing Set		
	R	**r^2**	**RMSE**	**R**	**r^2**	**RMSE**
Unclassified	0.531	0.282	5.067	0.244	-0.006	5.700
Model 1	0.533	0.283	5.062	0.244	-0.008	5.704
Model 2	0.569	0.324	4.917	0.465	0.064	5.497
Model 3	0.534	0.285	5.057	0.251	0.012	5.649
Model 4	0.552	0.304	4.989	0.272	-0.050	5.822
Model 5	0.538	0.289	5.041	0.382	0.076	5.461
Model 6	**0.555**	**0.307**	**4.977**	**0.565**	**0.266**	**4.870**
Model 7	0.611	0.373	4.733	0.481	0.209	5.055
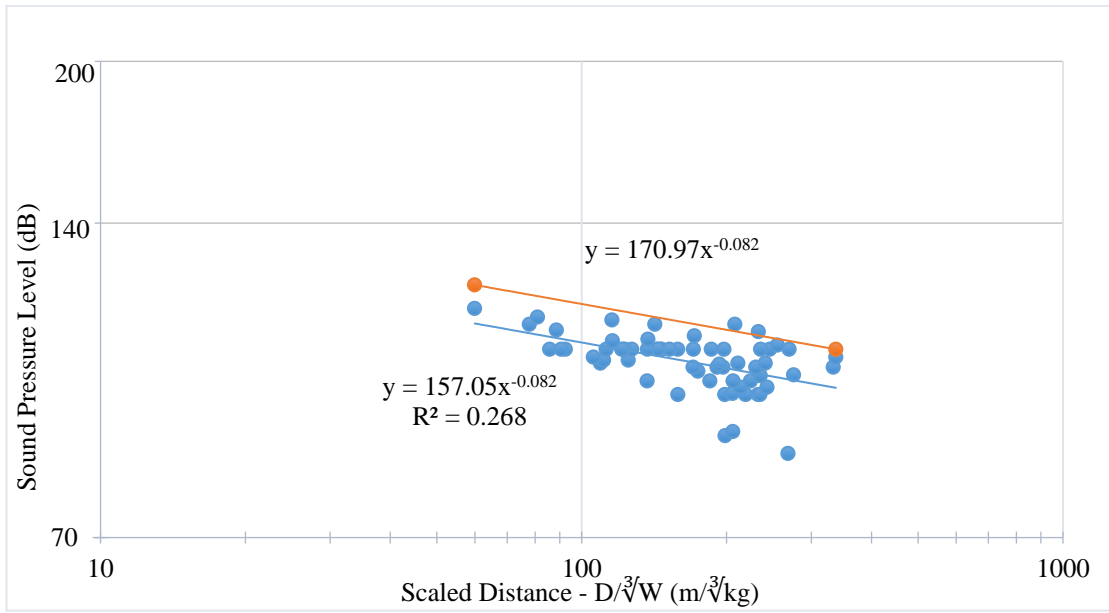
Figure 5.64 Gümüşkol Path 2 unclassified production blasting air blast overpressure levels in dB

Figure 5.65 Gümüşkol Path 2 production blasting air blast overpressure levels in dB (Northern winds-N, NE, NW)

151
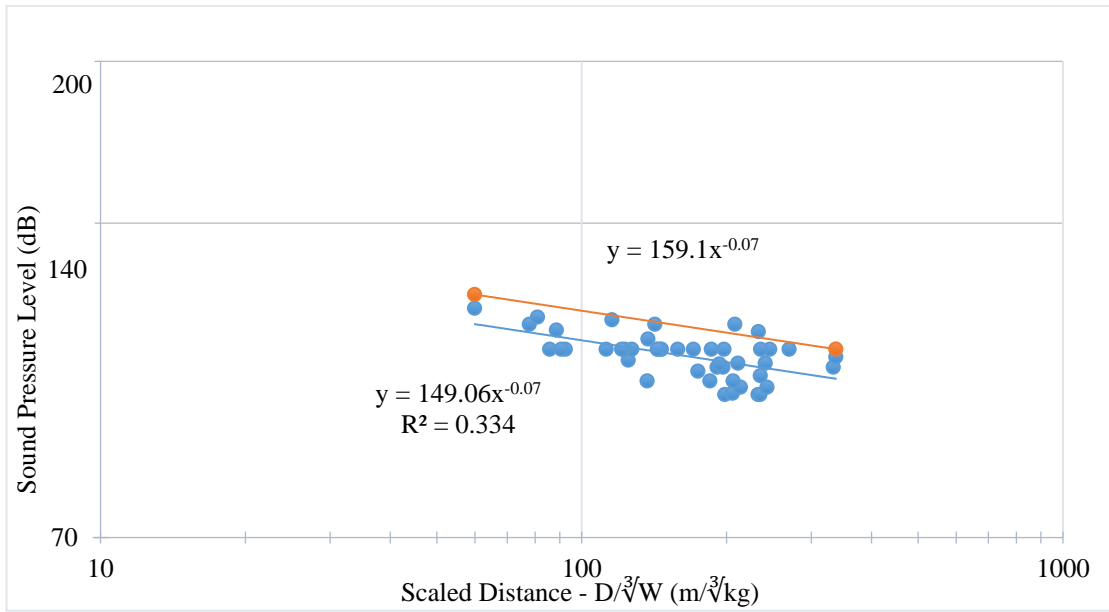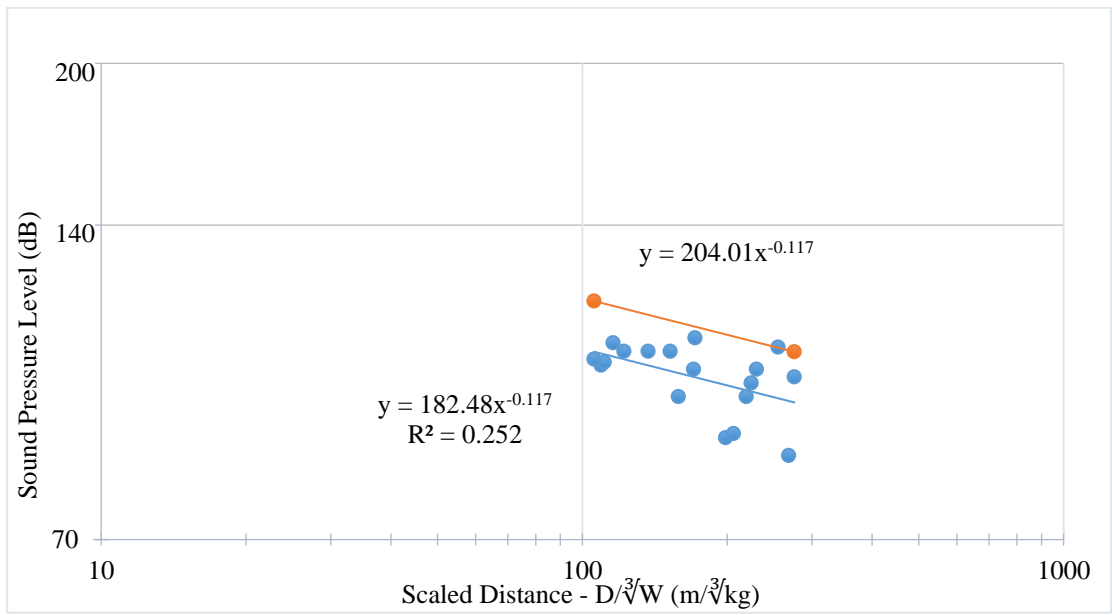
Figure 5.66 Gümüşkol Path 2 production blasting air blast overpressure levels in dB (Southern winds-SE, ESE)

$$y = 204.01x^{-0.117}$$

$$y = 182.48x^{-0.117}$$
$$R^2 = 0.252$$
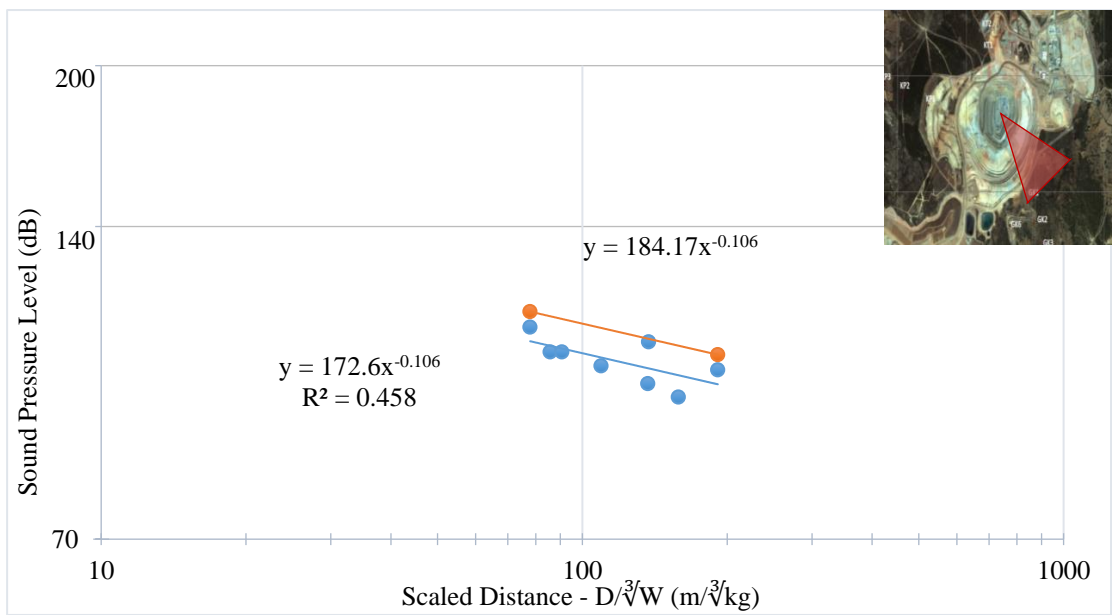
Figure 5.67 Gümüşkol Path 2 production blasting air blast overpressure levels in dB (Pit location- SE, SSE - in front of the pit)

$$y = 184.17x^{-0.106}$$

$$y = 172.6x^{-0.106}$$
$$R^2 = 0.458$$

152
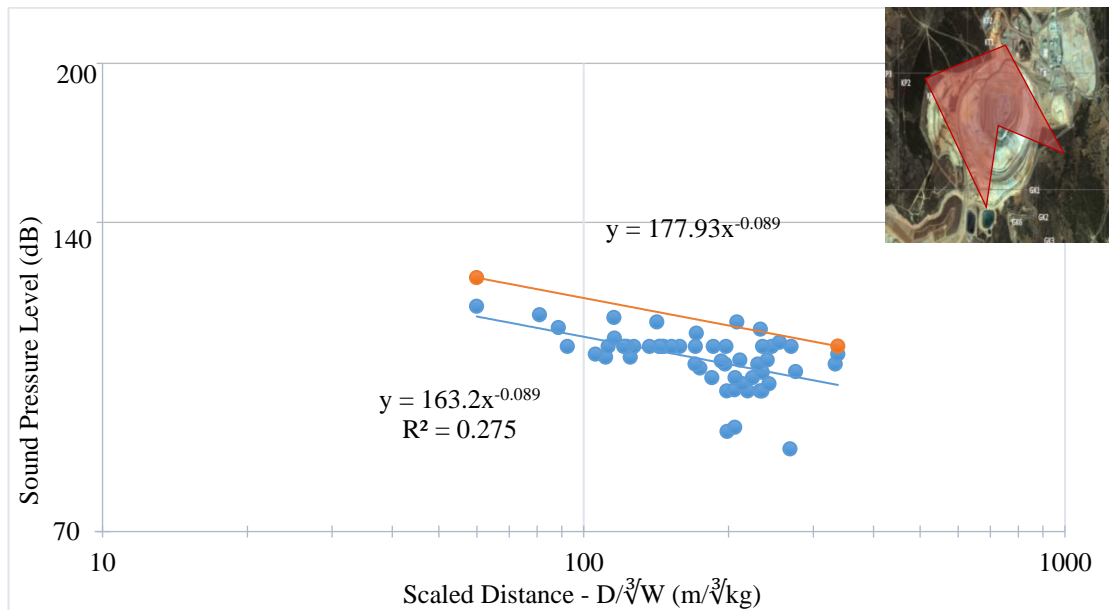
Figure 5.68 Gümüşkol Path 2 production blasting air blast overpressure levels in dB (Pit location- N, NE, E, S, SW, W, NNW - behind the pit)

5.3 Comparison of Ground Vibrations from 'In Front of the Pit' and 'Behind the Pit' Blasts

Table 5.28 tabulates the maximum air blast and ground vibration levels measured in each village at the nearest building to the mine. The highest ground vibration values measured in villages are 0.741 mm/s in Gümüşkol Path 1, 1.49 mm/s, in Gümüşkol Path 2, 2.372 mm/s in Karapınar and 1.876 mm/s in Katrancılar.

The lowest seismic wave dominant frequencies measured in the villages were 4.63 Hz for transverse component (0.270 mm/s) in Gümüşkol Path 1, 4.13 Hz for transverse component (0.317 mm/s) in Gümüşkol Path 2, 3.38 Hz for radial component (0.095 mm/s) in Karapınar, 3.81 Hz for vertical component (0.709 mm/s) in Katrancılar. The measured velocity values for the lowest frequencies are even less than the allowable particle velocity (5.00 mm/s) given for an explosion with 1 Hz frequency (in Figure 2.17). To prevent human disturbance the particle velocity should be less than 6.35 mm/s according to ANSI S3.29-1983 (in Table 2.6).

153

The highest seismic wave dominant frequencies were 31.94 Hz for vertical component (0.355 mm/s) in Gümüşkol Path 1, 35.50 Hz for vertical component (0.536 mm/s) in Gümüşkol Path 2, 15.44 Hz for vertical component (0.190 mm/s) in Karapınar, 14.38 Hz for radial component (0.952 mm/s) in Katrancılar. According to US OSM regulations for 14.38 Hz frequency allowable velocity value is 26.73 mm/s.

The highest ground vibration velocity is measured at KP4 station as 2.372 mm/s (with 7.94 Hz). According to US OSM regulations, this value is 12.5% of the maximum allowable ground vibration level (19 mm/s) for this frequency. Therefore, neither human disturbance nor structural damage are not possible. According to DIN 4150 (Table 2.5) standard for seismic waves with frequencies less than 10 Hz, maximum allowable ground vibration is 5 mm/s. So, it can be said that the measured velocity value is 47.44% of the allowable value. In other words, even if we take the allowable velocity value for buildings under a preservation order (3 mm/s), the measured value is still lower than the safe limits.

Table 5.28 The highest airblast and PPV levels at nearest location of settlements to the mine

| | Airblast level (dB) | | PPV (mm/s) |
	Presplit blasting	Production blasting	Production blasting
Gümüşkol Path 1	110.8 (9.81 Hz)	101.9 (3.63 Hz)	0.741 (12.81 Hz)
Gümüşkol Path 2	115.7 (9.25 Hz)	110.2 (3.13 Hz)	1.490 (13.13 Hz)
Katrancılar	112.0 (6.50 Hz)	104.9 (3.88 Hz)	1.876 (5.63 Hz)
Karapınar	112.0 (12.40 Hz)	110.6 (3.88 Hz)	2.372 (7.94 Hz)

Table 5.29 shows ground vibration prediction equations and PPV values calculated from the equations derived for production blasts at each village for the same square root scaled distance value (SRT SD=50). For Katrancılar and Karapınar PPV values are always higher when blast groups are 'in front of the pit' than 'behind the pit', as expected. However, for Gümüşkol path 1 and path 2, PPV values are higher when blast groups are located 'behind the pit' than blast groups located 'in front of the pit'. The reason might be attributed to the northeast-striking sub-vertical fault at the east part of the deposit and intrusive phases at that part of the deposit (Chapter 3.3, Figure 3.2). This fact may also be attributed to the strata replicating the probable shape of the actual stratovolcano which dips away from the deposit. A better understanding can be

achieved after obtaining velocity profile of the region which is not within the scope of this study. Moreover, the highest ground vibration values are expected in Gümüşkol path 1 from 'behind the pit' blasts for the same scaled distance.

Table 5.29 PPV values for 'in front of the pit' and 'behind the pit' conditions for SD=50

	in front of the pit	behind the pit
Katrancılar	$y = 529.48 \ x^{-1.326}$ PPV= 2.958 mm/s	$y = 881.28 \ x^{-1.55}$ PPV= 2.050 mm/s
Karapınar	$y = 891.1 \ x^{-1.445}$ PPV= 3.125 mm/s	$y = 1635.9 \ x^{-1.705}$ PPV= 2.075 mm/s
Gümüşkol Path 1	$y = 2607.3 \ x^{-1.761}$ PPV= 2.656 mm/s	$y = 110800 \ x^{-2.623}$ PPV= 3.874 mm/s
Gümüşkol Path 2	$y = 1367.6 \ x^{-1.549}$ PPV= 3.193 mm/s	$y = 673.75 \ x^{-1.349}$ PPV= 3.440 mm/s

5.4 Comparison of Air Blast Levels from Presplit and Production blasts

The results showed that, both for presplit and production blasts, blast group location is a better classification method than wind direction according to comparison of RMSE, r^2 and R of the models.

Table 5.30 and Table 5.31 show air blast levels calculated from the equations derived for presplit blasts and production blasts at each village for the same cube root scaled distance value (CRT SD=110), respectively. The predictions are obtained from 95% confidence interval line equation. It can be concluded that presplit blasts always result in higher air blast levels compared to production blasts. This is due to the fact that no stemming is applied in presplit blasts which results in higher air shock. Moreover, no matter it is a production or presplit blast if the blast group stands 'behind the pit' it results in higher air blast levels compared to 'in front of the pit' blasts. This is the expected result; the reason is topographic shielding in front of the villages which hinders the propagation of air shock towards the villages.

Table 5.30 Air blast levels for presplit blasts for 'in front of the pit' and 'behind the pit' conditions for SD=110

	in front of the pit	behind the pit
Katrancılar	$y = 425.95x^{-0.231}$ Air blast level= 143.8 dB	$y = 195.41x^{-0.091}$ Air blast level= 127.4 dB
Karapınar	$y = 244.66x^{-0.139}$ Air blast level= 127.3 dB	$y = 476.17x^{-0.255}$ Air blast level= 143.6 dB
Gümüşkol Path 1	$y = 214.99x^{-0.145}$ Air blast level= 108.7 dB	$y = 184.75x^{-0.082}$ Air blast level= 125.7 dB
Gümüşkol Path 2	$y = 196.03x^{-0.103}$ Air blast level= 120.8 dB	$y = 190.34x^{-0.087}$ Air blast level= 126.5 dB

Table 5.31 Air blast levels for production blasts for 'in front of the pit' and 'behind the pit' conditions for SD=110

	in front of the pit	behind the pit
Katrancılar	$y = 174.51x^{-0.098}$ Air blast level= 110.1 dB	$y = 196.2x^{-0.109}$ Air blast level= 117.5 dB
Karapınar	$y = 225.93x^{-0.135}$ Air blast level= 119.8 dB	$y = 312.95x^{-0.181}$ Air blast level= 133.7 dB
Gümüşkol Path 1	$y = 168.8x^{-0.094}$ Air blast level= 108.5 dB	$y = 195.22x^{-0.106}$ Air blast level= 118.6 dB
Gümüşkol Path 2	$y = 184.17x^{-0.106}$ Air blast level= 111.9 dB	$y = 177.93x^{-0.089}$ Air blast level= 117.1 dB

Figure 5.69 shows the contour map of the region with main topographical features which may create shielding effect as explained in Figure 2.8 and Figure 2.10. There is no topographical shielding in front of Katrancılar stations. Gökgöz Hill for Gümüşkol path 1 and path 2, and Tınas Hill for Karapınar serve as topographical shielding by blocking the air shocks from 'in front of the pit' blasts. The effect of topographical shielding decreases when the blast group stands behind the pit. The difference in air blast levels is not so obvious for production blasts since the use of stemming decreases the air shock levels. Air shock analyses from presplit blasts show that 'in front of the pit' blasts result in higher noise levels than 'behind the pit' blasts in Katrancılar village. This is on the contrary to the expected results; the reason might be the wind direction and speed at the time of blast.

Figure 5.69 Topographic map Uşak Kışladağ Open Pit Mine with final outline of pit, neighboring settlements and monitoring paths (Çakmak, 2007)

Table 5.32 and Table 5.33 show air blast levels from presplit and production blasts for wind classification, respectively. For Karapınar, wind direction does have only a small effect on air shock. For Katrancılar northern winds result in higher noise levels and for Gümüşkol path 1 and Gümüşkol path 2 southern winds result in higher noise levels. Further classification of the data according to wind speed, temperature is necessary, however the size of the dataset is not enough for further classification. The maximum difference in airblast levels is in the range of 2-3 dB, which was seen on Gümüşkol

path 1 and Gümüşkol path 2. Gökgöz hill hinders Gümüşkol path 2 stations completely and Gümüşkol path 1 stations partly. Therefore, higher air blast levels are expected on Gümüşkol path 1 for the same scaled distance. Besides, the effect of topography is more obvious when wind blows from north.

Table 5.32 Air blast levels for presplit blasts for wind classification for SD=110

	Northern (Western for Karapınar)	Southern (Eastern for Karapınar)
Katrancılar	$y = 205.08x^{-0.097}$ Air blast level= 130.0 dB	$y = 183.04x^{-0.077}$ Air blast level= 127.5 dB
Karapınar	$y = 264.02x^{-0.152}$ Air blast level= 129.2 dB	$y = 223x^{-0.116}$ Air blast level= 129.3 dB
Gümüşkol Path 1	$y = 170.97x^{-0.067}$ Air blast level= 124.8 dB	$y = 214.68x^{-0.111}$ Air blast level= 127.4 dB
Gümüşkol Path 2	$y = 141.76x^{-0.035}$ Air blast level= 120.3 dB	$y = 184.77x^{-0.081}$ Air blast level= 126.3 dB

Table 5.33 Air blast levels for production blasts for wind classification for SD=110

	Northern (Western for Karapınar)	Southern (Eastern for Karapınar)
Katrancılar	$y = 169.78x^{-0.083}$ Air blast level= 114.9 dB	$y = 164.29x^{-0.076}$ Air blast level= 114.9 dB
Karapınar	$y = 223.96x^{-0.131}$ Air blast level= 121.0 dB	$y = 212x^{-0.118}$ Air blast level= 121.7 dB
Gümüşkol Path 1	$y = 165.05x^{-0.074}$ Air blast level= 116.6 dB	$y = 202.48x^{-0.114}$ Air blast level= 118.5 dB
Gümüşkol Path 2	$y = 159.1x^{-0.07}$ Air blast level= 114.5 dB	$y = 204.01x^{-0.117}$ Air blast level= 117.7 dB

5.5 Safe Explosive Amounts for Sample Blasts at Each Quadrant of the Pit

To introduce safe explosive amount for a region is an important measure not to exceed allowable ground vibration limits. Figure 5.6, Figure 5.8, Figure 5.12, Figure 5.14, Figure 5.18, Figure 5.20, Figure 5.24, Figure 5.26 give the safe explosive amounts with respect to blast group location for each village separately. However, explosive amount that is safe for one village direction, can have a damaging effect for another direction. In order to obtain a unified graph, 4 sample blasts are chosen. That means one blast for each quadrant, and safe explosive amount graph is obtained for each

158

quadrant. The locations of the sample blasts and corresponding quadrants are given in Figure 5.70.

Figure 5.70 Location of sample blasts

Table 5.34 shows the coordinates of each blast and their positioning with respect to villages. Table 5.35 shows the distance between the sample blasts and the closest monitoring stations located in villages (GK5, Sami Y., KP4, KT5).

The maximum safe explosive amounts per delay are calculated for each blast (or quadrant) using the 'in front of the pit'-'behind the pit' formulas, given in previous sections, are summarized in Table 5.36. For example, for 'Blast 1' if the allowable ground vibration limit is selected as 3.00 mm/s (Table 2.5) the safe explosive amount for each village is calculated as follows by using the distances in Table 5.35.

Behind the pit formula is used for Karapınar for 2247.0 m distance and 3118.12 kg explosive is obtained. Behind the pit formula is used for Katrancılar for 2030.0 m

159

distance and 2698.74 kg explosive is obtained. In front of the pit formula is used for Gümüşkol Path 1 for 1332.7 m distance and 814.54 kg explosive is obtained. In front of the pit formula is used for Gümüşkol Path 2 for 1229.6 m distance and 559.16 kg explosive is obtained. Among all the calculated explosive amounts, 559.16 kg/delay is the lowest and should not be exceeded. Otherwise, structural damage may take place for the buildings in Gümüşkol Path 2.

Table 5.34 Coordinates of sample blasts and their positioning with respect to villages

| | X | Y | Location of sample blasts with respect to villages | | | |
			Karapınar	Katrancılar	Gümüşkol Path 1	Gümüşkol Path 2
Blast 1	687712.5	4261325.0	Behind the pit	Behind the pit	In front of the pit	In front of the pit
Blast 2	687725.0	4261925.0	Behind the pit	In front of the pit	In front of the pit	Behind the pit
Blast 3	687237.5	4261925.0	In front of the pit	In front of the pit	Behind the pit	Behind the pit
Blast 4	687237.5	4261312.5	In front of the pit	Behind the pit	In front of the pit	In front of the pit

Table 5.35 Distances between sample blasts and monitoring stations

	Karapınar	Katrancılar	Gümüşkol Path 1	Gümüşkol Path 2
Blast 1	2247.0 m	2030.0 m	1332.7 m	1229.6 m
Blast 2	2167.0 m	1520.2 m	1887.2 m	1827.3 m
Blast 3	1679.6 m	1293.5 m	2086.3 m	1915.7 m
Blast 4	1801.2 m	1884.4 m	1588.4 m	1345.2 m

Table 5.36 Calculated explosive amounts per delay from sample blasts for each village

	Karapınar	Katrancılar	Gümüşkol Path 1	Gümüşkol Path 2	Recommended MIC
Blast 1	3118.12	2698.74	814.54	559.16	**559.16**
Blast 2	2900.00	942.35	1633.36	1087.80	942.35
Blast 3	1067.98	682.25	1434.62	1195.56	682.25
Blast 4	1228.20	2325.50	1157.09	669.24	669.24

The maximum explosive amount that can be blasted per delay not to exceed safe ground vibration limits are given in the form of graphs. The safe explosive amount graphs for sample blasts located in each quadrant are drawn for 3.00 mm/s and 5 mm/s vibration limits in Figure 5.71 and Figure 5.72, respectively.
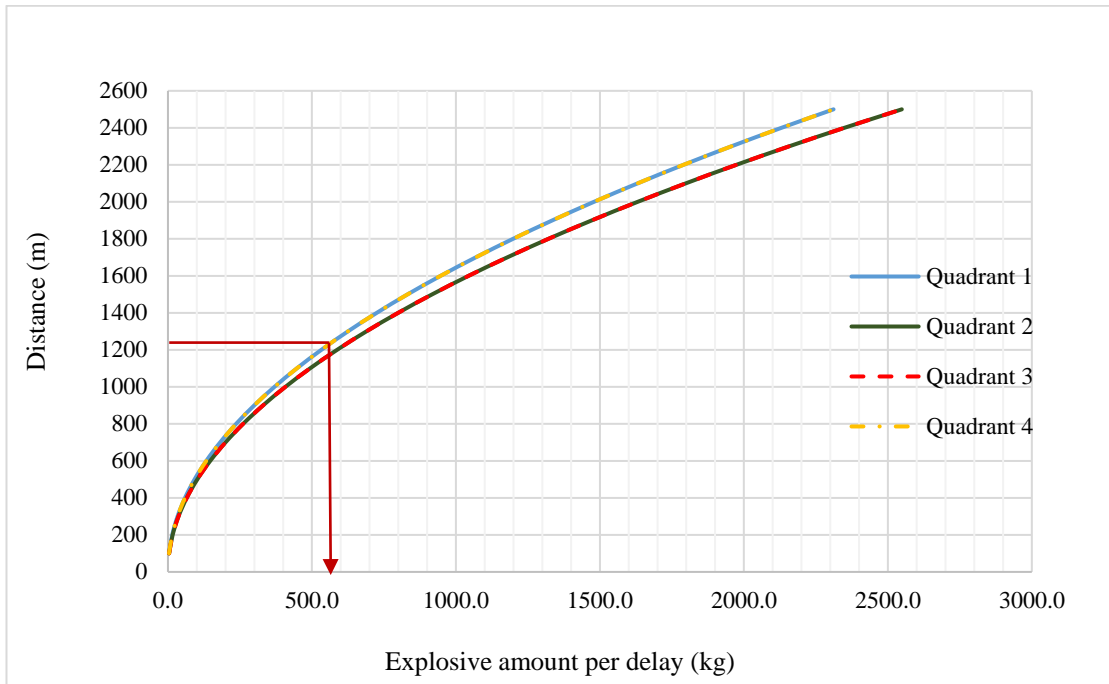
Figure 5.71 Safe explosive amounts for each quadrant not to exceed 3.00 mm/s in villages
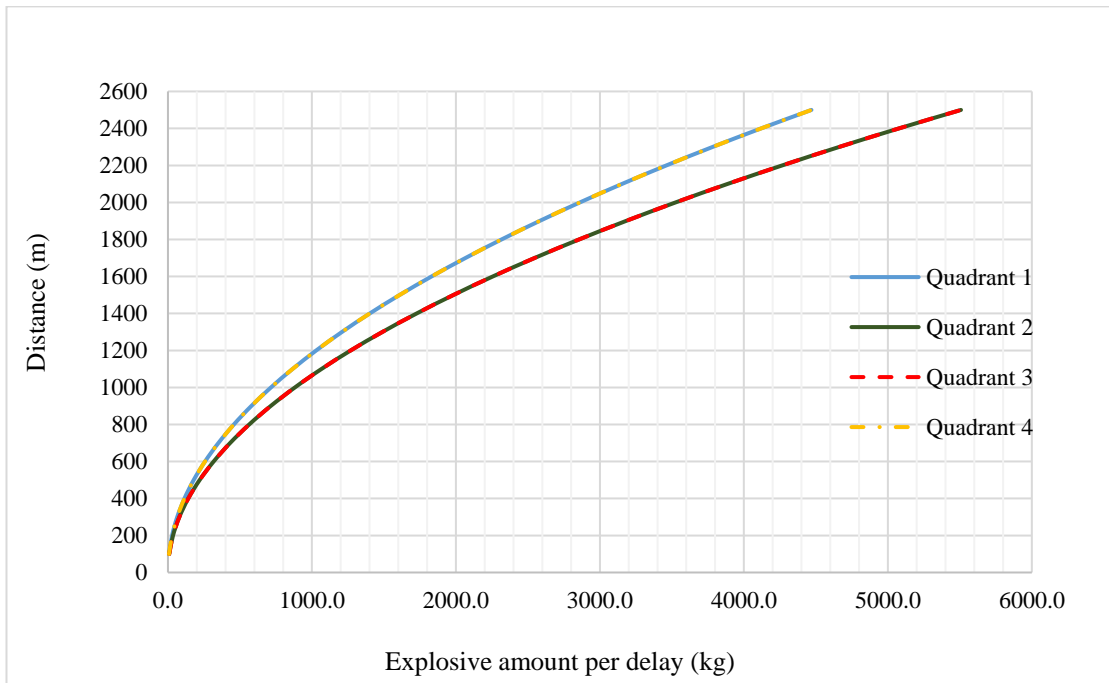
Figure 5.72 Safe explosive amounts for each quadrant not to exceed 5.00 mm/s in villages

161

If the buildings in the villages are classified as "buildings under preservation order" since they are mostly built by using mud mortar and rubble stone 3.00 mm/s ground vibration limit should not be exceeded (Table 2.5).

To use the graphs, the minimum distance is taken among distances to each village. For 'Blast 1', the minimum distance is 1229.6 m to Gümüşkol Path 2. Thus, the maximum safe explosive amount is calculated as 559.16 kg/delay. The collected data proved that the maximum charge amount/delay in practice in this mine was 519.00 kg/delay which can not create ground vibrations higher than 3.00 mm/s at the villages. In fact, the maximum ground vibration measured in the villages was 2.372 mm/s.

CHAPTER 6

MULTIPLE LINEAR REGRESSION ANALYSES OF GROUND VIBRATION AND AIR BLAST

In this chapter it was aimed to model ground vibration and airblast levels with more than one variable using multiple linear regression (MLR) analysis. The same datasets (both classified and unclassified sets) used for conventional regression analyses were used for MLR analyses.

The predictive equations for each case with S, R^2 and $R^2_{adjusted}$ are given in a table. Where S is the standard deviation between the predicted and measured values, the lower the S value, the better the model is. R^2 is the variation in model response in terms of percentage, the higher the R^2 value the better the model response is. $R^2_{adjusted}$ combines the number of predictors in the model, thus it is more reliable to compare $R^2_{adjusted}$ of models with different predictors. Since when a new predictor is added to the model R^2 value increases automatically even if there is no real improvement to the model. Moreover, root-mean square error (RMSE), correlation coefficient (R) and coefficient of determination (r^2) calculated from modelling and testing set were used as the performance indicators of the MLR models. The related definitions and equations were given in Chapter 5.

6.1   Ground Vibration Analyses

As a preliminary step to detailed ground vibration analyses, all the collected data were analyzed together. These values were later compared to regression analyses of the classified data. The best 'in front of the pit' and 'behind the pit' blast location combination determined in Chapter 5 was used for blast round location classification. Ground vibration analyses were conducted for each village and all possible input parameter combinations were tested to obtain the best model. For ground vibration

163

analyses 3 cases were tested each of which has different input parameters. The inputs for the 3 cases are listed below and PPV is the output for all models.

Case 1: scaled distance (SD), elevation difference (ED)

Case 2: charge weight (Q), distance (D)

Case 3: charge weight (Q), distance (D), elevation difference (ED)

Where elevation difference is the difference between explosion elevation and monitoring station elevation, $(ED = Explosion\ Elevation - Station\ Elevation)$.

The predictive equation for each case is given in Table 6.1. The performance indicators calculated for modelling and testing set are given in Table 6.2. The best result is obtained when charge weight, distance and elevation difference were inputs.

Table 6.1 Properties of the formed MLR models for whole production blast ground vibration data

	Predictive Equation	S	R^2	$R^2_{adjusted}$
Case 1	PPV=(0.6904 + 0.004823 SD - 0.000298 ED)$^{(-1/0.17917)}$	0.105	59.89%	59.72%
Case 2	PPV=(0.8778 - 0.000384 Q + 0.000236 D)$^{(-1/0.142962)}$	0.083	61.42%	61.25%
Case 3	PPV=(0.8601 - 0.000403 Q + 0.000243 D - 0.000252 ED)$^{-1/0.13686}$	0.078	62.86%	62.62%

Table 6.2 Performance indicators of MLR models for the cases whole ground vibration data

	Modelling Set			Testing Set		
	R	**r^2**	**RMSE**	**R**	**r^2**	**RMSE**
Case 1	0.688	0.307	2.235	0.743	0.360	2.115
Case 2	0.733	0.390	2.097	0.731	0.400	2.048
Case 3	**0.734**	**0.427**	**2.033**	**0.720**	**0.422**	**2.008**

6.1.1 Katrancılar Village

Table 6.3 shows predictive equations and Table 6.4 shows performance indicators for each case for unclassified Katrancılar ground vibration data. For unclassified ground vibration data, the best result was obtained when charge weight, distance and elevation difference were inputs. Table 6.5 shows predictive equations and Table 6.6 shows

performance indicators for each case for Katrancılar ground vibration data classified according to blast location. Case 1 combination yielded the lowest RMSE with the highest correlation coefficient and coefficient of determination for the testing set, therefore, square root scaled distance and elevation difference were used as inputs.

Table 6.3 Properties of the formed MLR models for unclassified data

	Predictive Equation	S	R^2	$R^2_{adjusted}$
Case 1	PPV=(0.7902 + 0.003220 SD - 0.000157 ED)$^{-1/0.121137}$	0.071	64.51%	64.03%
Case 2	PPV=exp(0.774 + 0.003516 Q - 0.001739 D)	0.561	68.31%	67.88%
Case 3	PPV=exp(1.037 + 0.003588 Q - 0.001897 D + 0.00238 ED)	0.555	69.23%	68.60%

Table 6.4 Performance indicators of MLR models for unclassified data

	Modelling Set			Testing Set		
	R	**r^2**	**RMSE**	**R**	**r^2**	**RMSE**
Case 1	-0.375	-1.067	3.033	-0.414	-1.314	2.684
Case 2	0.859	0.647	1.253	0.673	0.439	1.322
Case 3	**0.869**	**0.673**	**1.207**	**0.697**	**0.477**	**1.277**

Table 6.5 Performance indicators of MLR models for classified data

	Pit location	Predictive Equation	S	R^2	$R^2_{adjusted}$
Case 1	In front of the pit	PPV=(0.6969 + 0.004394 SD - 0.000039 ED)$^{-1/0.18599}$	0.088	65.73%	65.08%
	Behind the pit	PPV=(0.692 + 0.01130 SD + 0.00083 ED)$^{-2}$	0.387	49.31%	46.71%
Case 2	In front of the pit	PPV=exp(0.608 + 0.003841 Q - 0.001501 D)	0.498	68.32%	67.72%
	Behind the pit	PPV=(0.761 - 0.001617 Q + 0.000999 D)$^{-2}$	0.377	52.10%	49.65%
Case 3	In front of the pit	PPV=exp(0.705 + 0.003838 Q - 0.001562 D + 0.00077 ED)	0.499	68.45%	67.54%
	Behind the pit	PPV=(0.797 - 0.001568 Q + 0.000973 D + 0.00034 ED)$^{-2}$	0.381	52.14%	48.37%

Figure 6.1 shows measured versus MLR predicted PPV values with least-squares line for modelling set and testing sets.

Table 6.6 Performance indicators for classified data

	Modelling Set			Testing Set		
	R	**r^2**	**RMSE**	**R**	**r^2**	**RMSE**
Case 1	**0.836**	**0.571**	**1.382**	**0.930**	**0.720**	**0.934**
Case 2	0.848	0.657	1.235	0.690	0.421	1.343
Case 3	0.852	0.666	1.220	0.699	0.438	1.323
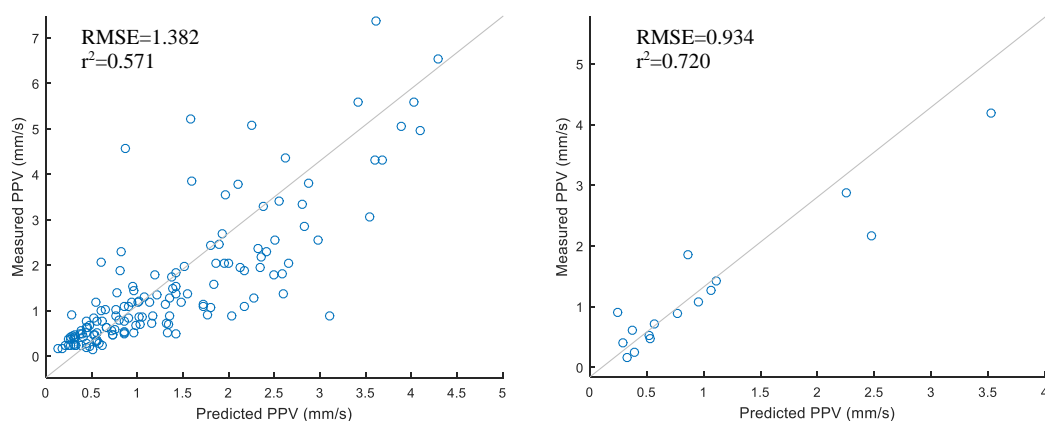
Figure 6.1 Predicted vs measured ground vibration levels for modeling set and testing set, respectively

6.1.2 Karapınar Village

Table 6.7 shows predictive equations and Table 6.8 shows performance indicators for each case for unclassified Karapınar ground vibration data. For unclassified ground vibration data, the best result was obtained when charge weight, distance and elevation difference were inputs. Table 6.9 shows predictive equations for ground vibration prediction.

Table 6.7 Properties of the formed MLR models for unclassified data

	Predictive Equation	S	R^2	$R^2_{adjusted}$
Case 1	$PPV=(0.4999 + 0.008673\ SD - 0.001132\ ED)^{(-1/0.309843)}$	0.191	65.79%	65.25%
Case 2	$PPV=(0.7080 - 0.000546\ Q + 0.000518\ D)^{(-1/0.307698)}$	0.193	64.50%	63.94%
Case 3	$PPV=(0.6756 - 0.000706\ Q + 0.000557\ D - 0.001016\ ED)^{-1/0.304895}$	0.173	70.91%	70.21%

Table 6.8 Performance indicators of MLR models for unclassified data

	Modelling Set			Testing Set		
	R	**r^2**	**RMSE**	**R**	**r^2**	**RMSE**
Case 1	0.541	0.176	3.799	0.640	0.202	3.703
Case 2	0.766	0.260	3.599	0.832	0.313	3.436
Case 3	**0.637**	**0.296**	**3.512**	**0.730**	**0.330**	**3.394**

Table 6.9 Properties of the formed MLR models for classified data

	Pit location	Predictive Equation	S	R^2	$R^2_{adjusted}$
Case 1	In front of the pit	PPV=(0.2851 + 0.012610 SD - 0.001331 ED)$^{-2}$	0.271	67.63%	66.94%
	Behind the pit	PPV=(-0.078 + 0.01969 SD - 0.00267 ED)$^{-2}$	0.415	53.38%	50.27%
Case 2	In front of the pit	PPV=(0.641 - 0.001044 Q + 0.000764 D)$^{-2}$	0.283	64.74%	63.99%
	Behind the pit	PPV=(0.934 - 0.001776 Q + 0.000942 D)$^{-2}$	0.417	52.84%	49.70%
Case 3	In front of the pit	PPV=(0.580 - 0.001190 Q + 0.000838 D - 0.001246 ED)$^{-2}$	0.265	69.42%	68.43%
	Behind the pit	PPV=(0.100 - 0.001648 Q + 0.001306 D - 0.00383 ED)$^{-2}$	0.392	59.79%	55.63%

Table 6.10 shows performance indicators for each case for Karapınar ground vibration data classified according to blast location. Case 3 combination yielded the lowest RMSE, when charge weight, distance and elevation difference were used for ground vibration prediction. Figure 6.2 shows measured versus MLR predicted PPV values with least-squares line for modelling set and testing sets.

Table 6.10 Performance indicators of MLR models for classified data

	Modelling Set			Testing Set		
	R	**r^2**	**RMSE**	**R**	**r^2**	**RMSE**
Case 1	0.578	0.185	3.778	0.683	0.219	3.665
Case 2	0.787	0.357	3.357	0.853	0.371	3.288
Case 3	**0.685**	**0.394**	**3.257**	**0.787**	**0.390**	**3.239**
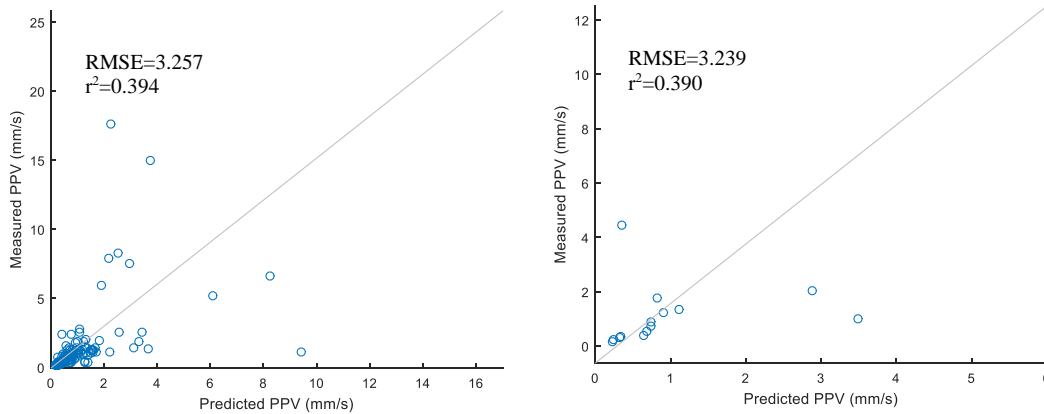
Figure 6.2 Predicted vs measured ground vibration levels for modeling set and testing set, respectively

6.1.3 Gümüşkol Village Path 1

Table 6.11 shows predictive equations and Table 6.12 shows performance indicators for each case for unclassified Gümüşkol Village Path 1 ground vibration data. For unclassified ground vibration data, the best result was obtained when scaled distance and elevation difference were inputs. Table 6.13 shows predictive equations and Table 6.14 shows performance indicators for each case for ground vibration data classified according to blast location. Case 3 combination yielded the lowest RMSE for the testing set, therefore, charge weight, distance and elevation difference were used for ground vibration prediction. Both unclassified and blast location classified data gave almost the same results. Figure 6.3 shows measured versus MLR predicted PPV values with least-squares line for modelling set and testing sets.

Table 6.11 Properties of the formed MLR models for unclassified data

	Predictive Equation	**S**	**R^2**	**R$^2_{adjusted}$**
Case 1	PPV=(0.6134 + 0.006635 SD - 0.000063 ED)$^{-1/0.205352}$	0.105	61.26%	60.57%
Case 2	PPV=exp(1.246 + 0.002769 Q - 0.002098 D)	0.537	60.63%	59.93%
Case 3	PPV=exp(1.271 + 0.002806 Q - 0.002116 D + 0.00019 ED)	0.539	60.64%	59.58%

Table 6.12 Performance indicators of MLR models for unclassified data

	Modelling Set			Testing Set		
	R	**r^2**	**RMSE**	**R**	**r^2**	**RMSE**
Case 1	**0.803**	**0.510**	**1.222**	**0.910**	**0.646**	**1.087**
Case 2	0.803	0.554	1.166	0.873	0.631	1.110
Case 3	0.802	0.556	1.163	0.872	0.632	1.108

Table 6.13 Properties of the formed MLR models for classified data

	Pit location	**Predictive Equation**	**S**	**R^2**	**$R^2_{adjusted}$**
Case 1	In front of the pit	$PPV=(0.6761 + 0.005601\ SD - 0.000001\ ED)^{-1/0.180012}$	0.090	63.79%	63.00%
	Behind the pit	$PPV=(-1.63 + 0.03060\ SD - 0.00675\ ED)^{-2}$	0.278	53.50%	48.33%
Case 2	In front of the pit	$PPV=\exp(1.385 + 0.002421\ Q - 0.002147\ D)$	0.520	64.02%	63.23%
	Behind the pit	$PPV=(1.114 - 0.00293\ Q + 0.000914\ D)^{-2}$	0.293	48.50%	42.78%
Case 3	In front of the pit	$PPV=\exp(1.427 + 0.002469\ Q - 0.002179\ D + 0.00029\ ED)$	0.523	64.04%	62.84%
	Behind the pit	$PPV=(-0.87 - 0.00305\ Q + 0.001766\ D - 0.00821\ ED)^{-2}$	0.291	51.89%	43.40%

Table 6.14 Performance indicators of MLR models for classified data

	Modelling Set			Testing Set		
	R	**r^2**	**RMSE**	**R**	**r^2**	**RMSE**
Case 1	0.808	0.503	1.231	0.908	0.618	1.128
Case 2	0.813	0.564	1.153	0.898	0.652	1.077
Case 3	**0.822**	**0.580**	**1.131**	**0.897**	**0.653**	**1.076**
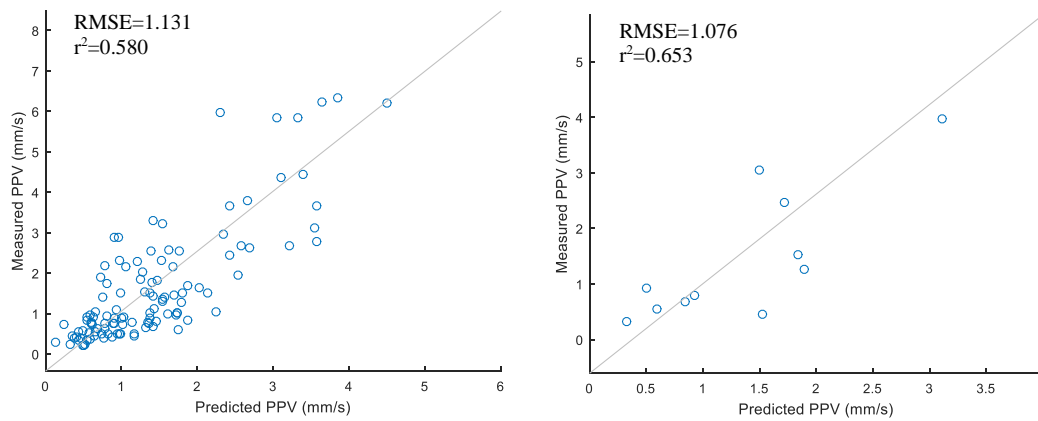
Figure 6.3 Predicted vs measured ground vibration levels for modeling set and testing set, respectively

6.1.4 Gümüşkol Village Path 2

Table 6.15 shows predictive equations and Table 6.16 shows performance indicators for each case for unclassified Gümüşkol Village Path 2 ground vibration data. For unclassified ground vibration data, the best result was obtained when charge weight, distance and elevation difference were inputs. Table 6.17 shows predictive equations and Table 6.18 shows performance indicators for each case for ground vibration data classified according to blast location.

Table 6.15 Properties of the formed MLR models for unclassified data

	Predictive Equation	S	R^2	$R^2_{adjusted}$
Case 1	PPV=exp(1.416 - 0.01977 SD - 0.00119 ED)	0.463	56.70%	55.44%
Case 2	PPV=exp(0.954 + 0.002372 Q - 0.001360 D)	0.466	56.16%	54.89%
Case 3	PPV=exp(0.880 + 0.002285 Q - 0.001300 D - 0.00068 ED)	0.468	56.40%	54.48%

Table 6.16 Performance indicators of MLR models for unclassified data

	Modelling Set			Testing Set		
	R	**r^2**	**RMSE**	**R**	**r^2**	**RMSE**
Case 1	0.746	0.530	0.634	0.948	0.566	0.703
Case 2	0.729	0.515	0.644	0.941	0.570	0.700
Case 3	**0.726**	**0.511**	**0.647**	**0.945**	**0.575**	**0.696**

Case 3 combination yielded the lowest RMSE for the testing set, therefore, charge weight, distance and elevation difference were used for ground vibration prediction. Figure 6.4 shows measured versus MLR predicted PPV values with least-squares line for modelling set and testing sets.

Table 6.17 Properties of the formed MLR models for classified data

	Pit location	Predictive Equation	S	R^2	$R^2_{adjusted}$
Case 1	In front of the pit	PPV=(1.60 - 0.0103 SD - 0.00472 ED)^2	0.249	70.67%	64.80%
	Behind the pit	PPV=exp(1.372 - 0.01901 SD - 0.00095 ED)	0.467	53.10%	51.42%
Case 2	In front of the pit	PPV=(1.505 + 0.00240 Q - 0.001054 D)^2	0.261	67.76%	61.31%
	Behind the pit	PPV=exp(0.942 + 0.002262 Q - 0.001319 D)	0.472	52.07%	50.36%
Case 3	In front of the pit	PPV=(0.36 + 0.00172 Q - 0.000064 D - 0.00822 ED)^2	0.255	72.22%	62.96%
	Behind the pit	PPV=exp(0.884 + 0.002193 Q - 0.001272 D - 0.00049 ED)	0.476	52.23%	49.62%

Table 6.18 Performance indicators of MLR models for classified data

	Modelling Set			Testing Set		
	R	r^2	RMSE	R	r^2	RMSE
Case 1	0.666	0.305	0.771	0.956	0.762	0.521
Case 2	0.723	0.447	0.688	0.941	0.562	0.706
Case 3	**0.521**	**-0.470**	**1.121**	**0.929**	**0.835**	**0.434**
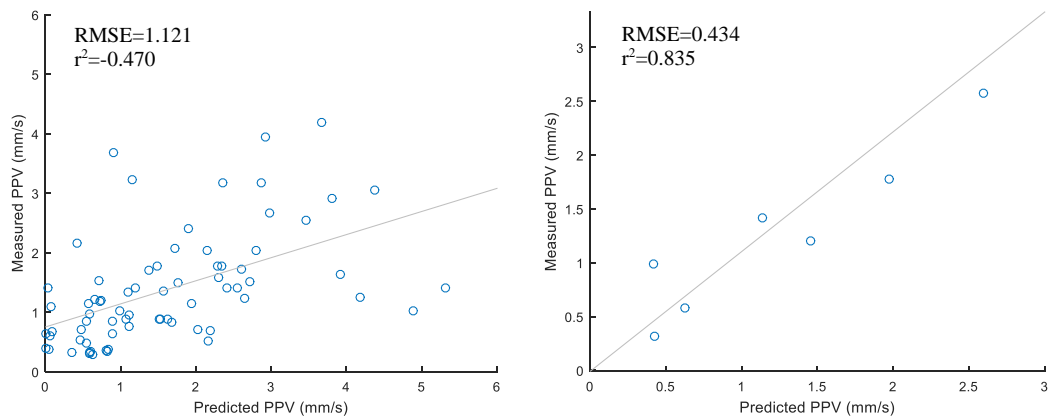
Figure 6.4 Predicted vs measured ground vibration levels for modeling set and testing set, respectively

6.2 Air shock Analyses

Air shock analyses were performed on presplit and production blasting data. The results will be presented for presplit and production blasts separately in the following sections.

6.2.1 Presplit Blasting Air Blast Analyses

As a preliminary step to detailed air blast analyses, all the collected data were analyzed together. These values were later compared to regression analyses of the classified data. The best 'in front of the pit' and 'behind the pit' blast location combination determined in Chapter 5 was used for blast round location classification. Air blast analyses were conducted for each village and all possible input parameter combinations were tested to obtain the best model. For analyses 3 cases were tested each of which has different input parameters. The inputs for the cases are listed below and air blast level is the output for all models.

Case 1: scaled distance (SD), elevation difference (ED)

Case 2: charge weight (Q), distance (D)

Case 3: charge weight (Q), distance (D), elevation difference (ED)

Where elevation difference is the difference between explosion elevation and monitoring station elevation $(ED = Explosion\ Elevation - Station\ Elevation)$.

The predictive equations for each case are given in Table 6.19. The performance indicators calculated for modelling and testing set are given in Table 6.20. The best result was obtained when charge weight, distance were inputs.

Table 6.19 Properties of the formed MLR models for whole presplit blast air blast data

	Predictive Equation	S	R^2	$R^2_{adjusted}$
Case 1	dB=exp(4.7996 - 0.000517 SD - 0.000151 ED)	0.061	41.41%	40.67%
Case 2	dB=exp(4.8369 + 0.000011 Q - 0.000115 D)	0.057	50.01%	49.37%
Case 3	dB=exp(4.8346 + 0.000011 Q - 0.000113 D - 0.000020 ED)	0.057	50.03%	49.07%

Table 6.20 Performance indicators of MLR models for air blast data

	Modelling Set			Testing Set		
	R	**r²**	**RMSE**	**R**	**r²**	**RMSE**
Case 1	0.696	0.465	6.411	0.765	0.509	6.471
Case 2	**0.718**	**0.515**	**6.103**	**0.783**	**0.592**	**5.895**
Case 3	0.718	0.515	6.102	0.780	0.590	5.910

6.2.1.1 Katrancılar Village

Table 6.21 shows predictive equations and Table 6.22 shows performance indicators for each case for unclassified air blast data from presplit blasts. The best result was obtained when charge weight, distance and elevation difference are inputs. Table 6.23 shows predictive equations and Table 6.24 shows performance indicators air blast data classified according to blast location. Case 3 combination yielded the lowest RMSE, when charge weight, distance and elevation difference were input parameters. Figure 6.5 shows measured versus MLR predicted air blast levels with least-squares line for modelling set and testing sets.

Table 6.21 Properties of the formed MLR models for unclassified data

	Predictive Equation	S	R²	R²$_{adjusted}$
Case 1	dB=exp(4.7757 - 0.000477 SD - 0.000339 ED)	0.068	31.68%	28.89%
Case 2	dB=exp(4.8308 + 0.000084 Q - 0.000115 D)	0.058	50.40%	48.37%
Case 3	dB=exp(4.9017 + 0.000046 Q - 0.000152 D + 0.000511 ED)	0.056	55.55%	52.77%

Table 6.22 Performance indicators of MLR models for unclassified data

	Modelling Set			Testing Set		
	R	**r²**	**RMSE**	**R**	**r²**	**RMSE**
Case 1	0.673	0.344	7.178	0.856	0.370	7.313
Case 2	0.715	0.511	6.197	0.858	0.689	5.138
Case 3	**0.750**	**0.562**	**5.864**	**0.839**	**0.702**	**5.032**

Table 6.23 Properties of the formed MLR models for classified data

	Pit location	Predictive Equation	S	R^2	$R^2_{adjusted}$
Case 1	In front of the pit	dB=exp(4.8844 - 0.000706 SD + 0.000488 ED)	0.053	54.65%	51.63%
	Behind the pit	dB=exp(4.9632 - 0.002563 SD + 0.000006 ED)	0.052	66.85%	62.71%
Case 2	In front of the pit	dB= exp(4.8532 - 0.000020 Q - 0.000138 D)	0.054	52.83%	49.68%
	Behind the pit	dB=exp(4.790 + 0.000869 Q - 0.000181 D)	0.054	64.84%	60.45%
Case 3	In front of the pit	dB=exp(5.0075 - 0.000115 Q - 0.000221 D + 0.001062 ED)	0.042	73.04%	70.25%
	Behind the pit	dB=exp(4.788 + 0.000863 Q - 0.000179 D - 0.000029 ED)	0.056	64.86%	57.84%

Table 6.24 Performance indicators of MLR models for classified data

	Modelling Set			Testing Set		
	R	r^2	RMSE	R	r^2	RMSE
Case 1	0.516	-4.555	20.883	0.338	-2.758	17.862
Case 2	0.776	0.602	5.592	0.896	0.638	5.541
Case 3	**0.843**	**0.710**	**4.774**	**0.862**	**0.732**	**4.766**
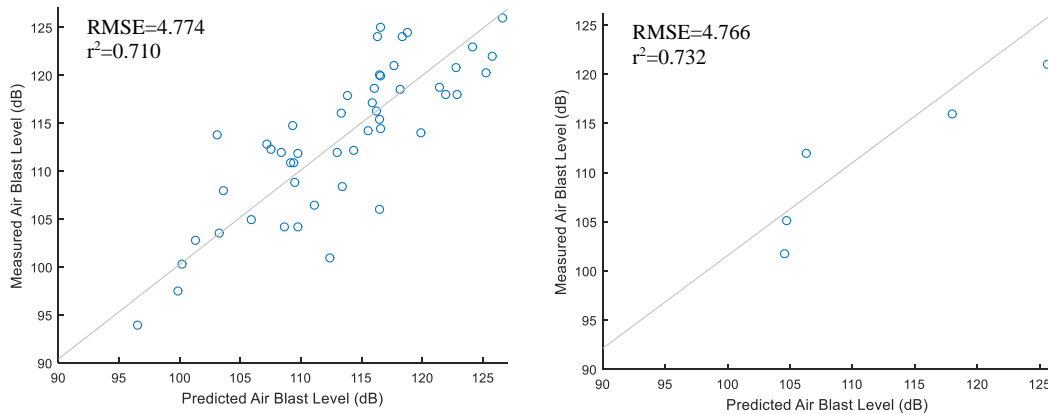
Figure 6.5 Predicted vs measured air blast levels for modeling set and testing set, respectively

6.2.1.2 Karapınar Village

Table 6.25 shows predictive equations and Table 6.26 shows performance indicators for each case for unclassified air blast data from presplit blasts. The best result was obtained when charge weight, distance and elevation difference were inputs. Table

174

6.27 shows predictive equations and Table 6.28 shows performance indicators for air blast data classified according to blast location. Case 3 combination for unclassified data yielded the lowest RMSE, when charge weight, distance and elevation difference were used as inputs. The analysis from unclassified data was better than classified data, therefore it can be concluded that blast round location does not affect air blast levels in Karapınar. Figure 6.6 shows measured versus MLR predicted air blast levels with least-squares line for modelling set and testing sets of the unclassified model.

Table 6.25 Properties of the formed MLR models for unclassified data

	Predictive Equation	S	R^2	$R^2_{adjusted}$
Case 1	dB=exp(4.8690 - 0.000852 SD - 0.000142 ED)	0.056	66.94%	65.53%
Case 2	dB=exp(4.9377 - 0.000187 Q - 0.000184 D)	0.048	75.59%	74.55%
Case 3	dB=exp(4.9266 - 0.000170 Q - 0.000178 D - 0.000102 ED)	0.048	76.35%	74.81%

Table 6.26 Performance indicators of MLR models for unclassified data

	Modelling Set			Testing Set		
	R	r^2	RMSE	R	r^2	RMSE
Case 1	0.829	0.687	5.858	0.932	0.727	5.925
Case 2	0.876	0.768	5.044	0.913	0.799	5.080
Case 3	**0.879**	**0.773**	**4.985**	**0.924**	**0.813**	**4.896**

Table 6.27 Properties of the formed MLR models for classified data

	Pit location	Predictive Equation	S	R^2	$R^2_{adjusted}$
Case 1	In front of the pit	dB= exp(4.8918 - 0.001045 SD - 0.000034 ED)	0.053	70.81%	68.99%
	Behind the pit	dB=exp(4.8302 - 0.000665 SD - 0.000455 ED)	0.058	64.21%	58.24%
Case 2	In front of the pit	dB=exp(4.9463 - 0.000170 Q - 0.000213 D)	0.039	84.02%	83.02%
	Behind the pit	dB=exp(5.090 - 0.000558 Q - 0.000227 D)	0.054	69.06%	63.90%
Case 3	In front of the pit	dB=exp(4.9485 - 0.000173 Q - 0.000215 D + 0.000018 ED)	0.039	84.05%	82.50%
	Behind the pit	dB=exp(5.021 - 0.000466 Q - 0.000195 D - 0.000275 ED)	0.054	71.46%	63.67%

Table 6.28 Performance indicators of MLR models for classified data

	Modelling Set			Testing Set		
	R	**r^2**	**RMSE**	**R**	**r^2**	**RMSE**
Case 1	0.294	-14.724	41.496	0.892	0.694	6.275
Case 2	0.322	-14.626	41.366	0.873	0.756	5.596
Case 3	**0.321**	**-14.621**	**41.359**	**0.874**	**0.761**	**5.536**
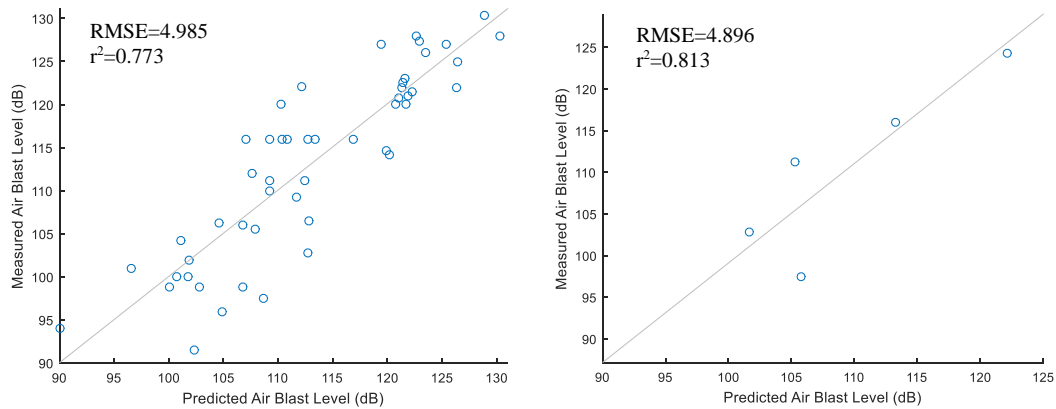
Figure 6.6 Predicted vs measured air blast levels for modeling set and testing set from, respectively

6.2.1.3 Gümüşkol Village Path 1

Table 6.29 shows predictive equations and Table 6.30 shows performance indicators for each case for unclassified air blast data from presplit blasts. The best result was obtained when charge weight, distance and elevation difference are inputs. Table 6.31 shows predictive equations and Table 6.32 shows performance indicators for air blast data classified according to blast location. Case 3 combination yielded the lowest RMSE, when charge weight, distance and elevation difference were inputs.

Table 6.29 Properties of the formed MLR models for unclassified data

	Predictive Equation	S	R^2	$R^2_{adjusted}$
Case 1	dB=exp(4.7805 - 0.000364 SD - 0.000066 ED)	0.048	38.17%	33.59%
Case 2	dB=exp(4.7917 + 0.000020 Q - 0.000072 D)	0.047	40.99%	36.61%
Case 3	dB=exp(4.7921 + 0.000020 Q - 0.000072 D + 0.000002 ED)	0.048	40.99%	34.18%

176

Table 6.30 Performance indicators of MLR models for unclassified data

	Modelling Set			Testing Set		
	R	**r^2**	**RMSE**	**R**	**r^2**	**RMSE**
Case 1	0.622	0.387	4.974	0.768	0.565	3.987
Case 2	0.644	0.415	4.859	0.844	0.642	3.619
Case 3	**0.644**	**0.415**	**4.859**	**0.845**	**0.642**	**3.618**

Table 6.31 Properties of the formed MLR models for classified data

	Pit location	**Predictive Equation**	**S**	**R^2**	**$R^2_{adjusted}$**
Case 1	In front of the pit	dB= exp(4.860 - 0.001737 SD - 0.000070 ED)	0	100.00%	100.00%
	Behind the pit	dB=exp(4.7904 - 0.000397 SD - 0.000058 ED)	0.048	40.85%	35.92%
Case 2	In front of the pit	dB= exp(4.834 + 0.000217 Q - 0.000313 D)	0	100.00%	100.00%
	Behind the pit	dB=exp(4.8046 + 0.000014 Q - 0.000079 D)	0.046	44.43%	39.79%
Case 3	In front of the pit	dB=exp(4.834 + 0.000217 Q - 0.000313 D)	0	100.00%	100.00%
	Behind the pit	dB=exp(4.8093 + 0.000014 Q - 0.000081 D + 0.000023 ED)	0.047	44.46%	37.22%

Table 6.32 Performance indicators of MLR models for classified data

	Modelling Set			Testing Set		
	R	**r^2**	**RMSE**	**R**	**r^2**	**RMSE**
Case 1	0.678	0.459	4.671	0.829	0.629	3.686
Case 2	0.702	0.493	4.524	0.925	0.708	3.271
Case 3	**0.703**	**0.494**	**4.519**	**0.934**	**0.723**	**3.182**

Figure 6.7 shows measured versus MLR predicted air blast levels with least-squares line for modelling set and testing sets.
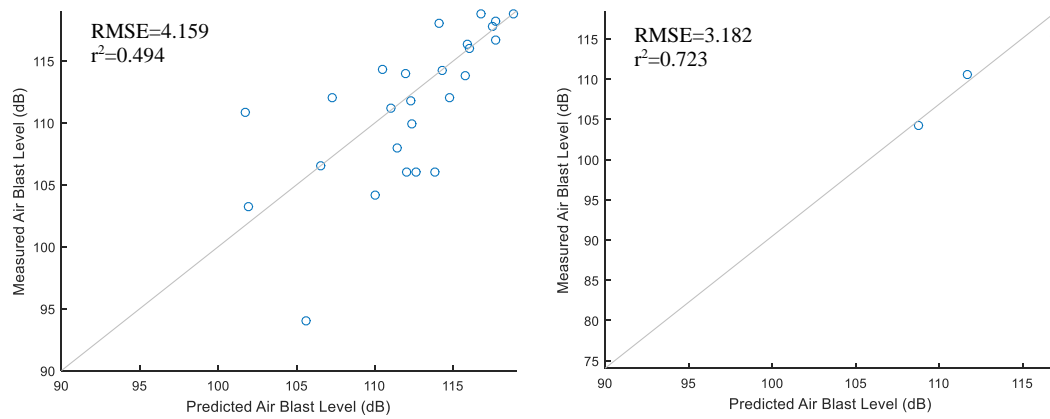
Figure 6.7 Predicted vs measured air blast levels for modeling set and testing set, respectively

6.2.1.4 Gümüşkol Village Path 2

Table 6.33 shows predictive equations and Table 6.34 shows performance indicators for each case for unclassified air blast data from presplit blasts. The best result was obtained when cube root scaled distance and elevation difference were inputs.

Table 6.33 Properties of the formed MLR models for unclassified data

	Predictive Equation	S	R^2	$R^2_{adjusted}$
Case 1	dB=exp(4.7374 - 0.000256 SD - 0.000174 ED)	0.054	21.05%	14.74%
Case 2	dB=exp(4.7509 + 0.000000 Q - 0.000050 D)	0.055	16.86%	10.20%
Case 3	dB=exp(4.7372 + 0.000006 Q - 0.000046 D - 0.000160 ED)	0.056	18.57%	8.39%

Table 6.34 Performance indicators of MLR models for unclassified data

	Modelling Set			Testing Set		
	R	r^2	RMSE	R	r^2	RMSE
Case 1	0.464	0.215	5.389	0.927	0.304	6.066
Case 2	0.420	0.176	5.521	0.164	0.001	7.264
Case 3	0.438	0.191	5.472	0.268	0.055	7.067

Table 6.35 shows predictive equations and Table 6.36 shows performance indicators for air blast data classified according to blast location. Case 1 combination yielded the

lowest RMSE for the testing set, therefore, cube root scaled distance and elevation difference were selected as inputs. Figure 6.8 shows measured versus MLR predicted air blast levels with least-squares line for modelling set and testing sets.

Table 6.35 Properties of the formed MLR models for classified data

	Pit location	Predictive Equation	S	R^2	$R^2_{adjusted}$
Case 1	In front of the pit	dB=exp(4.7799 - 0.000640 SD - 0.000294 ED)	0.044	63.13%	57.45%
	Behind the pit	dB=exp(4.8491 - 0.000479 SD + 0.000261 ED)	0.037	31.44%	16.20%
Case 2	In front of the pit	dB=exp(4.7938 + 0.000043 Q - 0.000123 D)	0.046	59.47%	53.24%
	Behind the pit	dB=exp(4.7199 + 0.000303 Q - 0.000047 D)	0.036	35.58%	21.26%
Case 3	In front of the pit	dB=exp(4.7816 + 0.000051 Q - 0.000123 D - 0.000229 ED)	0.046	62.11%	52.64%
	Behind the pit	dB=exp(4.773 + 0.000288 Q - 0.000074 D + 0.000180 ED)	0.038	36.45%	12.61%

Table 6.36 Performance indicators of MLR models for classified data

	Modelling Set			Testing Set		
	R	r^2	RMSE	R	r^2	RMSE
Case 1	0.758	0.574	3.972	0.972	0.478	5.253
Case 2	-0.063	-1.734	10.058	0.897	0.431	5.486
Case 3	0.763	0.582	3.932	0.925	0.411	5.581
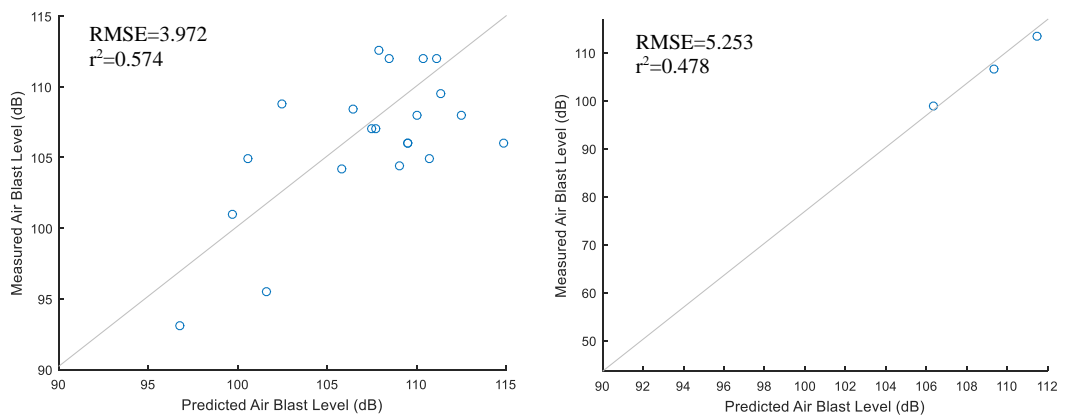
Figure 6.8 Predicted vs measured air blast levels for modeling set and testing set, respectively

6.2.2 Production Blasting Air Blast Analyses

As a preliminary step to detailed air blast analyses, all the air blast levels from production blasts were analyzed together. These values were later compared to regression analyses of the classified data. The best 'in front of the pit' and 'behind the pit' blast location combination determined in Chapter 5 was used for blast round location classification. Air blast analyses were conducted for each village and all possible input parameter combinations were tested to obtain the best model. For analyses 3 cases were tested each of which has different input parameters. The inputs for the cases are listed below and air blast level is the output for all models.

Case 1: scaled distance (SD), elevation difference (ED)

Case 2: charge weight (Q), distance (D)

Case 3: charge weight (Q), distance (D), elevation difference (ED)

Where elevation difference is the difference between explosion elevation and monitoring station elevation. The predictive equation for each case is given in Table 6.37. The performance indicators calculated for modelling and testing set are given in Table 6.38. The best result was obtained when charge weight, distance were inputs.

Table 6.37 Properties of the formed MLR models for whole production blast air blast data

	Predictive Equation	S	R^2	$R^2_{adjusted}$
Case 1	117.66 - 0.07880 SD + 0.00704 ED	5.894	41.89%	41.58%
Case 2	116.76 + 0.00311 Q - 0.012402 D	5.730	45.09%	44.80%
Case 3	117.26 + 0.00395 Q - 0.012772 D + 0.00604 ED	5.726	45.31%	44.87%

Table 6.38 Performance indicators of MLR models for whole air blast data

	Modelling Set			Testing Set		
	R	**r^2**	**RMSE**	**R**	**r^2**	**RMSE**
Case 1	**0.647**	**0.419**	**5.871**	**0.673**	**0.442**	**6.249**
Case 2	0.672	0.451	5.707	0.617	0.379	6.588
Case 3	0.673	0.453	5.695	0.620	0.383	6.569

6.2.2.1 Katrancılar Village

Table 6.39 shows predictive equations and Table 6.40 shows performance indicators for each case for unclassified air blast data from production blasts. The best result was obtained when charge weight, distance and elevation difference were inputs. Table 6.41 shows predictive equations and Table 6.42 shows performance indicators for air blast data classified according to blast location. Case 3 combination yielded the lowest RMSE, when charge weight, distance and elevation difference were inputs.

Table 6.39 Properties of the formed MLR models for unclassified data

	Predictive Equation	S	R^2	$R^2_{adjusted}$
Case 1	dB=118.91 - 0.08012 SD + 0.0477 ED	4.851	48.96%	48.01%
Case 2	dB=112.95 + 0.00477 Q - 0.01046 D	5.079	44.06%	43.01%
Case 3	dB=117.53 + 0.00796 Q - 0.01310 D + 0.0509 ED	4.698	52.58%	51.23%

Table 6.40 Performance indicators of MLR models for unclassified data

	Modelling Set			Testing Set		
	R	r^2	**RMSE**	**R**	r^2	**RMSE**
Case 1	0.701	0.491	4.777	0.868	0.677	3.961
Case 2	0.698	-1.162	9.847	0.741	0.535	4.756
Case 3	**0.726**	**0.527**	**4.605**	**0.879**	**0.713**	**3.733**

Table 6.41 Properties of the formed MLR models for classified data

	Pit location	Predictive Equation	S	R^2	$R^2_{adjusted}$
Case 1	In front of the pit	dB=120.39 - 0.1118 SD + 0.0453 ED	3.937	71.11%	69.67%
	Behind the pit	dB=119.93 - 0.0800 SD + 0.0428 ED	4.790	47.18%	45.53%
Case 2	In front of the pit	dB=113.40 + 0.00981 Q - 0.01623 D	3.868	72.11%	70.72%
	Behind the pit	dB=118.03 - 0.00403 Q - 0.01132 D	4.913	44.44%	42.71%
Case 3	In front of the pit	dB=115.57 + 0.01326 Q - 0.01722 D + 0.0339 ED	3.870	72.79%	70.69%
	Behind the pit	dB=123.17 - 0.00210 Q - 0.01427 D + 0.0486 ED	4.367	56.76%	54.70%

Figure 6.9 shows measured versus MLR predicted air blast levels with least-squares line for modelling set and testing sets.

Table 6.42 Performance indicators of MLR models for classified data

	Modelling Set			Testing Set		
	R	**r^2**	**RMSE**	**R**	**r^2**	**RMSE**
Case 1	0.760	0.578	4.351	0.958	0.844	2.757
Case 2	0.752	0.566	4.413	0.884	0.753	3.469
Case 3	**0.799**	**0.639**	**4.026**	**0.962**	**0.866**	**2.556**
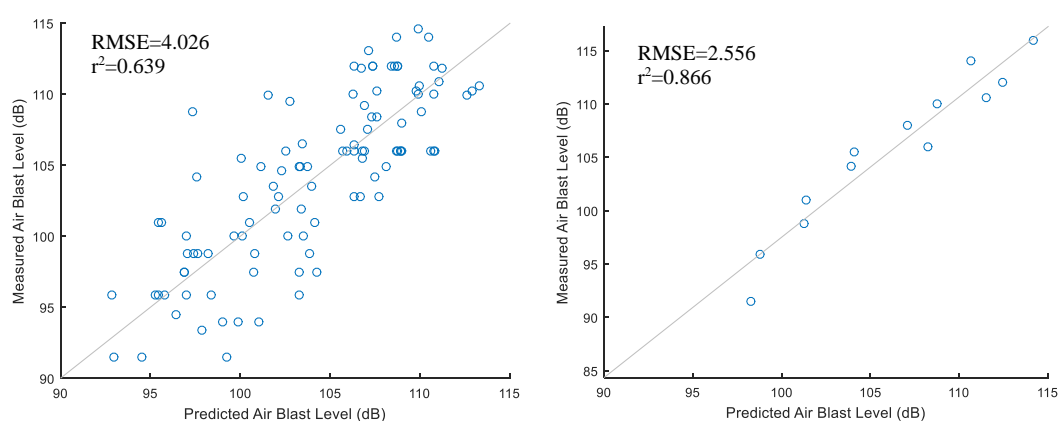
Figure 6.9 Predicted vs measured air blast levels for modeling set and testing set, respectively

6.2.2.2 Karapınar Village

Table 6.43 shows predictive equations and Table 6.44 shows performance indicators for each case for unclassified air blast data from presplit blasts. The best result was obtained when cube root scaled distance and elevation difference were inputs.

Table 6.43 Properties of the formed MLR models for unclassified data

	Predictive Equation	**S**	**R^2**	**$R^2_{adjusted}$**
Case 1	dB=120.75 - 0.09721 SD - 0.00736 ED	6.788	53.96%	53.12%
Case 2	dB=120.20 + 0.00496 Q - 0.01518 D	6.752	54.46%	53.62%
Case 3	dB=119.79 + 0.00394 Q - 0.01488 D - 0.00935 ED	6.743	54.99%	53.74%

Table 6.45 shows predictive equations and Table 6.46 shows performance indicators for air blast data classified according to blast location. Case 3 combination yielded the lowest RMSE for the testing set, when cube root scaled distance and elevation difference were inputs. Figure 6.10 shows measured versus MLR predicted air blast levels with least-squares line for modelling set and testing sets.

Table 6.44 Performance indicators of MLR models for unclassified data

	Modelling Set			Testing Set		
	R	**r^2**	**RMSE**	**R**	**r^2**	**RMSE**
Case 1	**0.735**	**0.540**	**6.695**	**0.812**	**0.618**	**7.011**
Case 2	0.738	0.545	6.658	0.731	0.516	7.885
Case 3	0.742	0.550	6.619	0.730	0.519	7.864

Table 6.45 Properties of the formed MLR models for classified data

	Pit location	Predictive Equation	S	R^2	$R^2_{adjusted}$
Case 1	In front of the pit	dB=121.93 - 0.10687 SD - 0.00003 ED	6.301	61.04%	60.21%
	Behind the pit	dB=111.1 - 0.0548 SD - 0.0686 ED	8.527	33.39%	22.29%
Case 2	In front of the pit	dB=120.18 + 0.00710 Q - 0.01647 D	6.243	61.75%	60.94%
	Behind the pit	dB=124.9 - 0.0043 Q - 0.01354 D	8.889	27.60%	15.54%
Case 3	In front of the pit	dB=120.09 + 0.00667 Q - 0.01636 D - 0.00282 ED	6.272	61.80%	60.57%
	Behind the pit	dB=111.2 + 0.0034 Q - 0.00859 D - 0.0601 ED	8.888	33.66%	15.57%

Table 6.46 Performance indicators of MLR models for classified data

	Modelling Set			Testing Set		
	R	**r^2**	**RMSE**	**R**	**r^2**	**RMSE**
Case 1	**0.760**	**0.578**	**6.410**	**0.867**	**0.672**	**6.494**
Case 2	0.760	0.577	6.414	0.812	0.606	7.113
Case 3	0.765	0.585	6.355	0.852	0.650	6.710
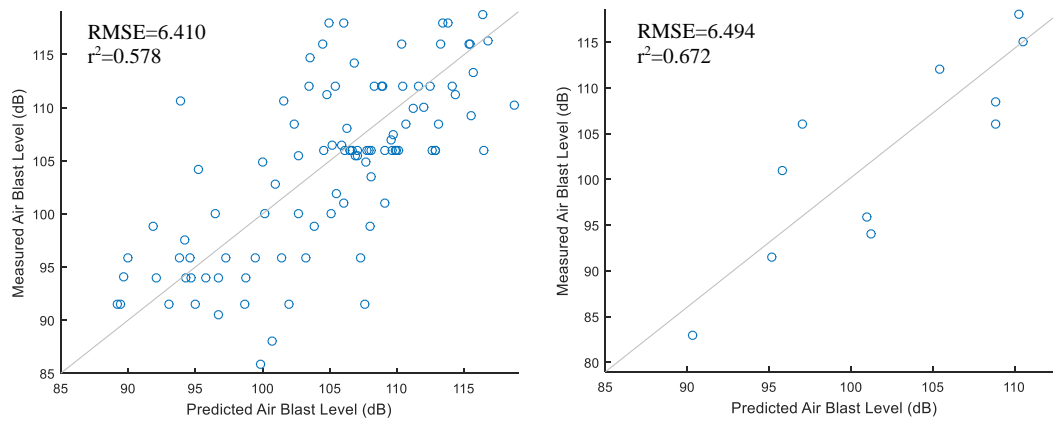
Figure 6.10 Predicted vs measured air blast levels for modeling set and testing set, respectively

6.2.2.3 Gümüşkol Village Path 1

Table 6.47 shows predictive equations and Table 6.48 shows performance indicators for each case for unclassified air blast data from presplit blasts. The best result was obtained when cube root scaled distance and elevation difference were inputs.

Table 6.47 Properties of the formed MLR models for unclassified data

	Predictive Equation	**S**	**R²**	**R²$_{adjusted}$**
Case 1	dB=116.46 - 0.0723 SD - 0.0014 ED	5.327	32.16%	30.62%
Case 2	dB=115.87 + 0.00456 Q - 0.01152 D	5.268	33.65%	32.14%
Case 3	dB=115.45 + 0.00415 Q - 0.01127 D - 0.0029 ED	5.297	33.69%	31.41%

Table 6.48 Performance indicators of MLR models for unclassified data

	Modelling Set			Testing Set		
	R	**r²**	**RMSE**	**R**	**r²**	**RMSE**
Case 1	**0.567**	**0.321**	**5.239**	**0.499**	**0.207**	**6.153**
Case 2	0.580	0.336	5.181	0.374	0.121	6.477
Case 3	0.580	0.337	5.180	0.381	0.125	6.465

Table 6.49 shows predictive equations and Table 6.50 shows performance indicators for air blast data classified according to blast location. Case 2 combination yielded the

lowest RMSE for the testing set, when charge weight and distance were inputs. When the data was classified according to blast round location, elevation difference did not affect the results too much. Figure 6.11 shows measured versus MLR predicted air blast levels with least-squares line for modelling set and testing sets.

Table 6.49 Properties of the formed MLR models for classified data

	Pit location	Predictive Equation	S	R^2	$R^2_{adjusted}$
Case 1	In front of the pit	dB=123.8 - 0.1266 SD + 0.041 ED	2.872	77.75%	72.81%
	Behind the pit	dB=118.32 - 0.0794 SD + 0.0026 ED	5.492	31.50%	29.70%
Case 2	In front of the pit	dB=107.48 + 0.0242 Q - 0.01328 D	2.833	78.35%	73.54%
	Behind the pit	dB=117.37 + 0.00413 Q - 0.01248 D	5.410	33.55%	31.80%
Case 3	In front of the pit	dB=113.5 + 0.0272 Q - 0.0173 D + 0.038 ED	2.985	78.64%	70.63%
	Behind the pit	dB=117.49 + 0.00426 Q - 0.01256 D + 0.0008 ED	5.446	33.55%	30.90%

Table 6.50 Performance indicators of MLR models for classified data

	Modelling Set			Testing Set		
	R	r^2	RMSE	R	r^2	RMSE
Case 1	0.597	0.357	5.101	0.756	0.462	5.070
Case 2	**0.613**	**0.376**	**5.024**	**0.866**	**0.533**	**4.720**
Case 3	0.613	0.376	5.023	0.868	0.532	4.730
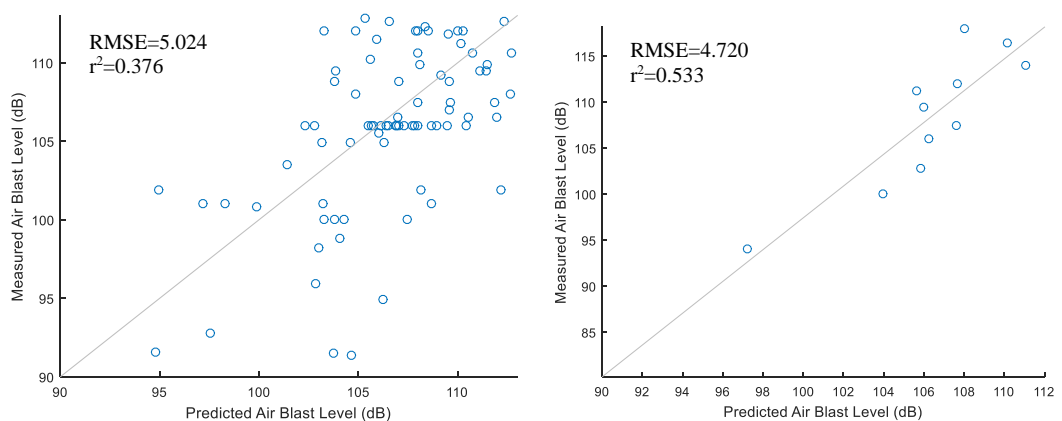
Figure 6.11 Predicted vs measured air blast levels for modeling set and testing set, respectively

6.2.2.4 Gümüşkol Village Path 2

Table 6.51 shows predictive equations and Table 6.52 shows performance indicators for each case for unclassified air blast data from presplit blasts. The best result was obtained when charge weight, distance and elevation difference were inputs. Table 6.53 shows predictive equations and Table 6.54 shows performance indicators for air blast data classified according to blast location. Case 1 combination yielded the lowest RMSE for the testing set, where the cube root scaled distance and elevation difference were used as inputs.

Table 6.51 Properties of the formed MLR models for unclassified data

	Predictive Equation	S	R^2	$R^2_{adjusted}$
Case 1	dB=115.22 - 0.0606 SD + 0.0227 ED	5.222	27.13%	24.74%
Case 2	dB=118.15 - 0.00783 Q - 0.01061 D	4.708	40.75%	38.81%
Case 3	dB=120.43 - 0.00349 Q - 0.01276 D + 0.0238 ED	4.571	45.07%	42.32%

Table 6.52 Performance indicators of MLR models for unclassified data

	Modelling Set			Testing Set		
	R	r^2	RMSE	R	r^2	RMSE
Case 1	0.521	0.271	5.105	0.402	0.157	5.216
Case 2	0.638	0.407	4.604	0.377	0.094	5.410
Case 3	**0.671**	**0.450**	**4.434**	**0.473**	**0.219**	**5.022**

Table 6.53 Properties of the formed MLR models for classified data

	Pit location	Predictive Equation	S	R^2	$R^2_{adjusted}$
Case 1	In front of the pit	dB=141.3 - 0.213 SD + 0.154 ED	4.385	49.17%	28.83%
	Behind the pit	dB=116.23 - 0.0641 SD + 0.0239 ED	5.306	28.65%	25.95%
Case 2	In front of the pit	dB=95.1 + 0.0519 Q - 0.00893 D	4.099	55.58%	37.81%
	Behind the pit	dB=120.35 - 0.00930 Q - 0.01172 D	4.621	45.88%	43.84%
Case 3	In front of the pit	dB=126.1 + 0.1122 Q - 0.0434 D + 0.299 ED	2.845	82.89%	70.05%
	Behind the pit	dB=122.77 - 0.00488 Q - 0.01396 D + 0.0243 ED	4.448	50.79%	47.95%

Figure 6.12 shows measured versus MLR predicted air blast levels with least-squares line for modelling set and testing sets.

Table 6.54 Performance indicators of MLR models for classified data

	Modelling Set			Testing Set		
	R	**r^2**	**RMSE**	**R**	**r^2**	**RMSE**
Case 1	**0.519**	**0.172**	**5.439**	**0.726**	**0.512**	**3.968**
Case 2	0.651	0.422	4.547	0.485	0.223	5.007
Case 3	0.618	-0.072	6.191	0.406	-0.267	6.396
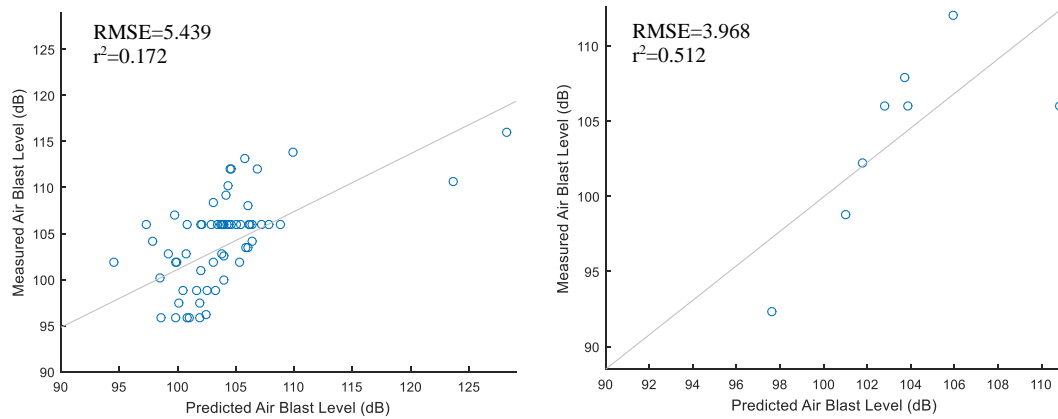
Figure 6.12 Predicted vs measured air blast levels for modeling set and testing set, respectively

6.3 Comparison of MLR Analysis Results

Inspection of the results showed that 'in front of the pit' analyses gave higher correlation than 'behind the pit' analyses for all villages. In order to see which input parameter is more effective on the ground vibration levels, data from unclassified and classified data are compared in Table 6.55.

Table 6.55 Comparison of MLR analyses results for ground vibration data

	Unclassified Data	Classified Data
Katrancılar	Case 3	Case 1
Karapınar	Case 3	Case 3
Gümüşkol Path 1	Case 2	Case 3
Gümüşkol Path 2	Case 3	Case 3

For all villages the ground vibration analysis from classified data according to pit location gave better results than the unclassified data. For whole ground vibration data, Case 3 gave better results where charge weight, distance and elevation difference were inputs. Table 6.56 shows results of air blast analyses from presplit blasts. Only for Karapınar unclassified data gave better results. Effect of input parameters on air blast levels from classified data analysis are consistent with the effect of input parameters from unclassified data analysis. Elevation difference is effective both for classified and unclassified data. For whole air blast data from presplit blasts Case 2 gave better results, where charge weight and distance were input parameters.

Table 6.56 Comparison of MLR analyses results for air blast data from presplit blasts

	Unclassified Data	Classified Data
Katrancılar	Case 3	Case 3
Karapınar	Case 3	Case 3
Gümüşkol Path 1	Case 3	Case 3
Gümüşkol Path 2	Case 1	Case 1

Table 6.57 shows results of air blast analyses from production blasts. For whole air blast data Case 1 gave better results, where scaled distance and elevation difference were input parameters. For all villages air blast analysis from classified data gave better results than unclassified data. Except for Gümüşkol village path 1 elevation difference is effective on the results.

Table 6.57 Comparison of MLR analyses results for air blast data from production blasts

	Unclassified Data	Classified Data
Katrancılar	Case 3	Case 3
Karapınar	Case 1	Case 1
Gümüşkol Path 1	Case 1	Case 2
Gümüşkol Path 2	Case 3	Case 1

CHAPTER 7

COMPARISON OF LINEAR REGRESSION AND MULTIPLE LINEAR REGRESSION ANALYSIS METHODS FOR GROUND VIBRATION AND AIR SHOCK ANALYSES

In this chapter the comparison between Linear Regression analysis and Multiple Linear Regression (MLR) method is given. Table 7.1 to Table 7.3 show performance indicators for the same modelling set-testing set combination for each village obtained with linear regression and MLR methods for the classified data according to blast round location. The measured and predicted values of testing data are given in tables in Appendix B. Conventional method used only scaled distance and blast group location as input parameters. Whereas, more inputs can be used to predict a response variable with MLR method. For PPV analyses the results from classified data is better than the unclassified data both for conventional and MLR methods. Table 7.1 shows the statistical parameters for the blast location classified data. Linear regression analysis method gives better results for all of the villages for ground vibration prediction (Table 7.1). Therefore, it can be concluded that only square root scaled distance and blast round location are enough to predict PPV.

Table 7.1 Comparison of performance indicators for PPV for conventional and MLR methods

	Method of Analysis	Modeling Set			Testing Set		
		RMSE	R	r^2	RMSE	R	r^2
Katrancılar	Conventional	**0.957**	**0.895**	**0.794**	**0.553**	**0.964**	**0.902**
	MLR	1.382	0.836	0.571	0.934	0.930	0.720
Karapınar	Conventional	**3.017**	**0.868**	**0.480**	**2.279**	**0.917**	**0.698**
	MLR	3.257	0.685	0.394	3.239	0.787	0.390
Gümüşkol Path 1	Conventional	**0.923**	**0.865**	**0.721**	**0.710**	**0.933**	**0.849**
	MLR	1.131	0.822	0.580	1.076	0.897	0.653
Gümüşkol Path 2	Conventional	**0.638**	**0.742**	**0.523**	**0.622**	**0.959**	**0.660**
	MLR	0.521	-0.470	1.121	0.434	0.929	0.835

For air blast prediction MLR method gives more reliable results than conventional method (Table 7.2, Table 7.3). When MLR is used instead of conventional regression

analysis for air blast prediction from presplit blasts, the decrease in RMSE are 30%, 20%, 4% and 11% for each village, respectively. For production blasts the decrease in RMSE are 27%, 14%, 12% and 18% for each village, respectively.

Table 7.2 Comparison of performance indicators for air blast levels from conventional and MLR methods for presplit blasts

	Method of Analysis	Modeling Set			Testing Set		
		RMSE	R	r^2	RMSE	R	r^2
Katrancılar	Conventional	5.706	0.765	0.585	6.880	0.705	0.442
	MLR	**4.774**	**0.843**	**0.710**	**4.766**	**0.862**	**0.732**
Karapınar	Conventional	5.679	0.840	0.706	6.088	0.900	0.711
	MLR	**41.359**	**0.321**	**-14.621**	**5.536**	**0.874**	**0.761**
Gümüşkol Path 1	Conventional	4.602	0.690	0.475	3.303	0.862	0.702
	MLR	**4.519**	**0.703**	**0.494**	**3.182**	**0.934**	**0.723**
Gümüşkol Path 2	Conventional	4.186	0.726	0.526	5.923	0.979	0.336
	MLR	**3.972**	**0.758**	**0.574**	**5.253**	**0.972**	**0.478**

Table 7.3 Comparison of performance indicators for air blast levels from conventional and MLR methods for production blasts

	Method of Analysis	Modeling Set			Testing Set		
		RMSE	R	r^2	RMSE	R	r^2
Katrancılar	Conventional	4.731	0.708	0.501	3.520	0.869	0.745
	MLR	**4.026**	**0.799**	**0.639**	**2.556**	**0.962**	**0.866**
Karapınar	Conventional	6.830	0.723	0.521	7.524	0.877	0.560
	MLR	**6.410**	**0.760**	**0.578**	**6.494**	**0.867**	**0.672**
Gümüşkol Path 1	Conventional	5.172	0.583	0.339	5.388	0.751	0.392
	MLR	**5.024**	**0.613**	**0.376**	**4.720**	**0.866**	**0.533**
Gümüşkol Path 2	Conventional	4.977	0.555	0.307	4.870	0.565	0.266
	MLR	**5.439**	**0.519**	**0.172**	**3.968**	**0.726**	**0.512**

CHAPTER 8

CONCLUSIONS AND RECOMMENDATIONS

8.1   Conclusions

In this thesis, the effect of blast related ground vibrations and air shock on structures and public health are investigated. Ground vibration and air shock were monitored on Gümüşkol Path 1, Gümüşkol Path 2, Karapınar and Katrancılar paths. The prediction performance of conventional (least square regression) analysis and MLR methods are compared in terms of statistical parameters (R, r^2, RMSE) and the best method is chosen.

With conventional linear regression analyses the effect of blast group location is tested only. Whereas, with MLR the performance of using scaled distance, charge weight, distance and elevation difference (separately and together) as inputs are tested for ground vibration and air shock analysis.

 Following conclusions can be drawn from this study:

1) For Katrancılar village, the highest PPV level from stripping and production blasting is 1.876 mm/s with 5.63 Hz predominant frequency (at 1447.3 m) for 'in front of the pit' blasts, and 1.429 mm/s with 13.88 Hz predominant frequency (at 1328.0 m) for 'behind the pit' blasts. The highest air blast level from stripping and production blasts is 104.9 dB with 3.88 Hz predominant frequency (at 1782.0 m). From presplit blasts the maximum air blast overpressure level at the house nearest to the pit border is 112 dB with 6.5 Hz predominant frequency (at 1824.0 m).

2) For Karapınar village, the highest PPV level from stripping and production blasting is 2.372 mm/s with 7.94 Hz predominant frequency (at 1381.0 m) for 'in front of the pit' blasts. The highest PPV level from production blasting is

191

0.780 mm/s with 8.25 Hz predominant frequency (at 1900.0 m) for 'behind the pit' blasts. The highest air blast level from stripping and production blasts is 110.6 dB with 3.88 Hz predominant frequency (at 2100.0 m). From presplit blasts the maximum air blast overpressure level at the house nearest to the pit border is 112 dB with 12.38 Hz predominant frequency (at 1078.9 m).

3) Gümüşkol village path 1, the highest PPV level from stripping and production blasting is 0.741 mm/s with 12.81 Hz predominant frequency (at 1707.9 m) for 'in front of the pit' blasts. The highest PPV level measured at GK4 station from production blasting is 0.968 mm/s with 34.63 Hz predominant frequency (at 1653.78 m) for 'behind the pit' blasts. The highest air blast level from stripping and production blasts is 101.9 dB with 3.63 Hz predominant frequency (at 1869.34 m). From presplit blasts the maximum air blast overpressure level at the house nearest to the pit border is 110.8 dB with 9.81 Hz predominant frequency (at 2331 m).

4) Gümüşkol village path 2, the highest PPV level measured at Sami Y.'s house from stripping and production blasting is 1.413 mm/s with 18.13 Hz predominant frequency (at 1262.03 m) for 'in front of the pit' blasts. The highest PPV level is 1.490 mm/s with 13.13 Hz predominant frequency (at 1641.16 m) for 'behind the pit' blasts. The highest air blast level from stripping and production blasts is 110.2 dB with 3.13 Hz predominant frequency (at 1558 m). From presplit blasts the maximum air blast overpressure level at the house nearest to the pit border is 115.7 dB with 9.25 Hz predominant frequency (at 1917.7 m).

5) For all villages both ground vibration and air blast levels are within the acceptable ranges and comply with the regulations, so they do not pose any risk in terms of structural damage, public disturbance and complaints.

6) The crack formation mechanism and damage in the buildings proved that they are not formed due to seismic effect. The probable reasons for damage might

be weak foundation, foundation settlement or water seepage into foundation. Construction type of buildings might be another factor of damage since they are mostly made of rubble stone-mud mortar and wooden beams are rarely used.

7) The radial velocity component is the dominant constituent of ground vibration (%54 of the vibration data).

8) Conventional analysis method is a better tool for ground vibration prediction. MLR analyses showed that blast group location has more effect on the magnitude of ground vibrations than elevation of blast group.

9) Multiple linear regression analysis is a better tool for air blast prediction from both presplit and production blasts. On the contrary to other villages, for Karapınar village blast group location does not have any effect on air blast levels from presplit blasts.

10) Elevation difference between blast group and monitoring station is an effective factor on measured air blast levels for both production and presplit blasts.

11) Regression analysis indicated that Katrancılar and Karapınar, 'in front of the pit' blast groups result in higher ground vibrations. Whereas, for Gümüşkol Path1 and Path2 'behind the pit' blast groups result in higher vibration levels. The reason might be attributed to the Northeast-striking sub-vertical fault at the east part of the deposit and the strata with bedding slopes replicating the probable shape of the actual stratovolcano which dips away from the deposit Gümüşkol village.

12) If the buildings in the villages are classified as buildings under preservation order since they are built by mud mortar and rubble stone, 3.00 mm/s ground vibration limit should not be exceeded. The maximum safe explosive amount, 559.16 kg/delay, should not be exceeded.

13) All in all, it can be concluded that MLR is more favorable if the dataset is not large enough or more than two parameters affect the results.

8.2 Recommendations

The following improvements can be made for the future studies:

1) In this research study the number of air blast records from presplit blasts were 58 for Katrancılar, 56 for Karapınar, 34 for Gümüşkol path 1 and 32 for Gümüşkol path 2. Although attempts were made to subclassify and analyze the data with respect to some other parameters, such as wind direction, wind speed etc., the results were not satisfying due to the limited size of the data.

2) Attenuation of ground vibration are mostly affected by geological structure and velocity profile of the region. By involving this highly prominent information, a better understanding on ground vibration propagation can be attained.

3) Despite the fact that a fully equipped meteorological station exists in the mine, only wind direction, wind speed and air temperature are not enough for air shock analysis. Rain, cloud cover and air inversion layer are also important factors that should be considered. By means of a seismograph attached to a drone, meteorological data and air shock data can be obtained on and above the ground and involved in analyses.

REFERENCES

Adhikari, G. R., Venkatesh, H. S., Theresraj, A., Roy, S., Balachander, R., Jain, N. K., & Gupta, R. (2005). Role of blast design parameters on ground vibration and correlation of vibration level to blasting damage to surface structures. Karnataka, India: National Institute of Rock Mechanics.

Adoko, A. C., & Wu, L. (2011). Fuzzy Inference Systems-based Approaches in Geotechnical Engineering- a Review. Electronic Journal of Geotechnical Engineering, 1543-1558.

Ak, H., Iphar, M., Yavuz, M., & Konuk, A. (2009). Evaluation of ground vibration effect of blasting operations in a magnesite mine. Soil Dynamics and Earthquake Engineering, 669–676.

Alcudia, A. D., & Stewart, R. R. (2008). Air blast attenuation by combining microphone and geophone signals in the time-frequency domain. Calgary: CREWES.

Alipour, A., & Ashtiani, M. (2011). Fuzzy modeling approaches for the prediction of maximum charge per delay in surface mining. International Journal of Rock Mechanics & Mining Sciences, 305–310.

American National Standards Institute. (1983). American National Standard Guide to the Evaluation of Human Exposure to Vibration in Buildings. ANSI S3.29-1983. USA.

Amnieh, H. B., Siamaki, A., & Soltani, S. (2012). Design of blasting pattern in proportion to the peak particle velocity (PPV): Artificial neural networks approach. Safety Science, 1913–1916.

Audell, H. (1996). Geotechnical Nomenclature and Classification System for Crack Patterns in Buildings. Environmental and Engineering Geoscience, II, 225-248.

Aydin, A. (2004). Fuzzy set approaches to classification of rock masses. Engineering Geology, 227–245.

Azimi, Y., Osanloo, M., Aakbarpour-Shirazi, M., & Bazzazi, A. A. (2010). Prediction of the blastability designation of rock masses using fuzzy sets. International Journal of Rock Mechanics & Mining Sciences, 1126-1140.

Bazzazi, A. A., & Esmaeili, M. (2012). Prediction of Backbreak in Open Pit Blasting by Adaptive Neuro-Fuzzy Inference System. Archives of Mining Sciences, 933–943. doi:10.2478/v10267-012-0062-x

Bender, W. L. (2006). Understanding Blast Vibration and Airblast, their Causes, and their Damage Potential. Retrieved from http://www.iseegoldenwest.org/articles/Blast%20Effects.pdf

Berta, G. (1990). Explosives: An Engineering Tool. Milano, Italy: Italesplosivi.

Bilgin, A. H., Tanrıseven, E. N., & Dağaşan, Y. (2014). Siirt Madenköy mevkiinde işletilen bakır madeni ocağı patlatmalarında ölçülen titreşimlerin analizine dayalı çevresel etki ve hasar etüt ara raporu. Ankara: ODTÜ.

Bilgin, H., Tanrıseven, E., Kahveci, S., Kılıç, M., & Ünlütürk, B. (2015). Kışladağ altın madeni patlatmaları kaynaklı çevresel etki ölçüm ve değerlendirme raporu. Ankara: ODTÜ.

Burgher, K. E. (2000). Determination of Air Blast Overpressure Levels. 26th Annual Conference on Explosives and Blasting Technique. International Society of Explosives Engineers.

Casarotti, E., Stupazzini, M., Lee, S. J., Komatitsch, D., Piersanti, A., & Tromp, J. (2007). CUBIT and Seismic Wave Propagation Based Upon the Spectral-element Method: An Advanced Unstructured Mesher for Complex 3D Geological Media. Proceedings of the 16th International Meshing Roundtable (pp. 579-597). Seattle: Springer.

Colombero, R., Kontoe, S., Foti, S., & Potts, D. (2015). Numerical modelling of drop load tests. Soil Dynamics and Earthquake Engineering, 279–289.

Çakmak, B. B. (2007, September). Investigation of Ground Vibrations Induced by Production Blasting at Uşak Kışladağ Gold Mine. Ankara, Turkey.

Dehghanin, H., & Ataee-pour, M. (2011). Development of a model to predict peak particle velocity in a blasting operation. International Journal of Rock Mechanics & Mining Sciences, 51-58.

DIN 4150–3:1999–02. (1999). Vibration in buildings—Part 3: Effects on Structures. Berlin.

Dixon, W. J. (1953). Processing Data for Outliers. Biometrics(9), 74-89.

Dowding, C. H. (1985). Blast Vibration Monitoring and Control. Prentice-Hall.

Dowding, C. H. (1992). Monitoring and Control of Blast Effects, SME Mining Engineering Handbook.

Ebeling, C. E. (2010). An Introduction to Reliability and Maintainability Engineering. Waveland Press Inc.

Ercan, T., Dincel, A., Metin, S., Turkecan, A., & Gunay, E. (1978). Uşak Yöresindeki Neojen Havzalarının Jeolojisi. Türkiye Jeoloji Kurumu Bülteni, 21, 97-106.

Fişne, A., Kuzu, C., & Hüdaverdi, T. (2011). Prediction of environmental impacts of quarry blasting operation using fuzzy logic. Environmental Monitoring and Assessment,174, 461-470.

Ghasemi, E., Sari, M., & Ataei, M. (2012). Development of an empirical model for predicting the effects of controllable blasting parameters on flyrock distance in surface mines. International Journal of Rock Mechanics & Mining Sciences, 163-170.

HATCH. (2003). Technical Report Kışladağ Project Feasibility Study. Vancouver, British Columbia: Eldorado Gold.

Hongmian, D., & Jing, Z. (2010). Digital Signal Processing Method to Air Blast Shock Wave. 2nd International Conference on Information Engineering and Computer Science (pp. 1-4). Wuhan: IEEE.

Hudaverdi, T. (2012). Application of multivariate analysis for prediction of blast-induced ground vibrations. Soil Dynamics and Earthquake Engineering, 300-308.

Jimeno, E. L., Jimino, C. L., & Carcedo, A. (1995). Drilling and Blasting of Rocks. New York: Taylor & Francis.

Juras, S., Miller, R., & Skayman, P. (2010). Technical Report for the Kışladağ Gold Mine, Turkey . Vancouver, British Columbia : Eldorado Gold.

Khandelwal, M., & Singh, T. (2006). Prediction of blast induced ground vibrations and frequency in opencast mine: A neural network approach. Journal of Sound and Vibration, 711–725.

Khandelwal, M., & Singh, T. (2007). Evaluation of blast-induced ground vibration predictors. Soil Dynamics and Earthquake Engineering, 116–125.

Khandelwal, M., & Singh, T. (2009). Prediction of blast-induced ground vibration using artificial neural network. International Journal of Rock Mechanics & Mining Sciences, 1214–1222.

Kima, D.-S., & Lee, J.-S. (2000). Propagation and attenuation characteristics of various ground vibrations. Soil Dynamics and Earthquake Engineering, 115-126.

Kışladağ Altın Madeni. (2013). Tüprag Metal Madencilik San. ve Tic. A.Ş. Retrieved from Tüprag Metal Madencilik Web site: https://www.tuprag.com.tr/tr/projelerimiz/Kışladağ-altin-madeni/7/jeoloji-ve-cevherlesme/27

Konya, A. J., & Konya, C. J. (2015). Air Overpressure Prediction Equation for Construction Blasting. 41st Annual Conference on Explosives and Blasting Technique (pp. 24-34). New Orleans: International Society of Explosive Engineers.

Konya, C. J., Otuonye, F., & Skidmore, D. (2000). Airblast Reduction From Effective Blasthole Stemming. 26th Annual Conference on Explosives and Blasting Technique (pp. 145-153). International Society of Explosives Engineers.

Kopp, J. W. (2000). Initiation Timing Influence on Ground Vibration and Airblast. 26th Annual Conference on Explosives and Blasting Technique. International Society of Explosives Engineers.

Kuzu, C., Fisne, A., & Ercelebi, S. (2009). Operational and geological parameters in the assessing blast induced airblast-overpressure in quarries. Applied Acoustics, 404–411.

Ladegaard-Pedersen, A., & Dally, J. W. (1975). *A Review of Factors Affecting Damage in Blasting.* Univ. of Maryland, Mech. Eng. Dept. College Park, Md: National Science Foundation.

Lewis Geoscience Services Inc. (2002). Report on Geological Mapping and Structural Analysis. Western Turkey: Kışladağ Au Project.

Mohamed, M. T. (2010). Vibration Control. Sciyo. Retrieved from http://cdn.intechopen.com/pdfs-wm/11902.pdf

Mohamed, M. T. (2011). Performance of fuzzy logic and artificial neural network in prediction of ground and air vibrations. International Journal of Rock Mechanics & Mining Sciences, 845–851.

Monjezi, M., & Rezaei, M. (2011). Developing a new fuzzy model to predict burden from rock geomechanical properties. Expert Systems with Applications, 9266–9273.

Office of Surface Mining Reclamation and Enforcement (OSM). (1983). Federal Register, 30 CFR Parts, 715, 780, 816 and 817, Vol. 48, No. 46, Rules and

Regulations (governing the blasts associated with surface and underground mines). Washington, DC: Department of the Interior.

Orhan, A. A. (2004). Geologic Investigation Report as a Basis for Local Construction Plan for Kışladağ Gold Mine. Uşak.

Pal Roy, P. (2005). Rock Blasting: Effects and Operations. A. A. Balkema Publishers.

Persson, P.-A., Holmberg, R., & Lee, . (1994). Rock Blasting and Explosives Engineering. Washington, D.C.: CRC Press. Retrieved January 3, 2016

Prdhan, S. K., & Das, A. (2007). Evaluation of Explosives Using Ground Vibration Criterion. Bachelor Thesis. Rourkela, Orissa, India: National Institute of Technology, Department of Mining Engineering.

Ratcliff, J., Sheehan, E., & Carte, K. (2011). Predictability of Airblast at Surface Coal Mines in West Virginia. West Virginia: West Virginia Department of Environmental Protection Office of Explosives And Blasting.

Rezaei, M., Monjezi, M., & Varjani, A. Y. (2011). Development of a fuzzy model to predict flyrock in surface mining. Safety Science, 298–305.

Richards, A. B. (2008). Blast vibration wavefront reinforcement model. Trans. Inst. Min. Metall., 117(4), 161–167.

Richards, A. B. (2010). Elliptical airblast overpressure model. Mining Technology, 119, 205-211.

Richards, A. B. (2013). Predictive modelling of airblast overpressure. Mining Technology, 215-220.

Richards, A. B., & Moore, A. J. (2003). The Eight Millisecond Time Window Myth. The 5th Large Open Pit Conference. Kalgoorlie, Australia: The Australasian Institute of Mining and Metallurgy.

Richards, A. B., & Moore, A. J. (2006). Airblast Control Techniques in Open Cut Mines. International Society of Explosives Engineers, II.

Richards, A. B., & Moore, A. J. (2009a). Blast Vibration Course: Measurement, Assessment, Control. Australia.

Richards, A. B., & Moore, A. J. (2009b). Real-Time Prediction of Meteorological Effects on Airblast Levels. 35th Annual Conference on Explosives and Blasting Technique. International Society of Explosives Engineers.

Singh, T. N., & Singh, V. (2005). An intelligent approach to prediction and control ground vibration in mines. Geotechnical and Geological Engineering, 249–262.

Siskind, D. E. (2000). Vibrations from Blasting. Cleveland, Ohio: International Society of Explosives Engineers.

Siskind, D. E., Stachura, V. J., Stagg, M. S., & Kopp, J. W. (1980). Structure response and damage produced by airblast from surface mining. United States Bureau of Mines.

Siskind, D. E., Stagg, M. S., Kopp, J. W., & Dowding, C. (1980). Structure Response and Damage Produced by Ground Vibration From Surface Mine Blasting, USBM RI 8507. Pittsburgh: United States Department of the Interior.

SOS-LIFE Earthquake early warning system. Quake Alarm. Earth Quake detector. (2015). Lamit Company.

Svinkin, M. R. (2008). Soil and structure vibrations from construction and industrial sources. Proc., 6th Int. Conf. on Case Histories in Geotechnical Engineering (pp. CD-ROM). Madison: OmniPress.

Svinkin, M. R. (2015). Tolerable Limits of Construction Vibrations. Practice Periodical on Structural Design and Construction, 20(2), 1-7. doi:10.1061/(ASCE)SC.1943-5576.0000223

Wu, C., & Hao, H. (2005). Modeling of simultaneous ground shock and airblast pressure on nearby structures from surface explosions. International Journal of Impact Engineering, 699-717.

Yazicigil, H., Karahanoglu, N., Yilmaz, K., Gundogdu, A., Sakiyan, J., Yesilnacar, E., & Tuzcu, B. (2000). Investigation and management of the Kucuk Menderes Basin groundwater. Ankara: Middle East Technical University.

APPENDIX A

COORDINATES OF MONITORING STATIONS

	X	Y	Z
GK6A	687632.6	4260816.2	1025.5
GK8	688448.3	4260195.4	955.1
GK0	687846.9	4261116.7	1057.7
GK1A	687902.8	4260984.1	1060.3
GK1	687875.2	4261021.3	1059.3
GK2	687997.5	4260743.9	1035.5
GK3	688081.4	4260567.2	1008.3
GK4	688169.6	4260382.9	984.5
GK5	688292.7	4260125.2	936.1
GK6	687698.9	4260757.4	1012.2
GK7	687722.9	4260428.7	978.1
A.tepe	687883.6	4261103.9	1061.3
Sami Y. House	687820.4	4260100.2	924.0
KP0	686819.9	4261673.9	984.9
KP1	686451.6	4261743.7	1051.9
KP2	686077.8	4261827.9	964.9
KP3	685809.2	4261912.3	921.2
KP4	685558.4	4261964.3	909.1
KT0	687369.4	4262117.6	998.2
KT1	687309.3	4262183.9	998.4
KT2	687135.2	4262533.6	994.6
KT3	686952.5	4262841.2	997.7
KT4	686827.2	4263151.7	981.0
KT5	686814.0	4263126.4	957.2

APPENDIX B

THE COMPARISON BETWEEN MEASURED AND PREDICTED GROUND VIBRATION AND AIR SHOCK LEVELS

Table B.1 Comparison between the recorded and predicted PPV from conventional method and MLR method

	Recorded	Predicted from Regression Analysis	Predicted from MLR
Katrancılar	0.159	0.304	0.326
	0.254	0.434	0.396
	0.402	0.406	0.292
	0.476	0.574	0.534
	0.524	0.658	0.525
	0.603	0.355	0.370
	0.709	0.621	0.564
	0.889	1.023	0.772
	0.905	0.366	0.247
	1.079	1.454	0.950
	1.270	0.956	1.068
	1.429	1.004	1.111
	1.857	1.216	0.864
	2.160	2.431	2.478
	2.873	2.122	2.251
	4.190	4.541	3.526
	7.370	5.593	3.879
Karapınar	0.159	0.244	0.227
	0.254	0.277	0.246
	0.333	0.337	0.327
	0.370	0.286	0.333
	0.381	0.927	0.644
	0.544	0.755	0.687
	0.725	0.801	0.744
	0.873	0.876	0.740
	1.020	3.439	3.487
	1.222	1.292	0.900
	1.333	0.904	1.108
	1.762	0.748	0.828
	2.030	2.542	2.881
	4.450	0.550	0.353
	17.19	9.775	5.675
Gümüşkol Path 1	0.315	0.221	0.323
	0.460	1.399	1.524
	0.556	0.750	0.590
	0.683	0.885	0.845
	0.788	0.685	0.927
	0.921	0.525	0.505
	1.270	1.792	1.891
	1.520	1.678	1.840
	2.461	1.523	1.722
	3.050	1.420	1.500
	3.969	3.104	3.107
	6.747	6.176	3.858
Gümüşkol Path 2	0.317	0.357	0.424
	0.583	0.616	0.624
	0.985	0.501	0.419
	1.206	0.875	1.456
	1.413	0.981	1.135
	1.778	0.750	1.976
	2.572	1.989	2.599
	3.810	2.731	2.813

Table B.2 Comparison between the recorded and predicted air blast level for presplit blasts from conventional method and MLR method

	Recorded	Predicted from Regression Analysis	Predicted from MLR
Katrancılar	101.7	104.4	104.6
	105.1	105.7	104.7
	112.0	106.6	106.3
	116.0	117.3	118.0
	121.0	126.9	125.6
	128.9	114.4	120.5
Karapınar	97.5	107.4	105.8
	102.8	104.7	101.7
	111.2	107.3	105.2
	116.0	115.5	113.3
	124.3	122.2	122.1
	130.0	119.9	124.9
Gümüşkol Path 1	104.2	108.5	108.8
	110.6	108.2	111.7
	115.4	116.5	116.9
	120.6	116.3	116.8
Gümüşkol Path 2	98.8	105.5	106.3
	106.5	106.9	109.3
	113.5	107.4	111.5
	118.0	108.0	111.6

Table B.3 Comparison between the recorded and predicted air blast level for production blasts from conventional method and MLR method

	Recorded	Predicted from Regression Analysis	Predicted from MLR
Katrancılar	91.5	99.1	98.2
	95.9	98.8	98.8
	98.8	101.7	101.2
	101.0	103.1	101.4
	104.2	100.1	103.9
	105.5	103.2	104.1
	106.0	109.9	108.2
	108.0	102.2	107.1
	110.0	108.0	108.8
	110.6	112.3	111.5
	112.0	112.7	112.4
	114.0	116.0	110.6
	116.0	115.5	114.2
Karapınar	82.9	94.5	90.3
	91.5	96.7	95.1
	94.0	100.1	101.3
	95.9	101.1	101.0
	101.0	97.0	95.8
	106.0	98.4	97.0
	106.0	106.4	108.8
	108.4	106.4	108.8
	112.0	103.2	105.4
	115.0	108.4	110.5
	118.0	108.1	110.2
	123.0	110.6	112.1
Gümüşkol Path 1	94.0	98.8	97.2
	100.0	104.3	104.0
	102.8	108.1	105.8
	106.0	104.7	106.2
	107.5	107.9	107.6
	109.5	104.6	106.0
	111.2	105.5	105.6
	112.0	107.5	107.7
	114.0	111.3	111.1
	116.4	109.1	110.1
	118.0	107.5	108.0
Gümüşkol Path 2	92.3	98.1	97.6
	98.8	99.4	101.0
	102.2	100.9	101.8
	106.0	103.1	102.8
	106.0	103.3	103.8
	106.0	110.9	110.8
	107.9	103.2	103.7
	112.0	102.5	105.9

CROSS SECTIONS OF MONITORING PATHS

From Pos: 3245306.521, 4620324.264   To Pos: 3245826.241, 4619113.862

Gümüşkol Path 1

From Pos: 3244903.054, 4620160.142   To Pos: 3245258.652, 4619134.378

Gümüşkol Path 2

From Pos: 3244718.416, 4621746.657   To Pos: 3244048.250, 4622984.412

Katrancılar

From Pos: 3243508.014, 4621267.967   To Pos: 3242434.381, 4621568.857

Karapınar

207
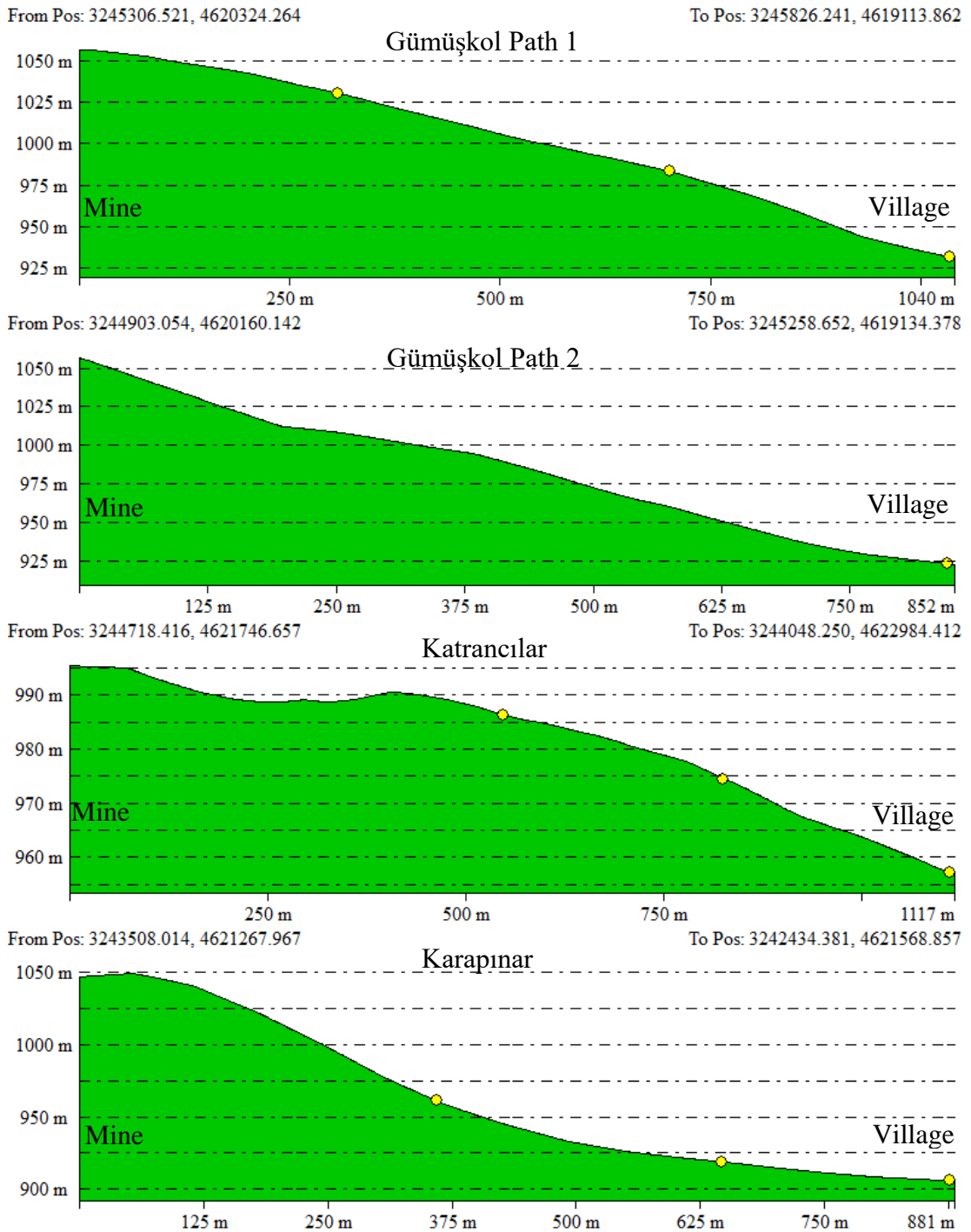
CURRICULUM VITAE

PERSONAL INFORMATION

Surname, Name: Tanrıseven, Esra Nur
Nationality: Turkish
Email: esra.gayretli@gmail.com

EDUCATION

Degree	Institution	Year of Graduation
PhD	METU Mining Engineering	2018
MS	METU Mining Engineering	2012
BS	METU Mining Engineering	2009

WORK EXPERIENCE

TUBITAK Scholar, Researcher, The Department of Earth and Environmental Sciences, Geophysics, Ludwig-Maximilians-University in Munich, Germany, 2017 – 2018.

Research Assistant, Middle East Technical University, Assistantship of Rock Mechanics, Mine System Analysis, Mine Design, Underground Mining, Rock Fragmentation Courses, August 2009 -2018.

Researcher, Middle East Technical University, Scientific Research Project, Environmental Impact Assessment of Siirt Madenkoy Blasting Operations, Siirt, 2015.

Researcher, Middle East Technical University, Scientific Research Project, Zonguldak-Amasra-Kurucaşile Road Turkish State Railways No: 50 Tunnel Stability Assessment, 2016.

Researcher, Middle East Technical University, Scientific Research Project, Environmental Impact Assessment of Eldorado Gold-Uşak Kışladağ Gold Mine Blasting Operations, Uşak, 2015-2016.

Internship at Underground Mining Operations, Çayırhan Coal Mine- Ciner Group, Ankara – Turkey, 2006.

Internship at Copper Processing Plant, Çayeli Copper Enterprises-Inmet Mining, Rize – Turkey, 2007.

Internship at Gold Processing Plant, Tüprag Metal Mining Company- Eldorado Gold Corporation, Usak – Turkey, 2007

FOREIGN LANGUAGES

Advanced English, Beginner German

PUBLICATIONS

1. Dagasan Y., Bilgin Hasan A. and Tanriseven Esra N., "Effect of non-accurate blasthole depth on the cost analysis of a foundation excavation blasting", European Federation of Explosive Engineers 8th World Conference on Explosives & Blasting, Lyon, France, 87-91 (26-28 April 2015)

2. Tanriseven Esra N., Bilgin Hasan A. and Duzgun Sebnem H., "Determination of Shear Strength Parameters of Dam Body Material using Disturbed Sampling". 68th Canadian Geotechnical Conference (GeoQuebec 2015), Quebec, Canada (20-23 September 2015)

3. Tanriseven Esra N., Bilgin Hasan A. and Duzgun Sebnem H., "Modulus of Elasticity Estimation with One Dimensional Consolidation Test", XV Panamerican Conference on Soil Mechanics and Geotechnical Engineering, Buenos Aires, Argentina, DOI: 10.3233/978-1-61499-603-3-2426, 2426 – 2433 (15-18 November 2015)

4. Tanriseven Esra N., Unluturk Burcu, Bilgin Hasan A. and Tutluoglu Levend, "Coupled stability analyses of a road cut slope and a railway tunnel in use ", 2016 ISRM International Symposium (EUROCK 2016), Cappadocia, Turkey (29-31 August 2016)

5. Tanriseven Esra N., Bilgin Hasan A. and Duzgun Sebnem H., "Effect of Ponded Water Level on Stability of a Tailings Dam", 51st US Rock Mechanics/Geomechanics Symposium, San Francisco, California, USA (25-28 June 2017)

6. Tanriseven Esra N., Igel Heiner and Bilgin Hasan A., "Comparison of Dominant Frequency Analysis Methods for Blast Induced Ground Vibrations", 14th IEEE International Conference on Signal Processing (ICSP2018), Beijing, China (12-16 August 2018)

HOBBIES

Tennis, Archery